A PARAMETRIC PHYSICS BASED CREEP LIFE PREDICTION APPROACH TO GAS TURBINE BLADE CONCEPTUAL DESIGN

A Thesis
Presented to
The Academic Faculty

by

Marcus Edward Brockbank Smith

In Partial Fulfillment
of the Requirements for the Degree
Doctor of Philosophy in the
School of Aerospace Engineering

Georgia Institute of Technology
April, 2008

A PARAMETRIC PHYSICS BASED CREEP LIFE PREDICTION APPROACH TO GAS TURBINE BLADE CONCEPTUAL DESIGN

Approved by:

Dr. Dimitri Mavris, Advisor
School of Aerospace Engineering
Georgia Institute of Technology

Mr. Russell Denney
School of Aerospace Engineering
Georgia Institute of Technology

Dr. Vitali Volovoi
School of Aerospace Engineering
Georgia Institute of Technology

Dr. Viren Kumar
GE Energy Service Engineering
Atlanta, GA

Dr. Zhimin Liu
School of Aerospace Engineering
Georgia Institute of Technology

Date Approved: March,28,2008

Writing a book is an adventure; to begin with it is a toy and an amusement, then it becomes a master, and then it becomes a tyrant; and … just as you are about to be reconciled to your servitude – you kill the monster and fling him … to the public.

- Winston Churchill

To my Parents and Laura

ACKNOWLEDGEMENTS

There are many people throughout my time here at Georgia Tech that have helped me though my Doctorate, I can but acknowledge a few herein. I would like to start by thanking my advisor, Professor Dimitri Mavris for the opportunities, encouragement and support he has provided through his excellent program here at the Aerospace Systems Design Laboratory. It was he that persuaded me to come to Atlanta, the first time I ever set foot on US soil was to attend the first day of classes here back in 2002, and without him my doctoral experience would not have been possible. I am pleased to extend my thanks to Professor Vitali Volovoi, Dr. Zhimin Liu and Mr. Russell Denney for their help and encouragement throughout the five years of working on the NASA/DoD URETI UAPT projects that lead in some part to the focus of this research work. Additionally, I would like to thank the last member of my committee, Dr. Virendra Kumar of GE Energy, who though entered my committee later provided some very useful insight and direction at the critical moments. Beyond the members of my committee, I would like to thank Dr. Jimmy Tai, Dr. Michelle Kirby and Mr. Mike Ward for their help along the thesis process with issues, from modeling to analysis.

Throughout my tenure here at Georgia Tech, I have had the support and encouragement of many friends of varied backgrounds, whether it be from within ASDL, Georgia Tech itself or the wider Atlanta community through my

work with the local field hockey clubs, for that I would like to thank you all. I have many fond memories, be it the days and nights spent at the "Golden Pheasant" thanks in part to Mr. Richard Neal, or days fishing with Mr. Henry Won and others in the backwoods of Georgia.

All those along my educational journey, I would like to extend my deepest gratitude. It is those grades and experiences that brought me up to this point in my life. Additionally I would like to thank the Royal Air Force selection officer, for asking what I thought I was doing trying to be an engineer with the quality of degree I had, instead I should follow the plan that eventually lead me here to Atlanta. A situation I would not have been in had Dr Simon Ritchie not told me of the opportunities across the pond, where would I be now without that?

I would like to extend my thanks to my family around the world that have given me their support on either side of the Atlantic. These thanks especially goes to my parents that have over the years helped to provide me with the schooling for me to overcome my Dyslexia, leading to my seeking of a doctoral degree here at Georgia Tech.

Finally I would like to thank a woman who I hold dear to my heart, my fiancée Dr. Laura Draucker. We met over three years ago playing field hockey, and through thick and thin she has been there for me. Her patience and support has helped me through this process, and has never faltered. I look forward to spending the rest of my life with you.

TABLE OF CONTENTS

	Page
ACKNOWLEDGEMENTS	v
LIST OF TABLES	xii
LIST OF FIGURES	xiii
NOMENCLATURE	xix
SUMMARY	xxii
1. INTRODUCTION	1
1.1 Motivating interest	1
1.1.2 Changes in Market Practices	5
1.1.3 Expanding Market	9
1.1.4 Research and Development Costs	11
1.2 Design for Life	15
1.3 Current Lifing Design Approach	18
1.3.1 Early/Conceptual Design	20
1.3.2 Preliminary Design	22
1.3.3 Detailed Design	22
1.3.4 Current Approach Drawbacks	25
1.4 Area for Consideration	26
1.4.1 Fan	29
1.4.2 Compressor	32
1.4.3 Combustor	35
1.4.4 Turbine	37

1.4.5 Selection of Research Focus 38
1.5 Inherent Problems 40
1.5.1 Aero-Thermal 42
1.5.2 Materials 44
1.5.3 Integration 45
1.5.4 Common Failure Modes 46
1.6 Identified Need 51
1.6.1 Intended Implementation 54
2. RESEARCH QUESTIONS & HYPOTHESES 57
3. FORMULATION 62
3.1 Modeling and Simulation Requirements 64
3.2 Analysis & Modeling Environment 72
3.2.1 Phoenix Integration Model Center ™ 72
3.2.2 Pacelab Suite 75
3.2.3 Modeling and Integration Tool Selection 78
3.2 Appropriate Fidelity Engine Modeling 79
3.3.1 Numerical Propulsion System Simulation (NPSS) 81
3.3.2 NASA/GE E^3 Engine Model 82
3.3.3 NASA WATE ++ 85
3.3.4 Velocity Triangle Analysis 91
3.3.5 Meanline Loss Model 95
3.3.6 Blade Cooling Consideration 106
3.3.7 Materials Modeling 116
3.3.8 Heat Transfer Analysis 120

3.3.8.1 Low Fidelity Thermal Analysis 121
3.3.9 Stress Analysis 126
3.3.9.1 Gas Bending Stress 127
3.3.9.2 Centrifugal Stress 129
3.3.9.3 Thermal Stress 130
3.3.9.4 Stress Combination 133
3.3.10 Blade Geometry Generation 135
3.4 Final Analysis Environment 139
3.5 Modeling and Simulation Requirements 144
3.6 Surrogate Modeling 145
3.6.1 Design of Experiments 147
3.6.1.1 Types of DoE Methods 148
3.6.2 Response Surface Methods 149
3.6.2.1 Definitions of Model Tests 151
3.6.2.2 How to Create an RSE 152
3.6.3 Neural Networks 154
3.6.4 Kriging 162
3.7 Surrogate Modeling Implementation Considerations 165
3.8 Analysis Environment Modeling and Visualization 169
4. COMPUTATIONAL EXPERIMENTS & RESULTS 175
4.1 Turbine and Blade Study 176
4.1.1 Design Variable Selection 177
4.1.2 Design Response Selection 182
4.1.3 Turbine and Blade Design Study Results 185

4.2 System & Materials Study 206
4.2.1 Design Variable Selection 207
4.2.2 Model Response Selection 211
4.2.3 Second Model Results 212
4.3 Design Space Exploration 221
4.3.1 Sensitivity Analysis 222
4.3.1.1 Turbine Stage and Blade Design Study Analysis 222
4.3.1.2 System and Material Study Analysis 227
4.3.2 Multivariate Analysis 231
4.3.2.1 Turbine and Blade Study 238
4.3.2.2 System and Material Study 240
5. CONCLUSION 245
5.1 Review of Research Questions and Hypotheses 245
5.2 Overall Benefits of Approach 252
5.3 Summary of Contributions 258
5.4 Recommendations for Future Research 259
APPENDIX A: EDUCATIONAL REPORT 262
A1. Parametric Physics Based Design Environment 263
A1.2 Analysis Environment User Information 267
A2. Computer Usage 272
APPENDIX B: ANALYSES OF PARTICULAR NOTE 273
B1. Loss Model NPSS Code 273
B2. Stress Code (NPSS version) 288
B3. Velocity Triangle Model (from Schobeiri) 298

APPENDIX C: MATERIAL DATABASE METALLIC COMPOSITIONS 311

REFERENCES 313

VITA 324

LIST OF TABLES

Page

Table 1: Selection of analysis integration environment 78

Table 2: Nominal chemical composition ranges of Nickel based Super-alloys 119

Table 3: Ranges for eleven design variables included in the Design of Experiments. 181

Table 4: Initial model fixed variables. 182

Table 5: Initial model Neural Net Settings 187

Table 6: Summary of initial model fit. 188

Table 7: Comparison of metallic composition of materials 1 and 14 195

Table 8: Continued comparison of composition for materials 1 and 14 195

Table 9: Ranges for eight design variables included in the Design of Experiments. 211

Table 10: Neural Net settings for system and material experiment. 213

Table 11: Second experiment simulation fitting history. 213

Table 12: Error report for second experiment responses 214

Table 13: Turbine and blade design model preferred values. 253

Table 14: Comparison of inputs for current and possible previous approach 255

Table 15: Summary of comparison of results for second design study, for both conceptual approaches 257

Table 16: Nickel superalloy properties utilized within thesis, part 1. 311

Table 17: Nickel superalloy compositions utilized within this thesis, part 2. 312

Table 18: Glossary of chemical compounds within metal compositions. 312

LIST OF FIGURES

Page

Figure 1: Sir Frank Whittles Patent Drawings 1

Figure 2: Rolls Royce Trent 1000 2

Figure 3: General Electric CFM-GE-CFM56-5C2 *(Flight International)* 3

Figure 4: Rolls-Royce gas turbine engine sales for year 2003 4

Figure 5: Rolls Royce total market prediction - 2003 *(After Singh)* 5

Figure 6: Rolls Royce balanced business portfolio 2006 *(CitiGroup)* 9

Figure 7: Civil market opportunity over next 20 years *(Rolls Royce)* 10

Figure 8: Rolls Royce investment in R&D, 1997 – 2006 *(Rolls-Royce)* 11

Figure 9: Turbine blade cooling technology comparison 14

Figure 10: Typical Design Process *(After Dieter)* 19

Figure 11: Typical design process breakdown 19

Figure 12: Visual representation of FEA and CFD results for a notional turbine blade. (*Ansys*) 23

Figure 13: Notional turbine detailed design process. 24

Figure 14: Gas turbine system breakdown. (*ASDL)* 28

Figure 15: Aero engine breakdown with temperature and pressure information. *(Rolls-Royce)* 29

Figure 16: GE 90 fan blade. *(Museum of Modern Art)* 31

Figure 17: Centrifugal Compressor 33

Figure 18: Diagrammatic representation of axial-flow turbine 34

Figure 19: Ideal Brayton cycle schematic 35

Figure 20: Notional turbine stage. (*After Mattingly*) 38

Figure 21: Notional HPT stage with film cooling 42

Figure 22: Development of Turbine Entry Temperatures (TeT) with time. *(After Spittle)* 44

Figure 23: Specific strength versus temperature for a variety of common aero engine metals. *(After Spittle)* 45

Figure 24: Notional creep behavior 47

Figure 25: The result of 2500 hour low altitude sea flight service on an uncoated and NiAl coated blade turbine blade 49

Figure 26: Schematic summary of the need 54

Figure 27: Summary of intended overall process 63

Figure 28: Morphological matrix of analysis alternatives 65

Figure 29: Pictorial representation of analysis level needs 66

Figure 30: Desired analysis consideration 67

Figure 31: System level modeling requirements 69

Figure 32: Requirements for consideration of part level influences on blade creep life 71

Figure 33: Example of Phoenix Integration Model Center Model. *(ASDL)* 74

Figure 35: Example PaceSuite Layout 76

Figure 36: Schematic Diagram of Baseline NPSS E^3 Model 84

Figure 37: Comparison of WATE ++ Model to E^3 FPS 85

Figure 38: Disk life flow chart. (*After Tong et al)* 86

Figure 39: Disk/Blade Assembly. *(After Tong et al)* 87

Figure 40: Notional Disk breakdown. (*After Tong et al)* 88

Figure 41: Stress Reference Frame 90

Figure 42: Representative axial turbine stage. *(after Schobeiri)* 92

Figure 43: Axial turbine stage velocity triangles. *(after Schobeiri)* 92

Figure 44: Profile loss correlation of Ainley and Mathieson. *(After Jepikse)* 98

Figure 45: Empirical Relation for *f*. *(after Cohen)* 102

Figure 46: Trailing edge thickness correction factor. *(after Cohen)* 103

Figure 47: COOLIT cooling configurations. *(NASA)* 113

Figure 48: Materials Classification Chart (Strength against Density). *(After Ashby)* 117

Figure 49: Notional turbine blade heat transfer problem 120

Figure 50: Simplified 1-d turbine blade aerofoil model. *(NASA)* 122

Figure 51: Notional heat transfer model 124

Figure 52: Representative cooled turbine blade 130

Figure 53: Tresca Yield Envelope. *(after McGuire)* 134

Figure 54: Von Mises Yield Envelope. *(after McGuire)* 135

Figure 55: Prichard's Eleven Parameters. *(after Prichard)* 137

Figure 56: Prichard's five key points and surface functions. *(after Prichard)* 137

Figure 57: Changes to Prichard's Geometry Model 138

Figure 58: Finalized turbine blade lifing approach 140

Figure 59: Simplified depiction of analysis model 141

Figure 60: Assembled creep lifing analysis approach 143

Figure 61: Requirements set through hypothesis six 145

Figure 62: Vertical offsets and perpendicular offsets 153

Figure 63: Neural Network Conceptual Diagram. *(after Johnson and Schutte)* 156

Figure 64: Hierarchical, surrogate modeling environment for systems-of-systems analysis 171

Figure 65: Notional multivariate approach. *(NASA/DoD URETI)* 173

Figure 66: Initial experiemt neural net graphical representation. 188

Figure 67: Discrete data handling model results for initial experiment. 189

Figure 68: Zoom on Discrete data handling and other Prediction Profiler highlights. 189

Figure 69: Turbine and blade design study interactive parametric trade-off environment 192

Figure 70: Creep life actual by predicted for initial experiment 193

Figure 71: Materials performance with respect to lifing. 194

Figure 72: Initial experiment flare angle actual by predicted 197

Figure 73: Initial experiment flare angle residual by predicted 198

Figure 74: Initial experiment swirl angle actual by predicted 199

Figure 75: Initial experiment swirl angle residual by predicted 200

Figure 76: Initial experiment actual by predicted for stage efficiency 201

Figure 77: Initial experiment stage efficiency residual by predicted 202

Figure 78: Consideration of the variation of the reaction 204

Figure 79: Consideration of the variation of the radius ratio 205

Figure 80: Second experiment lifing actual by predicted. 215

Figure 81: Second experiment AN^2 actual by predicted 215

Figure 82: Second experiment cooled efficiency actual by predicted 216

Figure 83: Second experiment life residual by predicted 217

Figure 84: Second experiment AN^2 residual by predicted 218

Figure 85: Second experiment cooled efficiency residual by predicted 218

Figure 86: System and materials experiment parametric interactive trade-off environment 220

Figure 87: Shortened Pareto Analysis for the first experiment creep lifing 223

Figure 88: Shortened model one stage efficiency Pareto analysis 224

Figure 89: Shortened initial model swirl angle Pareto analysis 225

Figure 90: Shortened initial experiment flare angle Pareto analysis 226

Figure 91: Second experiment creep life Pareto analysis. 227

Figure 92: Second experiment cooled efficiency Pareto analysis. 229

Figure 93: Second experiment AN^2 Pareto analysis 230

Figure 94: Monte-Carlo filtering example using results from the developed integrated environment 234

Figure 95: Model one simulator environment. 237

Figure 96: Initial model multivariate analysis environment pre filtering 238

Figure 97: Initial Model contour profiler results 239

Figure 98: System and material simulator environment 240

Figure 99: Model two multivariate environment 241

Figure 100: Model two lifing CDF with constraints 242

Figure 101: Surface representation of second model design space 244

Figure 102: Summary of H. 1 contributions 246

Figure 103: Summary of H. 2 contributions 247

Figure 104: Summary of H. 3 contributions 248

Figure 105: Summary of H. 4 contributions 249

Figure 106: Summary of H. 5 contributions 250

Figure 107: Summary of H. 6 contributions 251

Figure 108: Reminder of initial model results. 253

Figure 109: Reminder of second study results 256

Figure 110: Integrated turbine blade creep life analysis environment 264

Figure 111: Model Center ™ based design environment 268

Figure 112: Location of model inputs and outputs 269

Figure 113: Using the integrated DoE tools within Model Center™ 270

Figure 114: Model Center ™ DoE tool, design table input 271

Figure 115: Pareto plot for blade creep life from sample analysis 272

NOMENCLATURE

$	United States Dollars
£	Pound Sterling
N	Symbol
NASA	National Aeronautical and Space Administration
ASDL	Aerospace Systems Design Laboratory
NPSS	Numerical Propulsion System Simulation
URETI	University Research and Technology Institutes
UAPT	URETI on Aeropropulsion and Power Technology
WATE	Weight…
DoD	Department of Defense
GE	General Electric
RR	Rolls-Royce
DoE	Design of Experiments
RSM	Response Surface Methods
bn	Billion
USD	United States Dollar
GBP	Great British Pounds (Pounds Sterling)
RSE	Response Surface Equations
0/1/2/3D	1, 2 or 3 Dimensions
ANOVA	Analysis of Variance
Pr	Prandtl Number
Re	Reynolds Number

Nu	Nussult Number
k	Thermal Conductivity
h	Heat Transfer Coefficient
RPM	Revolutions per Minute
T_4	Turbine Inlet Temperature
W_2	Mass Flow Rate
TBC	Thermal Barrier Coating
AN^2	Disk Stress Factor
λ	Stage Loading
ν	Radius Ratio
φ	Flow Coefficient
μ	Velocity Ratio
α_3	Swirl Angle
t/c	Blade Thickness to Chord Ratio
CPF	Combustor Pattern Factor
r	Stage Reaction
AR	Aspect Ratio
s/c	Pitch to Chord Ratio
U_3	Perpendicular Rotor Exit Velocity
°R	Degree Rankine
°F	Degree Fahrenheit
°C	Degree Centigrade
HPT	High Pressure Turbine
LPT	Low Pressure Turbine

HPC	High Pressure Compressor
LPC	Low Pressure Compressor
Al	Aluminium
Ni	Nickel
Fe	Iron
Co	Cobalt
Cr	Chromium
Hf	Hafnium
CO_2	Carbon Dioxide
NO_x	Nitrogen Oxide
LCF	Low Cycle Fatigue
HCF	High Cycle Fatigue
LHC	Latin Hypercube
CCD	Central Composite Design
BBD	Box-Behnken Design
E^3	Energy Efficient Engine
σ_{GB}	Gas Bending Stress
σ_{CF}	Centrifugal Stress
σ_{TH}	Thermal Stress
FEA	Finite Element Analysis
CFD	Computational Fluid Dynamics

SUMMARY

The required useful service lives of gas turbine components and parts are naturally one of the major design constraints limiting the gas turbine design space. For example, the required service life of a turbine blade limits the firing temperature in the combustor, which in turn limits the performance of the gas turbine. For a cooled turbine blade, it also determines the necessary cooling flow, which has a strong impact on the turbine efficiency.

In most gas turbine design practices, the life prediction is only emphasized during or after the detailed design has been completed. Limited life prediction efforts have been made in the early design stages, but these efforts capture only a few of the necessary key factors, such as centrifugal stress. Furthermore, the early stage prediction methods are usually hard coded in the gas turbine system design tools and hidden from the system designer's view.

The common failure mechanisms affecting the service life, such as creep, fatigue and oxidation, are highly sensitive to the material temperatures and/or stresses. Calculation of these temperatures and stresses requires that the geometry, material properties, and operating conditions be known; information not typically available in early stages of design. Even without awareness of the errors, the resulting inaccuracy in the life prediction may mislead the system designers when examining a design space which is bounded indirectly by the

inaccurate required life constraints. Furthermore, because intensive creep lifing analysis is possible only towards the end of the design process, any errors or changes will cost the engine manufacturer significant money; money that could be saved if more comprehensive creep lifing predictions were possible in the early stages of design. A rapid, physics-based life prediction method could address this problem by enabling the system designer to investigate the design space more thoroughly and accurately. Although not meant as a final decision method, the realistic trends will help to reduce risk, by providing greater insight into the bounded space at an earlier stage of the design.

The method proposed by this thesis was developed by first identifying the missing pieces in the system conceptual design tools. Then, by bringing some key features from later stages of design and analysis forward through 0/1/2Ds dimensional modeling and simulation, the method allows estimation of the geometry, material selection, and the loading stemming from the operating conditions. Finally, after integration with a system design platform, the method provides a rapid and more complete way to allow system designers to better investigate the required life constraints. It also extracts the creep life as a system level metric to allow the designers to see the impact of their design decisions on life. The method was first applied to a cooled gas turbine blade and could be further developed for other critical parts. These new developments are integrated to allow the system designers to better capture the blade creep life as well as its impact on the overall design.

CHAPTER 1

INTRODUCTION

1.1 Motivating interest

The gas turbine engine has progressed significantly since its inception under Sir Frank Whittle in the early 1930's. The engine portrayed in his patent at that time consisted of a 2 stage axial compressor, followed by an axial cannular combustor with fuel nozzles and a single stage axial turbine as shown in Figure 1 [1].

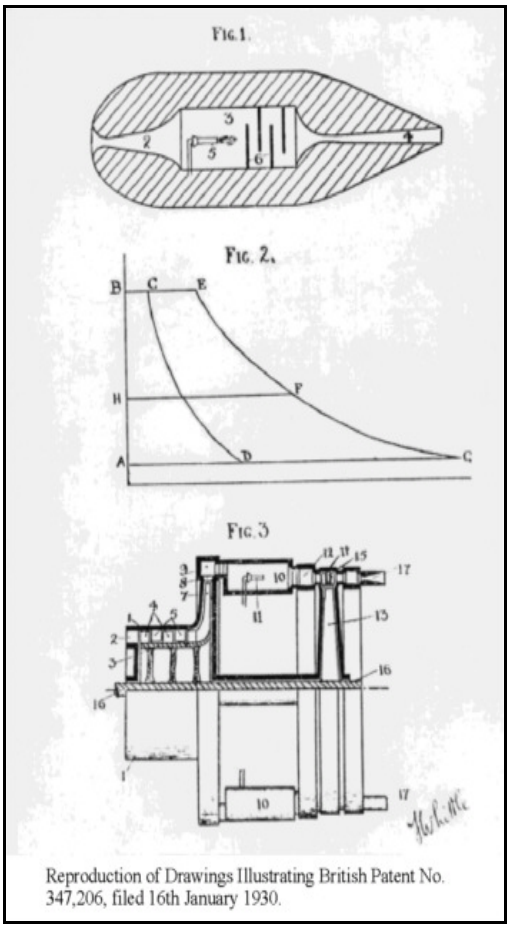

Figure 1: Sir Frank Whittles Patent Drawings.[2]

It has been said that the gas turbine engine is considered one of the most complex pieces of machinery available. Civil aviation engines, such as the Rolls Royce Trent 1000 in Figure 2, consists of several stages of low and high pressure turbines and compressors, fans, and the very latest in combustor technology. These technologies hope to achieve the best propulsive efficiency and thrust, whilst remaining within the limits placed by noise and other regulations. These limits need to be considered whist a gas turbine engine design progresses.

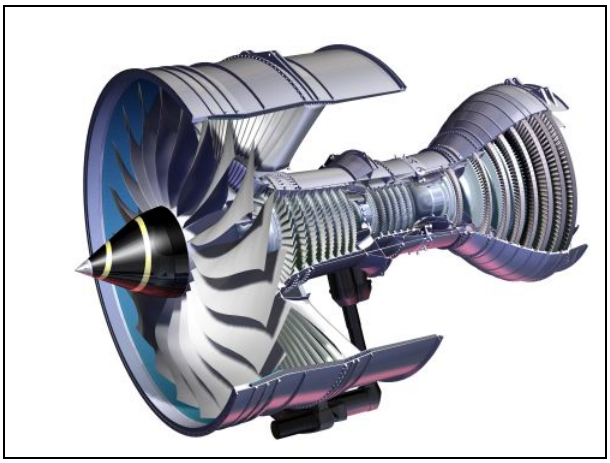

Figure 2: Rolls Royce Trent 1000. [3]

Developing an engine of the complexity illustrated in Figure 3 requires copious investment, material and facilities. Therefore companies involved in engine development are generally of considerable size, and often carry a diverse portfolio of uses for their engines. Spreading the engine's use provides greater market opportunities for the manufacture's to ensure a return on research investment, similar to that expected through the development of derivative aircraft by civil aircraft manufacturers.

The cost involved in the engine development process greatly precludes the mass manufacturing cost-reduction benefits other industries see. The number of engine manufacturers has increased over recent years, however, there are still only 3 main players: the two North American conglomerates General Electric and Pratt and Whitney, and the British conglomerate Rolls-Royce. The newer smaller companies concentrate on the smaller engines, leaving development of the big civilian engines to the previously mentioned three companies.

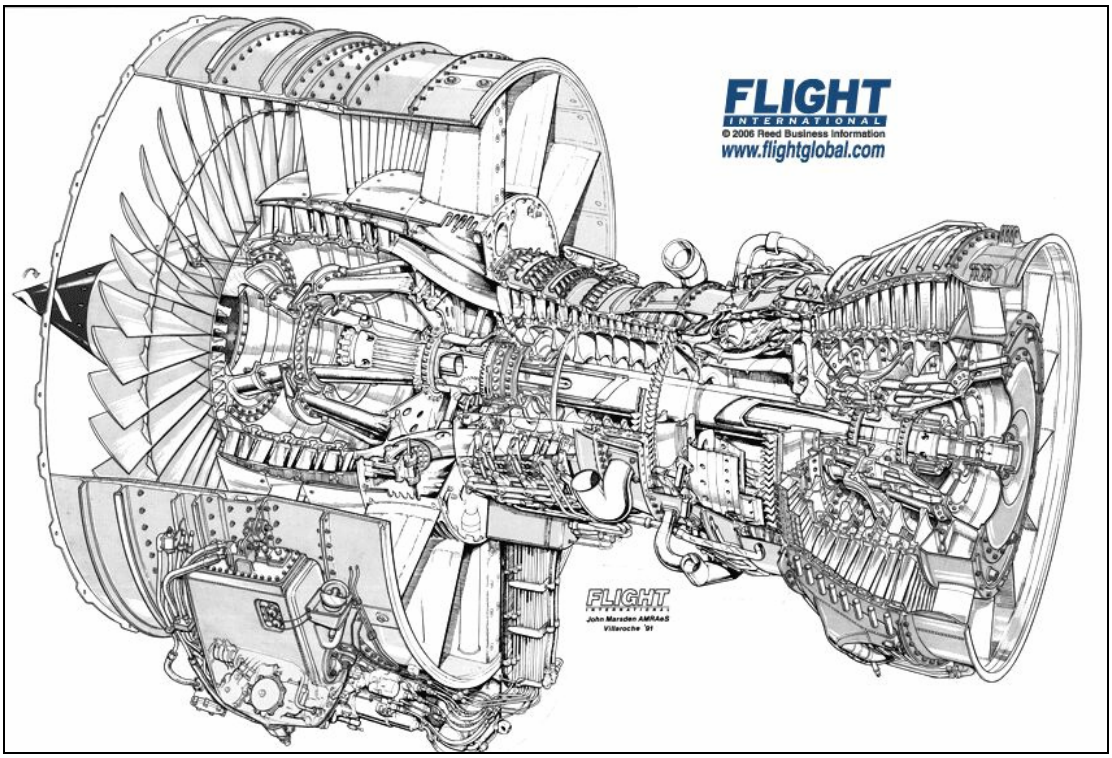

Figure 3: General Electric CFM-GE-CFM56-5C2 *(Flight International)*

The civilian engine market, i.e. engines fitted to civilian aircraft, is the largest original equipment sales market for engine manufacturers. The graph in Figure 4 illustrates this with sales figures from Rolls-Royce for their 2003

financial year; 48% of the 11.2 billion dollar total was for civilian engines. Similar figures are found for financial years up to the present and for differing manufacturers [4]. GE Aircraft engines provides data suggesting in 2006 $13.6 billion in total sales [5].

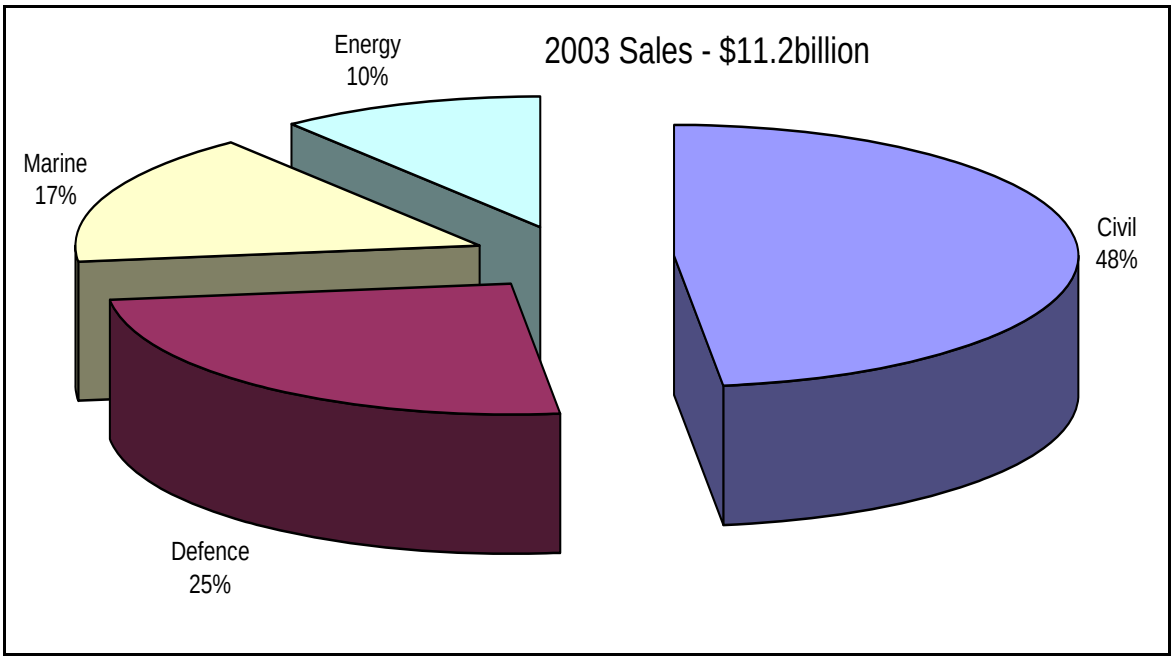

Figure 4: Rolls-Royce gas turbine engine sales for year 2003

Therefore, considering the information above, one might consider the civilian sector the most dynamic; prone to the effects of competition and having the most privately funded research input. The defense sector is often heavily subsidized through government inputs [6, 7], and the marine and energy sectors together only have half the market of the civil sector and often feed off their developments. Considering all this, it seems most pertinent to look into engines in the civilian sector for possible improvement work.

1.1.2 Changes in Market Practices

Research shows that not only does the civil engine sector drive the research and development activities of a company but it can also drive its business practices. Until recently, the aircraft engine industry was generally split into development/manufacture (depicted as original equipment sales in Figure 5 [8]) and after sales service (depicted as maintenance repair and overhaul in the same figure). The maintenance repair and overhaul industry until recently was being led by 3rd party manufacturers. Because of this, both the engine maintenance and after market parts were significant market opportunities being missed by engine manufacturers.

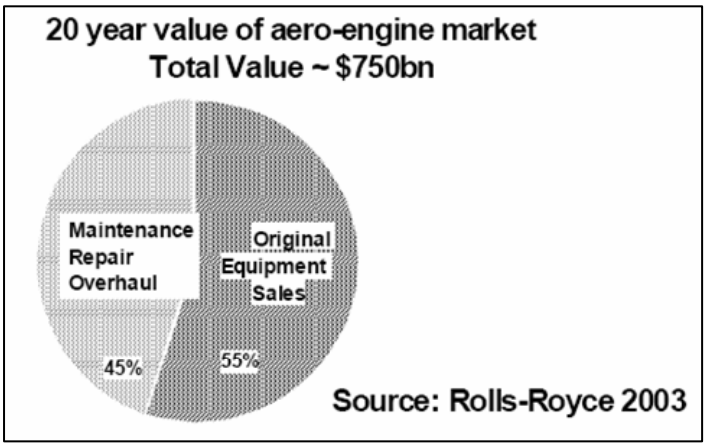

Figure 5: Rolls Royce total market prediction - 2003**.** *(After Singh)*

Companies came to realize that they were loosing business to third party component manufacturers and service and overhaul companies. Once the engines had been sold to the airlines and aircraft leasers, the manufacturers were seeing little return. In order to save money on engine maintenance, airlines often

sourced their spare parts from third party manufacturers which not only took useful income away from the engine manufacturers in the form of spare parts, but failures in the lower grade products tainted the reputation of their products. Thus engine manufactures began looking for new ways to improve sales practices and after-market maintenance.

The move away from traditional sales practices was not only based on the will of the engine manufacturers. Low cost airlines began looking for ways to reduce unanticipated costs and overheads that self-maintenance created. Practices at the time had the airlines carrying out their own non-critical engine maintenance, sending the engines to the manufacturers only for major offline servicing. With the competition in the airline market driving companies to lower overheads, so came the move to finding better practices.

Engine companies sensed this desire for change in the market and developed service packages which offered the operator (typically the airlines) "power by the hour". Such agreements span a 10 year period and involve the provision of comprehensive maintenance, at a set cost calculated on flying hours, as in the Rolls-Royce deal with Continental Airlines for the RB211 engines [9] . For the RB211 engine in particular, the London Stock Exchange press release for investors reported that with the addition of the service agreement in 2001, 60 percent of the RB211 engines operating on aircraft in the United States were by then operating under various Total Care ™ Support packages. [9]

The full range of services that Total Care™ packages typically offer is described in an article in the industry magazine Aviation Maintenance [10]. The packages are themselves individually tailored to each engine customer's needs [11]. However, the basics of the package are approximately the same, components of which include [10]:

- Off-wing maintenance
- Information and engine health monitoring
- In-service support
- Inventory management

All the above are provided by the engine manufacturer (Rolls-Royce), providing the operator the following added benefits to its business model [10]:

- More effective resource management
- Release from maintenance hassle
- Predictable cost, greater financial planning flexibility through agreed fix cost per hour
- Reduced financial risks, manufacturer absorbs unforeseen maintenance costs, fixed cost does not change
- Minimized operational disruption, spare engines provided under operations planning
- Reduced total operating cost for operator.

Thus, with the success of Total Care™, current aircraft engine manufacturers' business models have moved to include similar services, adding

significantly to the total profitability of engines over their lifetime. Of course, if the engine is built to last longer, the company would further improve profits by reducing maintenance costs. This suggests that considerations made now, whilst designing future engines, to limit the life cycle cost of the engine would maximize the return on these service plans and save considerable money. Life cycle cost as defined here is the expense of the system over its entire lifetime. Limiting maintenance cost and repair requirements will enable engine companies to increase their revenues.

The benefits of this current sales practice is shown in the model created for Rolls Royce by Citi Group for the 2006 financial year. This model, shown in Figure 6, compares all aspects of gas turbine applications from aviation to marine. Because of its success in the civilian industry, Rolls-Royce has begun expanding the aftermarket Total Care schemes to include the other markets for its engines. This includes offering packages to defense markets [12], as countries such as the United Kingdom look to reduce the size of their armed forces maintenance fleet in a post cold war era. These packages would continue even through a possible war with even more potential benefit to the customer; given that the engines involved are often for the flight trainers, the maintenance covered in the agreements can be carried out away from the theatre of operations, greatly reducing the risk to the engine companies' employees and business assets.

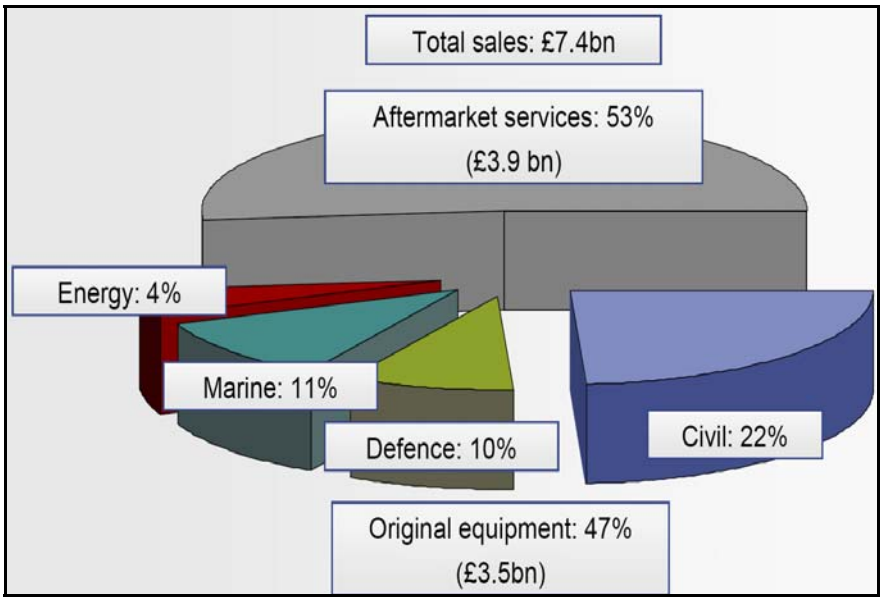

Figure 6: Rolls Royce balanced business portfolio 2006. *(CitiGroup)*

1.1.3 Expanding Market

Even without the increased profitability due to aftermarket maintenance, civil engine manufacturers have predicted continued market growth over the next 20 years, as shown in Figure 7. This market outlook for major companies such as Rolls Royce and General Electric puts large civil engines as the leading share in the original equipment portfolio.

The massive predicted growth provides a large incentive for companies to increase their market share. The best method of increasing one's market share is to provide a superior or equal product or service. Thus, the quest for technological superiority is a high priority for the firms in the aircraft engine sector.

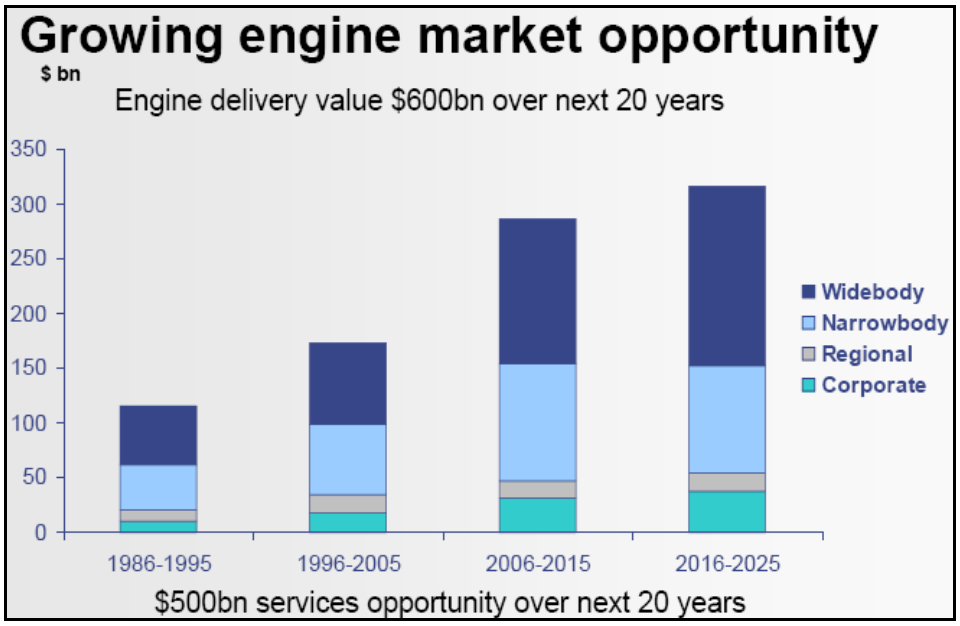

Figure 7: Civil market opportunity over next 20 years. *(Rolls Royce)*

Concurrently, the investment cost involved in designing a new engine in the large aero engine market is currently between $500 million - 2500 million (United States Dollars, USD)), profits of which are only seen after some 15 to 25 years.[8] Thus, the money necessary to advance expertise and investment is imperative as aero engine company's push to maintain their competitive edge in a rapidly growing market.

1.1.4 Research and Development Costs

Although important, investment in equipment alone is not enough to remain a leader in this market; therefore, a large amount of money is also placed in research and development. The overall yearly research and development investment of Rolls Royce is illustrated below in Figure 8 (the values being in Pounds Sterling (GBP)) along with their supported family of gas turbines. This figure shows how significant investments in expertise are, and how valued this expertise is to an engine development company. R&D investment is further put into context when one considers that in 2006 overall company sales were £546m with only £18m received as profit [13].

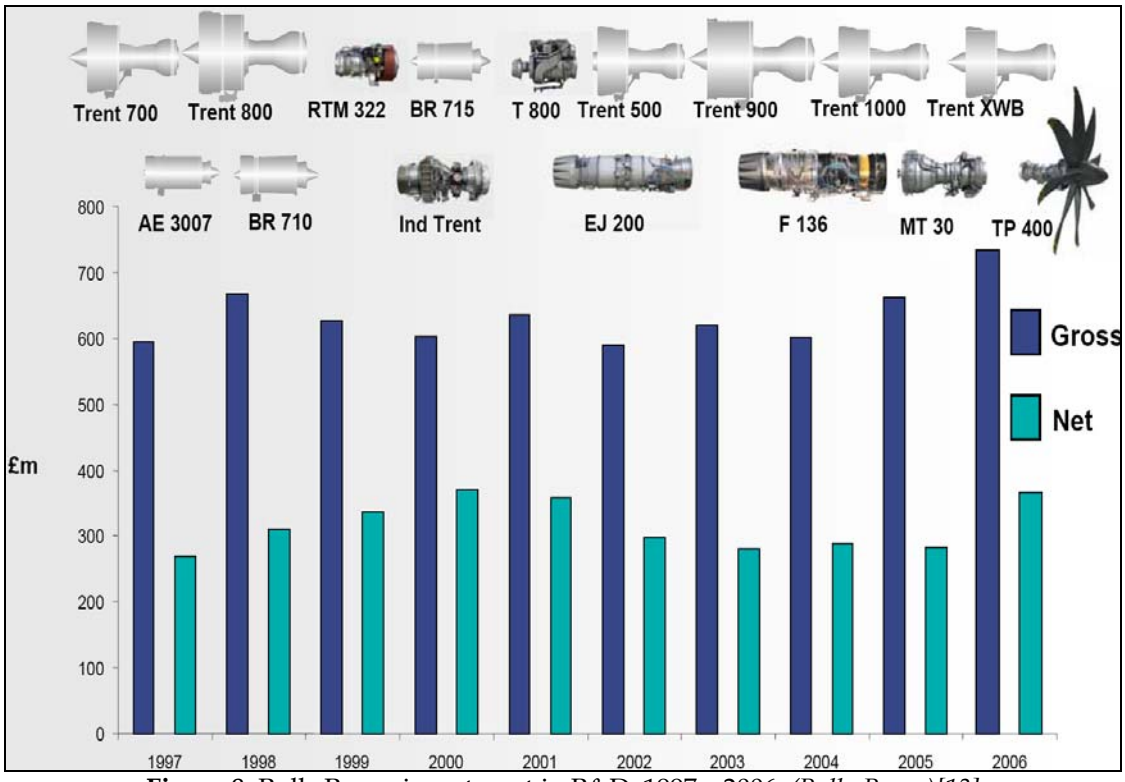

Figure 8: Rolls Royce investment in R&D, 1997 – 2006. *(Rolls-Royce)[13]*

Whilst companies are seeing some profit, a push for improved engine performance, efficiencies and cost reductions are required to maintain a competitive/technical edge. As current technical boundaries are reached and smaller companies begin to emerge, the demands on engine designers as well as increasing research costs will create difficulties for large, established companies. Therefore, reducing the sunk cost of R&D while improving engine design would be an attractive asset to a company, and often even the smallest changes may help in the long term. Modern techniques in complex system design suggest that the best method for achieving maximum return with minimal expenditure utilizes an integrated approach. An integrated approach considers the full life cycle of the engine, which in turn optimizes the engine for its given operating conditions and customer desires.

In a bid to remain at the forefront of technological development as well as a technical expert to United States industry, NASA identified the need for an improved design process within the civilian aero engine industry, in hopes of improving their market share, reducing time to market, and minimizing research costs [14]. This effort fell under the NASA/DOD University Research, Engineering and Technology Institutes (URETI) on Aeropropulsion and Power Technology (UAPT) initiative, designed to help improve overall engine performance and economics. Areas of interest included, but were not limited to,

high temperature materials, advancing turbine analysis techniques, and improving the overall engine design and analysis process. The latter interest called for the impact assessment of engine component technologies from the micro to system levels. [14]

Looking into these technologies to improve an engine, one needs to provide useful benchmarks from which comparisons can be made. If a superior product is going to be produced, analysis of the areas affected by the new product need to be considered. If this is not the case, significant money would be invested in designs that in the end prove to be impractical. A good example of the need for this type of analysis comes from determining the required service life of a turbine blade, which is limited by the exit temperature from the combustor and the material properties that in turn, limits the performance of the gas turbine. Ideally, the engine would operate at a high enough temperature to achieve the highest possible thrust rating [15], while at the same time maintaining an economic service life. This optimal operating temperature is a highly desirable design output, and consequently a good benchmark for future technology development, see equation one (based on Brayton cycle).

$$\text{Efficiency}, \eta = \frac{\text{net work output}}{\text{heat supplied}} = \frac{c_p\left(T_3 - T_4\right) - c_p\left(T_2 - T_1\right)}{c_p\left(T_3 - T_2\right)} \tag{1}$$

Currently, to address the issue of exit temperature, modern turbines utilize a cooled turbine blade to improve the possible rotor inlet temperature, and this necessary cooling flow has a strong impact on the turbine efficiency [16, 17]. By

improving cooling technology for a gas turbine blade it is possible to increase the combustor exit temperature sufficiently, therefore achieving good improvement in turbine efficiency and thrust [18]. Figure 9 shows the various cooling technology's ability to facilitate the increase in rotor inlet temperature.

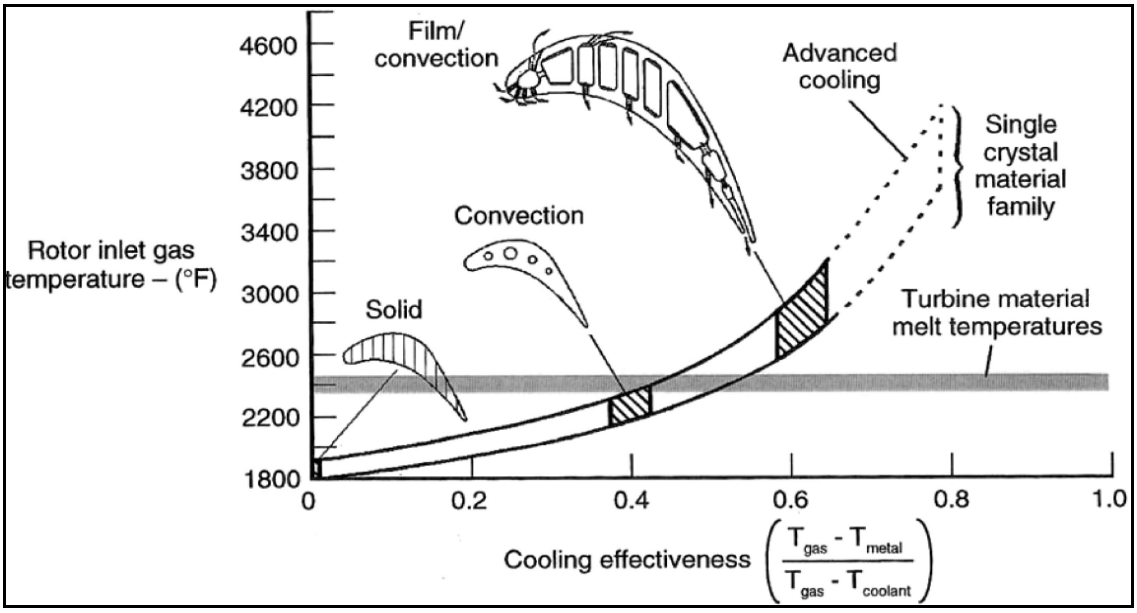

Figure 9: Turbine blade cooling technology comparison. [1]

However, this improvement does not prove viable when considering the complete process. The increase in cooling flow to the turbine blades and vanes takes bleed air away from the compressor, reducing its won efficiency. This detrimentally affects the efficiency of the whole system, such that the improvements in the turbine are eclipsed. Being able to track all these whilst looking at a particular component within an aircraft gas turbine, is obviously very desirable, especially at the early stages of a design. A successful design

process incorporates flexibility and freedom at the early conceptual stages and continuing as far into the design as possible, saving time and money in fixing problems that would have arisen had an investigation not taken place.

Looking into technologies to improve an engine, one needs to provide useful benchmarks from which comparisons can be made. If a superior product is going to be produced, analysis of the areas affected by the new product needs to be considered. If this is not the case a lot of money could be invested in designs that in the end prove to be impractical.

1.2 Design for Life

As previously discussed, the engine market has moved towards a service based business model which benefits both the manufacturer and the operator. To further capitalize on these benefits, the engine manufacturer needs to produce quality engines with a long useful life; but, how is the life of an engine characterized?

The length of useful service individual parts of a gas turbine engine provide is otherwise referred to as their part life or just life. This service life is often defined as the Mean Time Between Failure (MTBF) [19], with general maintenance scheduled around and to monitor this. The service lives of the many different parts of the engine vary primarily due to their location in the engine, role, and manufacture. Severe operating environments obviously shorten

the life of the part, through driving the more life critical parts to the high temperature or high stress type situations.

With Total Care™ type programs providing these scheduled maintenance intervals, a longer service interval is both beneficial to the manufacturer and airline alike. Therefore a full understanding of how one can control the service life is needed. We already explored the fact that the operating environment and manufacture really dictate the lifing issues that inherent with the components of the engine. But how are such problems accounted for or alleviated? How can one hope to extend the service life? First, it is necessary to identify what steps in the engine's life most affect its useful service; the design and the operation. There are several ways to extend an engine's life during these steps:

- Design
    - Design components to survive for a desired service life. This takes into account the perceived operating conditions, allowing designers to work with a design that best represents their final product.
    - The useful life left while the part is in service is also as important as how long a part will last. Designing a part so that should any problems arise during service, they are easily detectable and can be resolved without major damage.
- Operation

- In line with the design aspect, airlines can operate their aircraft such that the engines avoid exceptionally harsh operating regimes. Keeping conditions within the design limits, helps the parts to last for their designed service life.
- Flying in certain conditions also can have an adverse/beneficial effect on an engine.
- The operational side need not be considered as a purely airline problem. As the technology improves, engine control (also known as Full Authority Digital Electric Control (FADEC) [20]) systems evolve, which although are better they can still fail.

An example of adverse conditions effecting the life of an engine is the case of British Airways Flight 009 that flew through a cloud of volcanic ash from a recent eruption [21]. The ash clogged the engines which caused the flight crew to shutdown one engine and have trouble with the other. Flying through the cloud could have been avoided, but was thought not to pose a risk to the aircraft as a whole. Extreme events like these remind us that engine parts need to be reevaluated after participating in activities outside its design parameters. Conversely, engine control system failures are often the blame of the manufacturer, such as the early indications coming from the recent landing crash at Heathrow Airport [22]. This is only a short list of what to consider in the design and operation of an aircraft gas turbine engine, and considering all at once is beyond the scope of one tool. For this study, life determination focuses

only on the design stage of engine development; impact to the part life due to operational considerations is beyond the scope at this time.

1.3 Current Lifing Design Approach

The overall process and consideration of a design is very similar across the board in complex engineering systems. Asimow [23] and more recently Deiter [24] and others [25] [26] have set out the process, illustrated in Figure 10. The first step starts with full market development, whereby the manufacturer would determine the need for a new product or derivative of an existing design based on customer feedback and market trends, then moves through the initial conceptual design. With the initial stages of the design completed, a design team would then take the proposed product through the preliminary then detailed design stages to fully flesh out the design with a view to production. Although conceptual, the process as laid out does not specifically show how one would deal with the consideration of service life, especially pertaining to gas turbine engines. However, Dieter [24] does allude that these considerations need be included in design when he states: "*Quality cannot be built into a product unless it is designed into it [24]*

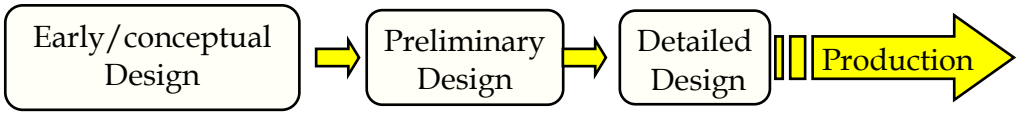

Figure 10: Typical Design Process. *(After Dieter)*

Treating service life as the quality that which Dieter speaks one can construe that such a consideration has been included in the current design methods. Looking now at how this design process is applied at the engine or part level, one needs to consider the previously described process at each stage for what it entails and requires in terms of component life consideration. A quick conclusion is drawn that this design conceptualization leads to the production and utilization of the whole engine. This leads to a more detailed design process, as shown in Figure 11. When designing an engine, several models and parameter considerations are needed throughout the process steps.

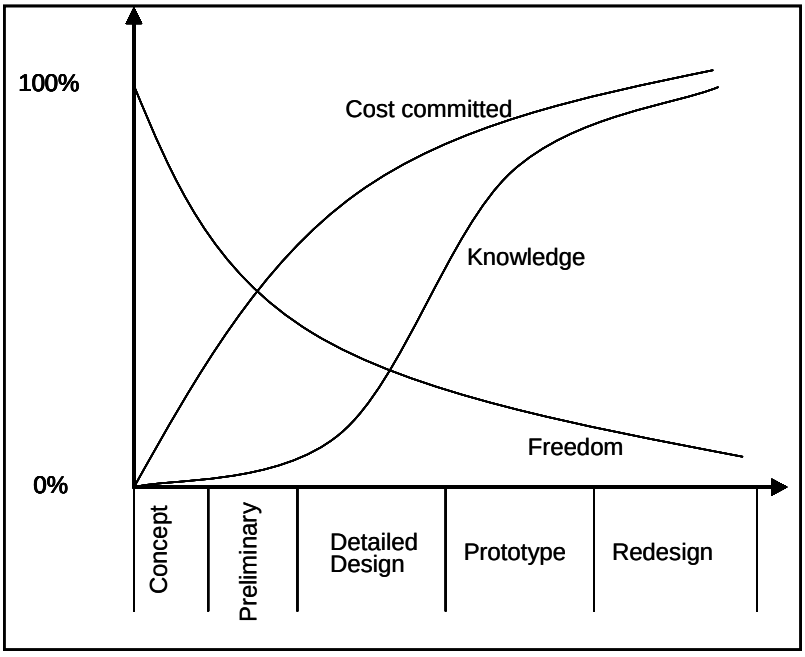

Figure 11: Typical design process breakdown.

1.3.1 Early/Conceptual Design

This is the earliest stage of the design process. During this stage, higher level considerations are made, working with desired engine thrust and other similar high level engine design factors, such as T_4 and stage efficiency. At the beginning of such a process there is a great deal of design freedom, working with requirements obtained from the aircraft manufacturers to thrash out the basis of the engine design.

Traditional low fidelity methods have been developed to model the engine at this stage to improve design. These methods employ mean-line or lower analysis to help the designer determine the designs end-goal and what is needed to achieve it. At this stage very little attention is paid to geometry of parts, other than that they are able to achieve the desired flow characteristics.

Looking into the life of the engine at this level is not particularly intuitive, and going into the required detail for the determination of a detailed part life prediction becomes futile. As previously discussed, the lifing of a component part of the engine is a complex affair depending very much on its failure mechanisms. Most often and most critically these are thermal, aerodynamic, centrifugal or a combination of the three. Determining these factors at this stage of design needs to be made using the least amount of detail to maintain the desired level of analysis and speed with which the analysis requires. At this early stage of design this really equates to understanding the physics of the problem,

through trends representing the behavior of the part life as other factors change. Further along the design process, those factors will be extensively studied, leading to a more accurate determination of part life.

The low fidelity methods enable fast trades when considering the higher level aero performance factors, but with the use of simplifying assumptions and bulk properties. These assumptions are then used with empirical relations and materials data to get the best indication of possible service life. Although fast, these relations can often restrict the design space due to narrowing assumptions behind them. Therefore, looking into new technologies at this stage usually requires going outside of these relationships.

These empirical relations have been developed over years of testing. These relate everything from blade section modulus and blade camber angle to turbine temperature drop and flow coefficient, and are often published within widely accepted books such as Cohen and Rodgers [27]. Utilizing these, especially when they are computerized, can produce rapidly generated results that provide a good indication of the performance of the design, both in terms of aerodynamics and service life. However, when using these relations it is important not to exceed their useful ranges or violate their assumptions.

1.3.2 Preliminary Design

In a typical design process, once the high level systems design has been chosen which skeletonizes an engine, a more complete process can begin. During this phase of the process more thought is put in to the geometry and flow of the engine, expanding the mean-line type analysis carried out previously. Dieter suggests that in this design phase decisions are made on strength, material selection, size shape and spatial capability. [24]

As more and more of the systems are fixed, the committed cost of the engine increases (see Figure 11). In addition, whilst the designers fix these factors, their knowledge of the design increases as more precise analysis and testing is brought to bear. All this goes on to help improve the design knowledge, most often based around improved information on the product and process that the earlier decisions and current analysis have enabled. As with this whole process, rethinking of the design is able to occur as this improved analysis may bring up unforeseen problems with previous design decisions.

1.3.3 Detailed Design

As the design progresses, the work is passed along into the detailed design stage. As the name suggests, this is the most detailed of the service life considerations during the design process; progressing into this stage requires many decisions about the design to be fixed. As the knowledge of the produce and process increases, so does the cost committed to said project. As, this is the

most costly of the design stages, it is generally approached using complex analysis techniques. These techniques generally work on specific parts of the engine only, say consider just the combustion system, without too much interaction with the rest of the system.

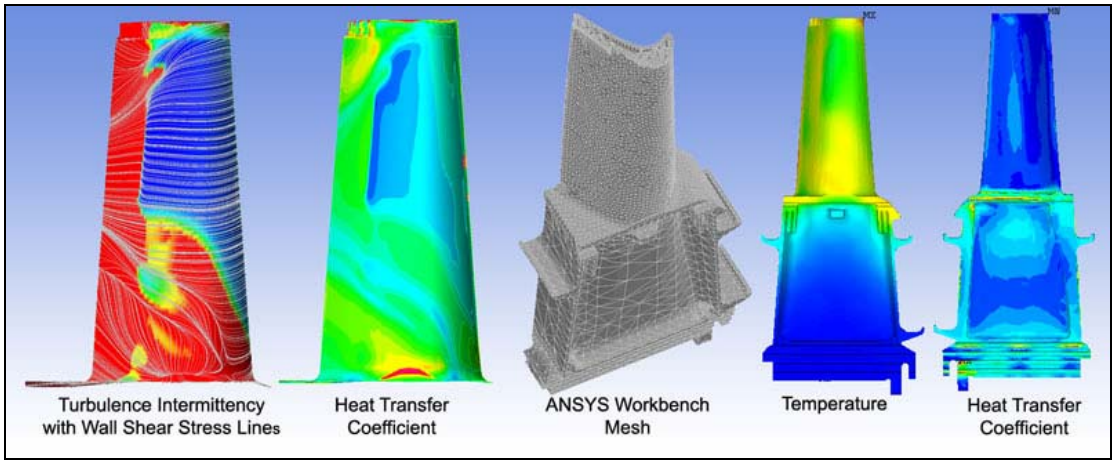

Figure 12: Visual representation of FEA and CFD results for a notional turbine blade. (*Ansys*)

The high fidelity analysis is carried out, utilizing Finite Element Analysis (FEA) and Computational Fluid Dynamics (CFD) as well as other methods, to provide the best simulation of a part or system in service. This work has been championed by Denton [28, 29] and others [30, 31]. An example of such work is provided in Figure 12 and a good review of current practices for CFD study of turbines is provided in Lynch [32]. Given the level of detail to which these methods can go they are obviously the most time consuming. In fact, when looking at the complex fluid flows inside the turbine and especially when considering both the primary and secondary (cooling) flows, this analysis often

takes months to run on just one design case and is often limit to a single case due to this.

However, it is using these approaches that provide the most comprehensive lifing consideration. This is especially important for parts of the engine where the determination of service life can be most complex, such as the turbine where a combination of centrifugal and aerodynamic forces acts along with the flows thermal conditions to stress the moving blades. The approach required to analyze this is depicted in Figure 13, from this one can see the required level of detail needed and the fixing of the design that would have demanded.

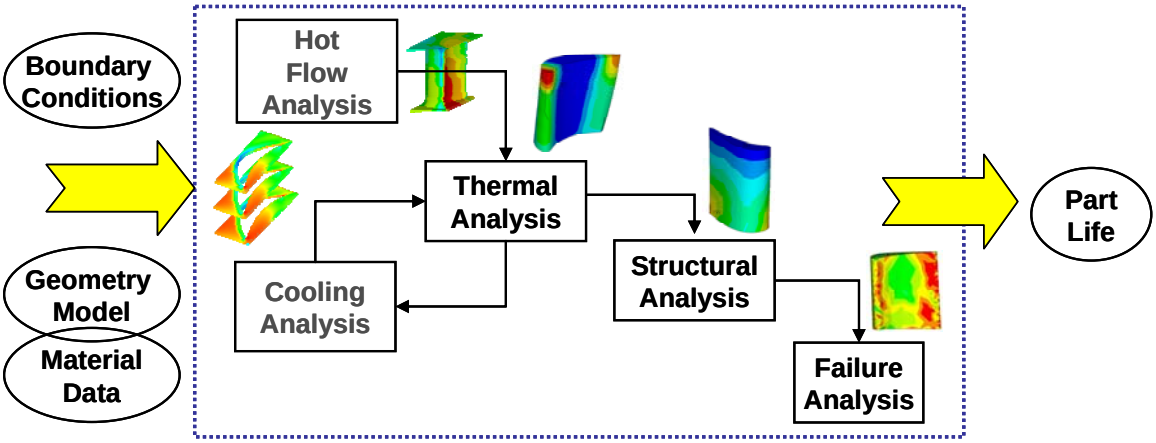

Figure 13: Notional turbine detailed design process.

Working at this detailed level captures the forces complex interactions, really helping with the detailed design of the parts and sometimes capturing even the smallest areas of concern. It goes without saying that any problems that this detailed analysis reveals in the design proves most costly to correct.

1.3.4 Current Approach Drawbacks

Previously it has been illustrated that current design methods tend only to provide comprehensive blade lifing consideration towards the end of the design process where detailed analysis could be used to provide a great level of certainty in any results. As the engine design progresses the lifing consideration progresses from empirical relations through to physics based considerations and on to detailed analysis. It is this work flow that currently limits the design freedom available as a design progresses. Thus, the further a design progresses into the more detailed analysis the more details that have already been fixed earlier in the process.

Furthermore at this the last stage in the process the design is most likely to only be checked to ensure that it meets a minimum life requirement. Full stress combinations are only considered as the level of fidelity increases, thus designs decisions are made conservatively. Additionally at this last stage in the process the designers are considering very limited numbers of design alternatives, such that should the intended design fail to meet these minimum criteria then a complete redesign is in order. Furthermore at this stage of the process little consideration is made between the part and system levels, all design considerations have been fixed and the concentration is on the part level.

What about trying to maximize the life? To consider such an idea one would need to understand the whole design space, not just the solution to the requirements. Current designs based on minimum lifing decisions neglect the

extent of the design space, working from existing, safe, approaches to incrementally improve designs. However, we have seen that the current environment requires thinking outside the box to maintain a competitive edge, and to maintain the edge in a customer care age.

There is a great need to bring the full stress consideration forward so that lifing issues can be considered at the same time as system level factors. This would help to bring designs away from meeting a goal and move toward a process that enables the designer to explore the limits of what's actually possible. However, such a process needs to be able to look beyond current limits imposed by the empirical relations, which is not yet fully available at the conceptual design stage. Currently these relations are based around tests of current machinery and limited by the test ranges. Thus an approach that brought the physics forward would be desirable.

The early conceptual design stage is when system trades and mean-line modeling are the main concentration. There brings forward a need to combine these with an appropriately complete lifing consideration. But what is an appropriate lifing consideration? How much of the engine should it involve, and what should it consider?

1.4 Area for Consideration

An engine can consist of many thousands of individual components. Consequently, attempting to gauge the service life of the engine based on all of

these components and parts would be beyond the scope of a conceptual rapid analysis approach. A simplified breakdown of an engine from the system through to the micro-scale level is provided in Figure 14. Looking at the micro-scale when considering the lifing of an aircraft engine is important, but the amount of variables needed would add significant detail and in turn negate the benefits (as previously mentioned) of a rapid analysis approach. Thus, stopping at the part level would enable the consideration of micro and meso-scale properties by grouping them under given material properties, as well as the system level considerations simultaneously. Thus a top down, bottom up methodology is brought to this approach, enabling the designer to consider a complete design space and providing the basis for an integrated conceptual design approach.

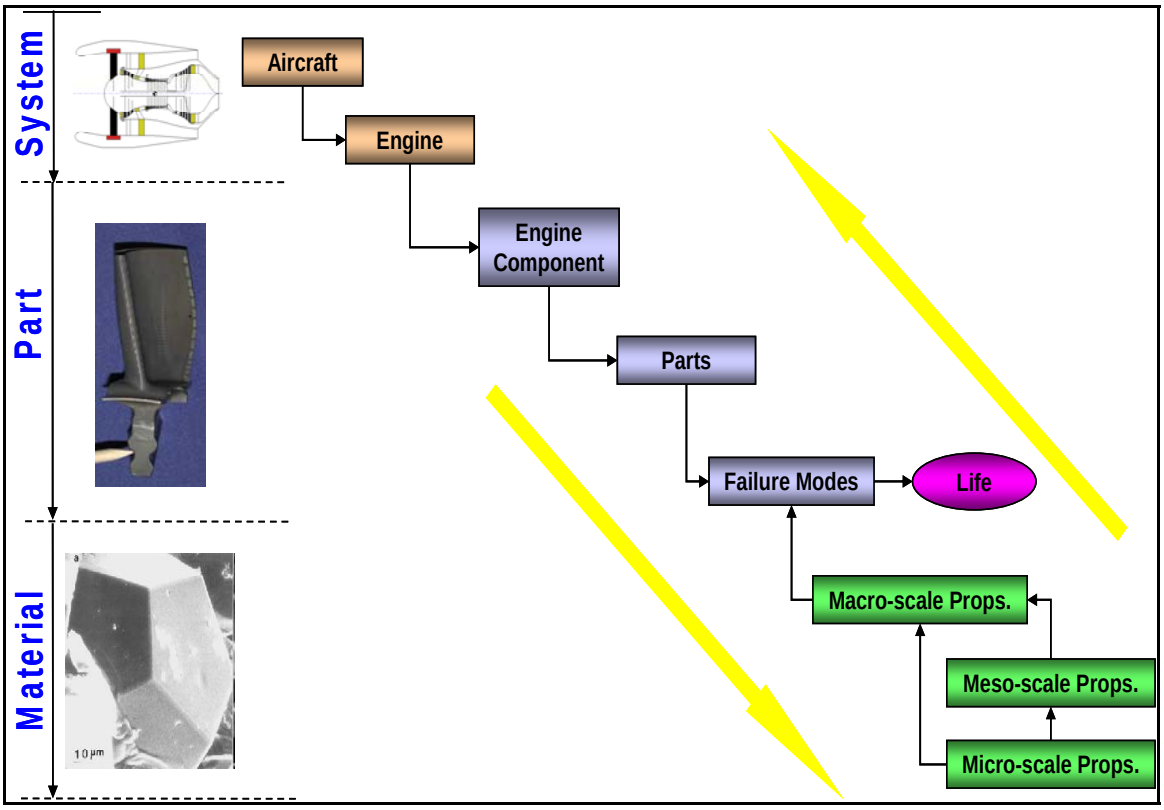

Figure 14: Gas turbine system breakdown. **(***ASDL)*

Now the question arises, what is the most life critical part of a gas turbine engine? Which part would benefit most from a design for life type approach which includes the ability to assess the possible impact of differing technologies? Answering this requires consideration of all parts individually, breaking the engine down its major parts and looking at their function (see Figure 15) and importance in a life critical prospective. These major parts will consist of either some or all the rotating or high temperature components. The list begins with the fan.

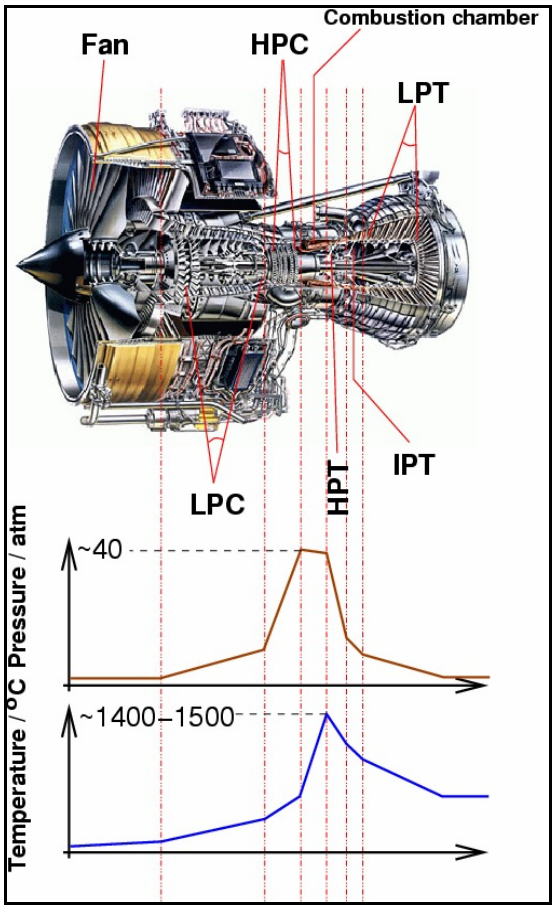

Figure 15: Aero engine breakdown with temperature and pressure information. *(Rolls-Royce)* [33]

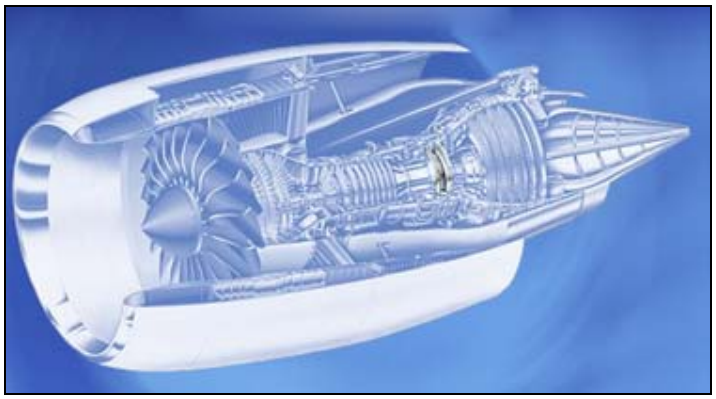

1.4.1 Fan

Working from the front of an engine, the fan is the first to be considered. This large component is in place to drastically increase the amount of air flowing

through the engine and thus increase the thrust produced. On the largest commercial aircraft engines these can be in the range of 10 feet in diameter (R-R Trent 900). Being this size, they can move a great amount of air both through the core and around it. It is this "bypass" air that drives the size of the fan, and the larger the diameter the better thrust for a given engine core which in turn improves its overall efficiency.

The size of these large fans for civilian engines is generally limited by the aerodynamics of the blades at the tips, and the ability of theses blades to cope with the great bending forces involved in moving so much air at such high speeds. Other than aerodynamic and centrifugal loads, the blades also have to be able to stand up to some Foreign Object Damage (F.O.D.). The blades themselves as you can see from the above picture have incredibly complex architectures, with their profile and twist changing almost along their entire span. The shapes are so complex that one has even found its way into the collection or the Museum of Modern Art in New York City. This GE fan blade is titanium tipped with a composite fiber resin core and a polyurethane coating.

Figure 16: GE 90 fan blade. *(Museum of Modern Art)*

Manufacturers use different materials to produce their blades. Rolls-Royce on the other hand has concentrated on purely titanium blades, while GE blades are fiber and polymer composites. The complex shapes of Rolls Royce blades are similar to those of the GE, but being all metal required the development of new manufacturing processes to minimize weight. The fan blades are formed through a process known as super plastic forming to produce a unique hollow blade. This technique enables a fifty percent weight saving over a solid alternative [3].

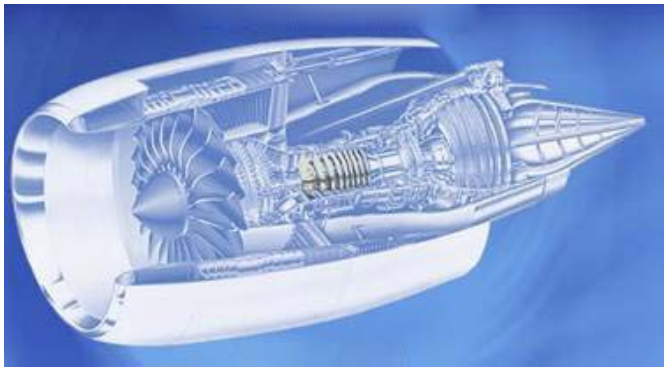

1.4.2 Compressor

Working our way through the engine, one tends next to consider the compressor (low pressure (LPC) and high pressure (HPC), see Figure 15). Consisting of many different stages, this part of the engine (as its name suggests) compresses the air in preparation for use in a combustion process, aiding the expansion within the turbine that helps to provide the thrust. The compressor comes in two forms, a centrifugal and an axial flow.

Early designs of gas turbine engine favored the centrifugal compressor, it is relatively easy to manufacture, robust and its use was better understood as it is widely used in superchargers. In fact the first engines developed by Sir Frank Whittle and Hans Von Ohain were based around this design. It is inherently more efficient and robust than the axial flow version, with no separate parts and no tip clearance losses. However the achievable compression ratio is limited, with few single stage centrifugal compressors able to achieve more than a compression ratio of greater than 10:1.

While this is not necessarily a problem for smaller engines, such as auxiliary power units, larger aircraft gas turbines need much more. Creating a 2 stage compressor goes some way to alleviate this, capable of raising the pressure ratio to 15:1. However these are still bulky and the large frontal area of the centrifugal compressor, out ways the efficiency gains that this type of compressor brings. Making these obsolete for aircraft engines really beyond the 1950's, once axial flow compressors had become more robust.

Figure 17: Centrifugal Compressor.

The most common form of compressor in aircraft gas turbine engines is the axial flow type. This version has been employed since the first production fighter aircraft (Messerschmitt, Me-262), and continue to be the favored form of

compressor for aero engine applications. One of the main benefits of this form of compressor is their smaller frontal profile when compared with the centrifugal design. Furthermore the axial-flow compressors produce a continuous flow of compressed air, and large mass flow capacity in relation to their frontal area. Several stages are required to achieve large pressure ratios [34], making them complex and expensive relative to centrifugal compressors.

The axial-flow compressor is split into two main parts, the disk and the blades (both rotational and stationary), see Figure 18. The disk as with other rotating disks is affects by issues with vibrational and centrifugal stress.

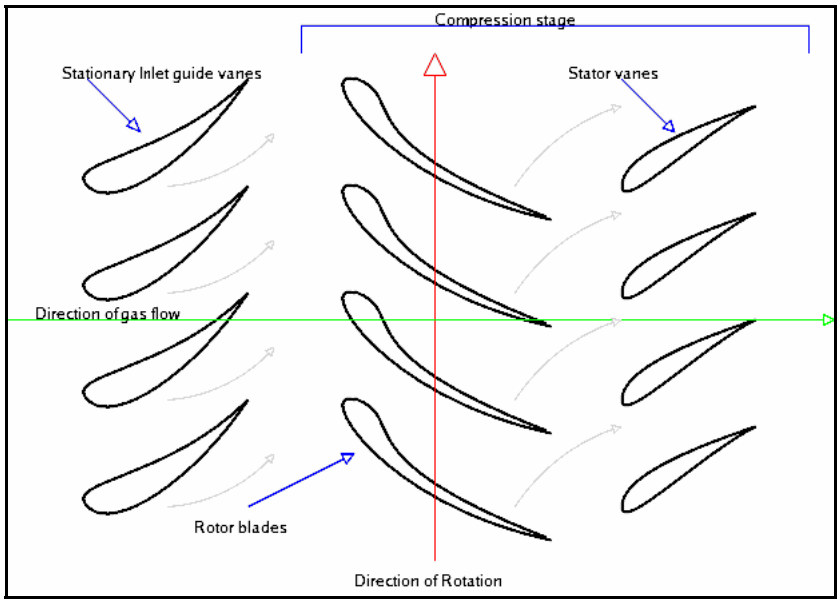

Figure 18: Diagrammatic representation of axial-flow turbine

Whereas the rotating blades are designed to withstand loading due to the aerodynamic forces on that force the air through the compressor blades. In

addition designers have to consider the centrifugal stress due to the high speed at which they rotate. A schematic representation of the use of the compressor in the ideal Brayton cycle is provided in the form of a temperature (T)/entropy (s) diagram, in Figure 19.

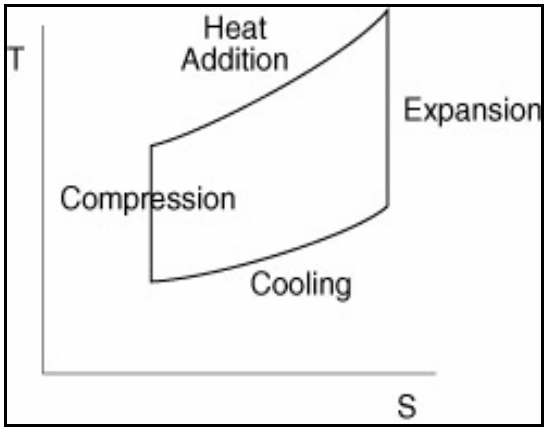

Figure 19: Ideal Brayton cycle schematic

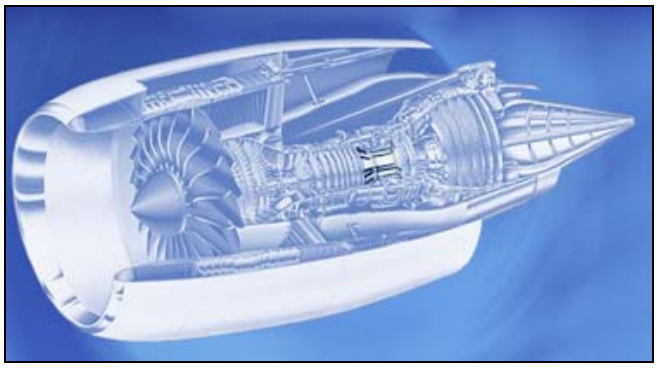

1.4.3 Combustor

The combustor (see Figure 15 and above) is one of the most important parts of a gas turbine engine. The combustion system provides the ability to burn a fuel/air mix to provide a hot gas flow, and thus the ability to extract useful

work from the flow. Most aircraft gas turbines burn liquid petroleum distillates but other forms of fuel can be used. To ensure the correct combustion of fuel/air mix whilst also ensuring that the combustor lasts for a suitable period of time is a necessarily complex design problem. This is currently being considered in a follow-up project based around the former NASA/DoD URETI UAPT [35] concerning the design of the combustor itself and the prediction of the emissions emanating from the combustion of the fuel/air mix within it.

It is a research desire to design combustors to produce the least amount of emissions while achieving a desired T_4 for the turbine. This T_4 obviously leads to the thrust outputted by the engine and its overall performance. These parts are often manufactured out of heat resistant alloys and now lined with ceramic liners to better improve the heat resistance of the combustors. All the 3 different types of combustor: Annular, Can and Can Annular; all require the use of complex shapes to aid the mixing of the fuel air combustion to achieve complete combustion, and therefore the lowest emissions.

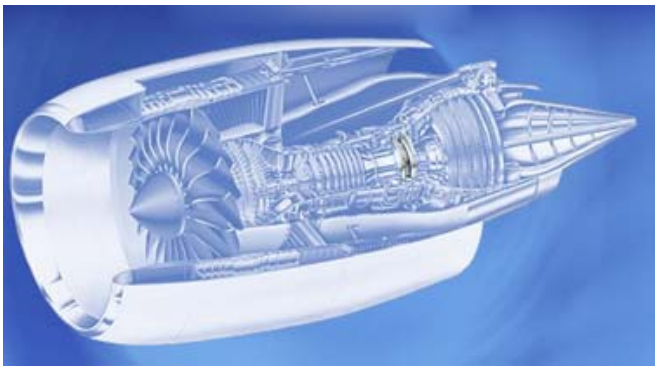

1.4.4 Turbine

The workhorse of the gas turbine engine is the turbine itself (both high pressure (HPT) and low pressure (LPT), see Figure 15 and above). The turbine extracts the energy from the flow to turn the compressor and fan. There are two types of turbines, radial and axial; however the axial is only suitable for the high temperature applications found in aircraft engines. Furthermore, axial turbines are more efficient for everything but the smallest of applications.[27]

The turbine consists of rows of rotors (rotating blades affixed to the disk) and stators (stationary blades attached to the outer casing of the engine). The most temperature critical part of the turbine is the high pressure side. The turbine is situated after the combustor and so experiences the highest temperatures as the flow enters the turbine post combustion. At this stage, complex cooling techniques are employed to keep the blades service life at a suitable level. These technologies include but are not limited to the use of Thermal Barrier Coatings (TBC) [36], and utilizing cooling bleed flows from the compressor through to the turbine blades [37].

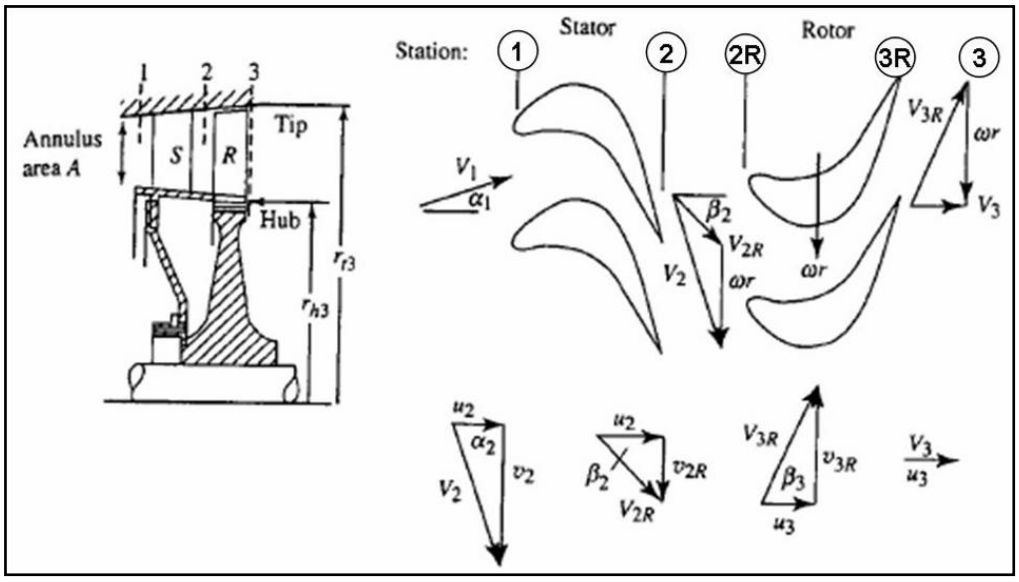

Figure 20: Notional turbine stage. (*After Mattingly*) [38]

The disk, is quite simply, what the turbine blades attach to and through which the torque is passed to the shaft. Various methods currently exist for the design of different types of turbine disk. The most promising lower fidelity methods include work by Tong et al as well as Melis and Zaretsky [39, 40]. All of these methods consider the disk at its most basic level to achieve the low fidelity analysis. However the method by Tong et al [41], considers the design of the disk at the same time as considering the design weight of the engine. This extra level of integration into the design process is what is desired at the early stage of the design process.

1.4.5 Selection of Research Focus

Considering all the above parts of a gas turbine engine, one can attest to how immense a full lifing consideration would be for an entire engine and its

components. Thus the decision needs to be made to narrow the scope of the research to a specific engine part. In doing this, one must consider the life criticality of the part, what research already exists, what analysis is already available, and how the parts overall importance effects operation of the engine.

This first step in this decision making process was to identify the parts that operate in the harsher environments within the engine, such as those involved during and after the fuel burn. Previous to the fuel burn, the compressor and fan operate in regions affected by vibrational and centrifugal/aerodynamic loads. These are important life considerations in their own right, but only focusing on these loads would omit other important parts of the aero engine. To best analyze the engine at the lowest fidelity one needs to consider a part where all the possible lifing factors come together. These would be thermal, centrifugal, aerodynamic and vibrational considerations. To combine these one needs to consider parts within the turbine, since this is the only section of the engine where parts can possibly operate with all those factors in play.

Thus the consideration is now narrowed to either the disk or blades within the turbine. It can be narrowed further into those parts within the HPT, since this part of the turbine experiences the highest operating temperatures. So what to study? Within the HPT one has to consider the disk. Failure of a disk due to improper life prediction during service causes the complete loss of the engine; if that failure is not contained, the aircraft is at risk. While not as safety

critical, the rotating blades have a greater affect on the general performance of the engine. Additionally, work to extend the life of a blade would be of economic benefit to the engine manufacturer in the current service centric business environment.

Thus, providing an approach by which the designer can consider the blade life along with the whole engine design would be highly advantageous. Consideration of the disk is currently available in some form through NASA codes, so combining this with a blade design approach would greatly expand the approaches possible application. However, such a blade design approach comes with some important considerations and possible stumbling blocks that need to be overcome.

1.5 Inherent Problems

When considering the turbine blade, one first has to understand the distinction between the rotating and stationary blades present within a turbine stage as both have different considerations when it comes to lifing. The rotating blades experience aerodynamic and centrifugal loads on top of the thermal loading, whereas the stationary blades (stators) are thought to be limited to the aerodynamic and thermal loading. It should be noted that the aerodynamic loading applied to each blade is different due to the fixed nature of the blade in comparison to the cantilever nature of the rotating blade.

Having previously mentioned the vibration loading of the blades as a factor for consideration within a lifing analysis, a short look into this phenomenon is needed. Vibration of the rotating blades can be attributed to a number of factors, these include:

- Vibration of engine shaft
- Balance or warping of the turbine disk
- Aerodynamic induced flutter

All of the above factors are really beyond the scope of analysis at this low fidelity end of the design process. This is especially so for dealing with the natural frequencies of the parts and operating conditions for an engine in flight, as well as including any effects of possible manufacturing defects. However, given the size of the turbine blades within the HPT, the aerodynamic flutter is not particularly significant. In fact, that is improved with the use of tip shrouds that help to secure the ends of the blades together. The tip shrouds also improve the aerodynamics of the tip and help to improve the stage efficiency [42, 43]. Choosing not to consider this form of blade loading does not necessarily penalize the analysis, as will be explained later the loading is not one of the main causes of blade failure. However this has helped to highlight just how complex the process of blade lifing can be. There are certain factors required for a system level analysis that even a physics-based process cannot capture with the low fidelity analysis. This is not the only consideration that needs to be made and not the only problem to overcome.

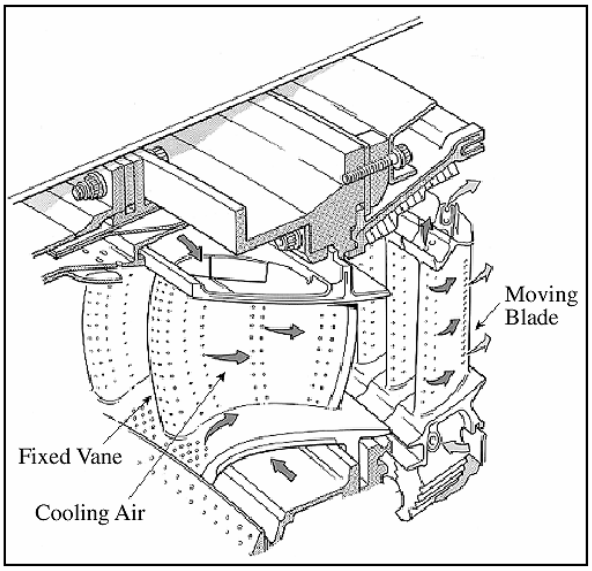

Figure 21: Notional HPT stage with film cooling [44]

1.5.1 Aero-Thermal

Some of the blade technologies which affect life, such as advanced turbine film cooling technologies (see Figure 21) and advanced materials, are applied at the part and material levels. However, lifing analysis (at the part level) and material modeling are necessarily far-removed from system-level evaluations and yet they have a major impact on the system. Thus a number of challenges exist, including:

- How to quickly and accurately evaluate the impact of changes at the micro- and meso-scales on system performance?
- How to set requirements for micro- and meso- scales based on system level requirement?

To improve current designs the consideration of all aspects of the gas turbine system is needed. Consequently one needs a part level analysis approach

to help assess the effects on the system level. For example, the current business environment calls for more efficient engines for reduced fuel usage as prices rise. To possibly answer this, one needs to consider how a turbine can be designed to improve the efficiency of the engine and what would that do to the blade life?

However, lifing analysis brings forth many different and conflicting requirements. For example, the efficiency is only one parameter of many that impacts an engine design; it needs to be balanced with performance, weight, life etc. When considering engine efficiency, the most direct way to increase this is through an increase in turbine inlet temperature. This potential leads to more fuel burn, which requires other developments to enable operation at the desired conditions. For example, there is a great need for development of improved materials and systems that can withstand higher inlet temperatures. These are parameters equally as important as efficiency when designing an engine to operate for its required life safely. If the required material properties alone cannot achieve the necessary improvement then other techniques, such as blade cooling, are needed to enable the engine to operate at that condition. However, introducing new blade cooling would also have detrimental effects on the overall engine efficiency, something that needs to be weighed against the benefits of increased inlet temperature.

Since the 1940's the development of the jet engine has demanded better materials for the hot sections as the drive to improve efficiency continues. This development has permitted the steady increase of peak metal temperatures to

withstand temperatures to over 1,100°C, whilst still achieving service lives of 10,000 hours or more [3, 15]. This increase in the temperature requirements is illustrated in Figure 22, using Rolls-Royce engines as data-points (the Trent series being the most modern) [3].

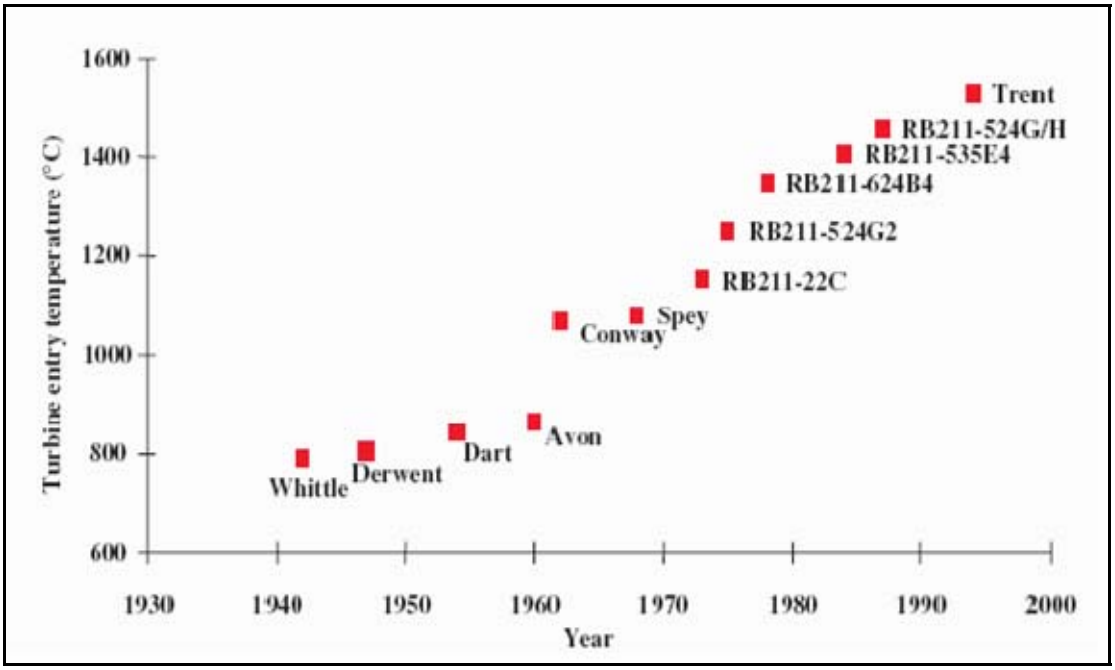

Figure 22: Development of Turbine Entry Temperatures (TeT) with time. *(After Spittle)*

1.5.2 Materials

Currently the only metals able to achieve the operating temperatures required are Nickel based super-alloys. This is due to the ability of the metal alloy's to maintain its strength even at elevated temperatures. A quick comparison is provided in Figure 23, illustrating the ability of Nickel Alloys against other common aero engine alloys [3].

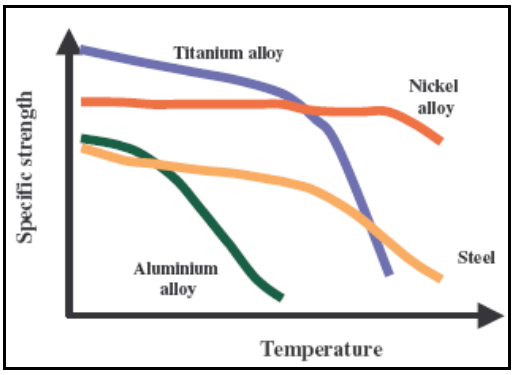

Figure 23: Specific strength versus temperature for a variety of common aero engine metals. *(After Spittle)*

Continual research is needed into materials to furnish the required properties for aero engine development. Schulz et al [45] point out that today's engines operate with hot gas temperatures that are more than 480°F above the melting temperature of the Nickel base alloys.

Thus to permit the operation with these increased inlet temperature there is need for the addition of cooling flow through the blades, as previously touched upon. This would reduce the need to develop new, high temperature withstanding materials, but would also reduce efficiency therefore negating the benefit of high inlet temperatures to begin with [46]. Therefore developing materials to improve their operation range would go some way to offset the need for the cooling flow that is detrimental on the efficiency.

1.5.3 Integration

When addressing these parameters separately, it is easy to see how some of these part interactions may be missed. Thus, an approach needs to be formulated that takes into consideration the big picture when developing a part

level method for design and technology assessment. This approach will provide a link connecting the system level requirements/performance to the macro/micro level materials modeling through the driver of turbine part failure modeling. Throughout the design process, this approach will save valuable time and money whilst improving the inherent safety of engine design.

The success of the design within the turbine can be looked at through a number of factors. When looking at the life of components, these factors often come in the form of figures of merit or percentages, allowing comparisons across engine types and applications when looking at component. These include:

- The thermal/structural properties in terms of length of useful service life
- The overall and stage efficiencies
- Emissions, both CO_2 and NOx
- Engine thrust to weight

1.5.4 Common Failure Modes

When considering the effect of differing conditions and designs on the turbine, one of the most important factors to consider is the envisaged service life of the engine. This is especially true when one takes into account the repercussions of the unexpected loss of a product in service. The structural/thermal loss of a component is dependent on many factors, from cyclical stresses to the effects of hot gasses on the metallic blades (explained in

more detail in the following section). Generally the loss of a turbine blade can be grouped into four main failure modes:

- Creep

  As shown in Figure 24, at a constant stress, the strain initially increases swiftly with time (primary or transient deformation), then increases more slowly in the secondary region at a steady rate (creep rate). Finally a fast increase in strain leads to failure in the tertiary region. Within a gas turbine the creep of the blades does not advance to the fracture limit. However, it does shorten the life of the blade once it extends beyond the inbuilt tolerances and interfaces with the casing.

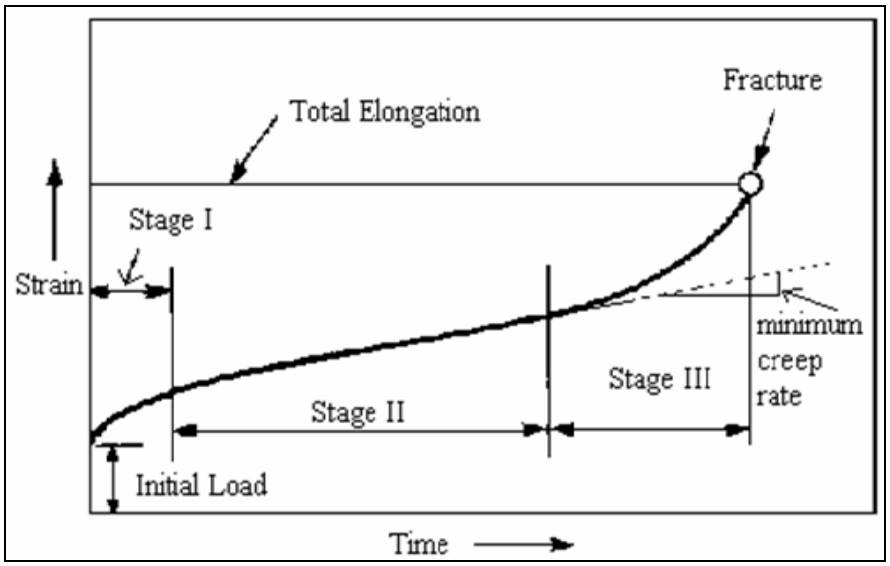

Figure 24: Notional creep behavior [47]

- Oxidation [48]

This is the reaction between the blade materials and the oxidants present in the hot gases from the combustion process. This effect varies greatly depending on the material composition and operating temperature. Great work has gone into developing materials that are more oxidation resistant as demands on the engines increase. Often companies employ coatings on top of the less resistant compositions to extend their service lives. This is a quick fix, and if a coating layer is compromised in any way, the service life of the blade is shortened drastically. More on the hot corrosion problem is mentioned later.

- Low Cycle Fatigue

  Where the stress is high enough for plastic deformation to occur, the account in terms of stress is less useful and the strain in the material offers a simpler description. Low-cycle fatigue is usually characterized by the Coffin-Manson relation [49] shown in equation 2:

$$\frac{\Delta\epsilon_p}{2} = \epsilon'_f(2N)^c \tag{2}$$

  where:

  - $\Delta\ \varepsilon_p\ /2$ is the plastic strain amplitude
  - ε_f' is an empirical constant known as the *fatigue ductility coefficient*, the failure strain for a single reversal
  - $2N$ is the number of reversals to failure (N cycles)

- c is an empirical constant known as the *fatigue ductility exponent* commonly ranging from -0.5 to -0.7 for metals

- Hot Corrosion

  Surface reactions with salts deposited in the vapor phase gradually erode away at metallic or coated surfaces [50]. It is one of the most severe environments faced by man made materials, which over time this leads to degradation of the aerodynamic performance of the blades. Developing materials for high temperature environments often leads to great mechanical properties; however, they also provide poor corrosion resistance, thus creating an extensive use of coatings for blades [51].

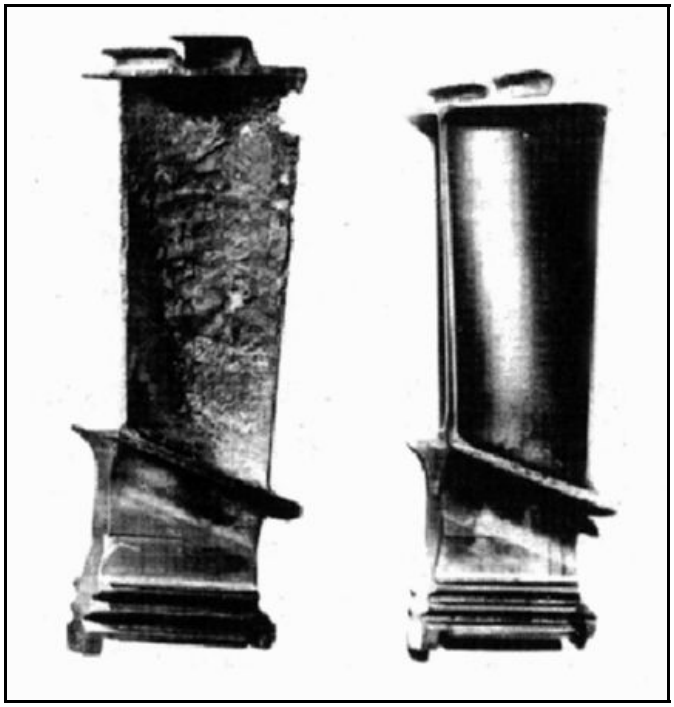

Figure 25: The result of 2500 hour low altitude sea flight service on an uncoated and NiAl coated blade turbine blade. [51]

With the use of suitable coatings, oxidation and hot corrosion can be suitably controlled [51] as shown in Figure 25. However the problems with creep and LCF persist, especially when the operating temperature approaches the metal melting point and the blade rotation causes considerable stresses. New materials are a possibility for improvement in the capability to operate at higher turbine inlet temperature, but guidance is needed as to the best materials to consider.

To combat these deign problems, development had previously been underway into a variable fidelity lifing approach for gas turbine design (covering from 3-D to 0-D) and was focusing on a 3-D/2-D methodology for the turbine part life [52, 53]. Previous research into such higher fidelity methodologies for blade life was carried out within ASDL under the NASA/DoD mantle. This research looked at the 3D behavior of the hot gas flow around the blade and the 3D finite element behavior of the blade in its stressed state. A demonstration of this approach proved the viability of the application of ASDL methodologies to the problem of gas turbine design, allowing for the inverse design techniques proposed in the initial plan for URETI. Utilizing neural networks, the effect of changing different operating requirements could be observed on blade life and materials composition.

By helping to speed up the gas turbine design process, such a methodology should also provide enablers for reducing development costs, aiding in the

elimination of costly later redesigns and tweaks common with more traditional design approaches. Considering more advanced features within the early conceptual design stage helps with their integration, and helping to realize the full benefits of such additions at both the component and system levels are key benefits to using this methodology.

Given its critical location within the engine, choosing to consider the turbine blades for this study greatly enhances the drive. This enables the designer the option of considering lifing/materials issues at the very beginning of the engine design process to prevent any unseen, unnecessary show stoppers later in the process. The lower fidelity approach is the most promising methodology, both for speed and ease of use. Trying to consider full internal and external flow path design is beyond this stage of the process, therefore generalizations and empirical relationships are best used to capture the physics of the problem.

1.6 Identified Need

The previous sections have indicated a number of issues relating to today's aircraft gas turbine design more specifically that of early turbine blade work. From these issues, it can be seen that there is a need to provide a methodology through an appropriate fidelity approach, whereby early stage design decisions can be analyzed "on the fly". Such a method can also be used to provide

indications for an area of interest, enabling the faster creation of a technologically superior design.

The previous sections have suggested that the focus of the approach should be concentrated on 0-D/1-D analysis to allow for much quicker computation and reflecting the level of knowledge available in the conceptual design phase. This new focus will still allow for consideration of the problem of failure within a gas turbine engine, which is of utmost importance within the aircraft industry. The author proposes to develop and implement an approach from system to part level and vice versa. In the most extreme of circumstances the loss of an engine in a dramatic fashion will most likely lead to the loss of that particular aircraft. Thus the ability to predict the life of an engine is of great importance.

However the goal of this proposed research is not only to improve the efficiency of the gas turbine engine but to provide a better overall design picture by considering other parameters. This framework will enable the system level designers to balance the conflicting needs, and thus yield a better design. This capability relies on the ability to understand the physics of the gas turbine cycle, captured in the use of an integrated interactive design environment. The development of material and other technologies to make this possible requires the development of a technology assessment tool. This project aims to produce such a tool that will provide the means for a full cycle analysis (represented through the engine core) while at the same time provide the designer a quick and

easy method to monitor the primary effect of both system, component, part and material level changes on the design environment. Overall this approach should aim to improve the R&D of gas turbine engines.

Through utilizing data from within NASA, it is hoped that any method created can be validated against this, working mainly from reports for the NASA/GE E^3 engine program. It is especially crucial to validate this method against such data since this is expected to be the only data available within the public domain. Not only is a higher fidelity method not suitable for such a stage in the engine design process, but a full comparison could not be completed for validation of the methodology given the privacy issues that engine companies tend to have, pushing the author towards a lower fidelity analysis methodology. A quick summary schematic is provided in Figure 26 which simply summarizes the topics raised within this section and provides a nice pictorial representation of some of the most significant.

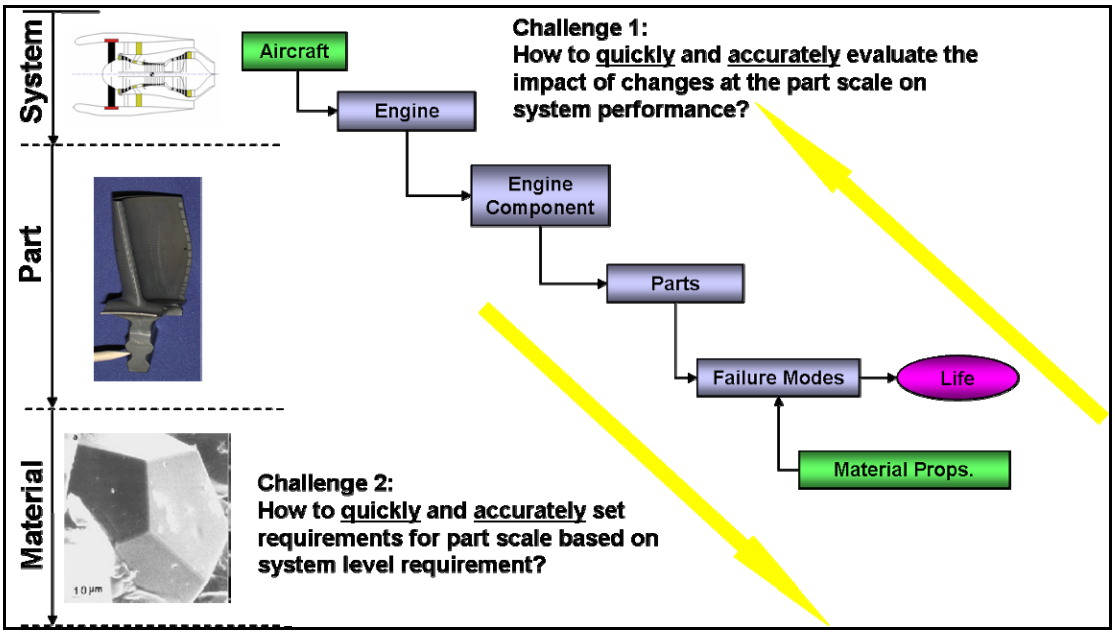

Figure 26: Schematic summary of the need.

1.6.1 Intended Implementation

The creation of this design environment needs not only be driven by the identified need but also its applicability within the current business environment. Such a market can be realistically broken down into two parts: pre and post-market. The pre-market reflects the design and production of the turbine blade and the post, reflects the maintenance, repair and overhaul end of the product life cycle. It is foreseen that the approach to be developed within the course of this thesis work could be applied to both situations, in different ways.

Beginning with the pre-market section of the product life cycle, the first utilization of this conceptual design approach would be for the reduction of the general design process time. Providing a suitable design direction through this conceptual phase analysis, avoids any later problems encountered during the

traditional process without the creep consideration. Thus, reducing the cycle time and need to revisit the design at a later stage, as new considerations are made during the process progression. Furthermore when beginning the new design of an engine, to tackle a situation not experienced before, the reliance on empirical data, typical of the traditional conceptual phase becomes stretched. Thus this physics based approach would provide great insight for the designer and enable a full quick design space exploration in search of favorable designs.

The addition of the creep life analysis will provide the designers a useful look into the materials level factors and encourage collaboration between the conceptual designers and their materials counterparts. This single approach would promote understanding and highlight possible trades throughout the design of the turbine blade within the whole cycle. Additionally, one can look beyond the effect of material selection on the design and begin to consider and compare the effects of technologies on the overall cycle and turbine stage and turbine blade. Overall there is a niche for this approach in the exploration of the complex interactions within a turbine engine, enable the consideration of uncertainty and help derive the suitable design directions for high temperature application.

Moving to the post-market sector, one can reiterate remarks made earlier. In order to improve upon a design within an MRO market, one must consider the effects of technologies on the baseline performance of a blade. MRO calls for performance, reliability and service life assessment, considering the creep life

within a rapid analysis approach greatly assists this goal. Thus this approach could aide the designers in technology selection in a creep life and performance aspect, as they strive for an improved design. This is especially important when you consider that any improvements made to a part after the beginning of an MRO contract reflects an increase in profits for the manufacture based on its fixed cost pricing.

Therefore it can be said that there are a number of possible implementations of the approach proposed within this thesis. Working towards the completion of the work for all of these applications would be beyond the work of a thesis. Tailoring the approach to meet one of these applications in no way rules out the use with another, in fact it can be seen that many of the discussed application can rely on aspects of the others in order to provide the desired result. In view of the current trends towards improvements in the gas turbine engine, it would be most appropriate therefore to consider this approach as an aide in the decision making process during the conceptual design phase and to assist in the reduction of the overall design cycle time and similarly cost. Thus, this thesis work should consider the pre-market conceptual work, but at the same time leave hooks within the approach to enable the other discussed applications at a later date. This requires the consideration of a "*plug and play*" type approach and would also enable the use of higher fidelity modeling within the analysis again at a later date, should the need arise.

CHAPTER 2

RESEARCH QUESTIONS & HYPOTHESES

Design of gas turbine engines is a very complex affair, and attempting to capture the physics of the problem in the conceptual phase is exceedingly difficult. The previous chapter has shown that there is a need for a multifaceted yet simplified method to analyze the life design of gas turbine blades when considered within a top down, bottom up approach. Researching this issue, based on previous work and perceived future requirements, has brought about the following questions on the intentions of the approach. In addition, solutions to these questions were hypothesized. The research questions posed investigate all levels of the necessary design approach and help to develop their associated hypotheses, starting from the system level (one and two), down to the part level (three and four) and considering the overall approach (five and six).

1. How can a conceptual phase creep lifing design approach be achieved without total reliance on historical and empirical methods?

   Hypothesis 1: An approach should consider the whole system, represented by the engine core, right down to the part level creep lifing design, to provide better understanding of the design space.

Current and previous methods within the conceptual phase of the design process rely heavily on empirical or historical methods, such methods include Weibull based approaches to service life prediction, such as that by Zaretsky [39].

These methods are often limited to just that particular type of engine and do not help to expand the knowledge of the designer at the conceptual phase. Considering the whole system at the same time as the blade creep lifing will help to improve the understanding of future design directions.

2. Can the system level and the part level characteristics be considered at the conceptual phase simultaneously? And if so how?

Hypothesis 2: Considering both issues requires the modeling of both considered at a low fidelity level to improve the information flow and thus assist in capturing the interactions.

Currently the cycle and part level analyses, especially in terms of creep are considered at different phases in the design process [54, 55]. Thus, providing analysis at the same phase and at the same fidelity level will improve the integration between each, in order to improve the information flow and design space exploration.

3. What is required to bring the blade creep lifing to the conceptual phase of design?

Hypothesis 3: A rapid, physics based analysis is needed to consider the blade creep life within an integrated conceptual engine design process.

The creep lifing of the blade is a complex affair and not something that can be accomplished through empirical or historical means [56, 57]. Low fidelity

physics based analysis that uses information from downstream within the engine will enable its use within the desired integrated environment, especially since Haubert et al suggest that the environment is on of the most important factors in the creep life determination[55].

4. How can one capture the creep life of the part early in the design process?

Hypothesis 4: One needs to capture the main stress components and thermal-mechanical factors that might combine to affect the service creep life of a turbine blade.

The physics based analysis mentioned within the previous hypothesis requires the consideration of all the possible factors in the determination of the creep life of the turbine blade. The analysis needs to be split into the consideration of three main stresses (gas bending, thermal and centrifugal) and the factors that effect these [27, 58], in order to achieve this.

5. How can one capture the turbine blade creep lifing interactions within a modern axial gas turbine?

Hypothesis 5: An approach should integrate the physics based analysis of the cycle, turbine stage and blade into a single design environment.

The integration of the system, component, part, and materials level analysis into a single environment has been shown to be the ideal means for

conceptual phase analysis. To achieve this, a single design environment needs to be utilized, so that information flow and analysis speed are not hindered in any way.

6. How can one help the designer understand the coupling between creep lifing and performance goals?

Hypothesis 6: An approach is needed that samples more of the design space, enables instantaneous trades through surrogate modeling techniques, and provides an informed design direction through interactive visualization.

The previous chapter has highlighted the fact that one major benefit of moving the consideration of the creep life up to the conceptual phase was to boost the designer's knowledge and considerations during the process. Achieving this requires the exploration of the design space through the use of DoE and surrogate modeling techniques, which will enable powerful parametric interactive visualization of the designs at hand. Given the level of fidelity the approach will provide a design approach rather than single point solutions to help understand the coupling between lifing and performance goals.

In summary, answering these research questions would require development of an approach that will enable the user to rapidly assess any changes to the engine design point whilst taking into account the effects on the whole engine. It is thus essential that such a tool have the following qualities, as previously described: Flexibility (modularity), short run times, accuracy, and the

ability to deal with the variability of the design. Considering this, the following research goal has been formulated:

"A fast conceptual level methodology can be formulated and implemented which may reduce the time required to explore the design space for a turbine blade design solution suited to high temperature applications."

CHAPTER 3

FORMULATION

The following chapter involves the formulation of the analysis environment, surrogate modeling and simulation, to work towards substantiating or disproving the postulated hypotheses. Following the flow of the hypotheses, this chapter will begin by formulating the analysis environment, to capture the system, component, part and material level analyses within a single environment. To permit the exploration of an intended turbine engine design space the use DoE methods and surrogate modeling will be explored. The closed form solution from these will then enable the visualization and other analysis, to improve the understanding and exploration for the preferred design direction, summarized in Figure 27, overleaf.

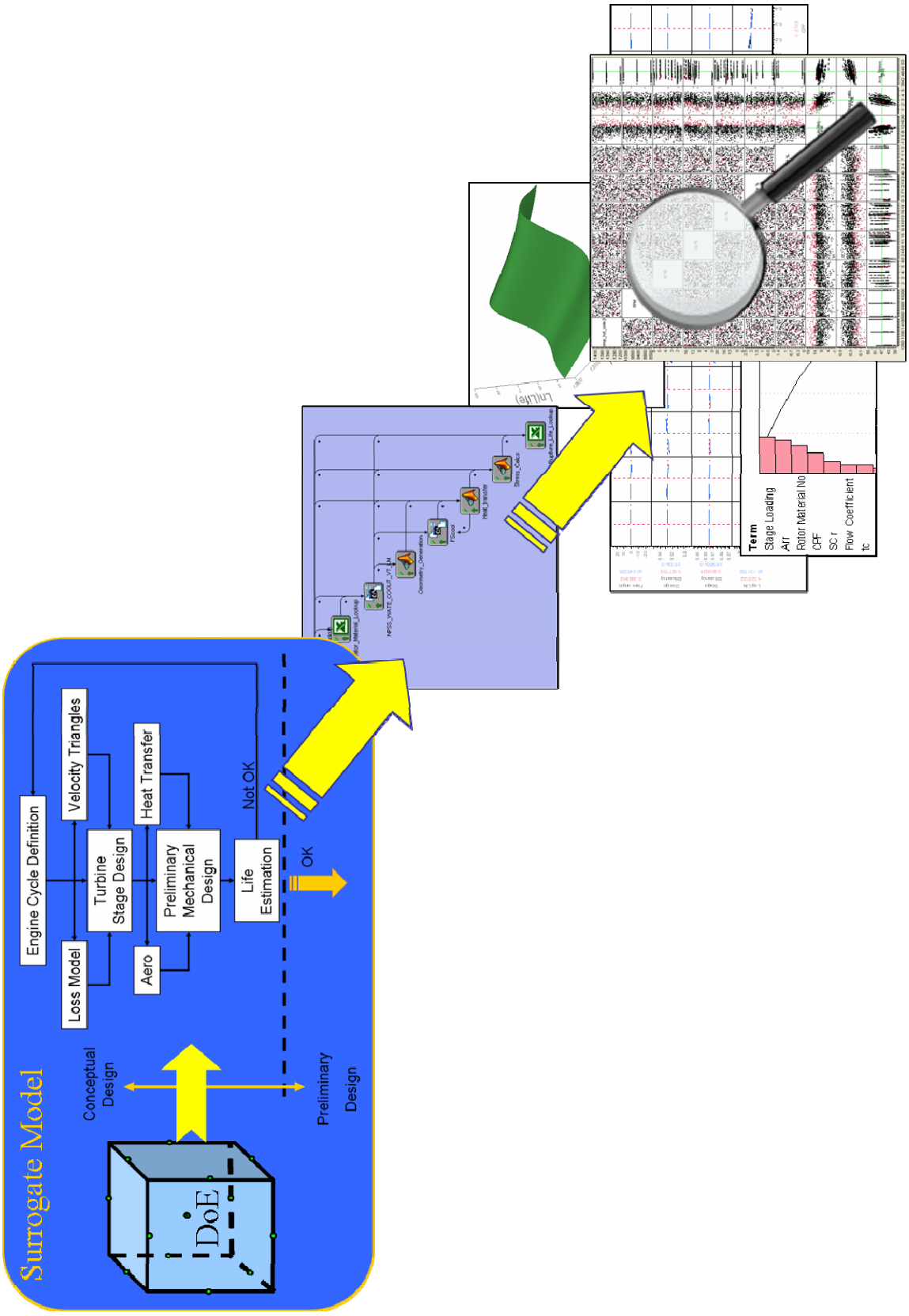

Figure 27: Summary of intended overall process

3.1 Modeling and Simulation Requirements

As one progresses through the scientific process and the problem at hand has been fully assessed and bounded through the hypotheses and research questions, a means to test the conjecture can be formulated. Chapter one called for a move towards a design for life approach for gas turbine design to meet the change in market practices and increasing competition within the market. This consideration would require the inclusion of part and component level analysis within the typically systems and performance based analysis of the conceptual design phase, with the ability of the relation of all aspects to each other should the need for such consideration arise. The hypotheses and research questions reflected this need, working from the system level through to the part level. The final two were concerned with a top-down/bottom-up approach, intended to aid the designer in the understanding of the considered design space.

Thus, working from the hypotheses and research questions, one can set out requirements for a suitable modeling and simulation environment. These requirements need to be ascertained through consideration of each of the hypotheses in turn, at he same time remaining true to the outlined research focus. To begin with, one needs to understand the desired level of fidelity of the research and the desired scope of the work. Recalling that the overall desire is to bring the scope of the detailed design phase, as see in Figure 13 in chapter one, to

the conceptual design phase. Figure 13, broke the turbine blade design consideration into six areas. The means to analyze these areas at the different fidelity levels is illustrated in Figure 28. It can be seen from this figure that the means by which the analysis involved within the research for this thesis, needs to be conducted based around physics based or empirical methods to comply with the low fidelity approach.

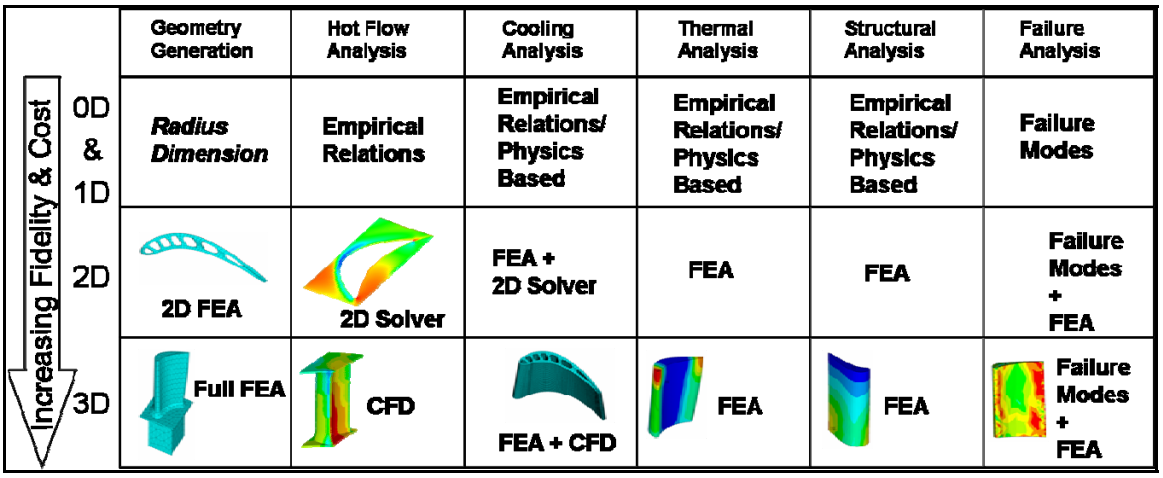

Figure 28: Morphological matrix of analysis alternatives

However the drive in technology development as described in chapter one, would push an approach that utilized physics based analysis rather than empirical relations regressed from existing designs. Though the physics based relations would never have the clarity of the FEA and CFD analyses involved in the normal 3D detailed design phase analysis, simplifying assumptions and other methods enable a good representation of the true results. Furthermore, as has been previously stated, maintaining a low fidelity analysis keeps the design

flexibility that is part of the conceptual phase. In addition hypothesis 3 suggests that physics based analysis is needed to consider the turbine blade creep life within the engine design, building on the limited data from empirical means.

Understanding this need hypotheses one and two suggest that the conceptual level modeling of the engine core, turbine and blade will provide the better understanding of the gas turbine design space. Additionally, within chapter one it was discussed that to consider the turbine blade in a design sense, not only should one consider the structural design but the material itself is of great importance. Consequently considering the system, part and material level within an analysis environment would be essential. Such an approach can be represented pictorially in Figure 29, showing the levels of the required analysis and the interactions between them.

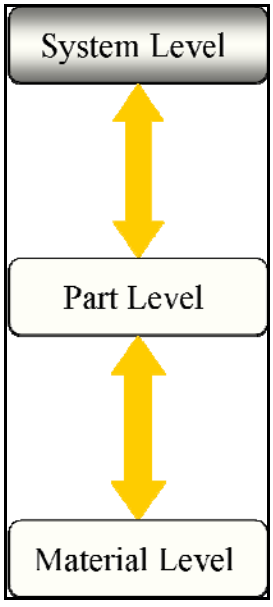

Figure 29: Pictorial representation of analysis level needs

This simplified breakdown highlights the key points laid out within the need and again represented in Figure 30. Therefore one can collate the aircraft engine and engine component analysis within the system level box in Figure 29, and the parts and failure modes are encompassed within the part level box. This leaves the materials considerations to the material level box in the analysis breakdown.

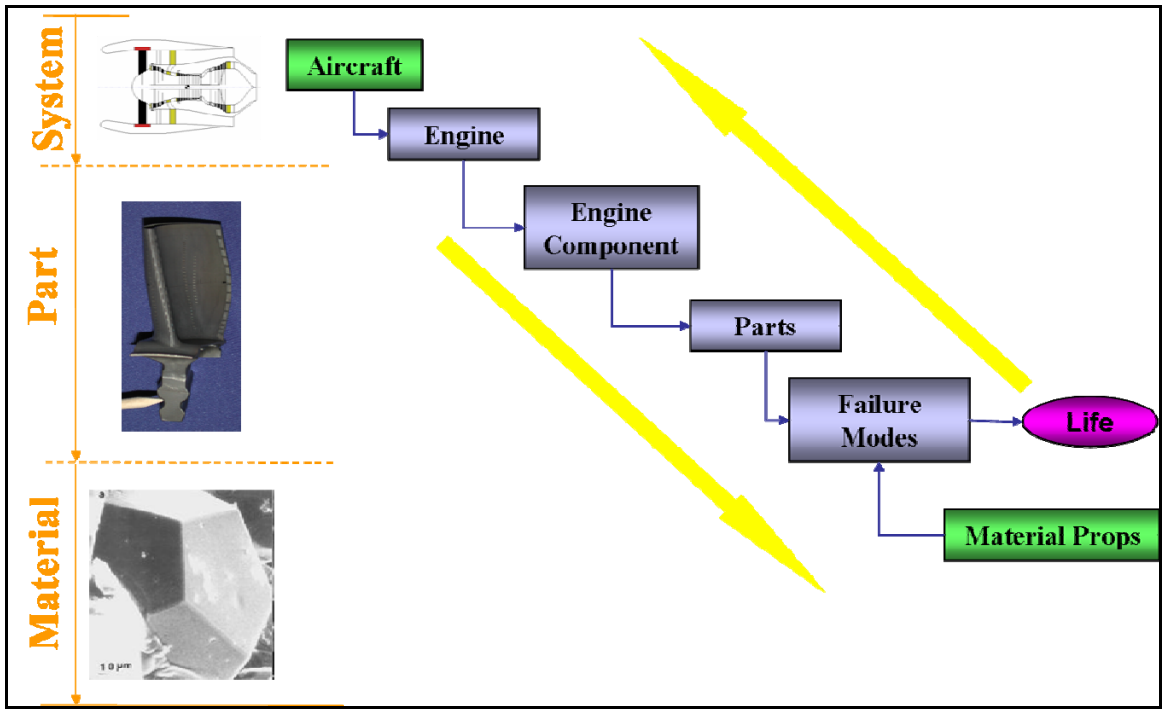

Figure 30: Desired analysis consideration

Constructing the approach of the desired analysis environment to meet the layout set in Figure 30, setting out the consideration of the system level is critical. It has already been discussed that considering the whole engine would add extra complexity to the work, given that the effects of upstream components

can be considered within a simpler engine core model. This would help to simplify the research and ease the validation of the hypotheses and research question, as to limit any problems within any code used to that being used for the work.

Capturing the performance and other characteristics of the core and the turbine for use within the intended integrated analysis process as called for by hypothesis one amongst others, requires the use of cycle modeling and turbine modeling methods. These methods need to be easily integrated and thus at the same fidelity level, to improve the information flow in line with hypothesis two. Additionally maintaining the same fidelity level throughout the analysis goes some way in avoiding propagating unnecessary errors between unequal analyses when seeking higher fidelity solutions.

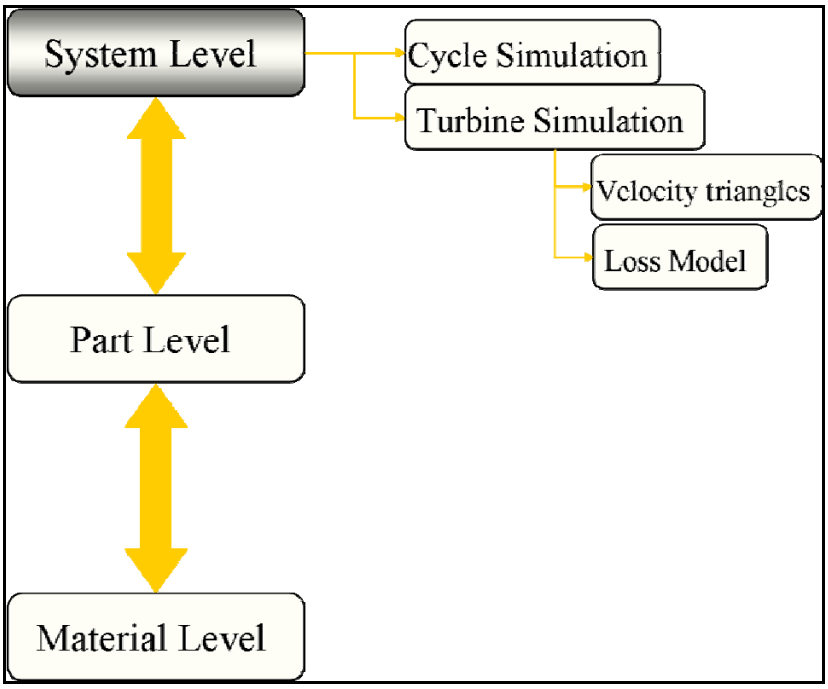

Figure 31: System level modeling requirements

The turbine simulation would require the use of both velocity triangle analysis and a meanline loss model to first decompose the flow through a stage then gauge the stage performance. The use of a meanline loss model is typical of the conceptual and preliminary stages of design when performance considerations are particularly important. Additionally, Haubert et al [55] have suggest that the mid span section of the blade is the life limiting section, thus, the study at the meanline is the most logical. Limiting assumptions obviously come with the use of such an approach but it is felt that for such a proof of concept as this work is these fit well within accepted practice.

As one considers the design analysis approach and continue following the information flow down, the next step is the consideration of the part level

analysis. This is additionally reflected in the consideration of the research questions and hypotheses that are driving the formulation of the modeling and simulation environment described herein. When considering the part in question, the turbine blade, more precisely the first stage HPT blade, the needs of the analysis require identification.

The fourth research question posed within the last chapter questions how the creep life (the failure mode of interest) can be brought within the conceptual phase design process. Thus it is postulated that the main stress components and additional aero-thermal-mechanical factors are needed for this to be achieved. Shephard identifies in his book [59] that the loading on a turbine blade is composed of direct centrifugal force and a bending force due to the fluid pressure and change of momentum. Halderman and Dunn [60] also suggest that significant effort is going into the determination of the thermal characteristics around the blade as temperatures within the turbine are pushed to their limits.

This thermal loading of the blade is an important factor to determine due to a number of factors. Firstly the creep properties of the blade material vary with the temperature of the metal, thus a means to determine this would be beneficial in addition to a means to determine these material properties as the temperature fluctuate. Secondly the need to maintain the temperature of the metal within acceptable bounds as the drive to increase the T_4 continues drives the need for improved blade cooling designs. As will be discussed later in this chapter, although the increase in flow temperature helps to improve the

efficiency of the stage the possible increase in cooling flows required can often negate this [46]. Thus in addition to the consideration of the heat transfer, which intrinsically requires some form of geometry definition (all be it ideally at the lowest level), the consideration of the cooling of the blade is absolutely necessary.

Thus, to test hypotheses three and four, an approach is needed that considers the aero-thermal characteristics within the turbine and blade, and the mechanical stresses that are associated with these or other cycle parameters. A simplification of the foreseen required analysis that will fit within an integrated engine design approach and how this ties in with hypotheses three and four is illustrated in Figure 32.

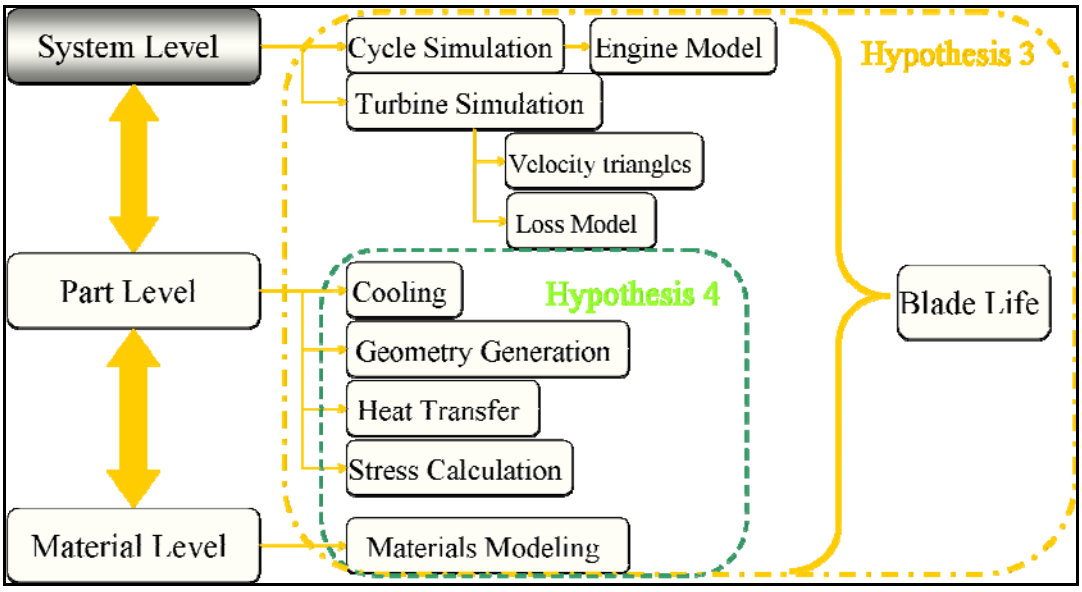

Figure 32: Requirements for consideration of part level influences on blade creep life

Therefore, with the consideration of the hypotheses and research questions, a framework for the analysis of the cycle, component, part and

material levels have been derived to meet the ideal set out initially in Figure 26 and then more practically in Figure 30. Now comes the task of filling in the blanks and determining the best methods to complete the analysis at the desired level of fidelity.

3.2 Analysis & Modeling Environment

With a view to provide the required flexibility dictated in the hypotheses and proposed approach, a suitable means to encompass the analysis methods into a single environment in line with hypothesis five was needed. Such software exists in the current market today. There are a number of players in the market, each with their own benefits, although none of them are free. The ASDL has access to the following three; Engineous' ISight, Phoenix Integration's Model Center, and Pacelab Suite. Given the nature of the work that is carried out within ASDL, these three software packages offer the best available capabilities. Therefore, considering other available software that would incur significant costs associated with a site license is unnecessary. Upon consideration of the benefits and disadvantages of each package, the Phoenix Integration Model Center provided the best platform for this design tool. The following summarizes each of the available software packages:

3.2.1 Phoenix Integration Model Center ™

Launched initially in 1999, Model Center has been intended to provide the designer software integration architecture for analysis and simulation. This

integration allows the designer much needed decision support for complex concept and systems analysis, with "on the fly" determination capabilities. The software enables a visual interface interaction with all the analysis codes, and easy integration within a DOE type approach. The software automates the process of running the engineering analysis, enabling the designer to concentrate on the results of the analysis. In fact, in one of Phoenix Integration's press releases Model Center is described as enabling the user to: *"quickly create an engineering process and then perform complex design exploration techniques to find the best design."* [61] The figure below illustrates an example engineering process model, used for preliminary research carried out in conjunction with Teledyne within the Aerospace Systems Design Lab. The contents of this are not meant to be important, it is included just to give the reader a basic idea of the interface.

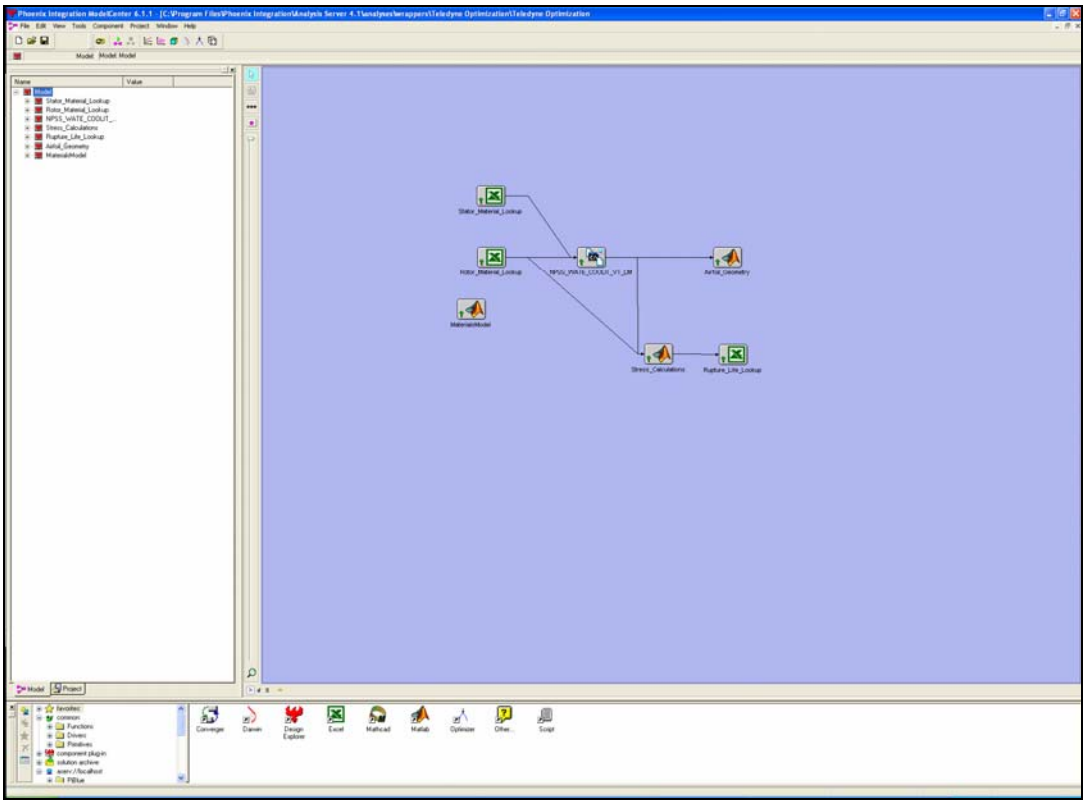

Figure 33: Notional example of Phoenix Integration Model Center model. *(ASDL)*

Working towards the goal that this work will be a baseline from which to expand this technique, Model Center is very dynamic. Therefore the users are able to adapt the engineering process to their particular needs at the time, possibly allowing for the increase/decrease in the fidelity of the analysis process. This ability would be highly desirable in the long run, looking beyond the development of this thesis.

Overall Model Center can be summarized in the following fashion, taken from Phoenix Integration themselves [62]:

- Easy to Deploy – Seamless integration with existing applications
- Better Designs – Enables linking of powerful tools to bring knowledge forward in design process

- Reduces Errors – Automation helps to reduce mistakes
- Saves Time – Eliminates manual transfer of data between applications
- Cohesive Team Environment – allows for data coordination across a network

3.2.2 Pacelab Suite

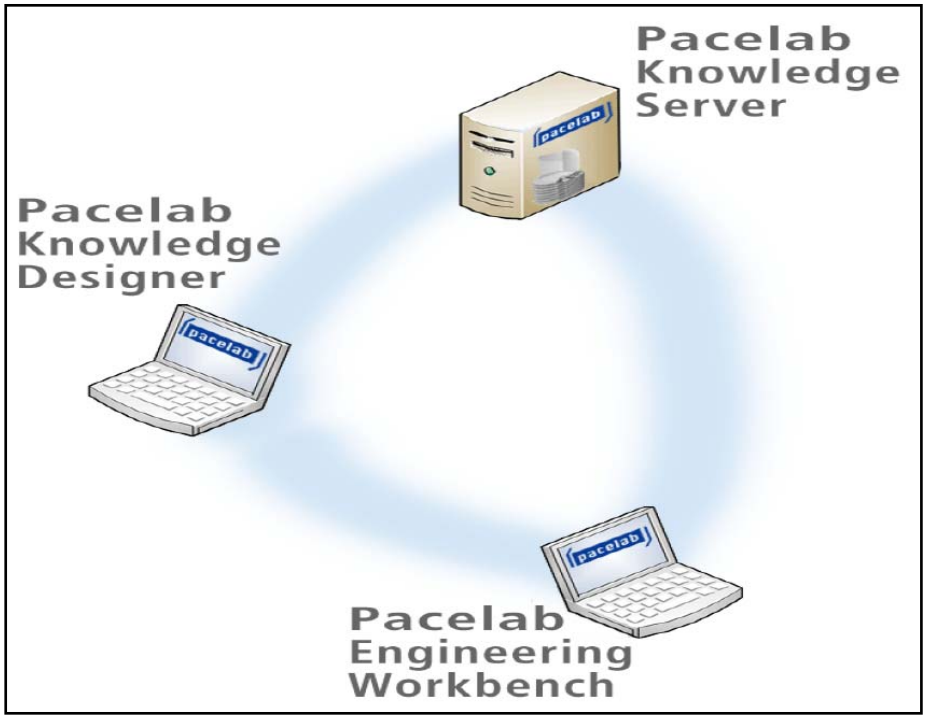

Figure 34: Representation of Pace Suite Constituents.

This program from German software developer PACE provides a single environment for preliminary design, allowing the designer to quickly investigate design alternatives. The biggest difference between this and the alternatives is that this environment has been created with an interest towards integrating user

developed codes more easily. These codes would be written in C Sharpe object orientated programming language using Knowledge Designer and then linked and adapted using Engineering Workbench, for use within a DOE type of approach. This software architecture developed by PACE with its separation of knowledge capturing and storage helps to speed up the process overall.

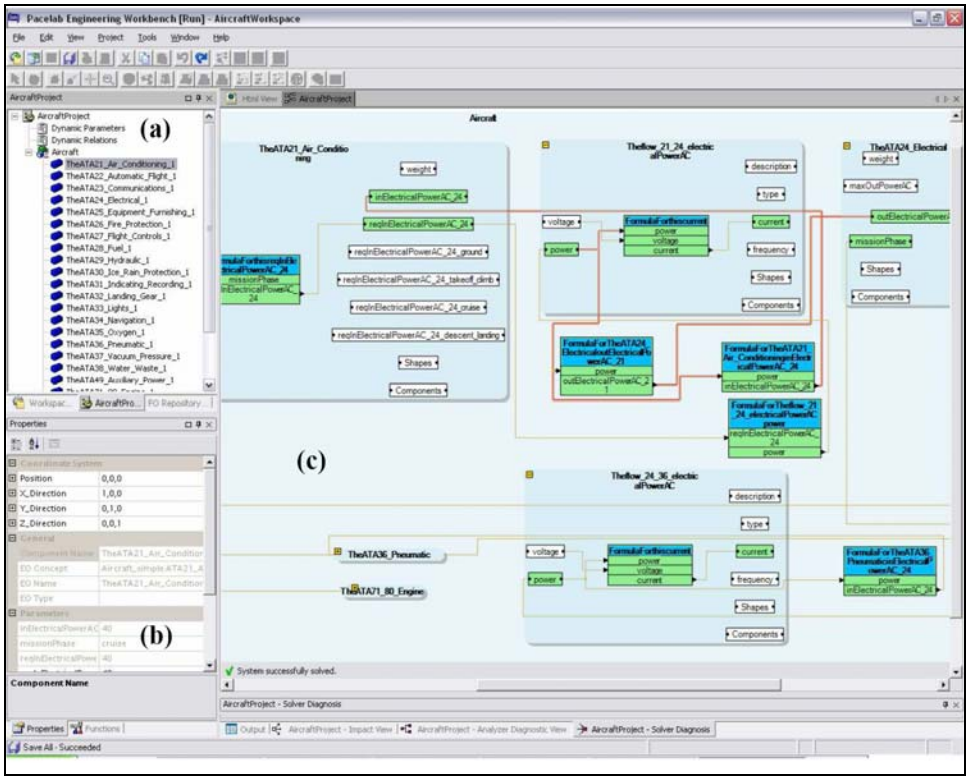

Figure 35: Example PaceSuite Layout.[63]

The example illustrated in Figure 35, highlights the areas of interest within the integrated environment implemented in the Engineering Workbench component of PACE Suite ™. As discussed by Mavris, Phan et al[63], in panel (a) the user can load and visualize the system, subsystem and their interfaces for the engineering problem studied. Panel (b) then lists all the properties of the selected

item in panel (a), as well as its parameters. The values not changed by any formula's can be changed there. This panel also has the ability to run previously laid down analysis routines. These complete the required analysis on the problem in question and record the results within an output file in the Pace Knowledge Server ™.

The third panel of the virtual environment, panel (c), provides the designer with an interactive graphical view of the model. Each subsystem is represented within the panel by an expandable box, all contained within a larger box representing the overall system of interest. Once selected, these expandable boxes enumerate the values of the parameters contained within the subsystem being represented. Panel (c) also graphically illustrates the links between the subsystems and system within the analysis. This is achieved through the use of lines in a similar fashion to those seen within Phoenix Integration Model Center.

Unfortunately, the architecture design of this software precludes its use with existing codes. The dependence on the C# language creates problems with codes that are generally programmed in older languages. The changes needed to operate with these add an unnecessary delay in the implementation of any approach working with this system. Given the intention of this thesis to create an interchangeable approach, having to rework any codes for use with this architecture would be excessive. Even with wrappers for the most common software tools like Microsoft Excel, which is underdevelopment at PACE, would not be available in time for use within this thesis work.

3.2.3 Modeling and Integration Tool Selection

Choosing the integration tool is not an easy choice given the selection available to the author. However considering the authors previous experience with Model Center ™, it would be pertinent to continue working with this software. We have seen that there would be no loss of modeling and integration capability through the use of this tool. In fact it would be an improvement over using PACELAB given the authors lack of experience in the tool. Model Center's ability to work with different codes and applications such as MATLAB and Microsoft's EXCEL, greatly enhances the ability of the intended analysis to achieve its stated goals. Furthermore the intended use of some industry codes for engine simulation tends to preclude the use of PACELAB, which has been developed more for use with user defined codes. Add to this the general lack of experience amongst piers with the use of ISIGHT and the field tends to narrow. Consequently the use of Model Center™ really comes as the most informed choice, balancing the advantages and disadvantages of the three different tools available to the author. A simple summary of the criteria chosen to perform this selection is given below in Table 1.

Table 1: Selection of analysis integration environment

	Handle Developed Codes	Handle Legacy Codes	Wrappers available?	Usability	DSM Based	Familiarity
iSight-FD	+	+	-	-	+	-
Model Center	+	+	+	+	+	+
Pacelab	+	+	+	+	-	-

3.2 Appropriate Fidelity Engine Modeling

Looking for a suitable engine cycle modeling tool one initially had to consider the fidelity at which the user desires to operate. The hypothesis and research questions guide the research behind this thesis into looking at the lower fidelity end of the scale, so suitable tools would fall within this range. Such tools would also need to be user friendly and fast to run, so that the conceptual designer can operate them with ease. An extensive search has identified two choices:

- Gas Turb – a code developed by a former MTU Aero Engines gas turbine performance engineer in his spare time. This program is GUI based with analysis based on open literature methods, working from predefined engine configurations [64]. These methods are widely accepted and of the desired fidelity.
- NPSS (NASA Numerical Propulsion System Simulation) – A NASA Glen Research Center developed code [65], designed to provide a full engine performance simulation from the lowest to the highest fidelity. To improve the fidelity the code can be used in conjunction with other analysis methods passing information to improve the overall cycle analysis.

To decide between the two for use within the intended integrated design approach, one needs to consider a multitude of factors. The integrated nature of the intended approach tends to favor a code that is developed with that in mind,

as NPSS was. Furthermore, NPSS is widely used by NASA and the American gas turbine engine manufacturers, these being the most likely users of such an approach, especially given the NASA/DoD URETI program.

Conversely, the drive to simplicity would favor the GasTurb system, with it's built in gas turbine models. This feature enables the user to go straight into the analysis of the performance of the engine, rather than first spending time developing and debugging an engine model for analysis. However, this advantage isn't enough to warrant the use of this code especially when considering further factors such as support and adaptability.

The knowledge base for NPSS within the Aerospace Systems Design Lab is very considerable. The code has been used within other NASA projects for some years now. Thus rather than having to contact the designer in Germany via a phone call, as the approach development progresses the author can utilize this internal knowledge base far more effectively and efficiently. In addition NPSS is designed to be used with some that are of particular interest to the author. These codes consider the cooling of the turbine stage and are easily integrated with the tool, the method of which will be approached later in this section. Thus, much time and effort would be saved rather than attempting to integrate the extra analysis with the stand alone tool, GasTurb.

Consequently it was decided to go with the use of NPSS as the cycle analysis tool of choice for the research. Even though the tool requires the development of an engine baseline model before executing the analysis,

additional research efforts with the NASA/DoD URETI framework developed one that was deemed suitable and thus negated any adverse effects on the development and operation of the intended approach. A short description of the tool follows.

3.3.1 Numerical Propulsion System Simulation (NPSS)

As mentioned previously, NPSS is a full engine performance simulation tool used by NASA and industry to predict and analyze the aero thermal cycle of a gas turbine engine [66]. It has been developed to reduce the time, effort, and expense necessary to design and test new gas turbine engines. According to a NASA [67] the end goal for NPSS is: *"create a numerical 'test cell' that enables engineers to create complete engine simulations overnight on cost-effective computing platforms"*. NASA even goes on to claim that utilizing this code will half the development time of a gas turbine engine down to 5 years, along with a similar effect on the development costs [68].

This code is to be used as the performance generation part of the methodology. This provides the user the necessary umbrella for the rapid lifing work, allowing for the calculation of the necessary inputs and then utilizing the outputs from the work to highlight any effects on the overall engine. The following are the main points of NPSS as utilized:

- Low fidelity Cycle analysis
- Generates WATE ++ input

- Internal solvers for other code utilization

The following NASA/GE engine model, E^3, was utilized to provide the baseline for the desired analysis. The model helped provide a link from the part to the system level and visa versa, later in the approach development and utilization.

3.3.2 NASA/GE E^3 Engine Model

Work within the NASA/DoD URETI UAPT program provided a useable engine model as a baseline for the work within the thesis. The General Electric/NASA Energy Efficient Engine (E^3) was chosen as this baseline engine model to use for verification and demonstration of the intended approach. This section describes some of the features of the NPSS model for this engine. Design data was taken from the following NASA reports:

- NASA CR-168070 , Fan and Quarter Stage Component Performance Report [69]
- NASA CR-165558, High Pressure Compressor Detail Design Report [70]
- NASA CR-168289, High Pressure Turbine Component Test Performance Report [71]
- NASA CR-167955, High Pressure Turbine Test Hardware Detailed Design Report [72]

- NASA CR-168290, Low Pressure Turbine Scaled Test Vehicle Performance Report [73]
- NASA CR-167956, Low Pressure Turbine Test Hardware Detailed Design Report [74]
- NASA CR-168211, Integrated Core/Low Spool Design and Performance Report [75]
- NASA CR-168069, Core Design and Performance Report [76]

The engine components and structure of the model file are shown schematically in Figure 36 below. The purposes of the major components of this model have been covered earlier within this thesis. The engine is designed to be a demonstration platform for the high tech energy efficiency devices, available at the time of the tests. Though the development of this engine dates back to the 1980's, it is the only publicly available data source of its type, and certainly the only one available with such a wealth of knowledge. Furthermore in view of the fact that the project for which it was developed was NASA funded, it made sense that this data was used.

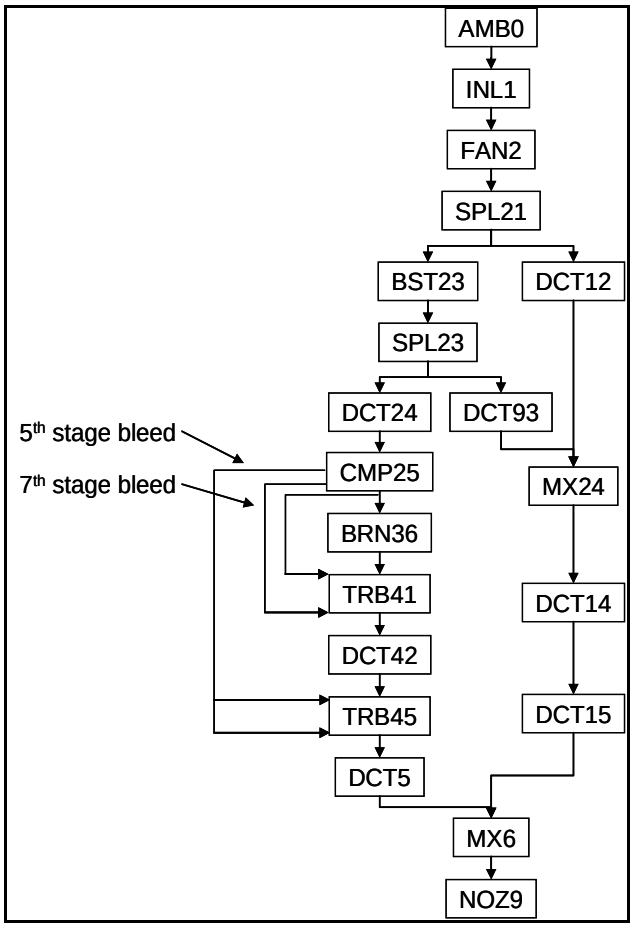

Figure 36: Schematic Diagram of Baseline NPSS E^3 Model.

For the purposes of this analysis, it is sufficient to only consider the core model. Given that the analysis is considering the lifing of the turbine blade, using more than just the core model, though possible, would be an extra burden on this proof on concept research. One need not consider this a loss of analysis integrity; boundary conditions for this core model and required inputs easily represent the effects of system and other level changes up or down stream of the core.

3.3.3 NASA WATE ++

This is a NASA developed code for the estimation of the size and weight of gas turbine engines. The code is designed to handle both small and large engines, thus aiding with the scope of this project. The original code was developed in the 1960's but has been updated over time by NASA [77]. The latest update included a new module for the calculation of turbine disk life, along with greater integration to the NPSS cycle analysis. Working from the E^3 NPSS model used within this analysis, the model produced by WATE++ was matched to the reported test data from the NASA reports [69-76], to produce the following model in Figure 37. A depiction of the actual engine has been included for comparison.

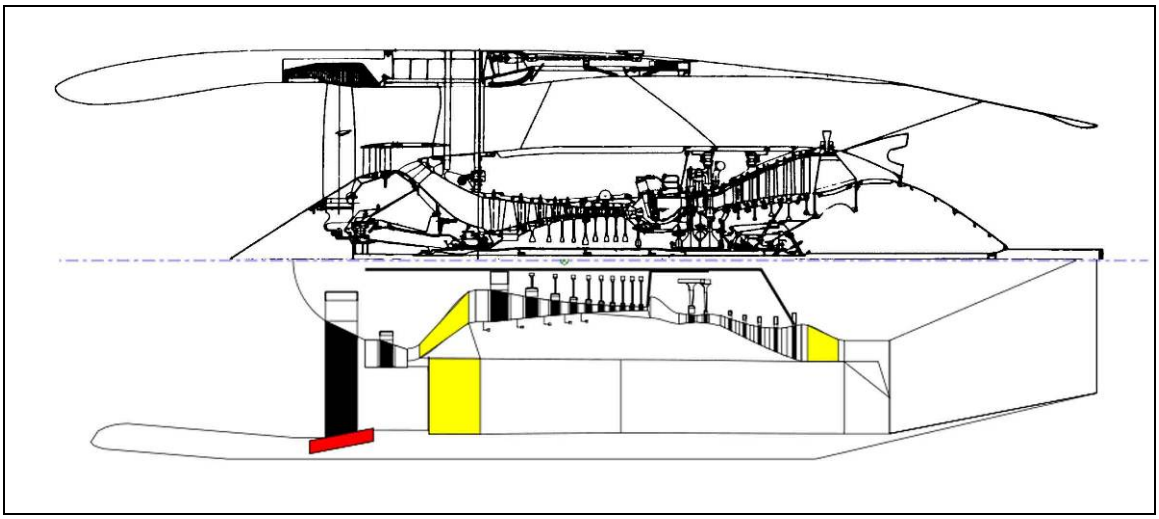

Figure 37: Comparison of WATE ++ Model to E^3 FPS. [35]

The following is a description of the turbine disk capability that WATE ++ contains. This will be used in addition to the blade lifing approach, to provide an added capability to enable the consideration of another critical engine part

within the lifing approach. The basic approach is illustrated in the flow chart in Figure 38.

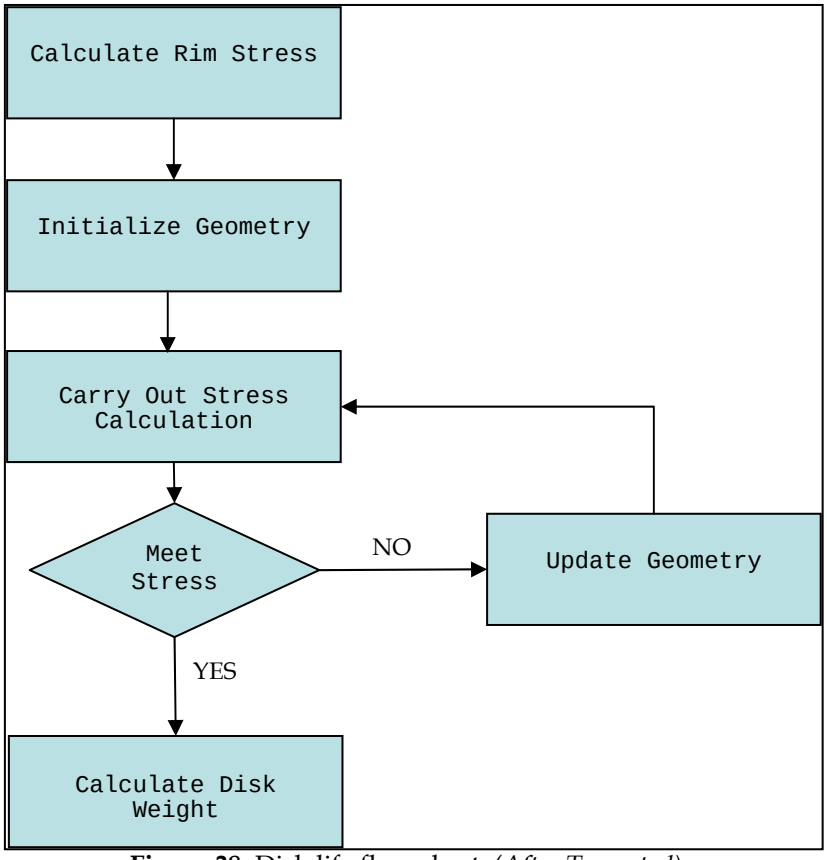

Figure 38: Disk life flow chart. (*After Tong et al)*

Going through the flow chart, the rim stress is calculated using the following equation:

$$Rim\,Stress = \frac{(dead\ weight)(\#blades)(dead\ weight\ CoG)(2\pi\omega/60)^2}{2\pi \times GC \times hub\,chord\,thickness} \qquad (3)$$

The concept of 'dead weight' is illustrated below in Figure 39. Only the portion of the disk inboard of the blade root is considered to carry the stresses, and this is referred to as the live disk. The parts of the disk between the blade roots (posts), as well as the blade roots themselves and the airfoils constitute dead weight.

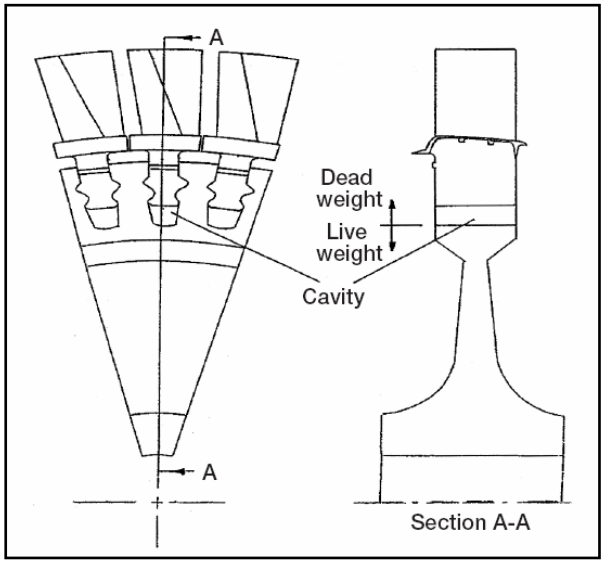

Figure 39: Disk/Blade Assembly. *(After Tong et al) [41]*

The calculation of disk stress is outlined here, taking the geometry data from WATE++ with the new module providing the calculations:

1. Determine CG location of dead weight based on blade weight and geometry
2. Calculate centrifugal stress at outer radius of live disk
3. Initialize disk geometry
4. Call the FEM subroutine to determine stress

a. Divide disk into 5 sections (Figure 40)

b. Divide each section into 9 slices

5. Check to see if constraints are met at current configuration.

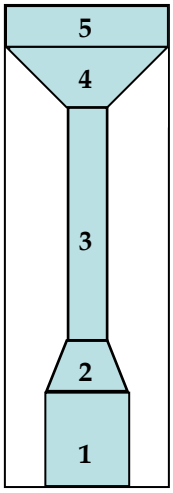

Figure 40: Notional Disk breakdown. (*After Tong et al [41]*)

The steps in the finite difference method applied over the 5 disk sections follow the procedure below:

- Apply boundary conditions at the inner surface of the section
- For each slice beginning with r + dr, (9 in all)
    - Store the radius in "ra"
    - Calculate the thickness of the slice
    - Call temp and material subroutines
    - Fill a row of the "a" matrix
    - Enter a value in the "b" (load) vector

- Calculate the volume of the slice; volumes are stored in "asec" and at each slice, the total volume is added to the model.

Currently this method utilizes tabulated materials data called in the materials subroutine. However it is the intention of this research to update this data with the JMatPro (defined later) data to allow for the latest disk materials. The inclusion of this data will allow, at a later stage, for the capability to be built in for the generation of materials data similar to the blade module. Then the materials composition can be determined from the disk lifing requirements from the materials meta-model.

The temp subroutine is used to establish the thermal boundary conditions at the bore. The temperature distribution is specifically dependant on the type of disk. This module considers the following types:

1. Ring disk
2. Web disk
3. Hyperbolic disk

The stress analysis also considers the thermal stress calculations based on boundary conditions determined previously. The equation below assumes a radial steady-state distribution from Fourier's law of conduction[78]:

$$T = T_{Bore} + \frac{\Delta T}{\ln\left(\frac{r_0}{r_i}\right)} \ln\left(\frac{r}{r_i}\right) - T_0 \tag{4}$$

The distribution of stresses in both the r and θ direction can be calculated using expressions similar to the general theory below [78], assuming a hollow cylinder of outer radius, *b,* and inner radius, *a*, and that the ratio of thickness to the outer radius is small with respect to unity [78].

$$\sigma_{rr} = \frac{\alpha E}{r^2}\left[\frac{\left(r^2 - a^2\right)}{\left(b^2 - a^2\right)}\int_a^b Tr \cdot dr - \int_a^r Tr \cdot dr\right] \tag{5}$$

$$\sigma_{\theta\theta} = \frac{\alpha E}{r^2}\left[\frac{\left(r^2 - a^2\right)}{\left(b^2 - a^2\right)}\int_a^b Tr \cdot dr + \int_a^r Tr \cdot dr - Tr^2\right] \tag{6}$$

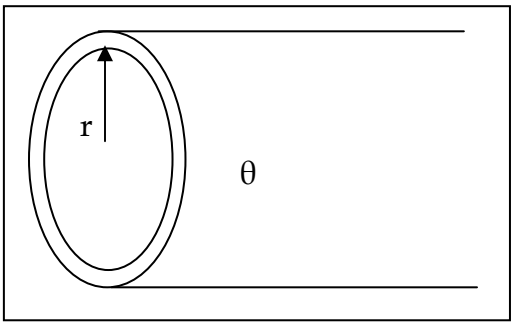

Figure 41: Stress Reference Frame

These thermal stresses are calculated for each of the 5 radial disk sections. The thermal stress term is then added to a total stress term and stored in an array. Once all the matrices are populated the stresses within the disk can be determined. This is done by calling another subroutine and establishing safety margins. Within this then the strain can be determined and thus the life calculated. This stress subroutine is called after each FEM call.

This explanation of the disk life flow chart shows a useful base for lifing analysis. However, it just analyzes the turbine disk and does not consider anything but the weight of the blade for this analysis. Through the use of NPSS and Model Center ™ this disk design capability can be easily integrated within the blade lifing analysis to extend its capability, as previously alluded to.

3.3.4 Velocity Triangle Analysis

In order to fully utilize the capabilities of low fidelity methods it is necessary to create a code to calculate the relative and absolute velocities of the gas flow through the turbine section. Classical gas turbine theory allows for the calculation of the angles of the gas flow through both a turbine and compressor. This approach is more interested in the turbine calculations, so for the sake of simplicity and applicability consideration will only be made for axial flow turbines. This is in light of the fact that expansion of the gases can be achieved rapidly with much less risk of instability.

Looking into utilization of the theory, it became necessary to provide an approach that could be utilized with minimal input. After a broad search though the classical and classically based literature an approach was considered that was based on elements from the works of Fielding [79], Cohen & Rogers [27] and Schobeiri [80]. This approach allows for minimal knowledge of a turbine stage concept, with the rest of the desired information being calculated though an

iterative process. This lends itself very nicely also to a DoE type approach, helping to reduce the number of design variables needed in the analysis.

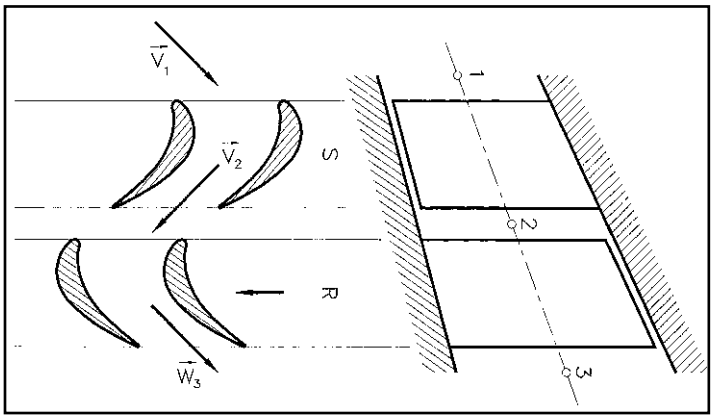

Figure 42: Representative axial turbine stage. *(after Schobeiri [80])*

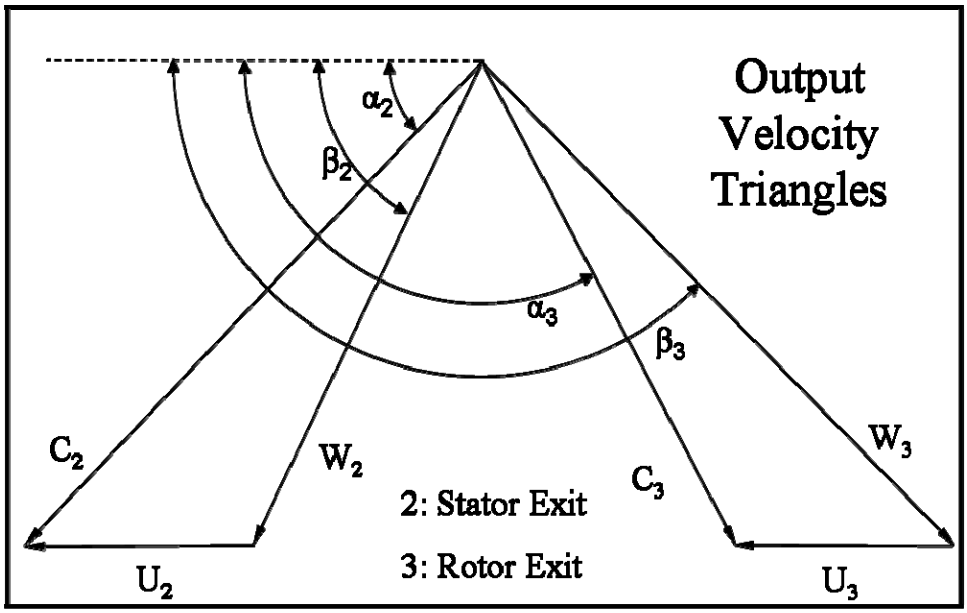

Figure 43: Axial turbine stage velocity triangles. *(after Schobeiri [80])*

The main part of the approach is derived from a method developed by Schobeiri. The method develops 5 dimensionless parameters for centripetal and axial, turbine and compressor stages. Working from Figure 43, these parameters

include Axial Velocity Ratio (μ), Flow coefficient (φ), Radius Ratio (ν), Stage Loading (λ) and reaction (r), as described below:

$$\mu = \frac{V_{m2}}{V_{m3}}, \nu = \frac{R_2}{R_3} = \frac{U_2}{U_3}, \phi = \frac{V_{m3}}{U_3}, \lambda = \frac{1_m}{U_3^2}, r = \frac{\Delta h''}{\Delta h' + \Delta h'' S} \tag{7}$$

With V_m and U from the velocity diagram, and $\Delta h''$ and $\Delta h'$, the specific static enthalpy difference in the rotor and stator can be calculated. Introducing these parameters into the equations of continuity, moment of momentum and degree of reaction, the stage is completely defined by a set of four equations:

$$\cot g\alpha_2 - \cot g\beta_2 = \frac{\nu}{\mu\phi} \tag{8}$$

$$\cot g\alpha_3 - \cot g\beta_3 = \frac{1}{\phi} \tag{9}$$

$$r = 1 + \frac{\phi^2}{2\lambda}\left[1 + \cot g^2\alpha_3 - \mu^2\left(1 + \cot g^2\alpha_2\right)\right] \tag{10}$$

$$\lambda = \phi\left(\mu\nu \cot g\alpha_2 - \cot g\beta_3\right) - 1 \tag{11}$$

The system of equations above (equations 8 through 11) contains nine unknown stage parameters. To find a solution, five parameters must be specified. Appropriate candidates for the first specification are: diameter ratio, $\nu = \frac{R_2}{R_3} = \frac{U_2}{U_3}$; the stator and rotor exit angles, α_2 and β_3; the exist flow angle, α_3; and the stage degree of reaction, r. In addition the stage flow coefficient, φ , can be estimated by inputting information about the mass flow and using the

continuity equation. Likewise, the stage load coefficient, λ can be estimated by employing the information about the turbine power. Once the five parameters are specified, the other 4 parameters can be determined through an iterative process around the previous four equations. In this case, the four parameters calculated fulfill the conservation laws for the particular turbine blade geometry for which five stage parameters were specified [80].

To simplify the process, the previous four equations can be expressed in terms of flow angles α_2, α_3, $\beta 2$ and β_3, and four non linear equations (12, 13, 14 & 15) that this simplification produces, calculate these gas angles within the stage. As before setting five of the nine, then iterating until a solution is reached utilizing a simple solver. This solver can be developed within NPSS to take advantage of an integrated analysis method.

$$0 = \left(\mu^2 \times \phi^2 \times \left(1-\eta^2\right) \times \cot\left(\alpha_2^2\right)\right) + \left(2 \times \mu \times \eta \times \phi \times \lambda \times \cot\left(\alpha_2\right)\right) - \lambda^2 - \left(2 \times (1-r) \times \lambda\right) + \left(\mu^2 - 1\right) \times \phi^2 \quad (12)$$

$$0 = \left(\phi^2 \times \left(1-\eta^2\right) \times \cot\left(\alpha_3^2\right)\right) + \left(2 \times \phi \times \lambda \times \cot\left(\alpha_3\right)\right) + \lambda^2 - \left(2 \times (1-r) \times \lambda \times \eta^2\right) + \left(\left(\mu^2 - 1\right) \times \phi^2 \times \eta^2\right) \quad (13)$$

$$0 = \left(1-\eta^2\right) \times \left(\mu \times \phi \times \cot\left(\beta_2\right) + \eta\right)^2 + \left(2 \times \eta \times \lambda \times \left(\phi \times \mu \times \cot\left(\beta_2\right)\right) + \eta\right) - \lambda^2 - \left(2 \times (1-r) \times \lambda\right) + \left(\left(\mu^2 - 1\right) \times \phi^2\right) \quad (14)$$

$$0 = \left(1-\eta^2\right) \times \left(\phi \times \cot\left(\beta_3\right) + 1\right)^2 + \left(2 \times \lambda \times \left(\phi \times \cot\left(\beta_3\right) + 1\right)\right) + \lambda^2 - \left(2 \times (1-r) \times \lambda \times \eta^2\right) + \left(\left(\mu^2 - 1\right) \times \phi^2 \times \eta^2\right) \quad (15)$$

It should be noted that Schobeiri's angle convention is 90 degrees off from typical convention hence the use of cotangent functions. This was reflected in the diagram in Figure 43.

3.3.5 Meanline Loss Model

In order to build on the abilities of the utilized NPSS engine simulation software, the need arose for a loss model analysis method to be employed. This method is also needed given the velocity triangle analysis that is intended to be employed in the analysis. As was pointed out in the previous section the method also requires a loss model to be used in conjunction with it to improve the accuracy and applicability.

The method needs to consider the turbine through the mean line, a common practice within early engine design. Furthermore, using information gained from the velocity triangle analysis will provide a better understanding of the effects of the gas flow on the turbine. These type of methods have been in development since the 1940's and 50's, with the most famous of these early methods being the so called Ainley & Mathieson approach [27, 81, 82], named after the authors. This is a well established approach spurring other similar work.

First published in 1951, the approach laid out a method by which the performance on flow conditions for an axial flow turbine at the mean diameter

could be estimated. The paper describes the calculation of performance over a wide range of operating conditions, but for an initial proof of concept approach, consideration of fewer points would be more fortuitous. Limiting the scope of this initial approach to that of the engine design point is the most logical, running the lifing analysis over the full engine regime for the thousands of cases I wish to pursue would be unhelpful. It is more important that the process and approach be correct by developing a base case, and then one can expand to explore new avenues at a later date. The extra steps needed would be simply added from the established theory.

Developing the process one needed to conduct a literature search of the most promising models. Most methods are built off Ainley and Mathieson, such as those from Japikse [82], Dunham and Came [81] and Cohen and Rogers [27]. Other model developers charted their own course. Most prominent of these was that of Rao and Gupta [83, 84] from 1980, and Young and Wilcock [85, 86] in 2001.

Based on this literature search, one turned to a model based on the Ainley & Mathieson [87] approach taken from books by Cohen and Rogers [27], and Japikse [82]. This will be used to determine the stage efficiency required for comparison with a simulation process, as previously discussed. Additionally these results could be used for inputs to a possible geometry generation process as well as with those from the velocity triangle method should be the need arise.

The model includes the following common possible performance loss considerations [82]:

- Profile loss – the loss arising from the growth of the blade surface boundary layers, and the attendant surface friction and blockage effects
- Shock loss – due to the shock waves that form in the between the blades under transonic flow conditions
- Secondary flow loss – due to the distortion of the fluid during the turning process in the blade passage, also includes boundary layer effects on the hub and shroud surfaces
- Tip clearance loss – due to fluid escaping from the flow through gaps between blade tip and shroud
- Trailing edge losses – due to wake shed from finite thickness of blade trailing edge
- Reynolds number effects – includes differences between desired operating Reynolds number and empirical data from which performance and loss estimates are made. Relations take into account the complex boundary layer situations found at differing Reynolds numbers.

Combining both of these texts [81, 82], the method begins by considering the two correlations in Figure 44 that show the empirical cascade data for

determining the profile loss coefficients, K_{P1} & K_{P2}. The two charts represent stator ($\alpha_1 = 0$) and repeating stage ($\alpha_1 = -\alpha_2$) blades.

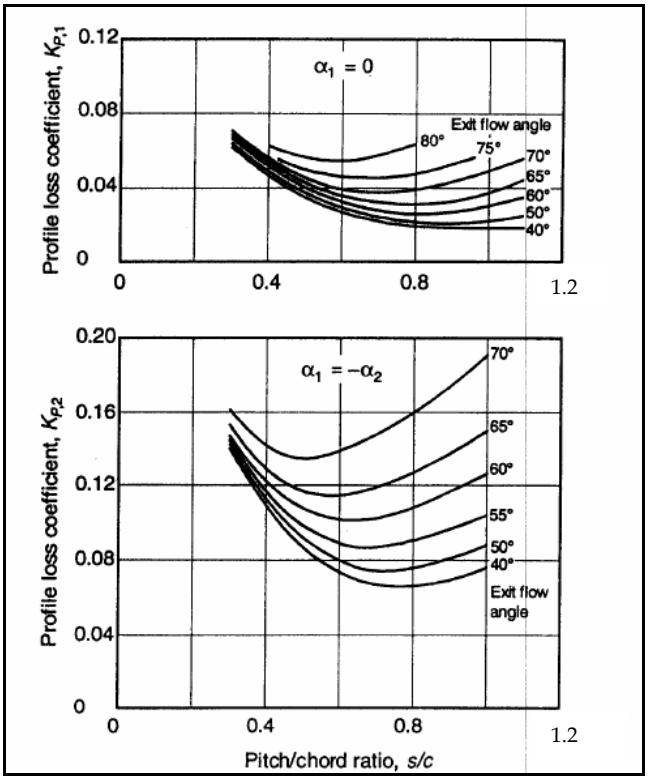

Figure 44: Profile loss correlation of Ainley and Mathieson. *(After Jepikse)[82]*

Both charts are read using the pitch-chord ratio and the exit angle of the blade row, and combined in equation 16.

$$K_{P,M<1} = \left[K_{P,1} + \left(\frac{\alpha_1}{\alpha_2} \right)^2 \left(K_{P,2} - K_{P,1} \right) \right] \left(\frac{t/c}{0.2} \right)^{\frac{\alpha_1}{\alpha_2}} \tag{16}$$

The following correction is applied for supersonic flow (M > 1) [81]:

$$K_P = K_{P,M<1} \left(1 + 60 (M-1)^2 \right) \tag{17}$$

It is convenient within this approach to treat both the secondary flow and tip loss factors simultaneously. Both Sieverding [88] and Dunham [89] provide useful discussions on the secondary flows in turbines, and along with Ainley and Mathieson [87] suggest that the following are factors influencing the losses it causes:

- Blade Shape – the vortices found in the blade passage and beyond are a function of the shape of the blade, obviously due to the turning that this implies on the flow. Therefore some correlation due to blade inlet and exit angles needs to be included.
- Pitch to chord ratio *(s/c)* – affects the loading of the blade, though its effect Sieverding [88] concludes can be offset by a change in the loading pattern.
- Aspect ratio *(h/c)* – occurring mainly near the end walls of the blade passage, Horlock [90, 91] showed a strong influence for smaller aspect ratio blades (less than an aspect ratio of 3), with little influence above that,. Ainley and Mathieson [87] argue that a change in height of the blade, *h*, is the more important of the two factors.
- Radius Ratio – in their article Ainley and Mathieson [87] point to this being one of the more important factors influencing secondary flow loss.

- Inlet boundary layer thickness – Dunham and Came [81] conclude that most turbines operate above the critical displacement thickness. Therefore no effect is seen on the secondary flow loss.
- Mach number – secondary losses appear to decrease with increasing Mach number, due to favorable pressure gradients at high exit mach numbers. In supersonic conditions the influence is uncertain.

Considering the turbine cascade based on similar compressor theory, the following is true (rotor blade notation applied):

$$\frac{C_L}{s/c} = 2\left(\tan\alpha_1 + \tan\alpha_2\right)\cos\alpha_m \tag{18}$$

Where:

$$\alpha_m = \tan^{-1}\left[\frac{\left(\tan\alpha_2 - \tan\alpha_1\right)}{2}\right] \tag{19}$$

Taking these factors into account the combined correlation for secondary and tip losses from the theory [81] is:

$$K_s + K_k = \left[\lambda_s + \frac{B}{AR}\left(\frac{k}{h}AR\right)^{0.78}\right]\left[\frac{C_L}{s/c}\right]^2\left[\frac{\cos^2\alpha_2}{\cos^3\alpha_m}\right] \tag{20}$$

where:

c = True Chord

h = Blade Height

AR = Aspect Ratio (inc. True Chord)

B = Clearance Constant (0.47 for un-shrouded, 0.37 for shrouded) [82]

C_L = Lift Coefficient

s = Pitch

a_m = Mean Angle of Flow

k = Clearance Gap

This is very much based on the theory for compressor blade rows (note the last two bracketed terms in equation 20). The secondary loss component, λ_s, however can be expressed as a function of the following, based on the previous discussion [82]:

$$\lambda_s = f\left\{\frac{\left(\frac{A_3\cos\beta_3}{A_2\cos\beta_2}\right)^2}{\left(1+\frac{r_r}{r_t}\right)}\right\} \tag{21}$$

Where the function, f, is given by the curve in Figure 45:

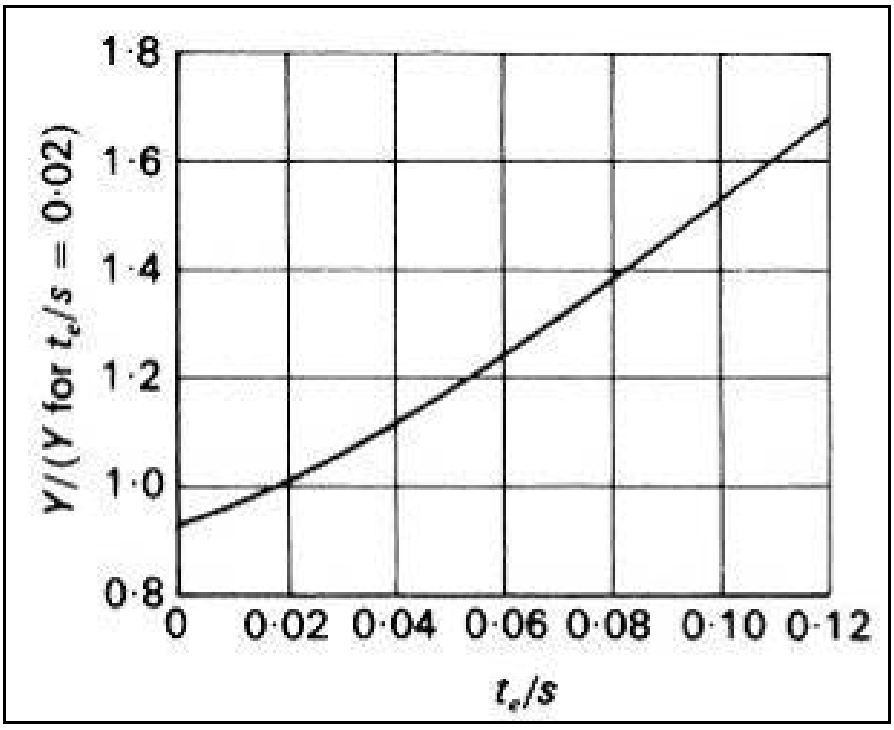

Figure 45: Empirical Relation for *f. (after Cohen)*

This can be simplified using simple momentum considerations [92] and cascade tests, which are then converted to Japiksian co-ordinates [82]. Thus, a more usable form can be developed inline with the rest of the approach as shown in equation 22.

$$\lambda_s = \left(\frac{0.0334}{AR}\right)\left(\frac{\cos\alpha_2}{\cos\alpha_1}\right) \tag{22}$$

Given that real turbine blades have a finite thickness at their trailing edge, corrections for the losses due to this are required. As discussed previously in this section, this is mostly due to the wake vortices that are shed at this point. The trailing edge thickness correction is applied based on the total losses, such that [27]:

$$Y = \left(K_p + \left[K_s + K_k\right]\right) \tag{23}$$

This result is then used in conjunction with Figure 46, to arrive at the loss factor based on the trailing edge thickness to pitch.

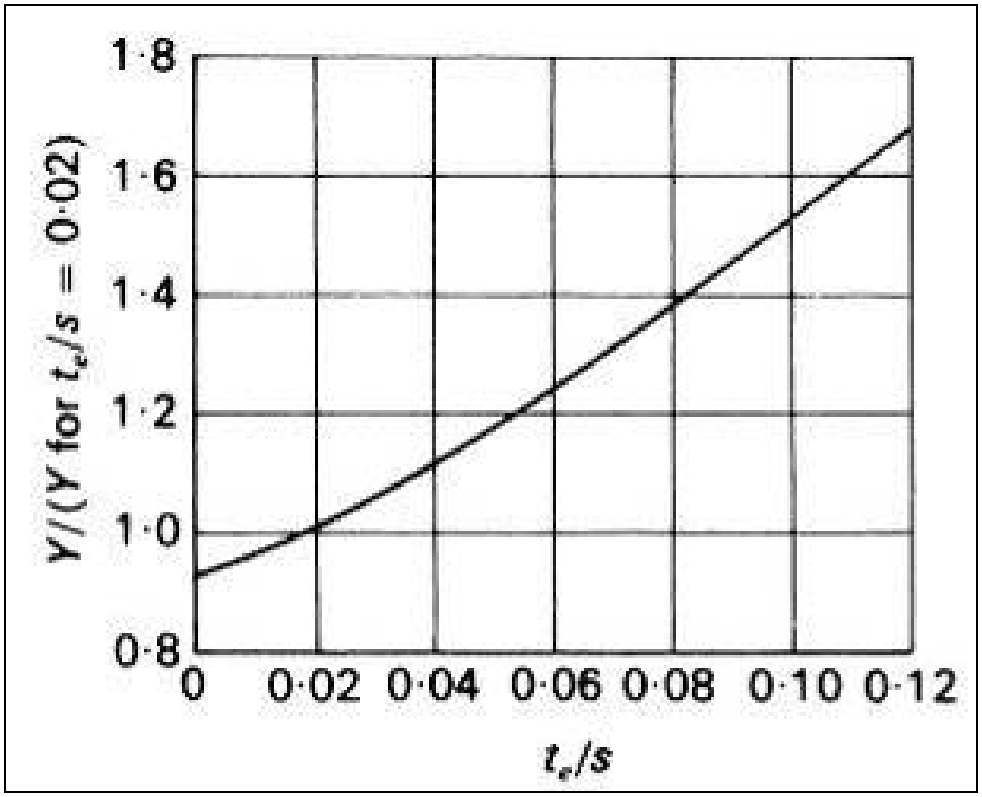

Figure 46: Trailing edge thickness correction factor. *(after Cohen)*

This factor is then applied in the following equation:

$$Y_{tot} = \frac{Y}{Y_{te/s=0.02}}\left(K_p + \left[K_s + K_k\right]\right) \tag{24}$$

The total pressure loss for each blade row can also be calculated based on the definition of the loss coefficient (relative total pressures are used for the rotor).

$$Y_{tot} = \frac{P_{t,in} - P_{t,out}}{P_{t,out} - P_{s,out}} \tag{25}$$

After determining the stage exit conditions based on the calculated losses, the stage efficiency is thus calculated with Reynolds number correction.

$$\eta_s = 1 - \left[\left(\frac{\mathrm{Re}}{2 \times 10^5} \right)^{-0.2} \left(1 - \frac{h_{t1} - h_{t3}}{h_{t1} - h_{t3isen}} \right) \right] \tag{26}$$

Finally, the loss model calculates the flowpath dimensions at the stage inlet, stator outlet/rotor inlet, and stage outlet based on the total pressure, temperature, mass flow, and axial velocity at each station.

However it has to be understood that although this is one of many methods available, it is one of those more commonly in use. Even with that, there are limitations understood with the method that need to be highlighted at this juncture.

- The method isn't perfect, obviously with ± 3% tolerance on stage efficiency [27, 81]. This is acceptable given the need for speed and simplicity that the author is looking for from this type of approach. Often even increasing the fidelity levels of the modeling techniques

does not necessarily guarantee any better accuracy for this metric though would provide more detailed understanding of the conditions behind it.

- As with any method of this lower fidelity type there will always be a compromise between simplicity and accuracy. This goes without saying, however some improvements are made through the utilization of test based curves and the like for corrections to the proposed equations and factors. These curves are dated but are still very applicable, modern design practices still use methods based on this classical approach as suggested by Dunn [93], though with improvements based on company proprietary data, beyond the reach of the author.
- The method loses accuracy at lower blade aspect ratios. Dunham and Came [81] provide suitable corrections to counter this issue. These will be included in this approach to allow for the consideration of all types of aeronautical gas turbines.
- This approach considers the turbine only at its meanline. This is popular with early stage performance calculation methods such as these; however, there can be considerable difference between the conditions at the meanline and those experienced at either the hub or tip of the blade. Approaches do exist to enable the calculation of conditions at these points based on scaling relations. [79]

- Reference data behind reference curves used within this methodology is based on conventional blade profiles. This is a major consideration when utilizing the approach. The users need to be aware of this and take it into account when interpreting the results from their work using this analysis.
- Allows for loss coefficients and efflux angles to vary by blade row with gas conditions. Therefore more accurate than simpler methods [94, 95] which used constant angles.

Interestingly, Ainley and Mathison [87] set out just how long it used to take to carry out these calculations back in the early 1950s: "*It has been found that to calculate the performance of a single stage turbine about two or three man hours of work is required to set down the relevant geometric data, estimate the variation of outlet gas angles with outlet Mach number, and estimate the variation of loss coefficient with incidence on the rotor and stator rows.*" Something that now can be achieved in minutes, in fact it is intended that thousands of DoE cases be run during such a time period for this thesis work.

3.3.6 Blade Cooling Consideration

NPSS can be used with an additional module available from NASA called COOLIT. This NASA developed code is for the calculation of turbine cooling flow and the resulting decrease in turbine efficiency. This code determines the quantity of required cooling flow and the corresponding decrease in stage

efficiency for each row of turbine aerofoils. These values are used to obtain the required compressor bleed flow and the decrease in cooled-turbine efficiency caused by cooling air injection into the hot gas stream. Obviously the calculations will depend on type and effectiveness of a given cooling configuration. This code was initially developed in the 1970's and designed to work with existing NASA analysis codes. To compensate some what for the advancements in technology over the years, the code requires the input of the production year which gives the allowable bulk metal temperature. This is taken from the extrapolation of early alloy data based on a notional improvement.

The code allows for different cooling configurations for each blade row, and the performance of each cooling configuration is represented by the cooling effectiveness, φ, as shown in equation 27.

$$\phi = \frac{(T - T_M)}{(T - T_C)} \tag{27}$$

Where:

T = hot gas temperature

T_M = allowable bulk metal temp

T_C = compressor bleed temp

Hot gas temperature entering a given row of airfoils is the average combustor exhaust temperature incremented to include the following seven effects:

1. Hot spot profile with pattern factor of around 0.3 for first stage stator, 0.13 for all other rows of cooled airfoils in the turbine.
    a. *Combustor Pattern factor (CPF)* is defined as the ratio of the difference between the hotspot and the average row inlet temperature to the difference between the average row inlet temperature and the combustor inlet temperature.

$$\mathrm{CPF} = \frac{\mathrm{T}_{4,\max} - \mathrm{T}_{4\,\mathrm{AVE}}}{\mathrm{T}_{4\,\mathrm{AVE}} - \mathrm{T}_{3}} \tag{28}$$

    b. To allow for improvements over time, COOLIT was updated with CPF calculations taking the following form (for Commercial turbo fans):

$$\mathrm{CPF} = 20.30 - \left(0.01 \times \mathrm{YEAR}\right) \tag{29}$$

2. Correction to the hot gas temperature due to the dilution of upstream cooling air is obtained from a mass average enthalpy from which a revised gas temperature is calculated.
3. *Relative total temperature of hot gas* – The heat transfer to a turbine rotor blade is governed by the relative total gas temperature, T'. As the blade only 'feels' the hot gas velocity relative to the moving blade, W. The difference between the total temperature, T', as the relative total temperature, T'' can be expressed as the following:

$$T'-T''=\frac{\left[V(I)^2-W(I)^2\right]}{2gJc_P} \tag{30}$$

Where,

W = Rotor blade speed

V = Absolute gas velocity

J = Blade polar moment of inertia.

Since the absolute gas velocity, V is greater than W then the relative total gas temperature will be less than the absolute. Therefore, the gas temperature at which the cooling effectiveness is evaluated must be decreased if:

a. The mid span turbine velocity triangles are known,

$$DTREL=\frac{\left[V(I)^2-W(I)^2\right]}{2gJc_P} \tag{31}$$

b. If the velocity triangles are not known, the following estimate is made within COOLIT:

$$DTREL=0.08\times TGAS(I) \tag{32}$$

4. The downstream rows of cooled vanes and blades are subjected to a lower gas temperature since work is previously extracted from the gas stream.

   a. Within COOLIT the power extracted by each stage can be entered with the aide of equation 33,

$$\mathrm{DH} = \frac{1}{2} g J \left(\mathrm{V}_1^2 - V_2^2 + U_1^2 - U_2^2 + W_2^2 - W_1^2 \right) \tag{33}$$

b. If the velocity triangles are unknown then suitable approximations are made. For a two stage turbine a power split of 56/44% between stages is assumed. Such that the second stage aerofoils see a hot gas temperature reduced but an amount:

$$\mathrm{DTPWR(I)} = 0.56 \left(\mathrm{T_{IN}} - T_{OUT} \right) \tag{34}$$

c. For higher stage turbine (N stages), an equal drop is suitably assumed, so that:

$$\mathrm{DTPWR(I)} = \left(\mathrm{T_{IN}} - T_{OUT} \right) \Big/ N \tag{35}$$

5. *Radial temperature profile.*

a. where *I* refers to the Ith row of cooled aerofoils.

$$\mathrm{PROFIL} = \frac{\mathrm{T_{G,MAX}}(I) - T_{G,AVE}(I)}{T_{G,AVE}(I) - T_3} \tag{36}$$

b. The latest version of Coolit updates the assumptions for this, after work by Adamczyk [96] showed that hot streaks migrate not only from the blade suction surface to blade pressure surface but also from blade hub to tip due to the gas density gradient within the gas flow.

c. The analyst can enter a radial profile for each row, with a default value of 0.10. This assumes that CPF is attenuated by half across the first stator.

6. *Safety factor* - The gas temperature used to determine the required cooling flow is first increased by a default value of 150 R to provide a safety factor for the cooled turbine airfoils. This can be altered should an assurance of the exact gas temperature is available.
7. *Yearly rate of improvement of materials technology* – as previously mentioned to account for improved materials properties for given technology years, the analyst can enter a specific YEAR(I) of technology for every row of aerofoils. This allows the representation of specific materials. These values are then used in the following equations to give the allowable metal temperature [96]:

$$TMETAL(I)=\left[-\frac{1}{8}\times YEAR(I)^2+505\times YEAR(I)-507677.5\right]-100\left[Log_{10}(ELIFE)-4\right] \quad (37)$$

Where,

ELIFE = desired life of the turbine blade.

This equation may be replaced with equations derived directly from the material properties of the material. Life can then be calculated at that temperature and iterated until an acceptable life/temperature is achieved.

COOLIT now has the capability to handle Thermal Barrier Coating on all of the included cooling configurations. The code assumes a 30 F per mm of TBC temperature drop, based on research by Dr R. Miller [96]. Thus the TBC can be used either to lower the blade surface temperature at the same cooling flow or to maintain the blade surface temperature but at a reduced cooling flow, or a combination of the two.

To determine the allowable bulk metal temperature, a specific TBC thickness, COAT(I), can be specified for each row (I) of turbine aerofoils. This will have the effect of adding 30 F per mm of allowable bulk metal temperature that is used for the calculation of cooling effectiveness. This will lead to a lower required cooling flow and is expressed in COOLIT as follows:

$$DTCOAT = 30 \times COAT(I) \tag{38}$$

The algorithm comes with eleven cooling configurations. However, much research is underway within the gas turbine manufacturers to come up with improved and more efficient cooling methods. The included configurations are depicted in Figure 47.

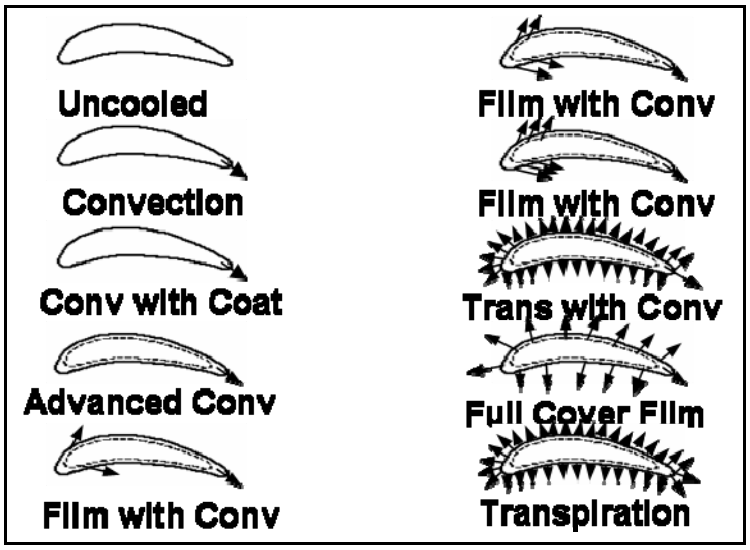

Figure 47: COOLIT cooling configurations. (NASA)[16]

Therefore COOLIT can cope with non-included methods such as [97] through the definition of a cooling effectiveness factor, φ. The analyst can input the factor, FACTOR(I) that relates the cooling effectiveness of a more advanced blade to a reference blade. If a cooling effectiveness and a corresponding cooling flow rate are known, then FACTOR(I) can be calculated as follows:

$$FACTOR(I) = \frac{\left(WC/WG\right)}{\left\{0.022\frac{\phi}{1-\phi}\right\}^{1.25}} \tag{39}$$

A default of 1.4 is suggested in the accompanying NASA report [16].

Dimensionless Cooling Flow, reflecting the 0D nature of this algorithm, after the cooling flow factor and the cooling effectiveness have been evaluated for the correct temperatures the dimensionless cooling flow can be calculated:

$$\frac{\mathrm{W(I)}}{\mathrm{WG}} = FACTOR * 0.022 * \left(\frac{\phi}{1-\phi} \right)^{1.25} \tag{40}$$

Where,

FACTOR = relative cooling flow, taken from tables in report [16].

Derived from a heat balance across the surface of a turbine blade, turbulent flow is assumed for both the hot gas and the cooling air. Further corrections are made to take into account the likes of end wall, shroud and disk cooling, and leakage. For this the dimensionless cooling flow for each row is increased by $4/3$. Though this figure obviously varies by engine, comparisons have shown this to be a reasonable assumption [16].

The efficiency of the cool turbine is then calculated within COOLIT. Initially the uncooled stage efficiency, EFF2, is calculated from the uncooled turbine efficiency, EFF1. The code assumes all uncooled-stage efficiencies and all stage pressure ratios are equal [98].

$$EFF2 = \frac{1 - \left[1 - EFF1 \left\{ 1 - \pi_t^{\frac{\gamma_t - 1}{\gamma_t}} \right\} \right]^{\frac{1}{N}}}{1 - \pi_t^{\frac{\gamma_t - 1}{\gamma_t N}}} \tag{41}$$

Where:

π_t = turbine pressure ratio

The decrease in thermodynamic efficiency of the turbine stage due to the cooling flow is calculated using the dimensionless cooling flow previously calculated. This decrease is equal to the product of the dimensionless cooling flow and the uncooled-stage efficiency. The cooled stage efficiency, EFF3, is calculated by subtracting the change in stage efficiency from EFF2:

$$EFF3 = EFF2 - \frac{\mathrm{W(I)}}{\mathrm{WG}} \times \nabla V \times EFF2 - \frac{\mathrm{W(I+1)}}{\mathrm{WG}} \times \nabla N \times EFF2 \quad (42)$$

To conclude the thermodynamic cooled-turbine efficiency, EFF4, the equation again taken from equations in [96], allows for different cooled-stage efficiency for each stage:

$$EFF4 = \frac{1 - \prod_{I=1}^{N} \left(1 - EFF3(I) \times \left\{ 1 - \pi_t^{\frac{\gamma_t - 1}{\gamma_t N}} \right\} \right)}{1 - \pi_t^{\frac{\gamma_t - 1}{\gamma_t}}} \quad (43)$$

This process loops until the desired blade life is achieved through the increasing or decreasing of the non dimensional cooling flow. With some further work this result can be linked into NPSS and the effect on the whole engine can be observed. Such as the loss of cooling flow etc, by passing information amongst the analysis constituents.

3.3.7 Materials Modeling

Charts are often used to help in the selection of suitable materials, and most used are similar to the ones proposed and utilized by Ashby [99]. These group the material possibilities using differing properties to separate and identify the best family of materials [100]. Such a plot is included in Figure 48 below to illustrate such a study, and one can gather from this chart that these studies have limitations. For an integrated approach such as this an approach based on charts of this kind would not be suitable, and thus a different approach is called for.

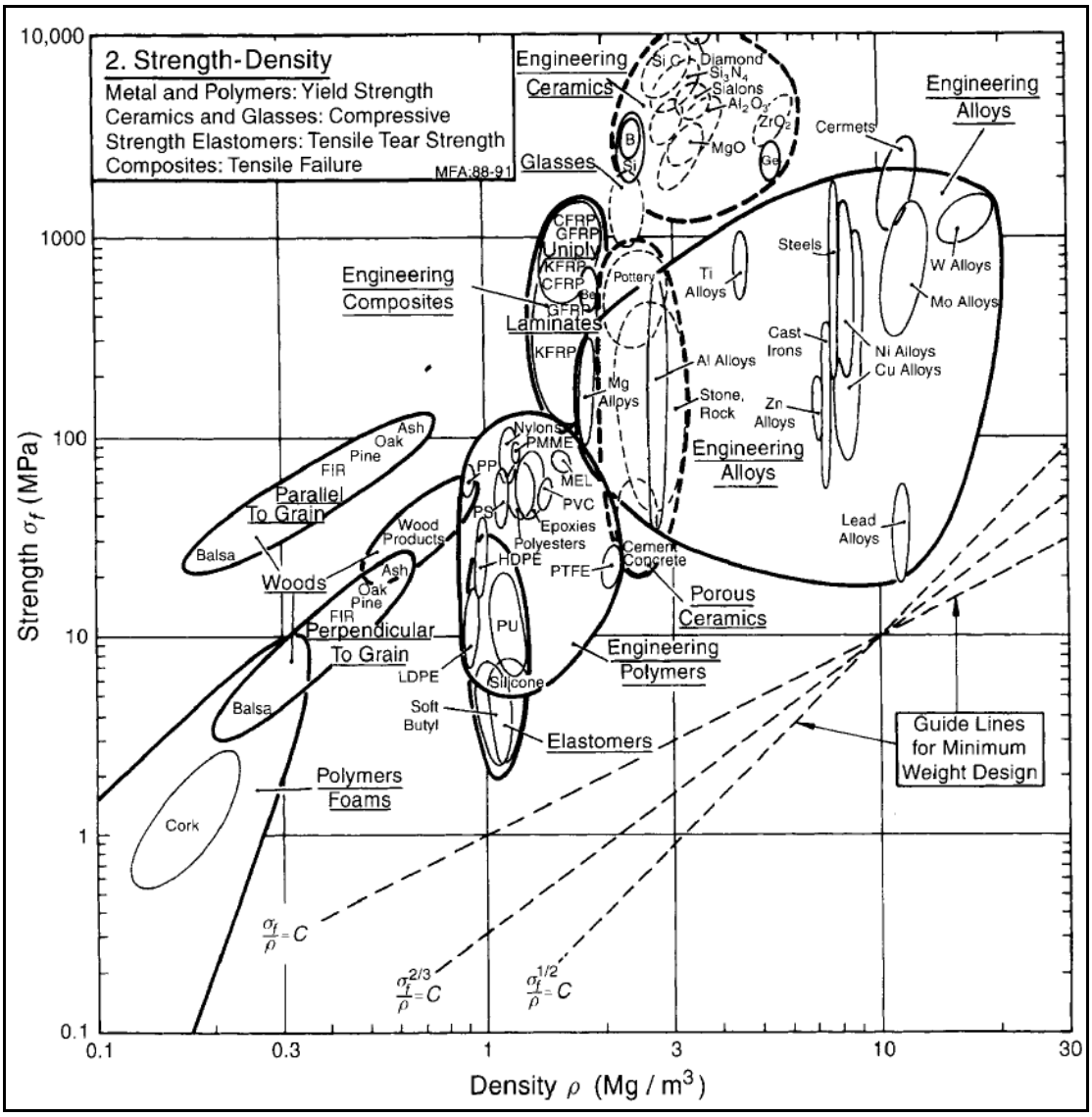

Figure 48: Materials Classification Chart (Strength against Density). *(After Ashby)* [101]

Seeing that the materials property study is running concurrently with this thesis work under the umbrella of URETI, there is a need for a material database to use during the application of the methodology. This took the form of existing metallic properties gathered from publicly available metallic data bases, for the work presented during the Year 3 review for NASA/DoD URETI [53]. These materials are all nickel based super alloys and all relevant properties are known

over the temperature ranges in question. The materials included were all taken from the limited number which were publicly available for the alloy manufacturer Special Metals ™ [102], or derivatives thereof, run through JMatPro, they are as follows (for full chemical compositions see Appendix D) :

1. Waspaloy
2. Waspaloy derivative
3. Waspaloy derivative
4. Nimonic115
5. Rene41
6. Udimet700
7. IN713LC
8. MarM002
9. MarM002 derivative
10. Astroloy derivative
11. Rene41 derivative
12. Udimet 700 derivative
13. Nimonic derivative
14. Waspaloy derivative
15. Arbitrary Material
16. Rene41 derivative
17. Udimet 700 derivative
18. Nimonic derivative

19. MarM002 derivative

20. Waspaloy derivative

The data is to be stored in a Microsoft Excel spreadsheet and accessed through a simple table look up via Model Center. This format simulates a typical DOE input that is anticipated from the materials meta-modeling generated by the materials sub task group. This will provide a reduction in lead time once the information is truly available, and is only meant as a stop gap measure until the composition based materials model developed by Mr Chul-Hwa Hong is available. With this rather than just material types, a full exploration of the material design space will be possible whilst exploring that of the turbine itself.

Table 2: Nominal chemical composition ranges of Nickel based Super-alloys [103].

Composition	Min	Max	Composition	Min	Max
Ni	(balanced)	(balanced)	Ru	0	4.5
Al	0	7.1	Si	0	0.5
Co	0	20	Ta	0	16
Cr	2	30	Ti	0	7.3
Fe	0	40	W	0	18.6
Hf	0	0.95	Zr	0	0.2
Mn	0	0.5	B	0	0.2
Mo	0	14.5	C	0	0.35
Nb	0	6.5	N	n/a	n/a
Re	0	6.1			

The input of materials composition, whose heat treatment temperature and metal operating temperature ranges are provided in Table 2, is then

furnished with the material properties at the temperature. This is achieved through the use of extensive neural networks based around the use of JMatPro™ and other materials considerations. Further explanation of this can be found in Mr Hong's work [104].

3.3.8 Heat Transfer Analysis

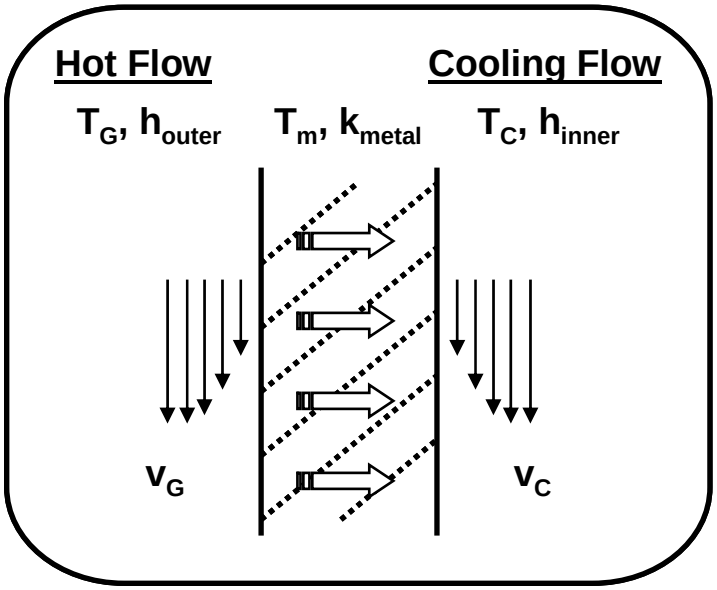

Figure 49: Notional turbine blade heat transfer problem.

The development of a physics based environment has worked towards answering of the hypothesis and research questions posed in chapter two. Thus as one works their way down to the part level through the overall methodology as set out earlier within this chapter, now moving to considering hypothesis four. Hypothesis 4 calls for the investigation of the stresses and other contributory factors in order to fully appreciate creep life of the turbine blade. This needs to be

investigated within the mandate of hypothesis three, the rapid physics based analysis that is being developed within this chapter.

In line with the fidelity levels used so far within this approach, the desire to calculate the bulk thermal stress for a turbine blade drove the need to develop a method for the calculation of the temperatures at points around the blade. Considering this, one has to make trades between the level of fidelity that you can afford. Low fidelity thermal stress calculations involve the calculation of the thermal gradient across the material in question as shown in Figure 49. This also takes into account the thermal properties of this material in the form of Poisons Ration, α, and Expansion Coefficient, as shown in equation 44:

$$\sigma_{Therm} \approx \alpha E \Delta T \tag{44}$$

3.3.8.1 Low Fidelity Thermal Analysis

Working within the framework of this low fidelity analysis method, an approach to discover the most useful and useable means to calculate the thermal gradient within the rotating turbine blade is required. Raymond Colladay [105] of NASA provides a simplified 1-d method for approximating cooling requirements based on different cooling methods. The schematic of which is shown in Figure 50.

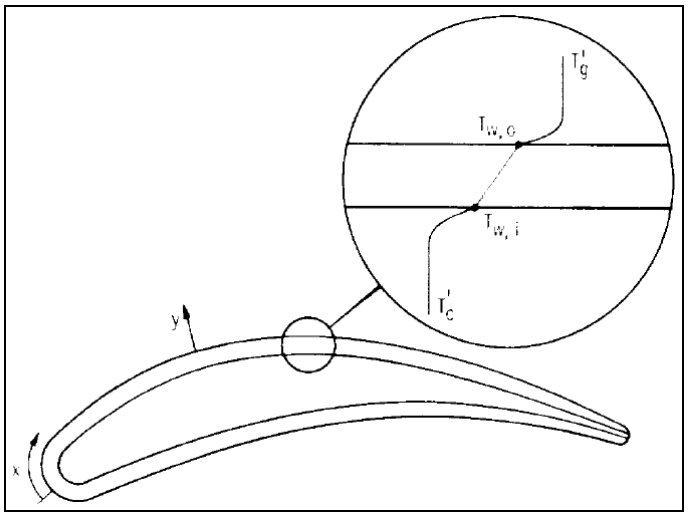

Figure 50: Simplified 1-d turbine blade aerofoil model. *NASA*

This model utilizes 1-d approximations to boundary layer equations, assuming the heat transfer coefficient on one of the sides is approximated by a flat-plate correlation for a cylinder, to yield results very similar to more complex calculations given the insensitivity of the Stanton Number to pressure gradient. This model also provides the gas temperature at the wall, and although a constant temperature is assumed allowances are made for turbulent flows. The calculated heat transfer coefficients take the form:

$$h_{x,x} = 0.332 \frac{k_g}{x} \mathrm{Re}_x^{1/2} \mathrm{Pr}^{1/3} \tag{45}$$

And for turbulent flow:

$$h_{g,x} = 0.0296 \frac{k_g}{x} \mathrm{Re}_x^{0.8} \mathrm{Pr}^{1/3} \tag{46}$$

With the ability to calculate the temperature at both wall surfaces, a better idea of the stress caused by the temperature gradient can be achieved. Although these temperatures will also depend on the thickness and the materials thermal properties, this approximation still provides a much better solution than what is presently used.

However, issues were raised with utilizing this approach when using COOLIT for other aspects of the design and with the accuracy of the flat plate assumptions necessary for the determination of the heat transfer coefficients. Considering that the whole methodology is aimed at the mean-line type low fidelity approach, the level of geometric definition required for this heat transfer determination is more than one would desire. The current model uses the geometry generation purely for area calculation, but based on current blade geometries some of the best geometries can be quite extreme. All this pushes the assumptions for the flat plate analysis beyond acceptable ranges.

Similarly COOLIT requires the user to fix the desired blade bulk metal temperature which is used to calculate the required cooling flow and efficiency, as explained in section 3.2.6. Thus utilizing a technique whereby the wall temperatures are calculated outside of the NPSS/COOLIT regime requires that the desired bulk temperature is set before the cycle analysis. This is to ensure that the calculated temperature and the bulk temperature for COOLIT are the related. Since this material temperature is required for the analysis even before the heat transfer coefficient would be calculated.

Taking a closer look at COOLIT, showed that it had allowances for Thermal Barrier Coating (TBC) thickness and thermal properties, increasing the complexity of the thermal equations. Therefore working with the bulk metal temperature, a method for the calculation of the blade wall temperatures was researched. In addition given that the blade design is considered at the design point, steady state constant temperature assumptions can be made.

The fact that using the blade bulk metal temperature as a heat source enabled the consideration of only the internal wall temperature. This greatly simplified the problem; now an internal wall temperature and therefore stress can be calculated without the need for stretched flat plate assumptions. Treating the cooling flow ducts within turbine blade as a smooth circular pipe, lead to the use of fully developed pipe flow theory to enable the calculation of the cooling air heat transfer coefficient, a notional example of which is show in Figure 51.

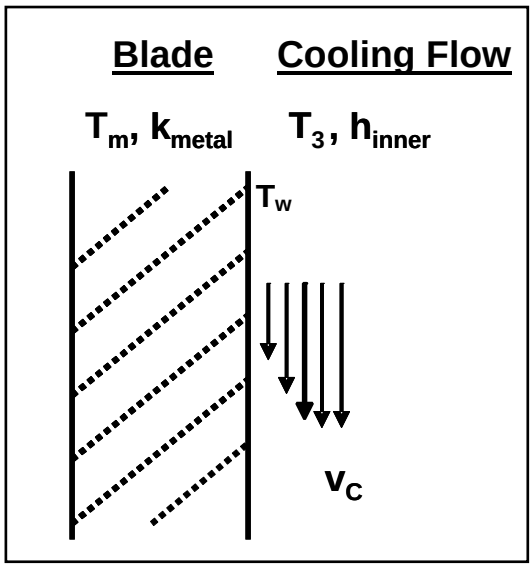

Figure 51: Notional heat transfer model.

Utilizing 1-d approximations to boundary layer equations and internal conduction, assuming the heat transfer coefficient on the cooling side is approximated by this fully developed pipe flow, to yield results very similar to more complex calculations. This provides the gas temperature at the wall on the cooling side. Constant temperature is assumed at the material mid line and allowances are made for turbulent flows within the assumed pipe, in line with accepted theory [93]. Therefore calculated heat transfer coefficients are taken from calculation of the Nusselt Number using the Dittus-Boelter Equation[106]:

$$Nu_{FD} = 0.023\,\mathrm{Re}_D^{4/5}\,\mathrm{Pr}^{0.8} \tag{47}$$

Where the heat transfer coefficient, h takes the form [107]:

$$h = \frac{k.Nu}{D_H} \tag{48}$$

Where the approximate hydraulic diameter, D_H is given by [107]:

$$D_H = \frac{4A}{U} \tag{49}$$

With the ability to calculate the temperature at the wall surface provides the designer a better idea of the stress caused by the temperature gradient. This will depend on the thickness and the materials thermal properties but will provide a much better solution than the present one. It is intended that an approximation of a suitable thickness can be made based on the cooling type and applied using the designers experience easily within the proposed methodology.

3.3.9 Stress Analysis

One of the most important sections of the modeling and simulation environment is the calculation of stress. Choosing the right method by which to calculate the stress and therefore the life of the part is critical. One must consider not only the most common modes of failure see section 1.4.4, but also the desired output from the analysis and the desired level of fidelity. Using expertise from Cohen and Rogers [27], amongst others [108] this work enables the most appropriate means of calculating the blade stresses at the desired lower fidelity.

The most detailed method to calculate blade stresses would involve full 3D FEA analysis through the likes of the ANSYS suite of software. The designer can then isolate the regions of highest stress at the design point, based on the boundary conditions from the downstream analysis and requirements. This type of analysis combines all the differing forms of stress to reach a solution, taking into account the thermal, aerodynamic, and structural effects of the operation of the engine at its design point. This data then can be compared with material property information to provide its rupture life at the operating temperature.

It is understood that this figure would be conservative even with the most complete stress analysis, since the engine would not be operating at its design point for the whole of its cycle. Calculating stresses over the full flight regime is both time consuming and unnecessary. Considering that the analysis is also intended to be at lower fidelity, the validity of the results means that performing

a full work up like this would not be pertinent. Considering just one condition does help to provide a good indication of the useful service life of the blade.

Working at the lowest fidelity means that to improve the accuracy the major stress components of the blade, each component needs to be addressed separately then combined once calculated to provide a total stress. Cohen and Rogers [27] suggest the consideration of both the aerodynamic forces through a "gas bending" and the rotational forces through a centrifugal stress.

3.3.9.1 Gas Bending Stress

The gas bending stress occurs when considering the bending moments in the blade due to the aerodynamic loads experienced. These loads arise due to the change in the flow angular momentum in the tangential direction, producing a bending moment about the axial direction, M_w. In addition there is a moment about the tangential direction M_a, due to a change in momentum in the axial direction. Resolving these bending moments into components about the principle axes of the blade [109]:

$$\sigma_{gb} = \frac{x}{I_{yy}}\left(M_a \cos\phi - M_w \sin\phi\right) + \frac{y}{I_{xx}}\left(M_w \cos\phi + M_a \sin\phi\right) \tag{50}$$

Twisted and tapered blades need to be considered in sections of height, δh, and the moments calculated from the averages over each section. This stress will be tensile on the leading and trailing edges and compressive in the back of the blade. In general the maximum stress is found to occur at either the leading or trailing of the root section. A useful approximation by Cohen and Rogers [27]

suggests for early design purposes to make use of the fact that the Principle X axis deviates little from the axial direction so the following can be approximated:

$$\left(\sigma_{gb}\right)_{\max} \approx \frac{\dot{m}\left(C_{W2m} + C_{W3m}\right)}{n} \times \frac{h}{2} \times \frac{1}{zc^3} \tag{51}$$

Where:

n = number of blades

z = is the smallest value of the root section modulus $\left(I_{xx}/y\right)$ of a blade with unit chord.

H = blade height

m = meanline fluid flow

The whirl velocities $\left(C_{W2m}\ \&\ C_{W3m}\right)$ are also considered at the meanline. In a more practical form as suggested by Japikse [82] the approximation is implemented as follows, with h_2 and h_3 taking into account the average height of the blade:

$$\sigma_{gb} = \left(\frac{\dot{m}}{g} \times \frac{\left(C_{W2} + C_{W3}\right)}{N_{Blades}}\right) \times \left(\frac{h_2 + h_3}{2}\right) \times \left(\frac{1}{z_s\, c_{true}^3}\right) \tag{52}$$

3.3.9.2 Centrifugal Stress

The typical gas turbine rotates at around 10000 rpm . Needless to say that having solid objects rotating at such high speeds puts great stresses on the parts including the blades. Working from simple Euler beam theory [109], the maximum centrifugal stress on the blade can be shown to be [27]:

$$\left(\sigma_{CF}\right)_{Max} = \frac{\rho_{Blade}\,\omega^2}{a_r}\int_{root}^{tip} ar\,dr \tag{53}$$

Where:

ρ_{Blade} = blade material density

ω = blade angular velocity

a = blade cross-sectional area (mid-span)

a_r = blade cross-sectional area (root)

Assuming both a uniform cross-section and the fact that taper reduces the stress by $2/3$ from an untapered blade, equation 54 is derived. The taper in this case is assumed to allow for a cross-sectional area ratio $\left(a_t/a_r\right)$ of between $1/4$ and $1/3$, suitable for preliminary design considerations, as is the stress reduction assumption. [27]

$$\sigma_{CF} = \frac{4}{3}\pi\left(\frac{RPM}{60}\right)^2 \rho_{Blade}\, A_{Annulus} \tag{54}$$

3.3.9.3 Thermal Stress

Naturally one also needs to consider the great amount of heat that is involved within a turbine stage. Thermal stress is caused due to a difference in temperature across a metal. In blade applications this can constitute the difference in temperature between the upper and lower surfaces of a solid blade. However, in the more common case of a cooled blade, the thermal stress is caused by the temperature difference between the outer surface in the heated flow and the inner cooled surface along the cooling channels.

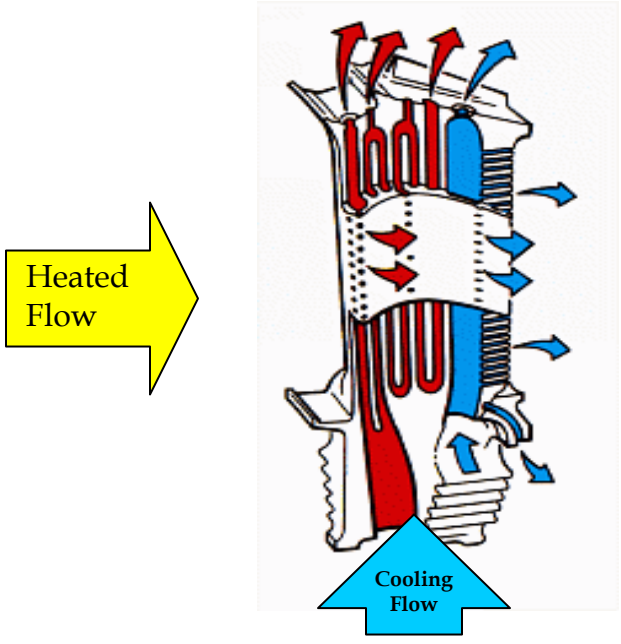

Figure 52: Representative cooled turbine blade

Earlier within this chapter, a method was developed to directly calculate the temperature at the blade inner wall, in view of the fact that the NASA code

COOLIT was being utilized within this approach. This method simplifies the calculation of the desired outputs. Recapping, this code requires the setting of a desired metal temperature then calculates the required cooling flow and subsequent loss in stage efficiency. Considering the internal flow properties and the bulk metal temperature enables this approach to avoid the pitfalls that the use of flat plate type assumptions based on the shapes of blades likely to be considered. The large flow deflections involved with turbine blades tend to push these assumptions to their very limit. The utilized stress equation takes the form of:

$$\sigma_{Therm} \approx \alpha E \Delta T \tag{55}$$

The stress is thus driven by the temperature through the material and the material thermal properties. This equation is the simplest form of heat transfer consideration in line with the rest of the methodology. The internal wall temperature necessary for the calculation of the temperature gradient was derived again using this same heat transfer theory. The equation for the wall temperature, T_W, takes the form:

$$T_W = \frac{\left(h_C \times T_C\right) + \left(k_M / t \times T_M\right)}{\left(h_C + k_M / t\right)} \tag{56}$$

Where:

T_C = Cooling flow temperature (also T_3) (^{o}R)

T_M = Bulk metal temperature (^oR)

h_C = Cooling flow heat transfer coefficient

k_M = blade material heat conduction coefficient

t = blade wall thickness (approximation in inches)

This blade wall thickness approximation was based on the NASA/GE E^3 engine and the cooling flow approximation. Within the heat transfer analysis, the fully developed pipe flow theory approximated the cooling flow tube based on the blade area and a scaling factor linked to the type of cooling chosen. Therefore, a blade wall material thickness approximation, t, should be taken from that, and within this model it takes the form:

$$t = \frac{\frac{Blade\ Area \times (1 - scale\ factor)}{s}}{12} \tag{57}$$

Where:

Blade area = blade area calculated from Prichard method (section 3.2.10)

Scale factor = cooling method based, area scale factor

s = blade circumference (section 3.2.10)

The method for calculating the stresses to be considered within this approach has now been determined. However, utilizing these different stresses individually with the materials creep/rupture life data is neither beneficial nor would it give a good indication as to the final performance of the blade material at the given temperature. Combining these three stresses provides one number

that can then be used with this data, providing a more complete picture of the expected material performance.

3.3.9.4 Stress Combination

Looking at how to combine these stresses one needs to reconsider how the stresses were first derived. This involves considering the principle axes of the stress, the direction of the forces involved and their magnitudes. Rather than developing a completely new and individual solution to this problem it is better to investigate methods already widely accepted. Many methods exist, though the most easily implemented are the now "classical" approaches, developed over the years.

The Tresca failure criterion, postulated by Henri Tresca back in 1864 [110], states that a material under a multi—axis state of stress will yield when the Maximum Shear Stress reaches a critical value. Using this assumption the yield envelope for a 2-D stress field is shown in Figure 53. The shape of this envelope can be derived through Mohr's Circle of Stress and can be found within Megson [108].

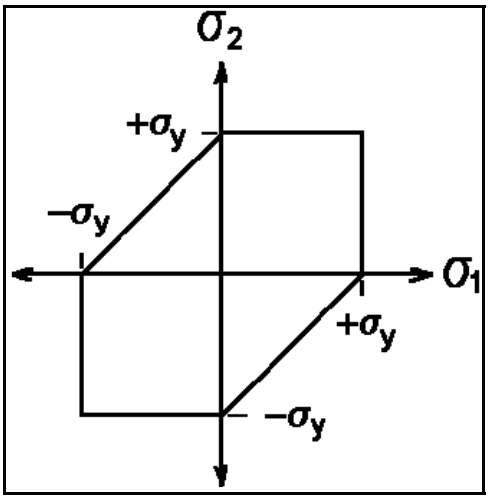

Figure 53: Tresca Yield Envelope. ***(after McGuire)*** **[111]**

Building off this work, Von Mises first postulated in 1913 [112], that a material fails when the distortional energy at a point in question reaches a critical value. This distortion energy can be written in terms of the 2D principal stresses:

$$\sigma_1^2 - \sigma_1\sigma_2 + \sigma_2^2 = \sigma_y^2 \tag{58}$$

On the plane $\sigma_1 - \sigma_2$ the equation represents an ellipse, which has been overplayed with the more conservative Tresca yield envelope to illustrate the relationship, in Figure 54.

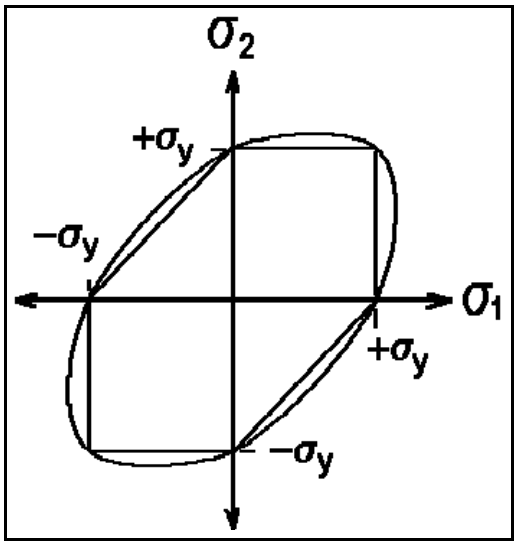

Figure 54: Von Mises Yield Envelope. *(after McGuire)* [111]

This solution provides a single equation (equation 57 below) that describes the envelope, convenient for use in a computer based method such as this. Its ability to capture and bound the principle stresses in a complex stress environment such as is to be found in a simplified turbine blade model. The equation as employed within my approach is shown below:

$$\sigma_{VM} = \sqrt{\frac{1}{2}\left[(\sigma_x - \sigma_y)^2 + (\sigma_x - \sigma_z)^2 + (\sigma_y - \sigma_z)^2\right]} \tag{59}$$

3.3.10 Blade Geometry Generation

Working with the idea of opening up the design process to make it more transparent and provide some guidance for the designer, a geometry generation tool was included in the methodology. This tool needed to be as simple as

possible given both the need for fast analysis and to match the low fidelity of the analysis. Following an extensive literature search, the work by L.J. Pritchard at Williams Aerospace [113], was utilized.

This work breaks the geometry of a turbine blade down into eleven parameters, as shown in Figure 55. These being:

- Aerofoil radius
- Axial chord
- Tangential chord
- Unguided turning angle
- Inlet blade angle
- Inlet wedge angle
- Leading edge radius
- Exit blade angle
- Trailing edge radius
- Number of blades
- Throat

These parameters are used as either design variables or taken from values calculated within the loss model.

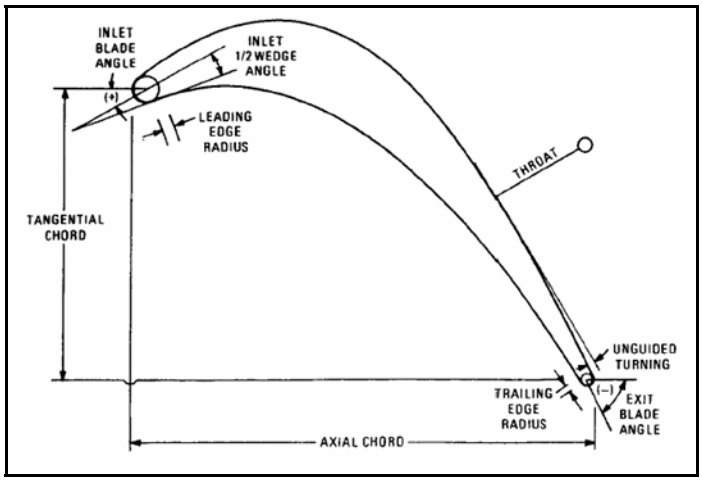

Figure 55: Prichard's Eleven Parameters. *(after Prichard)* [113]

These parameters are used to generate five key geometric points and surface functions, as shown in Figure 56. Circles are then used to close the ends of the geometry.

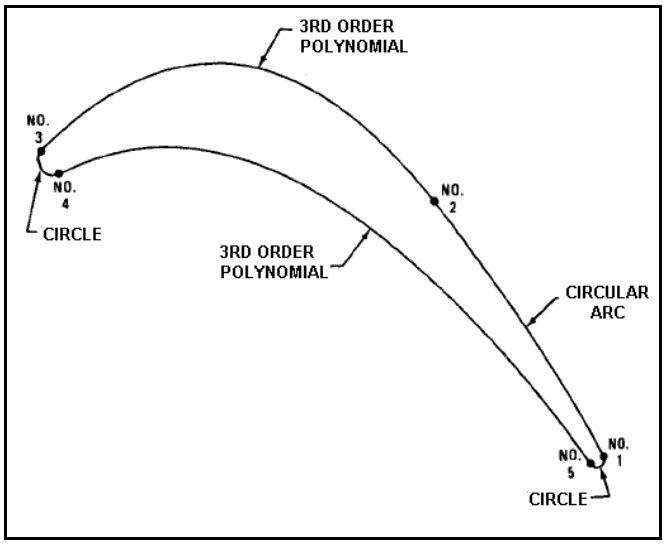

Figure 56: Prichard's five key points and surface functions. *(after Prichard)* [113]

Considering current industry opinion of the geometry model, research within ASDL was undertaken to modify the approach. Under the NASA/DoD URETI UAPT research this work was carried out through Task 2.1.1 to meet with current design standards [114]. The modifications are shown in Figure 57.

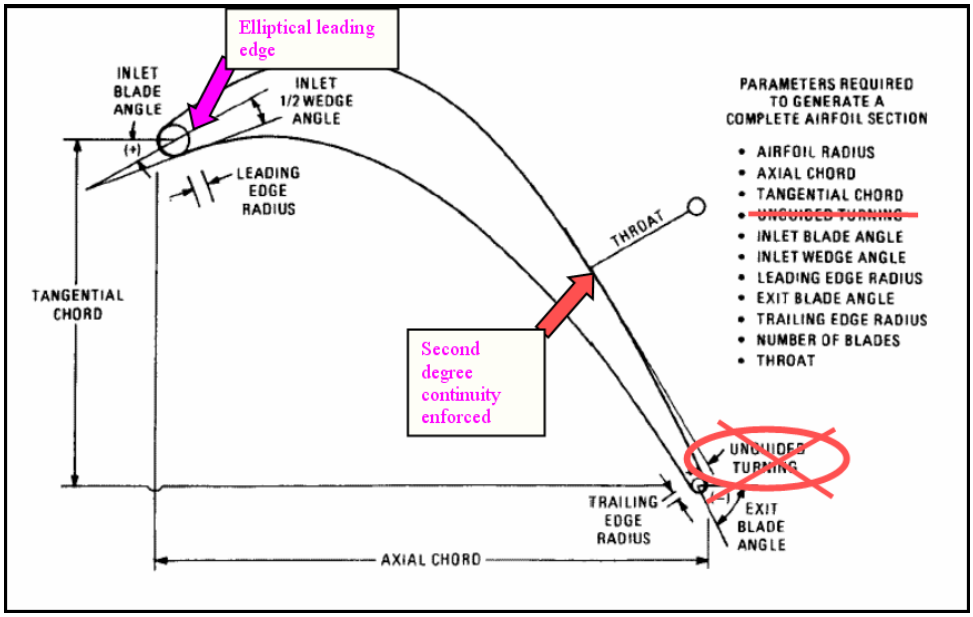

Figure 57: Changes to Prichard's Geometry Model. [114]

The main point of these modifications was to remove the assumption of circular leading and trailing edges. Modern blade designs considerations have moved towards an elliptical leading and trailing edge. Additionally, initial use of the Prichard method within a DoE type approach revealed that improbable designs for the upper blade surfaces could be realized. Working to correct this, the URETI research team headed by my esteemed colleague Mr Chung Lee, looked for solutions through new methods to describe this section of the blade

[114]. The new method they employed now prevents problems with the exterior shape of the blade through the use of improved boundary conditions at junctions with the leading and trailing edges.

As research progressed the need arose for a means to calculate the blade internal area for the improved heat transfer model. The easiest means of achieving this was to utilize inbuilt Matlab functions that enabled the calculation of the blade profile perimeter length and internal area. Because the original code was in Matlab, so only a small amount of extra coding was required. This information was then passed into heat transfer calculations through the Model Center interface. Thus not only is this tool used to improve the visual backing for a design decision but it is also an integral part of the analysis, brought together through the use of Model Center and the integration it's use enables.

3.4 Final Analysis Environment

With a view to the goal of creating a methodology to rapidly assess the life of a turbine blade in a dynamic and parametric manner, a process chart is needed from which the final design of the analysis model can be based. Working from the points raised within this and previous chapters, the process in Figure 58 is being proposed to investigate the validity of the hypothesis and research questions. This is the direct analysis process, which would then be encompassed within the modeling and simulation environment.

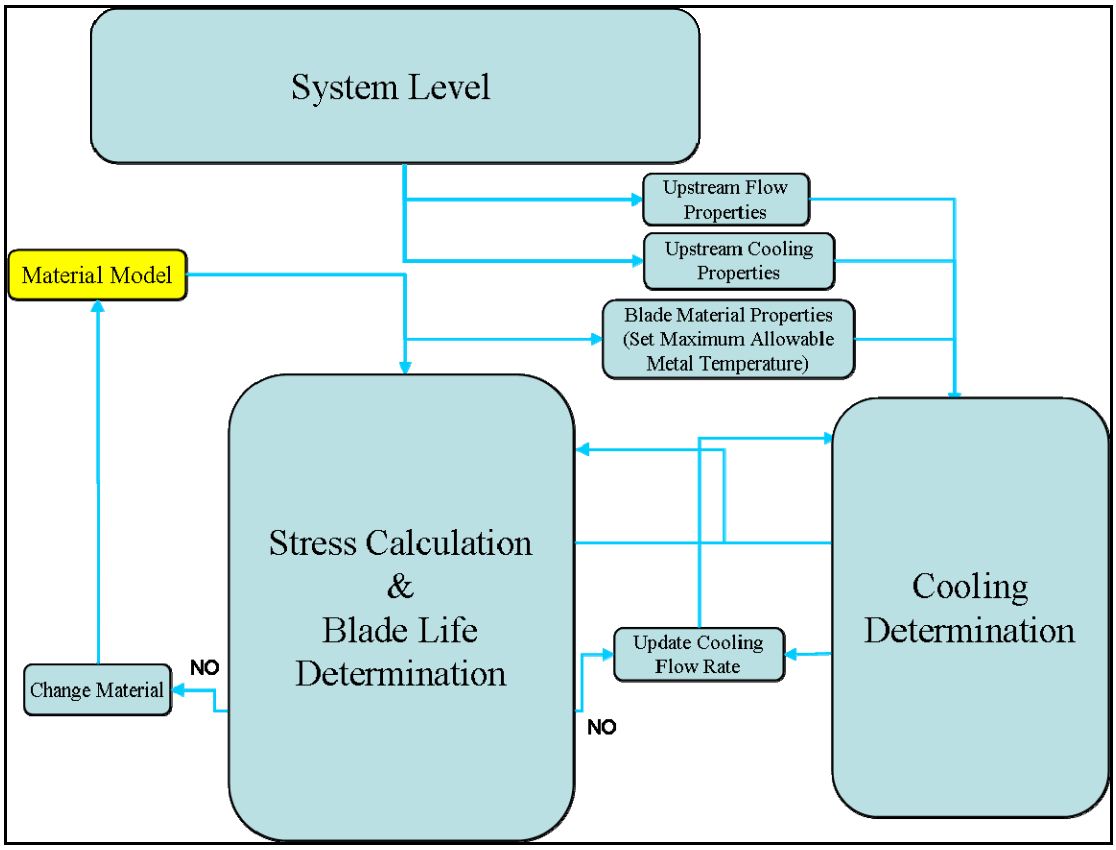

Figure 58: Finalized turbine blade lifing approach.

In Figure 58 the process breaks down into 4 main components:

- System level representation
- Materials
- Stress and lifing
- Cooling determination (including blade geometry)

This breakdown and the steps that this involves are depicted in Figure 59 below.

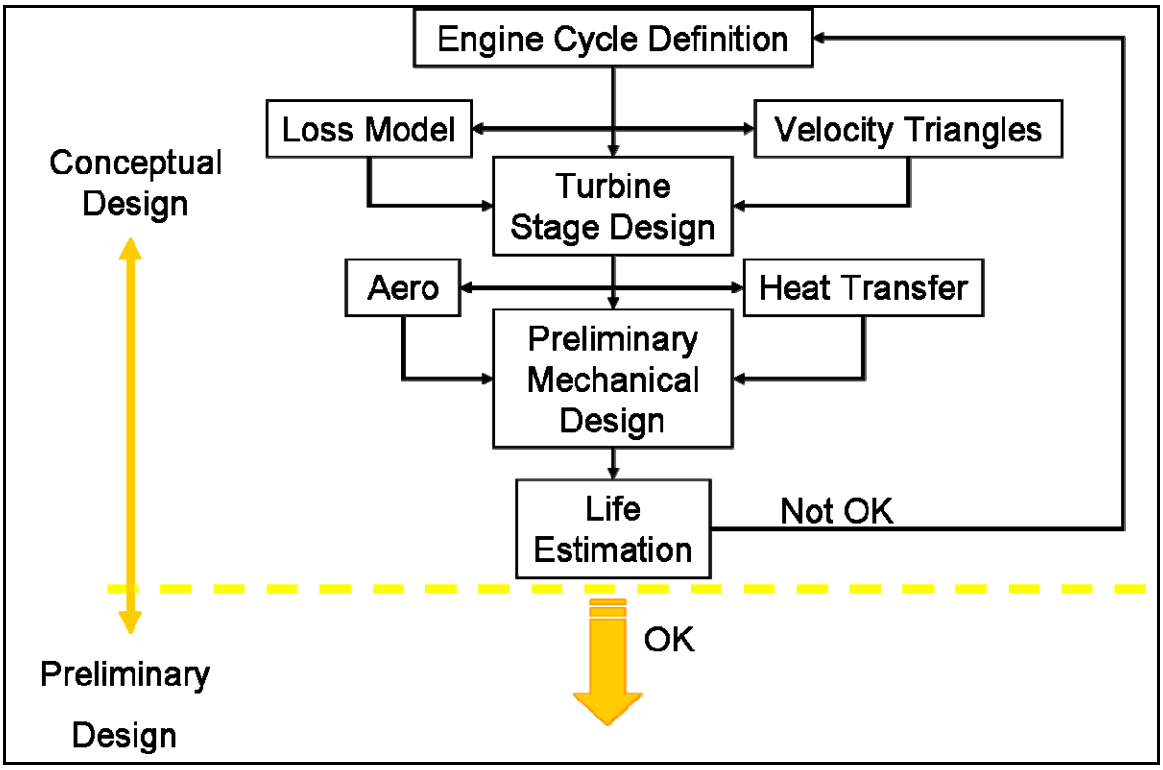

Figure 59: Simplified depiction of analysis model.

The system level process (as shown in Figure 59) encompasses the engine simulation and performance metric generation. The figures of interest are then passed along into the thermal cooling section labeled blade, and also the similar one for the disk. Based on a selected material the stress calculations are then used for life calculations. The actual metrics and numbers passed through this process are deliberately left blank illustrating the fact that the designer has the freedom to pick and choose what he wants to track and optimize for, along with the Life of the blade.

Having decided upon the formulation of the analysis approach, the next step is to assemble said approach. As previously discussed, in line with

hypothesis five, it had been decided to utilize Phoenix Integration Model Center to perform the model integration and construction. This program enables easier linking of codes, passing the data between them instantaneously without having to parse data from output files.

Thus the major part of this stage of the process was identifying the correct variables within the code to pass the information between. Ensuring the correct data flow is essential due to the large number of variables, especially in NPSS. The author found this out on a few occasions, with erroneous results coming from miss-linking and tracking of variables and the approach was validated. This was especially important when implementing the multiple stage consideration capability.

Taking a closer look at the final result the block FSCool in Figure 60 is used to provide the necessary flow information for the heat transfer module, using the NPSS architecture to provide the data. This information is used to calculate the internal heat transfer coefficients for the cooling flow. The different materials models in the figure are actually the the same data based just repeated to ease the integration within Model Center™.

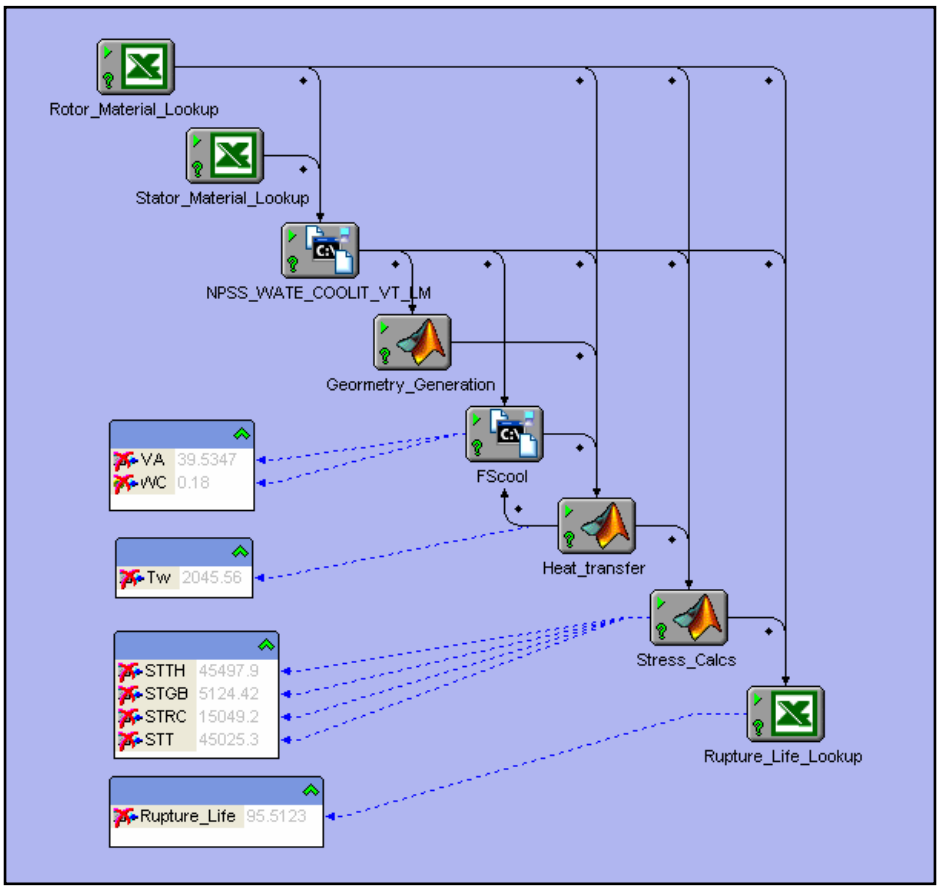

Figure 60: Assembled creep lifing analysis approach.

3.5 Modeling and Simulation Requirements

Having completed the formulation of the creep life analysis environment, one's attention again turns to the research questions and hypotheses for guidance with the commissioning of the rest of the research work. Within the previous chapter, the formulation of the analysis environment touched upon the requirements set through hypotheses one through five. The single integrated environment that has been developed lacks the inherent abilities to perform design space spanning and visualization that is necessary to meet the requirements set forth in hypothesis six.

This final hypothesis calls for the ability of the proposed approach to provide results from samples of a given engine design space to permit the use of surrogate modeling techniques. The use of the surrogate modeling techniques in turn enables the use of visualization techniques from the closed form solutions they provide. In turn permitting a means to consider the creep life of the blade at the part and system levels simultaneously as the hypotheses and research questions call for. In fact consideration for the part life would ideally be considered down to the material composition, should the modeling permit.

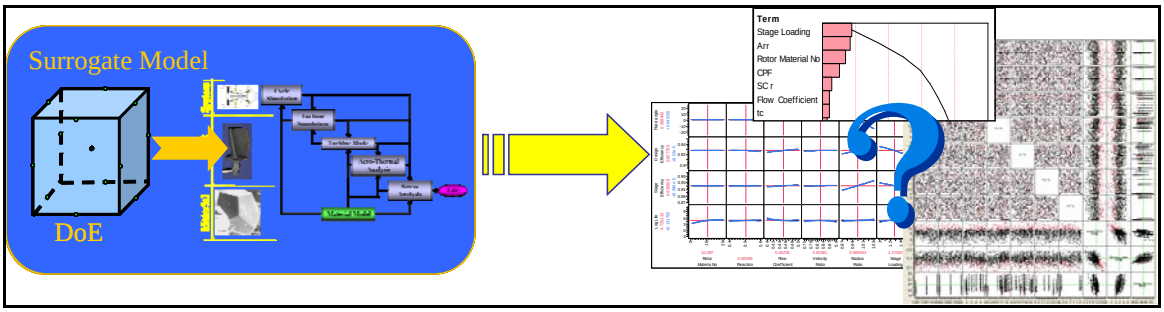

Figure 61: Requirements set through hypothesis six

The following chapter will further investigate the best methods to achieve a means to validate the postulation within hypothesis six. These approaches will follow the simplified ideas depicted in Figure 61, based around the notion of exploring and investigating a design space to provide insight and understanding to the conceptual phase designer.

3.6 Surrogate Modeling

To truly understand the physics behind a design problem such as this within the complex environment of a gas turbine engine, methods to simplify the problem into something manageable is desirable. Coming up with the best solution requires exploring this space necessitating the execution of the code at various design points. Should the studied conditions change then the design would have to be run again, and again and so on. Obviously depending on the fidelity level of the method being used, even just one execution of the code could take anything up to many months to retrieve the desired results. Utilizing methods to represent the time and resource consuming physics based models enables the designer to rapidly explore the effects of any changes in design

variables. This can be done at any time following the formation of these surrogates, allowing the execution of trades on the fly

Surrogate models are simplified models based on the complex analysis used in slower more extensive analysis. The set up for theses surrogates does require the execution of the utilized design codes over the design space, but after this the use of the model is split second within the correct environment. The fidelity of the design tools used for the creation of the environment drive the creation time for the surrogate model. However, as the fidelity of such a method increases, so does the benefit of providing surrogate models to the designer. The opportunity to observe any changes in a design' figures of merit based on alterations of system and design variables in real time, is especially desirable when a full analysis may take months.

This is particularly important when one is considering a wide range of variables and is looking for an optimal design. Running all the possibilities for the optimization would require an inordinate about of time. Beyond the possible time critical decision making often necessary during the early design stages of a project, allowing for quick trades on the fly, greatly improves the long running success of a design. It also provides the designer a better means of proving a business case to the company management or purchaser as to why the chosen design is the best available.

The generation of such surrogate models is described in the following sections. It begins with the decision on which design of experiments to use and continues with one of the most common methods of interpreting the results.

3.6.1 Design of Experiments

In the design of any complex system, there are a large number of variables and the physics behind the system can be too profound or esoteric to be fully understood. Experiments involving large sets of variables can be run using a full factorial combination, but the number of cases required increases exponentially with the number of variables. Thus, when a very complex system of numerous variables is considered, finding an optimum solution by varying each variable one at a time will be prohibitively expensive and time consuming. In this context, Design of Experiments (DoE) was developed in the 1920's for agricultural purposes [115].

DoE is a systematic way to plan, conduct and analyze a series of tests in which the input variables are changed in such a manner to obtain more intelligent information from the results. With the use of DoE, more information can be extracted with less time and money. DoE uses a statistical approach, which predicts the influences of variables and their interactions on the responses without running a full factorial experiment. There have been several methods developed which will be discussed later, but the purposes are same: to reduce

the number of the cases to run while extracting more knowledge from them. With DoE the following can be accomplished [116]:

· Determine the effect of each variable on the response.

· Find where to set the control variables to get the intended value of the response and,

· Find a robust solution so that the variability of the response is minimized.

3.6.1.1 Types of DoE Methods

A short description of a few of the most popular and well know models follow[117]:

· Full factorial Design – As aforementioned, this DoE varies only one of the variables at a time to see the effect of it on the response. Full factorial Design entails 2n number of cases to examine n variables at two levels. The number of cases required, thus, increases exponentially with the number of variables to be evaluated.

· Taguchi method – The Taguchi method uses an orthogonal array to plan the test. This method is very powerful and efficient, especially when the design space is small. Since the Taguchi method assumes linearity between the inputs and outputs, it cannot estimate quadratic or higher order effects. The Taguchi method is very useful for a parameter design or tolerance design, but has limitations in applying to conceptual design.

· Central Composite Design (CCD) – CCD is the DoE method used to get RSE's in this project. CCD considers 2*n* "cube points", 2*n* "star points" and one center point. When using star points in CCD, it is possible to investigate all the extremes of the design space, reducing extrapolation error.

· Box-Behnken Design (BBD) – This method runs fewer cases than CCD does, but can only be used for limited number of variables, due to its independent nature with elimination of the factorial design. Further more it does not test corners of the design space so that information of the unconsidered area requires extrapolation.

· D-optimal Design – Only run $(n+1)(n+2)/2$ number of cases for the n variables of 3 levels. In this method the matrices are not usually orthogonal and effect estimates are correlated. Typical reasons for using this method include: the need to reduce the number of runs over a factorial design and if the design space is constrained.

3.6.2 Response Surface Methods

For this work, the use of an all-encompassing model of the physical environment is required for the design space exploration. This exploration of a complex design space requires the use of a Response Surface Methodology (RSM) on the DoE results. RSM utilizes Response Surface Equations (RSE's) to represent a model of sophisticated analytical tools by relating an output variable or response to the levels of a number of input variables. The equation takes the

form of a polynomial approximation of the relationships across given ranges for the input variables. Within this project, the second-degree model of the form seen in equation 58 was used. In the RSE, b_0 is the intercept and b_n the respective regression coefficients of the subsequent terms. The x_i variable represents the normalization of each of the inputs that affect the response.

$$R = b_o + \sum_{i=1}^{n} b_i x_i + \sum_{i=1}^{n} b_{ii} x_i^{\,2} + \sum_{i=1}^{n-1} \sum_{j=i+1}^{n} b_{ij} x_i x_j \tag{60}$$

To obtain the regression coefficients, a design of experiments is carried out around the analysis of interest to provide certain test points and the RSE generated using the Least Squares Method (LSM). LSM is a mathematical method used to determine the best-fit equation to a given set of points by minimizing the sum of the squares of the vertical deviation between equation and test point. The sum of the squares of the vertical deviation is calculated and the R^2 and RSE found using a method described in section 3.6.2.1.

An equal number of linear equations and coefficients are created. Thus, when a quadratic RSE of n factors is created, there are $(n+1)(n+2)/2$ unknown coefficients. The same numbers of linear equations are also created, the coefficients are then found by solving these equations as explained in section 4.1.2.1 and once the RSE is found, the goodness of its fit is determined. There are certain ways and steps to check the goodness of fit involving comparisons of

both residual and predicted results, a common method that of the R^2 value is explained below.

3.6.2.1 Definitions of Model Tests

Residuals – "The residual is the sum of squares of deviations from a best-fit curve of arbitrary form" [118] which is defined mathematically as displayed in the equation 58.

$$\text{Residuals} = \sum [y_i - f(x_i, a_1, a_2, ..., a_n)]^2 \tag{61}$$

R^2 value - R^2 value is one of the indicators with which the goodness of the fit of the RSE can be measured. R^2 value is always between zero and one. When the RSE perfectly represents a real model, R^2 value becomes one. When the RSE in no way represents the real model, R^2 value becomes zero. Generally an R^2 value greater than 0.75 is considered acceptable. R^2 value is mathematically defined in equation 61 [119].To define R^2 value, SS_E and SS_Y should be defined first. Sum of the squares of the residuals is displayed in equation 59:

$$SS_E = \sum_{i=1}^{n} (y_i - \bar{y}_i)^2 = \sum_{i=1}^{n} e_i^2 \tag{62}$$

Total sum of squares is displayed in equation 60,

$$Syy = \sum_{i=1}^{n} \bar{y}_i^2 \tag{63}$$

and R^2 value is defined as below in equation 61:

$$R^2 value = 1 - \frac{SS_E}{Syy} \tag{64}$$

Whole model test – This implies that the test is run using a more sophisticated and complex model. A whole model is a model of a system which physically or empirically represents the real world model with high order accuracy. However the whole model test can not always be executed because it entails much computational work which takes too much time. Instead, a meta-model, which is a model of the model, can be used. A meta-model is generated mathematically using response surface methodology. Simulation with Meta-model may not be as accurate as a model but is much simpler and requires less computational work.

3.6.2.2 How to Create an RSE

The RSE is an equation which represents a model of sophisticated analytical tool. A relationship between input variables and the responses can be found with RSE. Most times, a second degree model RSE is appropriate.

Even though RSE can be any function such as exponential, sinusoidal or logarithms, it is proved that any type of function most data can be expressed as an infinite number of polynomials with a Taylor series expansion. Second order polynomial equations are quite accurate when the ranges are small around the nominal values. The second degree RSE takes the form of equation 62 [120]:

$$R = b_o + \sum_{i=1}^{n} b_i x_i + \sum_{i=1}^{n} b_{ii} x_i^{\,2} + \sum_{i=1}^{n-1} \sum_{j=i+1}^{n} b_{ij} x_i x_j \tag{65}$$

Since RSE is a regression equation, there must be a set of test points. In this project the points are the responses created using the DoE values. The RSE is then generated using Least Squares Method. Least Squares Method is a mathematical method used to find the best fitting equation out of given set of points by minimizing the sum of the squares of the vertical deviation between equation and test point. The difference between vertical deviation and perpendicular deviation is depicted in the Figure 62.

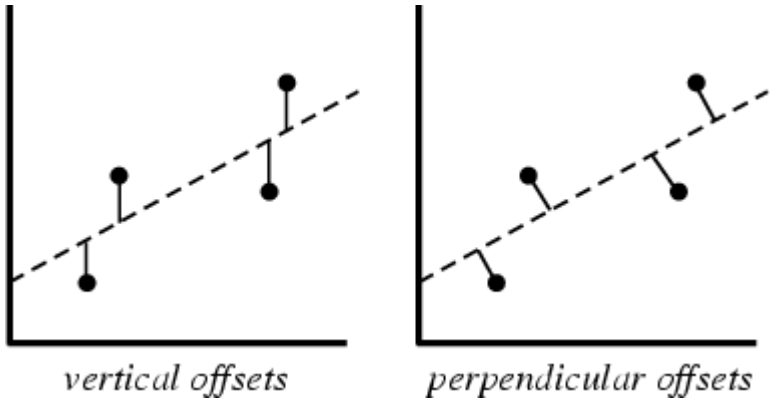

Figure 62: Vertical offsets and perpendicular offsets[116] **.**

Sum of the squares of the vertical deviation is represented in equation 58. Each coefficient of best fitting RSE can be found by taking differentiation of R^2 and set it to zero as represented in equation 63.

$$\frac{\partial(R^2)}{\partial a_i} = 0 \tag{66}$$

With equation 63, an equal number of linear equations and coefficients are found. For example, when the quadratic RSE of n factors is created, there are $(n+1)(n+2)/2$ coefficients or unknowns. $(n+1)(n+2)/2$ linear equations can then be derived from equation 63. The coefficients can then be found by solving those equations.

3.6.3 Neural Networks

Along with response surface methods another more popular multivariate modeling technique, is that encompassed by it's more common title, neural network techniques. Neural network techniques or more simply, Neural Networks are a different form of regression for highly non-linear or discrete problems. Fundamentally, Neural Networks are different only in form from Response Surface Methods.

Neural Networks are an alternative to Response Surface Methods (RSM) in the creation of meta-models for problems where the polynomial representation inherent in RSM fails to perform well. This failure being highlighted through the goodness of fit tests mentioned previously. The methods can be employed over both continuous and discrete responses, creating types known as function and classification approximations respectively. These types are based loosely on the low-level structure of actual biological neural networks. The idea being that mimicking the low level structure of the brain would be the

best method to achieve an artificial intelligence type result. These methods are utilized in a variety of roles, including[121]:

- Financial markets prediction
- Image processing software
- Complex engine management software
- Robotic control architecture
- Credit assignment

In order to provide a better understanding of this method including its pro's and con's, the author will turn to work by fellow Aerospace System Design Lab members Carl Johnson and Jeff Schutte. Mr Johnson and Mr Schutte have worked extensively on creating a Neural Network generation tool for mutli-disciplinary optimization. From his instruction manual for the tool, otherwise knows as Basic Regression Analysis for Integrated Neural Networks (BRAINN), a suitable in depth description of the theory and practice of Neural Networks can be gained. The following is an excerpt from this document describing the theory of the Neural Networks [122]:

"*Neural Nets work by mapping a set of input variables to a set of responses through a set of filters, called the hidden layer. There can be more than one hidden layer, but JMP only supports models with one hidden layer. One of the requirements in the development of BRAINN was compatibility with JMP, so it is also constrained to one hidden layer. The hidden layer consists of hidden nodes, analogous to neurons in the*

biological model. An example diagram illustrating the connections between the layers is shown in Figure 63.

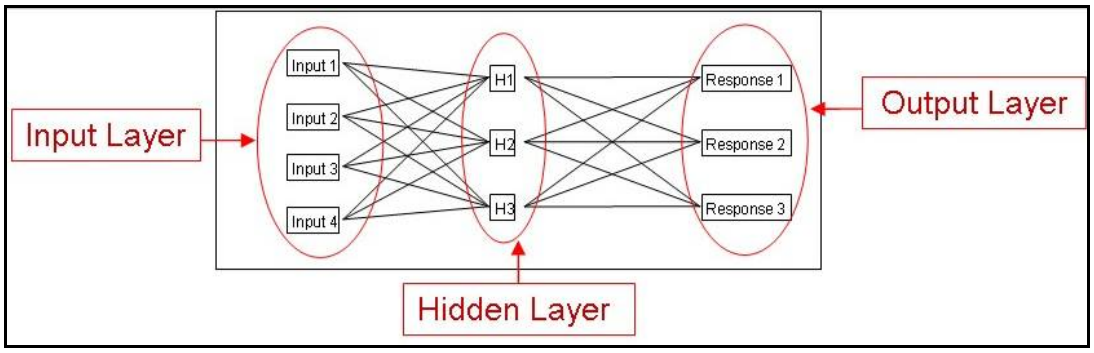

Figure 63: Neural Network Conceptual Diagram. *(after Johnson and Schutte)*

As a conceptual example, the input layer is like a person's five senses, receiving data from the outside world. The hidden layer is like the brain, processing this data. And the output layers would be a response to stimuli, like talking or typing. As the figure shows, each of the inputs has an influence on the hidden nodes and each of the hidden nodes has an influence on the responses. The correct number of hidden nodes depends very much on the problem; the procedure to select the number of hidden nodes will be discussed later.

A Neural Network, like all other forms of regression, fits an equation through a given set of data. The mathematical form of the Neural Net equation is described below. The data being regressed is called the training set for a Neural Network. The training algorithm is the optimization method used to determine the coefficients for the network that minimize the training error. A large variety of training algorithms are available in BRAINN and each will be described later in this document."

The math behind this approach is also documented for one of the hidden layers, it works from the initial biological primmest of the theory and develops the mathematics from that. Mr Johnson and Mr Schutte have laid out this work as follows [122]:

"In a biological system the neurons, as described above, are either sending or not sending a signal, based on the inputs they receive from other neurons. They therefore have a step function for their activation function- on or off. For a numerical regression the use of a step function is problematic because it is not continuous and differentiable. Most Neural Networks use something called the logistic function. The logistic sigmoid function, seen in (64), has the effect of "squishing" the inputs to it such that it always outputs a value between 0 and 1.

$$S(z) = \frac{1}{1+e^{-z}} \tag{67}$$

This logistic function is used to calculate the value for each of the hidden nodes for both the function approximation and classification problems. The value of the hidden node is taken by applying the logistic function to a linear term related to the input variables, as shown in (65).

$$H_j = S\left(a_j + \sum_{i=1}^{N}\left(b_{ij}X_i\right)\right) \tag{68}$$

Where: a_j is the intercept term for the j^{th} hidden node

b_{ij} is the coefficient for the i^{th} design variable

X_i is the value of the i^{th} design variable

H_j is the value of the j^{th} hidden node

and N is the number of input variables

The calculation of the final response will depend on the problem type. For function approximation, the value of the response is found through a linear term that depends on the value of the hidden nodes, as shown in (66).

$$R_k = e_k + \sum_{j=1}^{N_H} \left(f_{jk} H_j \right) \tag{69}$$

Where: e_k is the intercept term for the k^{th} response

f_{jk} is the coefficient for the j^{th} hidden node and k^{th} response

H_j is the value of the j^{th} hidden node (defined above)

and N_H is the number of hidden nodes

The different steps described above can be combined to create the following unified form of the Neural Net equation for function approximation.

$$R_k = e_k + \sum_{j=1}^{N_H} \left(f_{jk} \left(\frac{1}{1 + e^{-\left(a_j + \sum_{i=1}^{N} \left(b_{ij} X_i \right) \right)}} \right) \right) \tag{70}$$

Where: a_j is the intercept term for the j^{th} hidden node

b_{ij} is the coefficient for the i^{th} design variable

X_i is the value of the i^{th} design variable

N is the number of input variables

e_k is the intercept term for the k^{th} response

f_{jk} is the coefficient for the j^{th} hidden node and k^{th} response

and N_H is the number of hidden nodes

The four coefficients (a, b, e and f in the above) are modified to fit the training set as well as possible, minimizing the sum square error or mean square error of the training set, depending on the training algorithm selected.

For the classification problem, the output layer for the neural network consists of another layer of logistic sigmoid nodes instead of the linear transfer function used for function approximation. The number of nodes in the output layer depends on the number of discrete responses (1 node per discrete response). Thus, each output node is a logistic sigmoid function of a summation of logistic sigmoid functions as shown in (68).

$$O_k = S\left[c_k + \sum_{j=1}^{N_H} d_{jk} \left(S\left(a_j + \sum_{i=1}^{N} \left(b_{ij} X_i \right) \right) \right) \right] \tag{71}$$

Expanded out the equation becomes the following,

$$O_k = \frac{1}{1 + e^{-\left[c_k + \sum_{j=1}^{N_H} d_{jk} \left[\frac{1}{1 + e^{-\left(a_j + \sum_{i=1}^{N} b_{ij} X_i \right)}} \right] \right]}} \tag{72}$$

Where: a_j is the intercept term for the j^{th} hidden node

b_{ij} is the coefficient for the i^{th} design variable of the j^{th} hidden node

X_i is the value of the i^{th} design variable

N is the number of input variables

c_k is the intercept term for the k^{th} response

d_{jk} is the coefficient for the j^{th} hidden node and k^{th} output node

and N_H is the number of hidden nodes

The resulting output nodes of the classification Neural Network are therefore between 0 and 1 as opposed to the output of the function approximation Neural Network which can take on any value. The four coefficients (a, b, c and d) are modified to fit the training set by minimizing the sum square of errors. The training set will have been converted to 0's and 1's before the training process."[122]

Additionally suggested within the document, post processing of the Neural Network is often required to ensure that the output values reflect only one class for a set of given inputs. This is often achieved by simply rounding the output values from the logistic sigmoid nodes. However this does not necessarily guarantee the desired result. To resolve this the outputs of the nodes are ranked with the maximum value set to one, then the other output values to zero to ensure that only one class is selected.

Creating the Neural Network for use with a multi-disciplinary approach as outlined above requires the use of a data set, from the generated results from the blade lifing environment. Neural Networks use a percentage of the input data as validation to create the networks and equations that approximate the

results. The biggest problem with the use of this validation set is the correct choice of training parameters associated with the use of Neural Networks. These include the number of hidden nodes, training time and number of epochs. Though no current specific guidelines exist as to the general settings for these variables, rules of thumb do and can be explored through a simple DoE type exploration. Typically 75% of the data set is used for network training [122].

Depending on the software used to create the Neural Networks from the data set, the researcher has the possibility of utilizing different training algorithms. It is this choice of software that drives the algorithm choice. The options to the author include JMP and MATLAB/BRAINN, the first choice comes complete with all algorithm options fixed, the developers having decided what they felt to be the best approach for the intended use of the application. BRAINN/MATLAB comes with a selection of thirteen algorithms for the user to utilize, these are:

- Levenberg-Marquart
- Levenberg-Marquart with Bayesian Regularization
- Gradient Descent with Momentum and Adaptive Learning Rate
- Gradient Descent with Adaptive Learning Rate
- Gradient Descent with Momentum
- Gradient Descent
- Conjugate Gradient (Powell-Beale)
- Conjugate Gradient (Fletcher-Reeves)

- Conjugate Gradient (Polak-Ribiere)
- Scaled Conjugate Gradient
- Resilient Backpropagation
- One Step Secant Backpropagation
- BFGS quasi-Newton Backpropagation

These methods are all line search methods that are not domain spanning. Thus for a multi-model surface a true global minimum solution cannot be guaranteed. The goodness of the fit is then tested against the remaining test data, such that any problems can be identified and investigated before the networks are used for result predictions. These tests are almost exactly the same as with those for the Response Surface Methods, with more weight put on residual by predicted, actual by predicted and generalized error forms. Looking at the generalized error and the other information is a far better method of indicating any problems over highly non-linear spaces such that materials information can be.

3.6.4 Kriging

One further popular meta-modeling technique is that of Kriging, This is a form of Gaussian process [123] developed through the geostatistical field. This was first proposed by French Mathematician Georges Matheron [124], based on previous work by Daniel Krige, hence the term Kriging. This method has moved

from its base of geological exploration, where it was developed to more accurately determine the location of gold reserves, moving into areas such as:

- remote sensing
- computer modeling

The groups of techniques that make up kriging are aimed at interpolating from a current value in a random field out to a point in a nearby location in the same field, based on observations in the same area. This approach calculates the best linear estimator (unbiased) based on a stochastic model of the special dependence though various methods including, expectation and covariance of the field. This estimator, $\hat{Z}(x_0)$, is a linear combination in the form:

$$\hat{Z}(x_0) = \sum_{i=1}^{n} w_i(x_0) Z(x_i) \tag{73}$$

Where:

$Z(x_i)$ = observed values

$w_i(x_0)$ = weights

The number of observations, I, is chosen to minimize the kriging variance, $\sigma_k^2(x_0)$, subject to the expectation, $E\left[\hat{Z}(x) - Z(x)\right]$, being unbiased. This theoretical background forms the basis for eight classical types of Kriging, these being [125]:

- Simple
- Ordinary
- Universal

- IRFk
- Indicator
- Multiple-indicator
- Disjunctive
- Lognormal

Each of these types of Kriging differs from the rest through differing assumptions for μ*(x)*. The assumptions vary from implementing a constant trend through interpolation by logarithmic means. Looking at one of these types in detail to get a grasp of the details, we shall take the Simple Kriging approach with its assumption, $\mu(x) = 0$.

This is the simplest kind of Kriging approach, with a known expectation of the field and covariance function, $c(x,y) = Cov(Z(x), Z(y))$. The general equation system for simple Kriging provides the Kriging weights, w_i:

$$\begin{pmatrix} w_1 \\ \vdots \\ w_n \end{pmatrix} = \begin{pmatrix} c(x_1,x_1) & \cdots & c(x_1,x_n) \\ \vdots & \ddots & \vdots \\ c(x_n,x_1) & \cdots & c(x_n,x_n) \end{pmatrix}^{-1} \begin{pmatrix} c(x_1,x_0) \\ \vdots \\ c(x_n,x_0) \end{pmatrix} \tag{74}$$

Thus the Kriging weights have a no unbiasedness condition. Therefore the interpolation is given by:

$$\hat{Z}(x_0) = \begin{pmatrix} Z_1 \\ \vdots \\ Z_n \end{pmatrix}' \begin{pmatrix} c(x_1,x_1) & \cdots & c(x_1,x_n) \\ \vdots & \ddots & \vdots \\ c(x_n,x_1) & \cdots & c(x_n,x_n) \end{pmatrix}^{-1} \begin{pmatrix} c(x_1,x_0) \\ \vdots \\ c(x_n,x_0) \end{pmatrix} \tag{75}$$

With an expected error given by:

$$Var\left(\hat{Z}(x_0)-Z(x_0)\right)=\underbrace{c(x_0,x_0)}_{Var(\hat{Z}(x_0))}-\underbrace{\begin{pmatrix}c(x_1,x_0)\\ \vdots \\ c(x_n,x_0)\end{pmatrix}'\begin{pmatrix}c(x_1,x_1) & \cdots & c(x_1,x_n)\\ \vdots & \ddots & \vdots \\ c(x_n,x_1) & \cdots & c(x_n,x_n)\end{pmatrix}^{-1}\begin{pmatrix}c(x_1,x_0)\\ \vdots \\ c(x_n,x_0)\end{pmatrix}}_{Var(\hat{Z}(x))} \quad (76)$$

Which by Chiles & Delfiner [126] leads to the generalized least squares version of the Gauss-Markov Theorem:

$$Var(Z(x_0))=Var\left(\hat{Z}(x_0)\right)+Var\left(\hat{Z}(x_0)-Z(x_0)\right) \quad (77)$$

All the further methods start with the derivation of the Kriging weights and move on to the interpolations from there.

3.7 Surrogate Modeling Implementation Considerations

Having reviewed the three most suitable methods for this problem a choice is required as to which of the metal-modeling techniques is best suited for the application at hand. When making this decision one needs to take into account both inputs of the creep lifing environment and the needs of the designer. Thus, these into account and the requirements set out within the hypotheses, considerations need to be made as to which of the methods to

employ. To best achieve this it is beneficial to run through each of the methods investigating the advantages and disadvantages of their implementation.

Keeping to the order of the previous work, the first to be considered would be the response surface methods. It has been well documented [117, 127] since the beginning of the method under Box and Wilson [128], that the method is best used when the user is looking for:

- Rapid and efficient method
- Understanding of underlying response system
- Transparency of resulting meta-model, the resulting equations for the meta-model are easy to understand and manipulate.

Given that this is a well established methodology (beginning with Box and Wilson in 1951 [127]), there are:

- Well defined tools and processes [117]
- Minimal number of cases for resulting meta-model

However, every method comes with drawbacks and this is certainly true here. Firstly one needs to realize the major drawback for RSM that being its polynomial based expressions that form the basis for the generated meta-models. Consequently it proves unable to accommodate highly non-linear problems such as any materials modeling necessary. Furthermore problems can arise when dealing with large numbers of variables and wide ranges. Though this is unlikely to be an issue within this work, it does bring to the fore the need for careful range selection for the variables, something that needs to be accommodated

within the next chapter. More troubling though for this intended work, is that RSM is only able to handle continuous data. Unfortunately the way in which the metal properties are being gathered using the Excel spreadsheet organized by material number, suggests the use of discrete modeling of the materials given their distinct compositions.

With this in mind we now move onto the discussion of the advantages and disadvantages of implementing a neural network technique for this thesis work. This method as we have seen is capable of handling discrete and continuous data, such as that found within the intended analysis environment. This ability is due to the fact that the solution does not assume a functional form, such as the polynomial form taken by RSM. In addition therefore the method has the ability to handle highly non linear solutions with ease. As previously mentioned, though the cycle analysis results are expected to be relatively well behaved given the polynomial basis of NPSS, the materials modeling should it be required is highly non-linear. Previous efforts [103, 129, 130] to model the properties of nickel superalloys have all utilized neural networks in some way due to this reason. Furthermore this approach provides the designer with a closed form solution of the trace that represents the design space behavior. Greatly improving the usability of the resulting surrogate model

These advantages of using a neural networks based methods, do come at a cost. Johnson et al [122] point out that such an approach is stochastic and that it is therefore unrepeatable. Thus it is of paramount importance to save the best

neural net equations as soon as they are generated, in order to retain the model for later use. Methods to alleviate this during the selection of the best neural network variables, are discussed earlier, this included fixing the random starting point from which the neural network analysis begins. Additionally given the possible extended run times and the care that needs to be taken with the variable selection, on top of the basic implementation, neural networks require a more intensive utilization [131]. This is not only in computer resources but in user knowledge of the method at hand.

Considering now the Kriging method of surrogate modeling, one notices the similarity with it to Gaussian Processes. The method provides estimation of and the confidence interval for the response values. In addition, it like the neural networks is able to handle the use of both discrete and continuous variables. It is also able to fit through the exact data points of the response. And is the only method that can guarantee this.

The question might arise that with such a great capability why not look any further than the kriging method mentioned earlier. However in line with section 4.1.4, the method is based on storage matrix operations. Thus, any manipulation of the model and the creation of said model would require computationally intensive matrix manipulation, greatly increasing the creation and operation times on the usual desktop personal computers. This consideration limits the dimensionality of the problem, as increasing the number dimensions of the problem under study, would also increase the size of the

matrixes to be manipulated. Not something that is to be taken lightly and obviously makes it much more difficult to implement than RSM [131].

Looking back to the research questions and hypotheses, the fact that this method is to be used in a complex system becomes of great importance. Were there are an almost limitless number of variables that could be considered, the use of Kriging would hamper the speed and ease of use that this approach is intended to have. Therefore it comes down to the ability of Neural Networks to accommodate highly non-linear spaces including discontinuities making it much more suitable for this application than RSM. Furthermore neural networks are also able to cope with a high number of variables, another bonus given the intended problem. This along with the great visualization that using such a surrogate modeling technique will help the author answers the challenges set within the hypothesis and research questions.

3.8 Analysis Environment Modeling and Visualization

The hypotheses and research goal call for a fast top down bottom up approach to enable the capturing of the complex system that is the gas turbine engine and enable its relation to the blade life. Additionally it should be noted that there is no call for any optimization within the approach. The research questions and hypotheses look for a concentration of the understanding and visualization of the problem at hand.

Therefore one needs to look for a method that can enable the author and then the designers to put this into practice. In other words a method that provides the ability to help with the visualization and understanding of this top down/bottom up analysis. Villeneuve in 2007 [132] provides a good understanding of the latest path based methods such as Genetic Algorithm (GA), All At Once (AAO), Collaborative Optimization (CO) and Ant Colony Optimization (ACO), however, these do not meet the perceived requirements. These methods do provide excellent means to find global minimums in a complex design space. Therefore if at a later date a study was needed that looked for a single design rather than the design direction that this thesis considers, these would certainly be the option. Furthermore their significant computer resource and time requirement also goes against the hypothesis and research questions that the aforementioned techniques require.

Considering that the analysis is as mentioned designed to give a design direction rather than a singular point answer that others provide, methods that help to visualize trends would be more suitable. Additionally, it is intended that such an approach be applied to a variety design problems, leading to possible conflicts with different optimization methods is applied across the board. Ender in 2006 [133] introduces the use of a multivariate approach to systems design, moving away from the more complex Unified Tradeoff Environment (UTE), developed by Baker [134, 135]. The UTE enables more for more than one meta-model to be present within a system representation, such as an overall system

meta-model relying on the outputs of lower level, subsystem meta-models, to perform its analysis. Such a technique is considered unnecessary given the intended analysis model in Chapter Five which would carry out the analysis itself within one model negating the need to a use a hierarchical meta-model developed from Baker and utilized by Biltgen et al [136] in Figure 64.

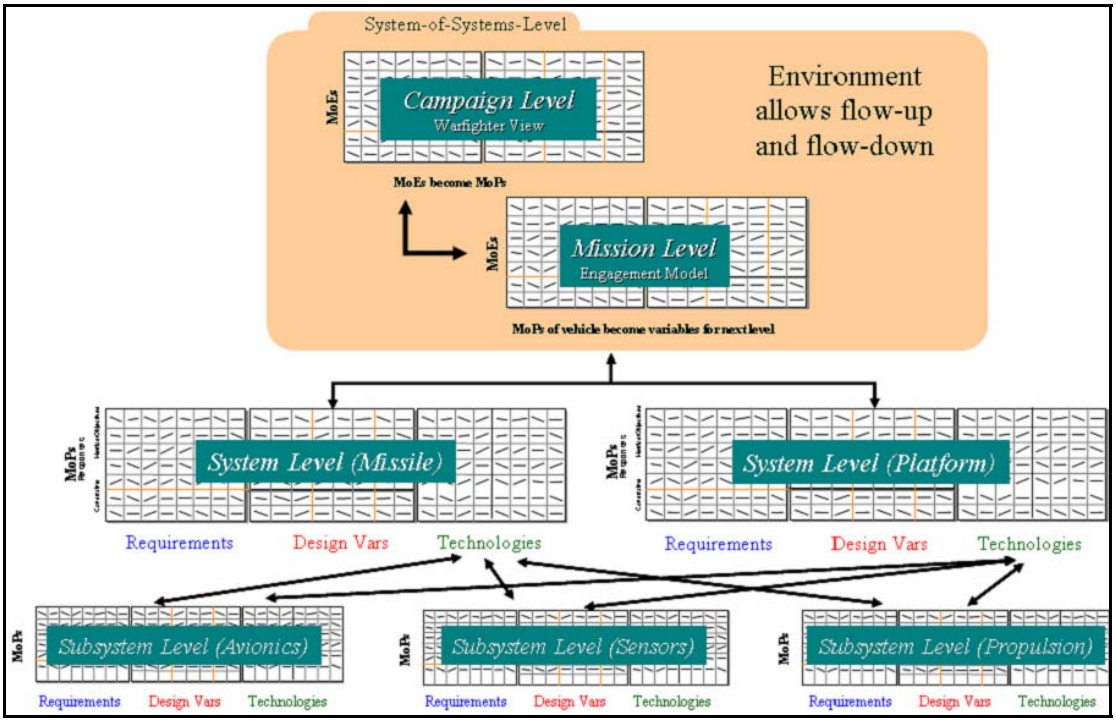

Figure 64: Hierarchical, surrogate modeling environment for systems-of-systems analysis. [136]

The multivariate approach as used by Ender [133], though intended for solely top down approach to design, does provide useful methods for this author to achieve the research goal. However, one needs to take a look at how the need for the inverse design techniques will allow for a very powerful approach to

turbine blade design. This inverse design is nothing more than a top down/ bottom up approach, thus enabling the designer to consider the system and part level simultaneously. Therefore using the visualization techniques that were used by Ender [136] in his subsystem analyses would allow the visualization of all dimensions of variables and responses simultaneously, enabling "inverse design". These "Multivariate" plots are generated within JMP ™ using a Monte-Carlo based sampling of the variables and the results generated from the previously developed neural nets. A similar approach was used previously for the 3D high fidelity approach [53]. The results of the environment are shown below in Figure 65.

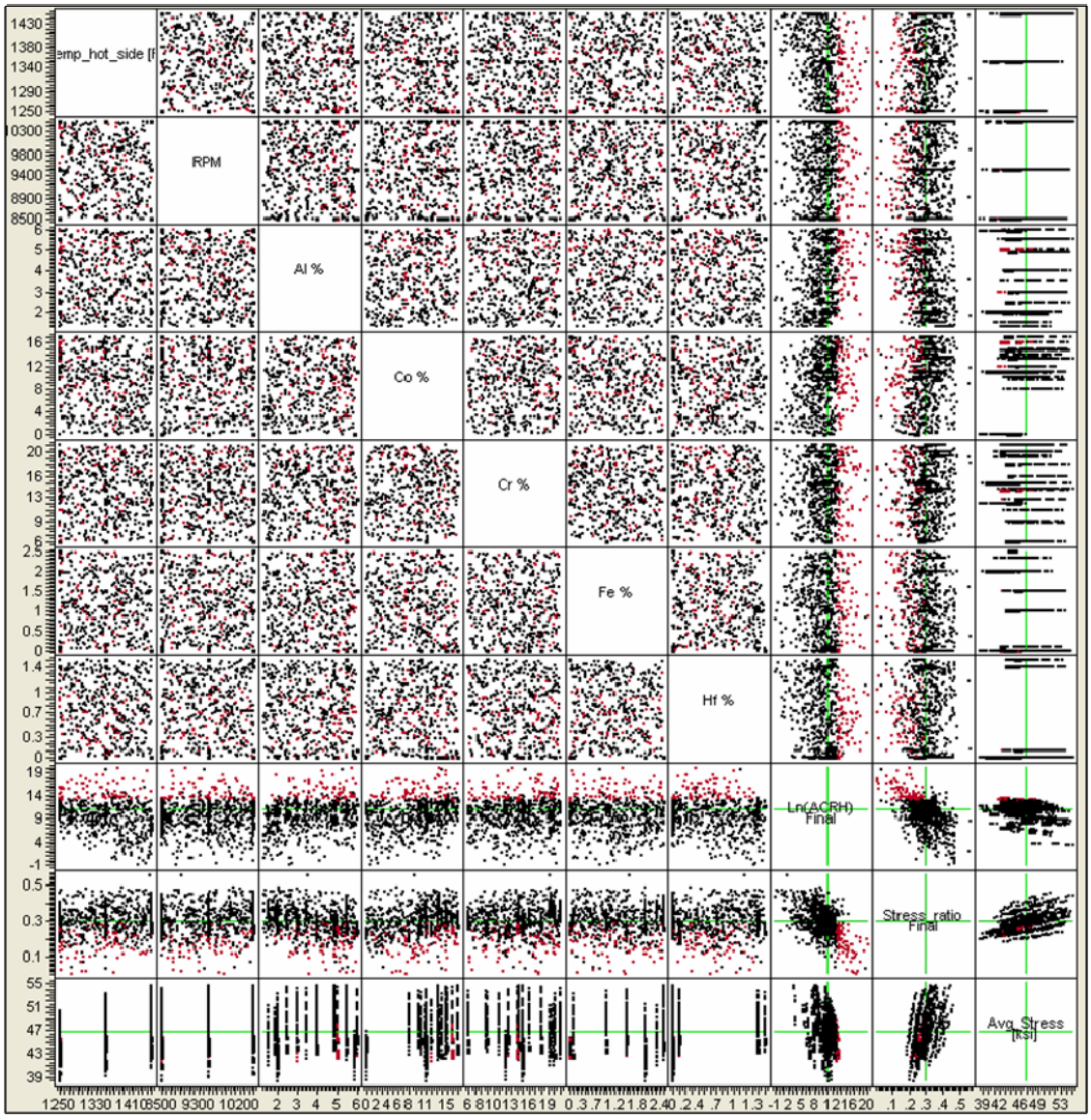

Figure 65: Notional multivariate approach. *(NASA/DoD URETI)[53]*

This system shows that the variation of any chosen design variable can be tracked with respect to the system, be it in this example (Figure 65) material composition changes reflect back to upstream conditions or changes in upstream conditions reflecting on changes in materials requirements and say cooling requirements. However it should be noted that using the low fidelity 0d/1d

methods as the research is intended will allow for a better exploration of the design space, taking advantage of the fast runtime of the codes to be utilized.

The exploration enabled by this Monte-Carlo based technique is truly impressive. They say that a picture is worth a thousand words, and this is the case here. The lower fidelity of the analysis does not particularly warrant a single point answer but the establishment of the trends within the system is paramount. The ease with which these can be observed and manipulated is a great asset to a designer. This enables a true exploration of the chosen design space, with full understanding of the system and the effects of the variables and responses. This is especially true when one wishes to consider the truly complex and multi-model design space of the nickel super alloys. [103], being able to visually explore the space would be most useful. The results of the implementation of this will be included within the following chapter.

CHAPTER 4

COMPUTATIONAL EXPERIMENTS & RESULTS

Now that the formulation of the modeling and simulation approach has been completed, one moves on to the experimentation stage. We have seen previously how the research questions and hypotheses have driven the work in the previous two chapters, and how they have bounded the issues highlighted within the first chapter as well. It is now important that based upon these postulations, the need to test them, and validate the work to date, the overall problem is revisited.

Several areas need to be considered when validating the necessary experiments. An experiment needs to provide supporting results for the evaluation for the hypotheses and research questions, while keeping with the experimental framework envisioned for the eventual design space. An experiment should also provide the author with any possible limitations on the current method to open up more opportunities for study. An LHC/CCD DoE comes with the necessary number of runs for it to remain orthogonal and produce unbiased results. Thus the choice of the number of variables to investigate determines the number of cases required and the length of time the analysis takes. Therefore, in choosing the correct number of variables, one needs to carefully consider what information can be gathered and the importance of that information in relation to the time required for analysis.

The hypotheses and research questions look for a method that approaches an inverse problem, looking from the system level down to the part level and visa versa in terms of turbine blade creep life. This means that simultaneously one needs to be able to explore the effects of any change to some design variables on factors influencing the system and part levels. For example, if the designer wants to maximize the creep life of the turbine blade, what is necessary to achieve this at the system and part levels, and what is its affect? Thus the scope of this investigation is most important, leading one to either a simple experiment or complex one depending on the experimental setup.

4.1 Turbine and Blade Study

The initial experiment conducted utilizing the integrated design environment was intended as a proof of concept study. The bounds set through the hypotheses and research questions are fairly broad, and as previously discussed look for the exploration of the gas turbine design space whilst considering turbine blade creep life. Thus it was decided that this first experiment should consider the blade design to ascertain the suitability of the analysis methods used within the design environment.

Keeping the goal of this initial experiment in mind, one needs to consider design variables for which known output trends exist and can be compared against. Choosing the correct form for this work is essential and requires much consideration including possible industrial applications and the necessary steps

for answering the hypothesis and research questions, amongst other things. Overall however, the intention for this and any other research models within this thesis is the needs of the industry. The needs of industry should drive the research.

The previous two chapters have gone over the development of the analysis model, with surrogate modeling and visualization techniques that best meet the expectations being described within chapter three. These have provided the author and future designers with an approach that is intended to provide a top-down/bottom-up approach to the conceptual design of gas turbine engines. This approach needs to be tested, thus considering the blade life along with other blade level design decisions along with other upstream design constraints. An experiment that considers as much whilst proving the method would be beneficial to progress of this research.

4.1.1 Design Variable Selection

Considering the observations within the first two chapters, especially the identified short falls of the current methods, one can build the base for the first implementation of the approach. The consideration of the blade at the conceptual design stage was limited until now. The inclusion of the velocity triangle and meanline loss models, allows for the great simplification of the overall turbine stage. Consequently the design of this stage can be considered in a fast an informed manner and providing useful building blocks for blade design.

The gas angles generated through the conceptual design stage methods is then used to generate an approximate blade profile, with its height and other factors (including cooling) being calculated with NPSS and the Meanline Loss Model. Therefore the engine can be considered down to the typical conceptual design parameters for turbine stage design, and encompass the blade design at the same time. Considering the engine in its simplest form speeds up the design process and enables the designers to use widely understood factors for design variables. These factors of interest being the 5 inputs for the Schobeiri velocity triangle:

- Reaction, $r = \frac{\Delta h''}{\Delta h' + \Delta h'' S}$ (78)
- Velocity ration, $\mu = \frac{V_{m2}}{V_{m3}}$ (79)
- Flow coefficient, $\phi = \frac{V_{m3}}{U_3}$ (80)
- Stage loading, $\lambda = \frac{1}{U_3^2}$ (81)
- Radius ration, $\nu = \frac{R_2}{R_3}$ (82)

These five coefficients form a good basis for a blade study. One can observe the effects of these changes on the blade, turbine and engine as a whole. To enable the consideration of the blade lifing, materials data is needed. This information is to be provided using the materials data sheets as in section 3.3.7,

accessed through Model Center. Therefore one further variable in this study should be the material number, from one to twenty representing the available material property information.

Cumulatively this brings six design variables. Keeping this blade design requirement for this first model, further blade centric design variables need to be decided. Again turning to the analysis, the geometry model requires extra variables other than the gas angles derived from the velocity triangle analysis to complete its blade generation. Pritchard's eleven variables consisted of [113]:

- Airfoil radius
- Axial chord
- Tangential chord
- Unguided turning angle
- Inlet blade angle
- Inlet wedge angle
- Leading edge radius
- Exit blade angle
- Trailing edge angle
- Number of blades
- Throat

While most of the above are calculated through the velocity triangle, meanline or NPSS analysis, there are still some factors requiring and input for

blade profile generation. Fixing the leading edge ellipsoidal characteristics does not detract form the worth of the study, but greatly simplifies the approach. The calculation of the throat however does some use input. This can be calculated from the factor 1/Solidity (otherwise known as the pitch/chord ratio), including this for both the rotor and stator would enable the designer to consider changes on the whole stage. The thickness to chord ratio will also be included to allow the consideration of blade thickness on stage efficiency and blade lifing.

NPSS further requires the input of a blade aspect ratio for its turbine sizing routines, so this would be a perfect variable to include in this first model given its goal. This would again be for both the rotor and stator, to help illustrate the effects on the turbine. In addition to bring some vestige of the whole engine design and to consider the effects on cooling, the combustor pattern factor (CPF) was included in the list of variables. Bringing this factor into the list will also help to bring a little technology consideration into the analysis with most modern engines looking to reduce the CPF to help with the temperature problems in the turbine inlet. Therefore the initial model consists of 12 variables (11 continuous and 1 discrete), the ranges being selected based around the GE/NASA E^3 engine parameters. These were as follows in Table 3.

Table 3: Ranges for eleven design variables included in the Design of Experiments.

Design Variable	Description	Lower Bound	Upper Bound
Reaction	Rotor enthalpy change / total enthalpy change	0.4	0.6
Flow Coefficient	Axial flow / blade speed	0.4	0.5
Axial Velocity Ratio	Stator axial flow / rotor axial flow	0.75	0.9
Radius Ratio	Stator exit radius / rotor exit radius	0.97	1.03
Stage Loading	Total enthalpy change / (blade speed)^2	1	1.6
S/c_r	Rotor pitch-chord ratio	1.2	1.6
S/c_s	Stator pitch-chord ratio	0.9	1.2
AR_r	Blade height / true chord	0.6	1
AR_s	Vane height / true chord	0.6	1
t/c	Blade thickness-chord ratio	0.15	0.3
CPF	Combustion pattern factor	0.15	0.4

The remaining required inputs for the analysis were fixed at the start of the analysis to match as closely as they could be to conditions found within the NASA/GE E^3 engine (Table 4, overleaf). The multistage calculations within the analysis model were kept to 2 stages with the settings for the variables being exactly the same as for the first.

Table 4: Initial model fixed variables.

Design Variable	Description	
Rotor Metal Temp	Desired metal temp.	2100
T3	Cooling flow temp.	1465
T4	Turbine inlet temp	2858
RPM	Engine RPM	12650
TBC Thickness	TBC Thickness (mm)	2
te_s_st		0.02
te_s_rot		0.02
Vane cooling type	Cooling type for COOLIT	1.2
Rotor cooling type	Cooling type for COOLIT	1.2
epsilon_in	Inlet wedge half angle	15
Zeta		5
Scale_f	Cooling method scaling factor	0.65

4.1.2 Design Response Selection

Now one needs to consider the desired outputs. Therefore, one needs to review what is needed from the model at this stage. The approach is as yet unproven, so a method that can help to verify the approach would be desirable. It is known that the tools/techniques within the approach run well on there own, but there is a need to prove their integration and any necessary debugging.

Therefore the desired outputs need to be chosen in such a way that they provide useful approach to this verification. However this also needs to be considered within the requirements set within the research questions and hypotheses in chapter 4. These call for the consideration of blade design in terms

of creep life and of system part level factors in a fully integrated environment. Therefore the first response to be considered should be the first to be considered. This being taken after the stresses have been compared with the T_4 and the combined stress, against the gathered public data.

To help verify the codes one needs to consider if the stress adheres to an accepted pattern. Without the creep lifing data to compare to one needs to consider, are the largest stress values where you would expect them? Do the stresses react accordingly to change in the input variables? In other words, does increasing the height of the blades increase the centrifugal stress and the like?

Proving the analysis through the derivation of the correct trends is not solely sufficient using just one response, extra responses are required. Creep lifing is not the only intended response of concern within this thesis. Means of reflecting the effects of designing for life on the overall performance of the engine is also required. One such response would be the consideration of stage efficiency. The variables that have been chosen for use within this first model are likely to have an effect on the efficiency of the engine. There really isn't a point in in improving the life of a turbine if the performance of the engine is made to suffer. This is especially of concern when airlines are sold the guaranteed performance of an engine.

Changing the turbine stage layout will affect the flow conditions of the stage and a means of capturing design decisions that these effects would be beneficial. Therefore the consideration of the exit angles and turbine cross section

would be something to note. Starting with the gas angles, the stage exit angle, also known as the swirl angle (α_3), if too great causes issues when moving from the HPT to the LPT, or onto the next stage if more than one HPT stage. Therefore a design with an α_3 of as close to zero as possible is desirable to ensure the best aerodynamic performance of the turbine stages. However should the analysis indicate that a better blade designed for life would have to have an α_3 of greater than zero, then the use of an exit guide vane to correct the airflow could be considered. This would possibly add unnecessary cost and complexity to the design, and is a trade that would need to be well thought-out only if the benefits gained outweighed the costs. This approach will enable these trades to occur on the fly, in line with the requirements within the research and hypotheses. This not only greatly expands the possible design space but the knowledge that the designer can rely on through his decision making process.

Moving onto the next and really the last of the considered responses, Flare angle, any more than four would really crowd the analysis and prevent a good representation of the approach within this document. Flare angle is the change in flow path angle through the turbine stage in other works the deviation of the flow from the meanline, due to the shape of the turbine stage. The angle is calculated through at the exact same time as the stress in the same module. The deviation can either be with or against the expanding flow, depending on the flow conditions and turbine design. There is a need to match this up with the considered blade designs and stage in order to help with the validation of the

approach. Too great of a flare angle creates aerodynamic instabilities through the turbine stage and reduces the efficiency of the stage. Working from the NASA/GE E^3 engine model [76]and with accepted design norms [27] the flare angle can be within the range $\pm 20^o$ to be within these accepted design limits. This limit unlike the swirl angle cannot be corrected for with the use of the guide vane, therefore this limit should be used more as a check to see that improved designs are within the accepted limits. Thus, all designs outside this range would have to be rejected from consideration, or investigated further should the results warrant, determining the exact detrimental effect.

The approach as a whole has the ability to track all of the system outputs in a large file should the need require, thanks to the work of Mr Eric Hendricks. Thus should one realize that an output factor is missing and crucial to the desired analysis then the data can be added to the metamodel without rerunning the whole analysis again?

4.1.3 Turbine and Blade Design Study Results

Running the DoE analysis did reveal some pitfalls in the initial assumptions and these were addressed promptly. The range for radius ratio was initially set to between 0.9 – 1.1 but problems with stress and flare angle required narrowing of the design ranges (see Table 3) to improve the analysis results. This and other pitfalls highlighted a need for the careful initial selection of design

variable ranges that are required in DoE analysis. The changes in question were only small and highlighted in the previous section.

To run this analysis the DoE table was read into the model and associated with the desired input design variables. The Model Center DoE tool is utilized to run the model altering the values of the design variables whilst keeping the rest of the model constant. These other variables have been set to replicate a typical NASA E^3 engine set up, helping to base the research in a real industrial situation. Still however no lifing data is available to the author. However this is not the issue, through using the classical solutions to the stress analysis the author can provide a conservative solution that provides a trend over the ranges of the design variables.

The DoE results from the model are outputted from Model Center in a format that is easily entered into the statistical analysis software JMP. The software was deemed to be the best method to achieve the desired mix of neural net capability and result visualization and manipulation that the hypotheses alluded to. Choosing the correct factors for the neural net for the first model, was based on work carried out based on previous experience gained with the NASA/DoD URETI research from some three years ago [53]. This work as previously mentioned worked with a high fidelity approach, however using the neural net settings as a baseline was useful given the consideration of life in both approaches. JMP has a limited number of variables that can be changed, greatly improving the simplicity of its use for a project such as this. A table consisting

the setting as used in the creation of this model is noted in Table 5. To achieve this numerous runs were attempted until the fit of the model was sufficiently precise. Judging this fit is described in chapter four, these results called for an R^2 value as close to one as could be achieved.

Table 5: Initial model Neural Net Settings

Fit Variables	Settings
Hidden Nodes	10
Over-fit Penalty	0.001
Number of Tours	30
Max Iterations	300
Converge Criterion	0.00001

It should be noted however that simply reentering these results is not a guarantee of achieving the same fit running the same model multiple times as previously explained. However to help with this the random seed that provided the best results can be set so that the model is more consistent as the exploration of the neural net settings is carried out. A full DoE analysis of the optimal values for the neural net settings can be carried out, however the computer power available to the author is limited and the time required to run the full analysis is not seen as beneficial, when considering the good results that have been achieved with a simple variation from the baseline. The net result of this was a neural net, represented in the following pictogram.

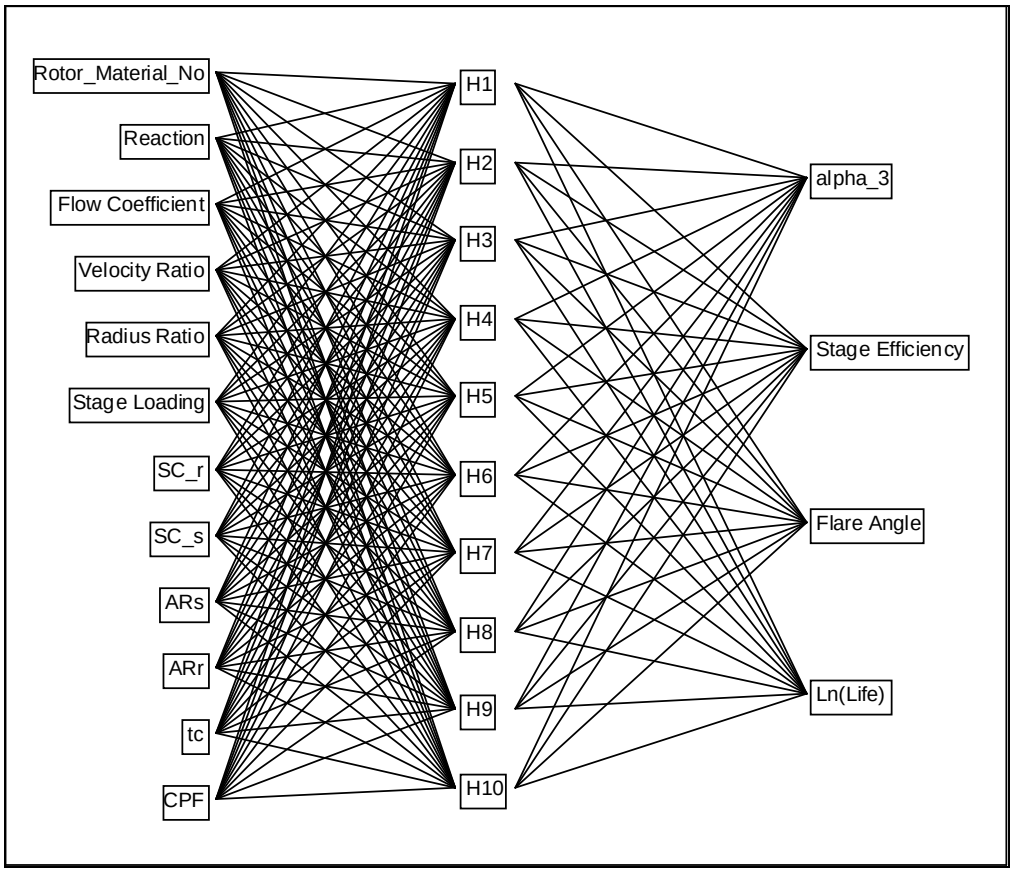

Figure 66: Initial experiemt neural net graphical representation.

The fit achieved with the setting listed in Table 5 produced a model with an excellent goodness of fit. The behavior of the responses has been mapped very well. A quick summary of the fit for this first model is provided in Table 6.

Table 6: Summary of initial model fit.

RESPONSE	RMSE	RMSE SCALED	R SQUARE
Swirl Angle	1.49708502	0.07572471	0.9943
Stage Efficiency	0.00121566	0.06820447	0.9954
Flare Angle	0.35855774	0.02660955	0.9993
Ln(Life)	0.38255465	0.15348949	0.9765

The results which gave a total R^2 of 0.99137, a figure that is to be expected in some part due to the assumptions and calculations within the cycle analysis in NPSS, in addition the fit achieved with the discrete material numbers was very pleasing (see Figure 67 and Figure 68, below) . This helps to illustrate the ease

that the neural nets have with dealing with data of both discrete and continuous types. This is its real advantage over other methods for this application in particular.

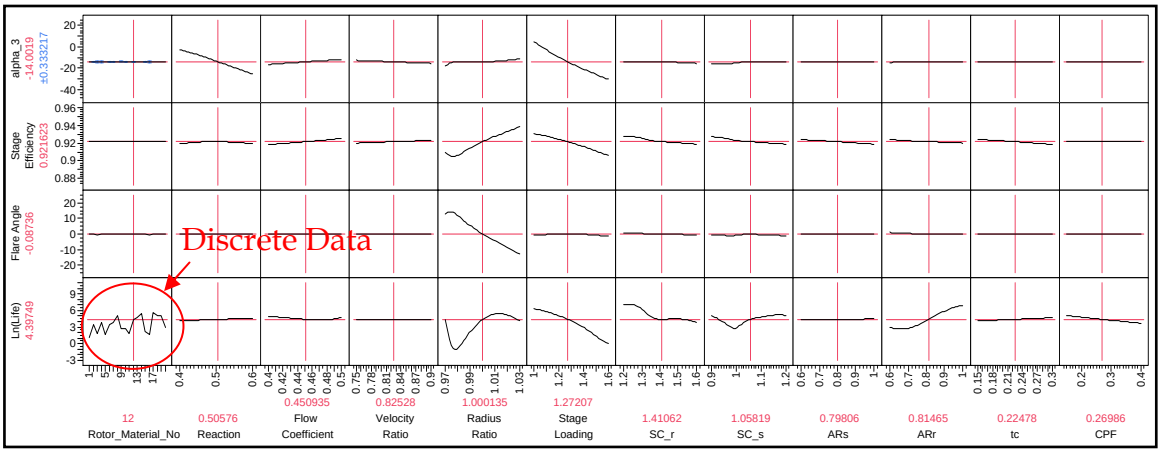

Figure 67: Discrete data handling model results for initial experiment.

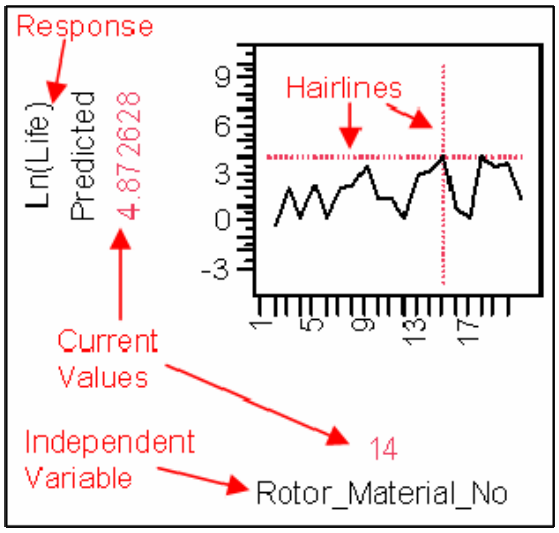

Figure 68: Zoom on Discrete data handling and other Prediction Profiler highlights.

The plots from JMP shown in Figure 67 & Figure 68 are known as the Prediction Profilers. The Help file within JMP [137], describes them as: "*the display of the prediction traces for each x variable. A prediction trace is the predicted*

response as one variable is changed while the others are held constant at the current values. The prediction profile can then recompute the traces as you vary the value of an x variable." This prediction profiler as the previous sentences allude to, provides a great visual understanding of the model, with the curve of the slope of the traces representing the impact of a particular independent variable. Using the hairlines (the vertical red dotted lines in Figure 67) the values of the independent variables can be altered on the fly, by just altering their position by dragging the lines with the mouse. The values of the responses are then instantly calculated and the new values reflected in the position of the red horizontal dashed lines.

Overall these profilers fulfill a variety of roles for the designer these being:

- Debugging – Providing the ability to review the prediction traces for each independent variable, checking for responses that don't make sense.
- Fidelity – Adjusting the independent variables to visualize their impact on the studied responses.
- Technology – Modeling the impact of new technologies through the independent variable inputs and then visually and analytically evaluating their impact on the studied responses.
- Total Derivative – The span of the y-values is indicative of the design space size and how the responses vary as the set of x-values (independent variables) are changed over their ranges.

The prediction profiler is a very powerful visual representation of the effects of the independent variables on the studied responses. The final results from the modeling of the analysis data is depicted in Figure 69, overleaf. The results depicted follow the expected trends and will be discussed in detail following this figure.

Figure 69 is used to present the traces of the studied inputs and responses in an easy means to visualize the effects and the behavior of the design space. One of the most convenient forms of this is through the prediction profiler as mentioned earlier which this figure depicts. This technique helps to ensure that the desired trends are being seen in the model for verification purposes.

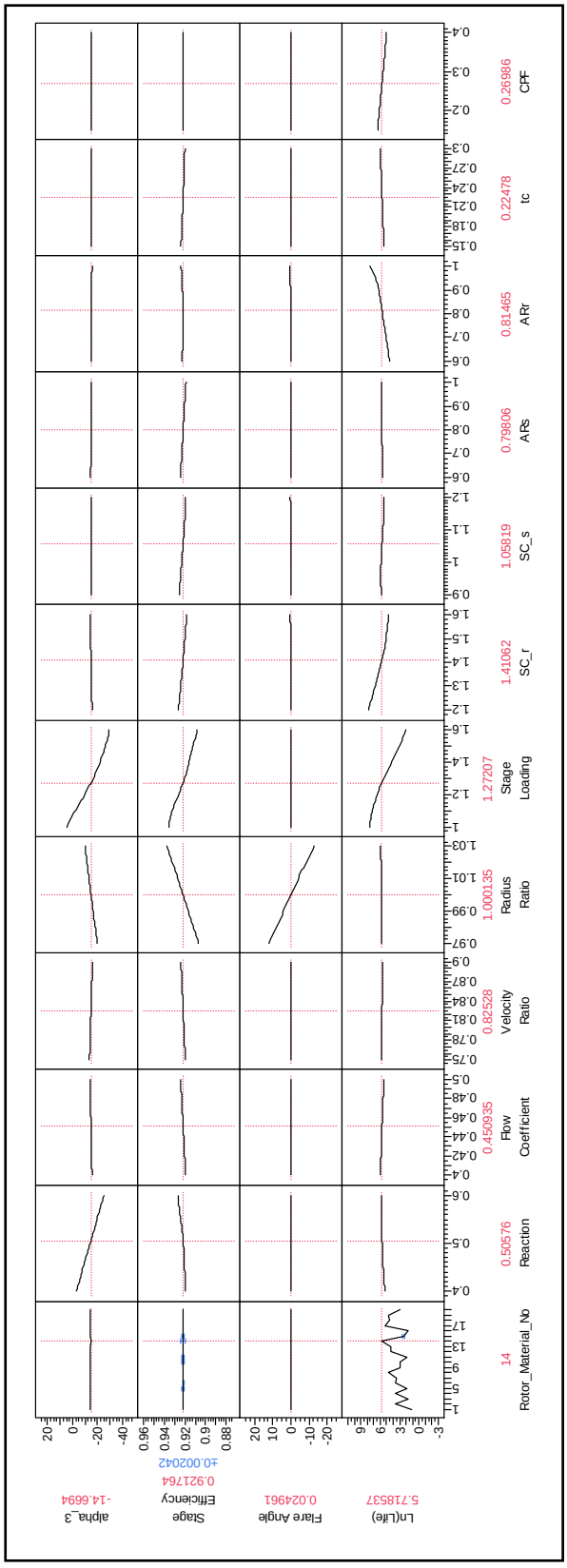

Figure 69: Turbine and blade design study interactive parametric trade-off environment

The trends that the traces in the profiler follow are very promising and looking at each response in turn will help better understand the results. Starting with the blade creep life, the natural log of this figure was used during the modeling process to better help the fitting of the model, smoothing out the design space. This is a common technique to use and does not adversely affect the resulting model, shown in Figure 70.

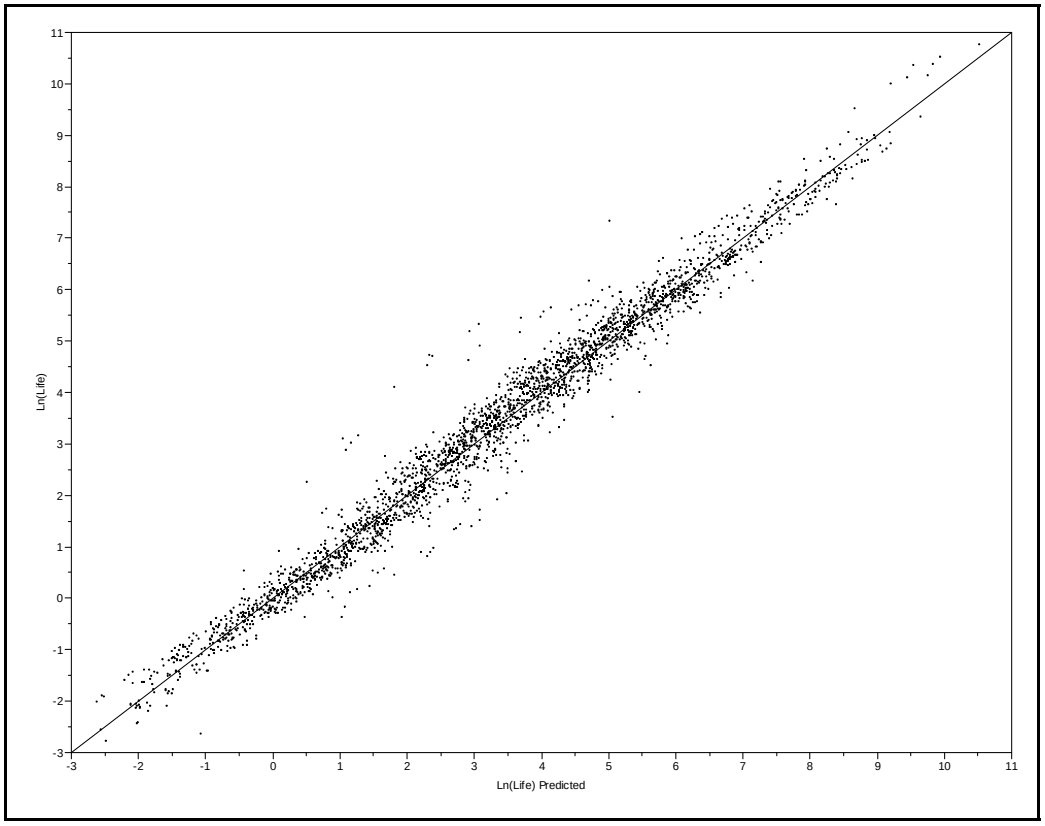

Figure 70: Creep life actual by predicted for initial experiment

Another great way of visualizing the ranges of the materials is through a so called bubble plot. This graphically illustrates the range of results for the different materials types in terms of the log of life. A better understanding of the material performance within the design study can then be achieved. The results

depicted in Figure 71 reflect those found in Figure 69, with the best material for the design study being material fourteen. This is a Waspaloy derivative, and apparently the most robust metal within the selection. In this plot the darker the circles the more numerous the results they represent, a simple visual histogram in some ways.

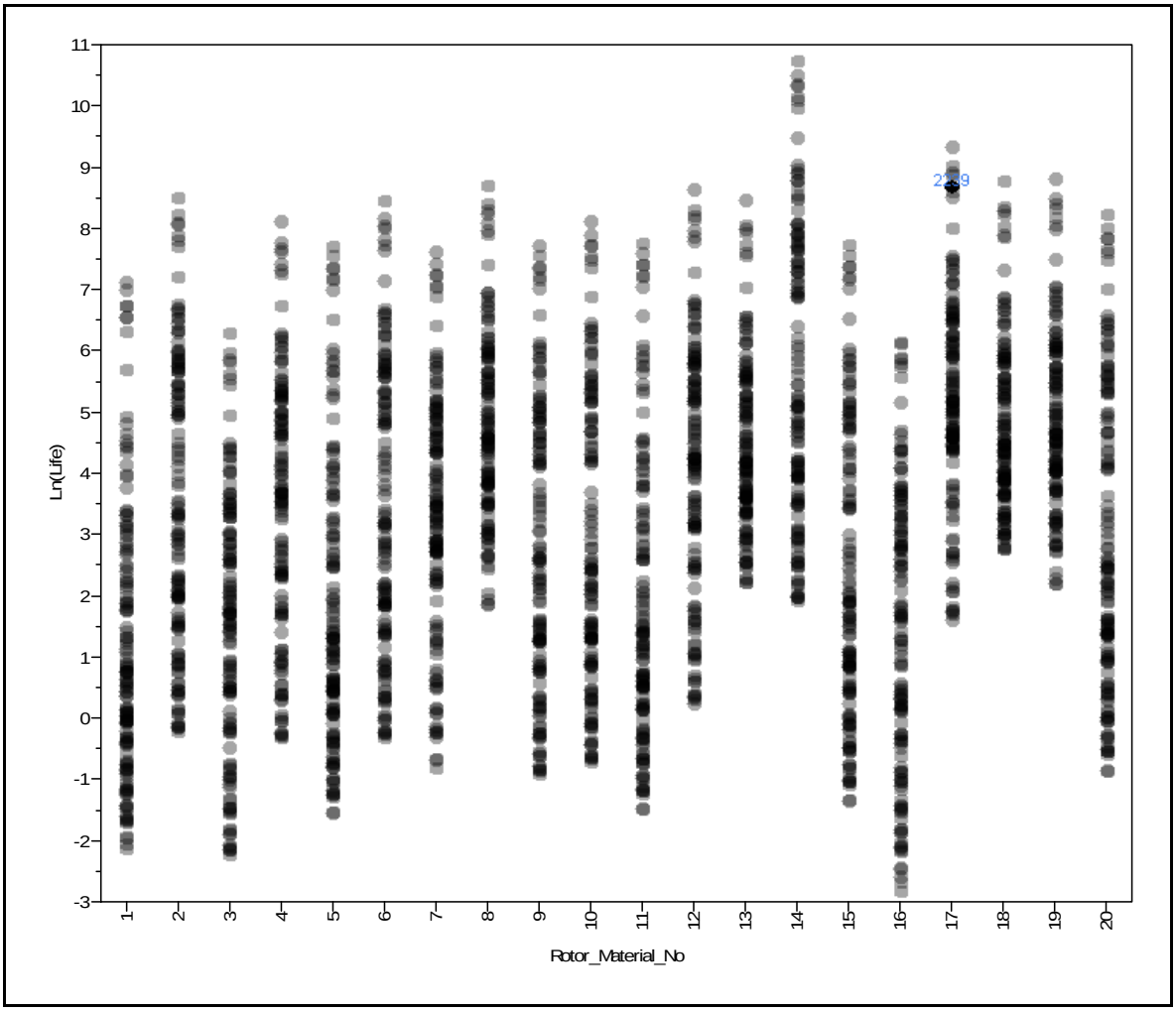

Figure 71: Materials performance with respect to lifing.

It should be noted that WASPALOY is generally considered to be an alloy unsuitable for blade utilization. However the material indicated for best use, fourteen, is listed as a derivative of WASPALOY. The composition for this had been taken from the composition of this metal and altered then the values run through JMatPro ™ to determine the thermal-mechanical properties. This derivative is significantly different to the original (material number one), not only in the composition (see Table 7 & Table 8) but also in terms of service life in the studied situations (Figure 71). Thus it could be said that the naming of the material is a little misleading but was done given the based of the variation.

Table 7: Comparison of metallic composition of materials 1 and 14

Materials		Percent Composition									
		Ni	Al	Co	Cr	Fe	Hf	Mn	Mo	Nb	Re
1	Waspaloy	61.4	1.3	13.5	19.5	0	0	0	4.3	0	0
14	Waspaloy derivative	57	3.5	14.7	21	0	0	0	3.8	0	0

Table 8: Continued comparison of composition for materials 1 and 14

Material		Percent Composition								
		Ru	Si	Ta	Ti	W	Zr	B	C	N
1	Waspaloy	0	0	0	3	0	0	0.006	0.08	0
14	Waspaloy derivative	0	0	0	2.87	0	0	0.007	0.09	0

Altering the nickel content through the addition of significant Aluminium and chromium additions improved the creep lifing capabilities significantly. This was also along with small changes to other compound contents and thus a full investigation would be required to find the underlying causes. However, this is

beyond the scope of this thesis work. Though at the time the selection of the material composition was somewhat random, in order to fill out the database, it was certainly positive as we have seen.

The results for the flare angle are some what interesting. Given the nature of the DoE used (a LHC/CCD mix) to capture the eleven continuous variables and the fact that this then needed to be repeated twenty times to reflect the different material types in the data sheet, a great deal of repetition in the model was going to occur. This is represented in the model with the stratification of the results. Furthermore it was discovered that some of the methods used within this analysis had limited accuracy, which at this level of design isn't a particularly big issue. This lack of accuracy was due to their inability to handle data down to the number of significant digits that the DoE was providing.

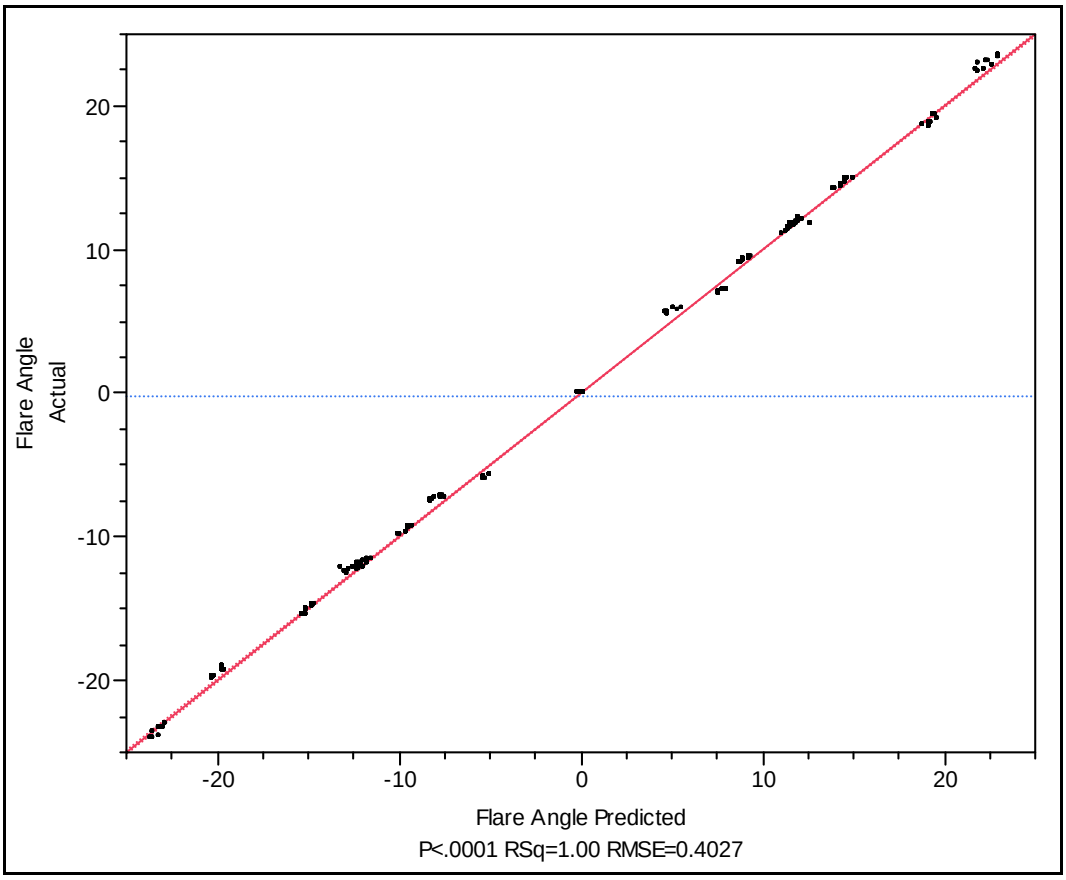

Figure 72: Initial experiment flare angle actual by predicted

This just meant that there were clumping around certain response values. The excessive repetition of the values proved problematic for the modeling techniques, though the effect was not significant. Figure 73 illustrates this with the bands of residuals, but their relative size compare to the predicted is within an acceptable band of error.

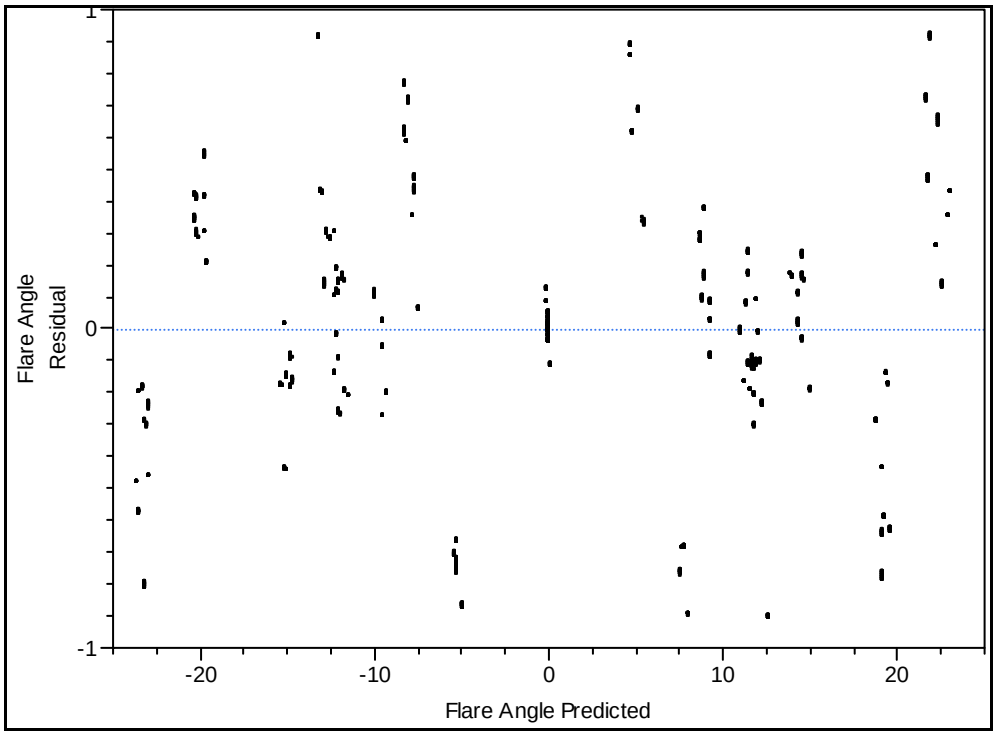

Figure 73: Initial experiment flare angle residual by predicted

The main point of consideration once it has been determined that the response fit is suitable, is how the response reacts to the variation of the input parameters. Thus, the traces that are found within Figure 67 are studied for the flare angle. This analysis reveals that the main factor for this response is the radius ratio. This should be expected given that it is the radius ratio, ν, which determines the radius of the stage and thus the flare angle, from geometry it is:

$$Flare\ Angle = \frac{Radius - (\nu \times Radius)}{Blade\ chord + {blade\ height}/{12}} \tag{83}$$

The other response that was affected by this clumping of values, the swirl angle (α_3), or the exit flow angle as it is otherwise known (see Figure 74 and Figure 75). The fact that these repossesses were the ones affected leads the author to believe that it was the developed stage and stress codes that are the ones causing this issue, due to precision issues within MATLAB. However the results that these produce are more than sufficient for the level of fidelity that this approach is meant to operate.

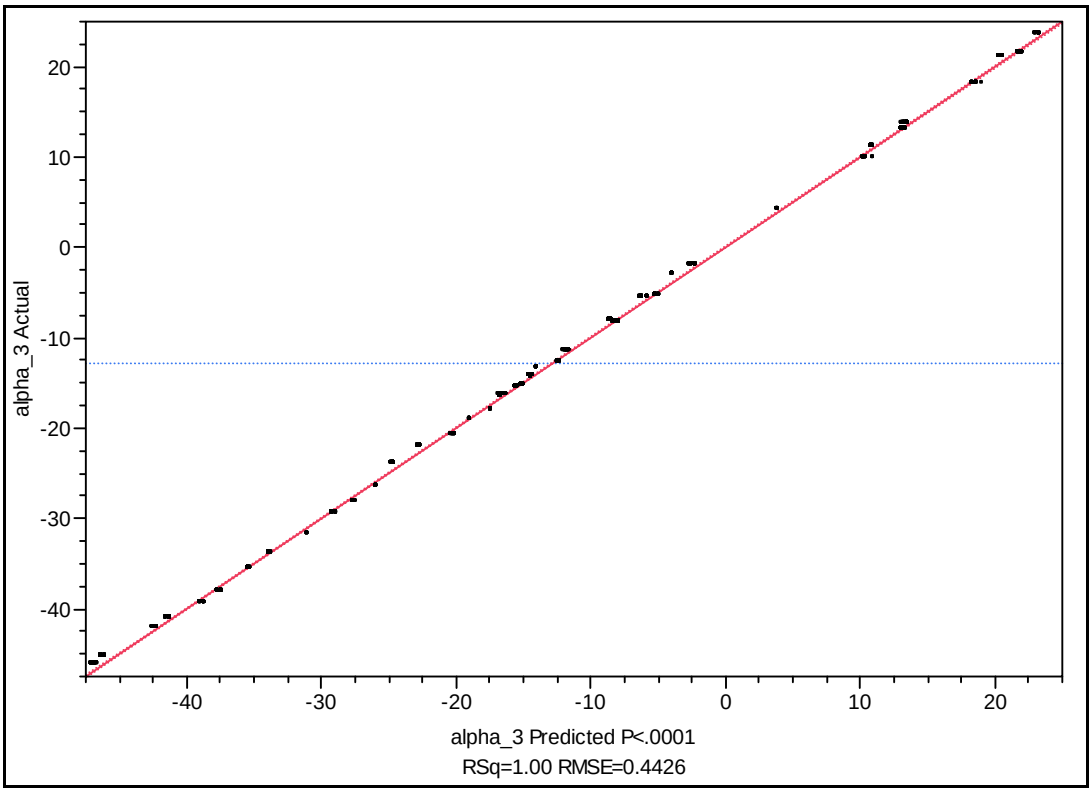

Figure 74: Initial experiment swirl angle actual by predicted

The lack of and skewing in the residual by predicted of the stratified layers, indicates the lack of detrimental effects that this has on the values of the

predicted model. Once more, the residuals from the neural net model are within acceptable limits.

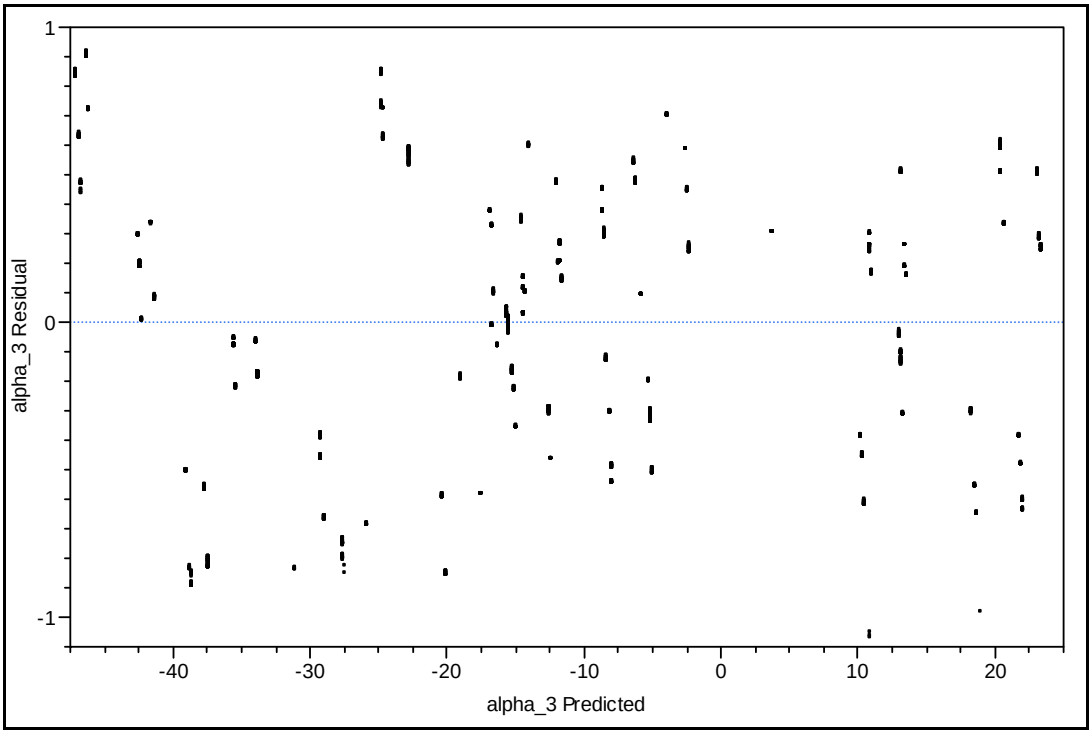

Figure 75: Initial experiment swirl angle residual by predicted

The stage reaction is one of the top three effects observed for the swirl angle in Figure 69. It would appear from these results to be the second most important variable, a figure that will possibly be corroborated in later sensitivity analysis. A full discussion of the routes of the effects will be considered at that time.

Finally the last consideration is that of the stage efficiency, this fit is particularly good. The clumping seen in the angular responses is not witnessed here and the results are relatively well distributed reflecting the multitude of input variables that affect this one particular response as will be discussed later.

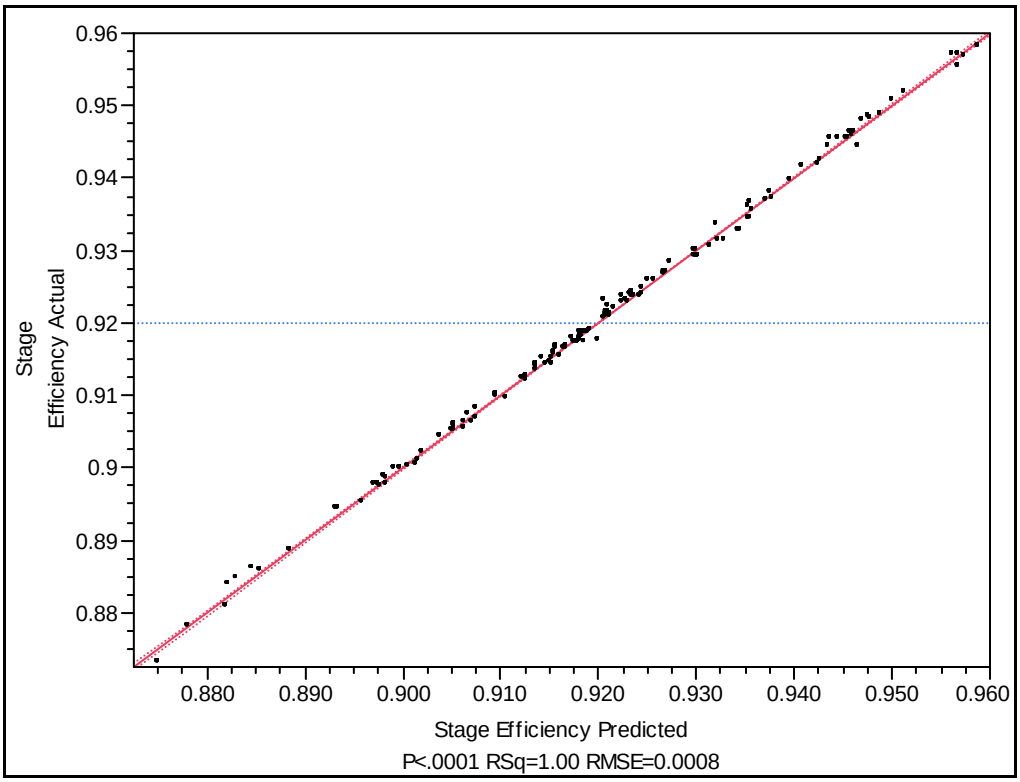

Figure 76: Initial experiment actual by predicted for stage efficiency

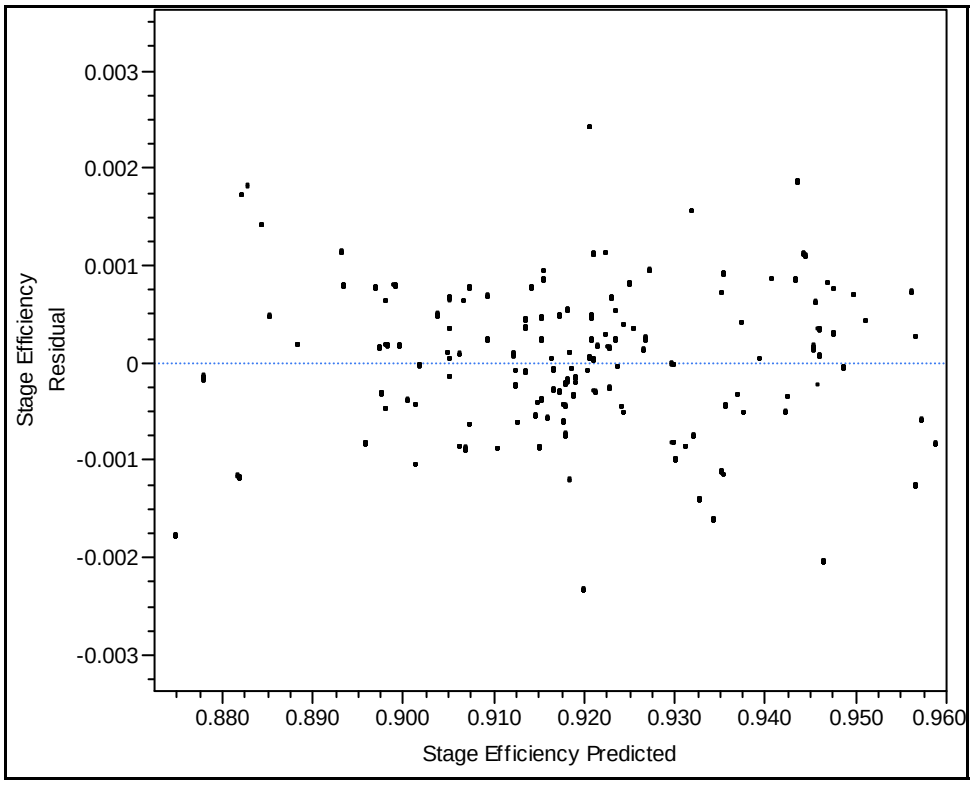

Figure 77: Initial experiment stage efficiency residual by predicted

Moving now the effect of the design variables on the response of the stage efficiency, as before a variable by variable approach will be taken. The response of the stage efficiency is, as mentioned earlier, well behaved, and thus the effects of the variables chosen followed the accepted theory. Figure 69, highlights two significant factors affecting the stage efficiency, these being: the radius ratio, ν, and the stage loading, λ. Beginning with the radius ratio, it can be seen that an increase in, ν, leads to an increase in the stage efficiency. This is to be expected due to the nature of the ratio, and its relation to the rotor and stator exit axial velocities, as highlighted in equation 84.

$$\nu = \frac{R_2}{R_3} = \frac{U_2}{U_3} \tag{84}$$

Further discussion on this matter can be found in section XX. The other major factor for the stage efficiency can be identified as the stage loading, λ. Again this can attributed to a reduction in rotor perpendicular exit velocity, U_3, along with the increase in the change in temperature gradient across the stage, from equation 85:

$$\lambda = \frac{1}{U_3^2} = \frac{2 c_p \Delta T}{U_3^2} \tag{85}$$

The results taken from this model have highlighted some interesting facts, both from the results themselves and their interactions. Investigating the traces within Figure 69 highlights some interesting interdependences between the design variables and the responses. Looking first at the responses based on the variation of the reaction, in Figure 78, one notes that in order to improve stage efficiency, issues arise with the magnitude of the swirl angle. Thus should the design depend on the increase in reaction to achieve the desired stage efficiency (since the life improvement tails off), allowances would have to be made for the addition of an exit guide vane to improve the aerodynamics for the following turbo-machinery.

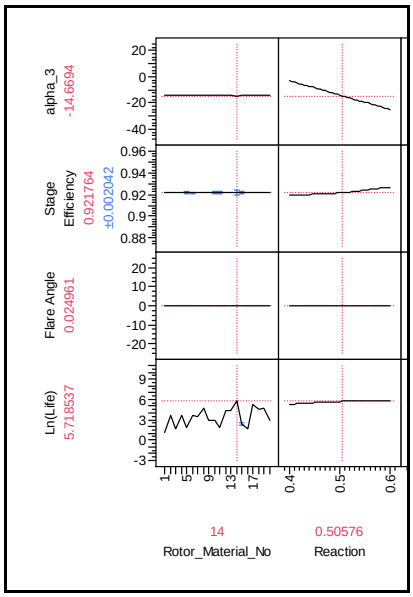

Figure 78: Consideration of the variation of the reaction

Reaction is not the only variable of interest. The radius ratio, in Figure 79, illustrates how sometimes the drive to improve the stage efficiency improves on one constraint (Swirl) only to show detrimental effects on the other. Increasing the radius ratio shows slight additional improvement in the creep life thus for both responses is desirable. However, taking the radius ratio to its limit, as would be needed, takes the flare angle beyond an acceptable value. Thus a trade-off is required to degrade the stage performance and creep life until an acceptable angle is achieved.

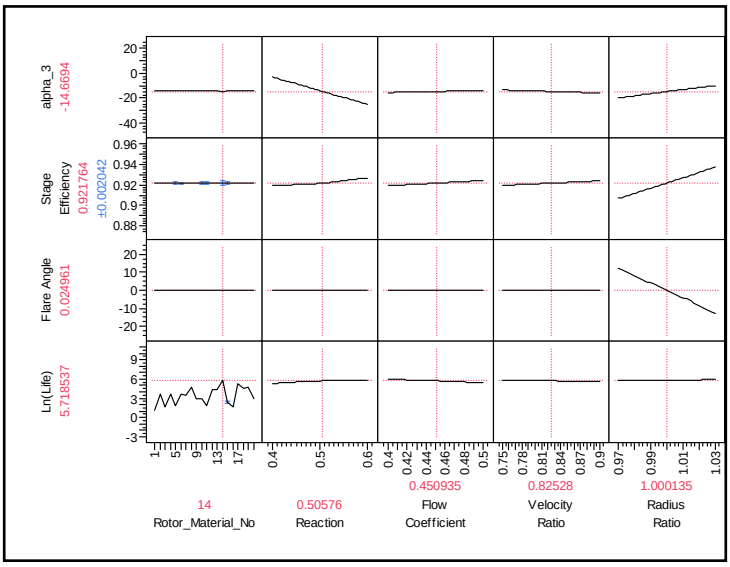

Figure 79: Consideration of the variation of the radius ratio

While these two variables are not the only ones exhibiting notable behavior these set the scene for the rest of the experiment. It should be noted that these results are all dependant on the assumptions based within the analysis environment and the ranges for the variables. Thus, through the validation of the responses from the turbine design model, a proof of concept has been achieved. The results have highlighted the fact that a creep based design solution can be reached, when considering the conceptual phase of the engine.

4.2 System & Materials Study

The results from the previous section have shown that the model is can be considered verified for design point case. The work provided the necessary knowledge of the analysis approach to proceed in the drive to provide supporting research for the research questions and hypotheses. We have seen how the blade lifing can be successfully modeled whilst considering life and other engine design metrics. If we recap back to the need, Figure 26 illustrated a desired flow of information about the design process, looking from the system level right down to the material composition level in terms of blade life. Though the previous model did very well at expanding the knowledge of the blade design process, it was limited in considering just the blade and turbine stage design. Consideration of any higher factors was limited to the consideration of the upstream combustor through the CPF. Thus to fulfill the work as set out within chapter 3, a study to look at the turbine engine as whole, from the materials through to the system level is required. Thus the question arises, just how can this be achieved? Before answering this, one needs to realize the desired scope of this research. It is the intention of the author to work to within the limitations necessary for presenting his work within this document. While is it possible to consider a large number of variables within the analysis environment, presenting and discussing the results from this work would be difficult, whilst achieving the desired visualization of the work. It is this visualization that is a

critical part of the work within this thesis and thus needs to be brought across strongly within the document, supporting the hypotheses that answer research questions five and six.

Therefore in an effort to maximize the usability of the work, it has been decided to fix the design of the turbine blade stage geometry and base the work around a design study on these. As a result, a design based on a production blade and stage was chosen. Given the wealth of data available, the NASA/GE E^3 [76]was utilized, therefore the author was not limited by industrial knowledge ownership considerations and all results could be published in their raw form. This design study is intended to enable the author to play the game whereby the geometry has been fixed by say external issues, and performance and lifing gains or trades are needed before the design is finalized. Say the possible inclusion of new technologies or the chance of the engine operating condition. This could also include the tradeoff between the inclusions of expensive technologies versus any detrimental effects that non inclusion would have.

4.2.1 Design Variable Selection

An exploration is now required to determine the options for the intended research around the fixed blade geometry design. Let us first consider the inclusion of some materials based research. In the previous model the materials effort was limited to the study of metals by number. Looking at the effect of the different materials on the blade life, well what about considering the metal at its

composition. In other words, what would be the best percentage chemical composition of the different compounds within the nickel superalloy? The full compositions of the alloys included in the materials model are describe in appendix D, from that we can see that there are 19 different possible compounds used for the compositions of nickel superalloys, some of which are extremely expensive to use. Each of these compounds has a specific purpose, whether it be to improve creep resistance or improve oxidation resistance amongst others. However each compound does not necessarily improve all the properties of the metal, in fact while improving say the oxidation resistance a compound can have a detrimental effect on the creep life. Therefore the design of a blade material is one big compromise. Considering these effects on blade life of all of these compounds at once would prove to be difficult with the available data, until Mr Hong's work [104] is complete. Until this time the data is limited to the 20 materials contained within the model. This cuts down on the variable compounds to consider, and limiting the consideration to the five major compounds of the superalloys (excluding Nickel). These being:

- Aluminium, Al
- Cobalt, Co
- Chromium, Cr
- Iron, Fe
- Hafnium, Hf

Though Iron only appears in a few of the alloy's composition it is a very important addition to the alloy. In fact the alloys containing this are considered their own sub group within the Nickel superalloy family, that of the Ni-Fe Alloys. To account for the affects of the varying compositions the usual material number will have to be entered into the analysis model and then the compositions considered during the metamodeling and visualization process. Without the full material property models and thus complex mixture designs necessary to ensure that the compositions always meet one hundred percent, this is the only means possible to achieve the desired solution. This effect will not be to the detriment of the accuracy of the research, in fact it will help to illustrate the typical interactions between the percentage compositions of each of the five compounds.

Now that the consideration of the material level has been made consideration for the system level needs to be addressed similarly. Therefore one needs to turn and decide on some easily determined variables that would best represent changes that would be made at the system level. These changes could be a desire for more thrust, to fly higher and maybe fly faster in addition. The easiest means for the engineer to represent the need for more thrust would be to increase the T_4. This would be an excellent variable to use since it would bring into play trades between it, materials considerations and cooling decisions. Would a lower T_4 be acceptable if a significant gain in lifing would be possible? The variation of T_4 could also be made to represent the choices in combustor

technology, something that could be very interesting as the engine company's move to a reduction in emissions.

Furthermore, one could consider the mass flow through the turbine. This would be determined from either the airspeed at which the engine is operating or the altitude, since $\dot{m} = \rho.A.V$. A change in flow velocity would obviously have a more significant effect than a slight change in density that would represent a change in cruising altitude of a hundred feet or so.

In addition one could also consider the turbine RPM as an input variable to the analysis model. Considering this would bring with it the consideration of disk stresses through the WATE ++ code and the centrifugal and gas bending blade life.

Now for the selection of the final input variable we shall move in a slightly different direction. Wanting a variable that would tie in well with the variation of T_4, one turns their attention to the consideration of TBC thickness. This is a major design choice, the coatings are expensive, and therefore could the same life be achieved with less coating, thus saving money. Not only on the cost saving side, but thick TBC coatings run into problems through delaminating under high stresses [45], so looking for an optimum thickness would be most beneficial.

It is intended therefore that through the selection of the independent variables this model will enable the consideration of trades between the system and part and material level within the one analysis. The ranges of the intended

inputs are included in, Table 9, below. To work with these design variables it is necessary to select the most appropriate responses to study, this continues below.

Table 9: Ranges for eight design variables included in the Design of Experiments.

Design Variable	Description	Lower Bound	Upper Bound
T_4	Turbine entry Temperature (°F)	2550	3150
RPM	Rotational speed (rpm)	11,500	13,500
TBC Thickness	TBC material thickness (mm)	0	4
W2	Turbine mass flow rate (lbm/s)	100	140
Al	% Aluminium	1.3	5.9
Co	% Cobalt	0	17
Cr	% Chromium	6	21.0
Fe	% Iron	0	2.5
Hf	% Hafnium	0	1.5

4.2.2 Model Response Selection

In view of the fact that this second model is intended to enable on the fly design trades, significant factors need to be identified for study. Obviously the first response for inclusion within this model will be the blade life, since the consideration of this is the mainstay of this thesis. Beyond this decisions are still open.

Considering that there is the consideration of the engine RPM amongst the design variable, it is only natural to consider AN^2. This is a product of the meanline annulus area and the rotational speed squared, and is an important blade stress and rim stress factor within the turbine. Providing limits for both

rim speed and material stresses [138]. Therefore along with the stress based lifing results, they come to form a useful consideration for design decisions.

The inclusion of T_4 and TBC thickness within the design variables invites the selection of the cooled turbine efficiency generated within COOLIT. Thus it would be possible to understand and investigate the direct effects of these variables on the efficiency of the engine based on their effect on the turbine blade cooling system.

The remaining input variables, including the turbine blade and stage geometry are set to directly replicate that of the NASA/GE E^3 aero engine. The DoE suitable for neural network surrogate modeling was, as with the previous model run through the Model Center ™ environment and the results from this then entered into the statistically analysis software JMP ™ for the modeling and visualization stage of this approach

4.2.3 Second Model Results

To begin the design space exploration for the purpose of the second model, a similar approach was taken to the DoE design as had been used within the first model. The mix of CCD and LHC had proved to work so well with the first model that the continued use in the second model would be appropriate. The mixed results over the twenty material points provided a DoE of one thousand two hundred and sixty cases (sixty three per material), perfectly sized

to provide the correct amount of data for the model whilst not consuming excessive computational resources.

Running the inputs through the Model Center ™ environment went smoothly with no failed cases. Obviously the fact that there was really little change within the cycle produces no failed aero-thermal nor structural cases. Combining these results with the NPSS output file results, provided the necessary outputs to cover all eventualities within the simulation. Using the previous neural net settings within JMP as a baseline to work with, the values in Table 10 were found to be the optimum in terms of computational time and accuracy.

Table 10: Neural Net settings for system and material experiment.

Variable	Value
Hidden Nodes	9
Overfit Penalty	0.001
Number of Tours	40
Max Iterations	200
Converge Criterion	0.00001

It was found as with the previous model that the number of hidden nodes around ten was required. However given the smaller size of the DoE a greater setting for the number of tours and iterations could be utilized whilst remaining within an acceptable user timeframe. The simulation results are very promising with an overall training and testing R^2 of 0.99872 as illustrated in Table 11.

Table 11: Second experiment simulation fitting history.

Nodes	Penalty	R^2	CV R^2	Training and Testing R^2
9	0.001	0.99869	0.99858	0.99872

Looking beyond the fitting history above, the results show particularly promising error values across the board. It would tend to suggest therefore that the design space under consideration could be more easily represented that the previous. But this is not necessarily so. The work within this design space was more concerned about the work around a baseline design and therefore the turbine stage and blade designs were mostly fixed, reducing the uncertainty associated. Additionally, the materials were decomposed into their compounds and thus an improved understanding of the material space was gained. The designer can then achieve a better understanding of the effects caused by changing the material types within the design space.

Table 12: Error report for second experiment responses

Response	SSE	RMSE	SSE Scaled	RMSE Scaled	R^2
Ln(Life)	53.694064136	0.20936067	3.4554757632	0.05311117	0.9972
AN2_1	1.6590982521	0.03680171	0.7557822871	0.02483878	0.9994
Cooled Efficiency	8.1565487e-6	0.0000816	0.4976478635	0.02015547	0.9996

Considering the just the data above would be short of confirming the success of the simulation of the second model were it to be the only measure. In addition to this data the most productive judges of fits are as previously discussed the actual by predicted and residual by predicted plots. The data within these is a great representation of the suitability of the model for the use to which it has been put. These plots (Figure 80,Figure 81 and Figure 82) validate the level of fit that was alluded to within Table 12, with the points along the and tight to the desired axis.

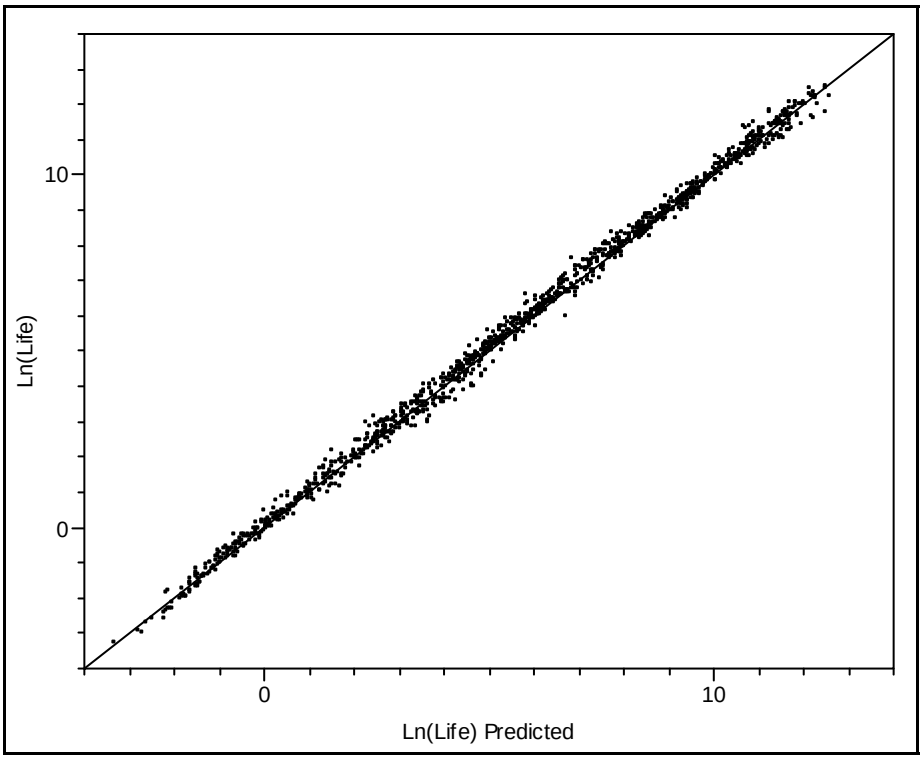

Figure 80: Second experiment lifing actual by predicted.

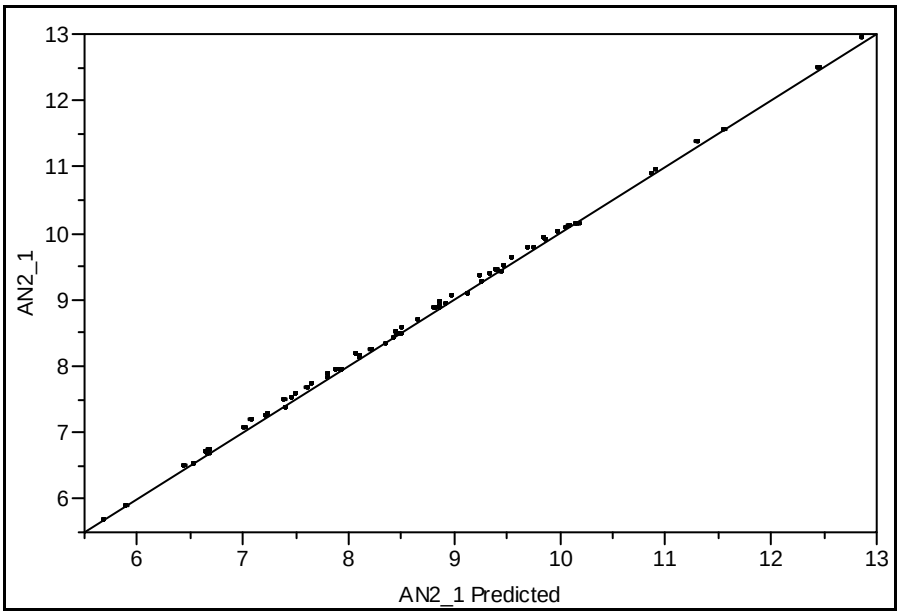

Figure 81: Second experiment AN^2 actual by predicted

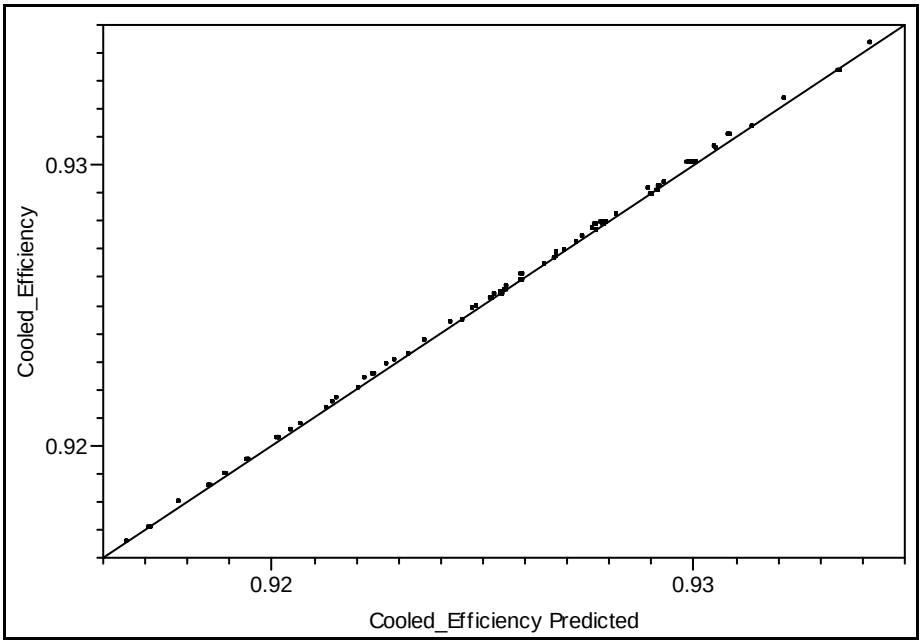

Figure 82: Second experiment cooled efficiency actual by predicted

The plots have also shown that the modeling of the material number as a discrete value has again let to the stratification of the outputs. However this is not the only reason for this result. As with the previous model the modeling environment itself does not accept nor output values down to the same numbers of significant digits as has been entered through the DoE, therefore the bunch is also attributed to the rounding that automatically occurs within the code. For example, the LHC requires that the TBC thickness is entered at the fourth significant digit to maintain the desired design space exploration. However COOLIT is not able to distinguish the thickness at this level and so rounds the numbers to its own level of accuracy. The code was designed to compare TBC

thicknesses but not down to the tenth of a millimeter. A true exploration of this phenomenon is possible through the manipulation of the results within JMP.

Moving on to the consideration of the residual error distributions, as with the previous model small residuals are desired when compared to the predicted values. Figure 83, Figure 84 and Figure 85 all show favorable results, though the creep lifing in Figure 83 boarders on the edge with near ten percent residual values in places. It is to be expected that the creep lifing had the higher residuals given its lower fit parameters as shown in Table 12.

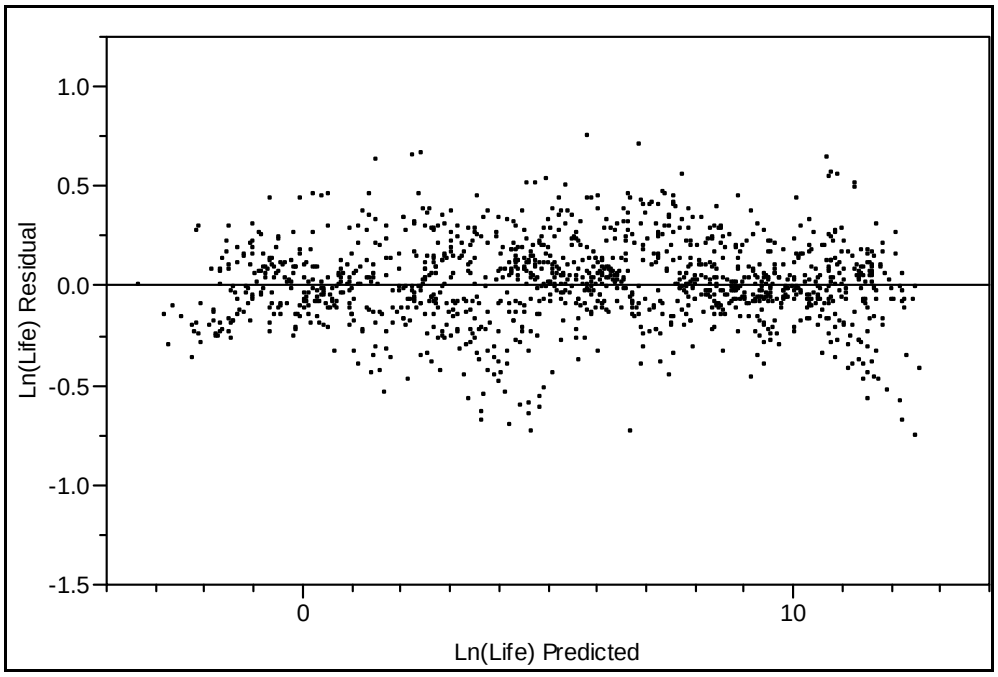

Figure 83: Second experiment life residual by predicted

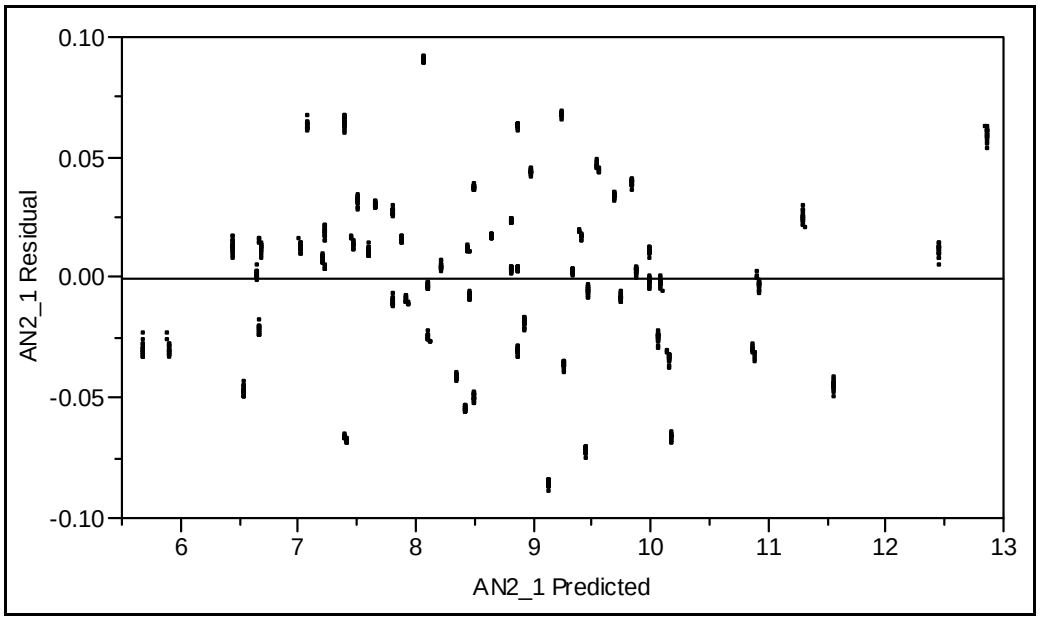

Figure 84: Second experiment AN^2 residual by predicted

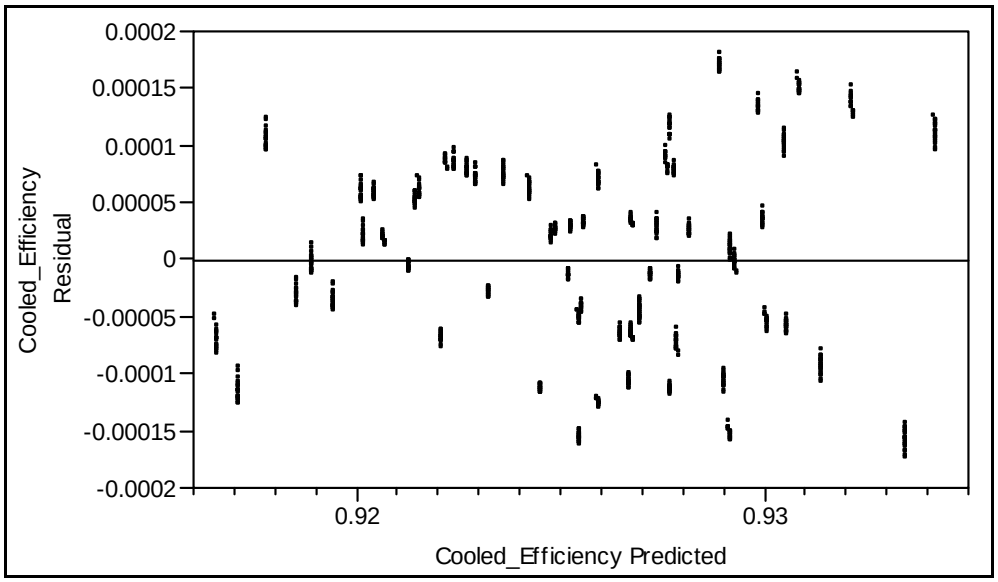

Figure 85: Second experiment cooled efficiency residual by predicted

The stratification is seen again in the residual by predicted plots, as with the previous work, and again has its causes within DoE structure and the methods utilized. However one will immediately recognize that the values are themselves negligible when put in comparison to the predicted values. Thus, any detrimental effects can really be ignored.

Now that a suitable surrogate model has been achieved to represent the results of the analysis, the real benefit of the intended approach can begin the visualization of the design space. The most appropriate method for this stage of the process is the use of the prediction profiler as mentioned earlier in this chapter. The prediction profiler for the second model is depicted in Figure 86. The results show how the materials work to alter the life of the blade as their compositions change. In addition, this profiler easily highlights the changes that the other input variables cause on the responses. The thermo dynamic effects all follow the expected theory as do the mechanical effects. The extent of the changes in the life of the blade due to the changes in the material properties are very interesting, and the ability to easily visualize these to improve the understanding will be discussed the next section, as will investigation of the responses of the other variables.

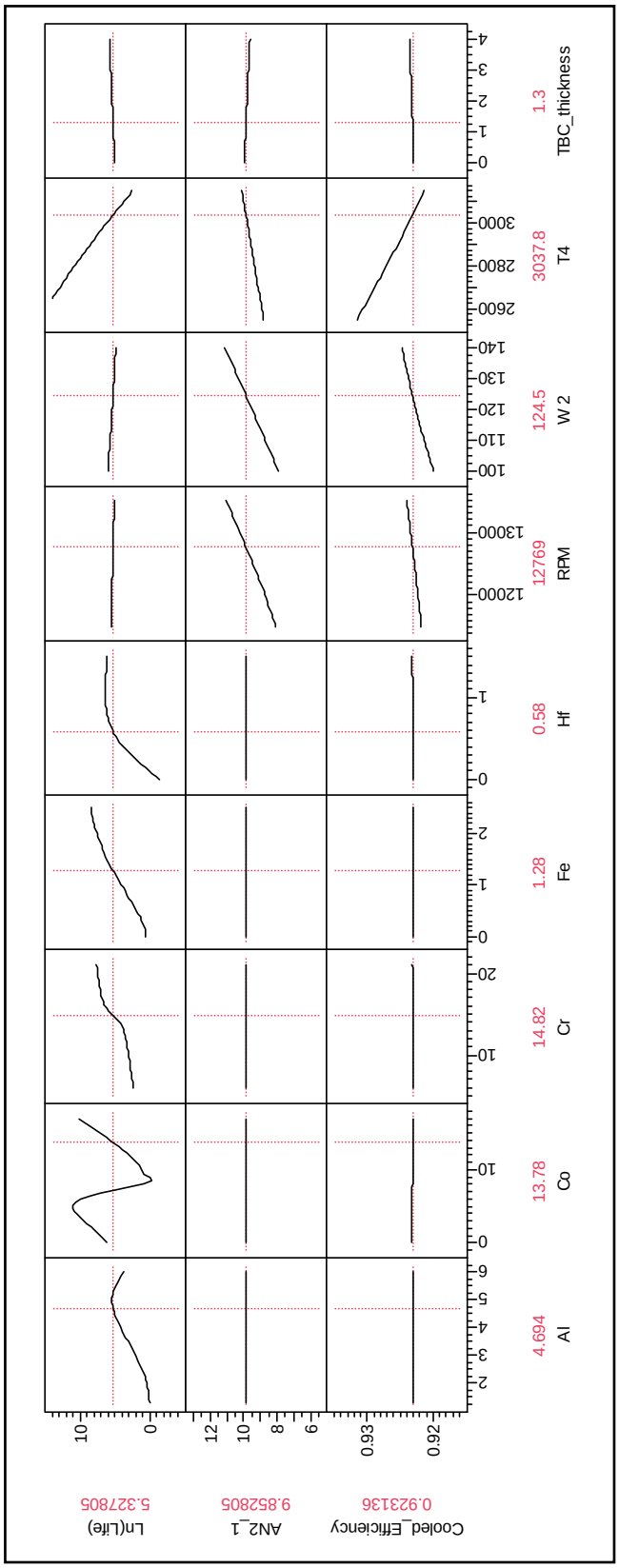

Figure 86: System and materials experiment parametric interactive trade-off environment

The non material related variables again illustrate the usefulness of this approach in highlighting the requirement for trade-offs between the performance and creep life considerations. While some of the trades are more obvious than others, the requirements can change and even small changes in a response can become critical. These trades only become obvious using a visual based method such as this. The creation of the parametric interactive trade-off environment is not the only approach available to the designer for design space visualization and understanding. The following section will explore further how to better answer the postulations of hypothesis six and how it applies to the first and second experiments.

4.3 Design Space Exploration

The implementation of the approach is only as good as the means by which it enables the user to understand the design space. The design space has been spanned through the use of the DoE methods. Selecting the correct ranges to encompass your desired area of interest is the key here. The selection of these is not the only consideration though. Through the utilization of the JMP statistical software the user is fully enabled to explore the results learning what they need from the data.

The package comes with some very powerful features to enable this design space exploration. The use of the multivariate approach has been discussed previously at the end of chapter five. This along with further methods

discussed herein provide the visualization necessary for this approach to support the conclusions in the hypotheses in chapter three. In addition to the capabilities provided through the multivariate approach a much simpler method exists that provides and easy visual and analytical representation of the sensitivity of a given response to its design variables. Through this the most important variables can be identified and a better understanding of the response gained.

4.3.1 Sensitivity Analysis

A simpler means for understanding the responses of the system to the inputs of design variables is the Pareto analysis method to ANOVA. This method is a statistical technique in decision making that is used more generally used for the selection of a limited number of tasks that produce the most significant overall effect. It uses the Pareto principle [139] whereby eighty percent of the response is caused by twenty percent of the variables.

4.3.1.1 Turbine Stage and Blade Design Study Analysis

Applying these principles to each of the four responses from model one will help to understand the behavior with respect to the variation within the input variables. Working with creep life response first as depicted in Figure 87, illustrates the effects of the turbine and blade sizing variables on the results along with which material would be used.

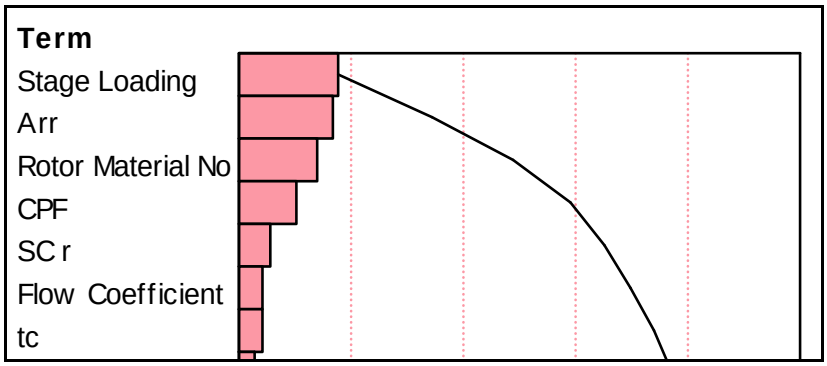

Figure 87: Shortened Pareto Analysis for the first experiment creep lifing.

Figure 87 illustrates just how significant the stage loading is in the determination of the blade creep life in this study. To understand the reason behind the importance of this factor, one needs to consider the formulation of the factor, as in equation 86.

$$\lambda = \frac{1}{U_3^2} = \frac{2c_p \Delta T}{U_3^2} \tag{86}$$

It can be seen that the stage loading is mainly affected by the change in temperature across the stage and the whirl velocity, U_3. These particular factors both form major components within the stress analysis, the temperature for the thermal stress and U_3 for the rotor gas bending stress, from the equation 87.

$$\sigma_{GB} = \left(\frac{\dot{m}}{g} \cdot \frac{(U_2 - U_3)}{N_{Blades}}\right) \cdot \left(\frac{h_2 + h_3}{2}\right) \cdot \left(\frac{1}{z_s \cdot c_{true}^3}\right) \tag{87}$$

Beyond the stage loading the thermal and geometric variables prove to be other important contributors to the variability of the blade creep life. This also

includes the variation of material type through the rotor material number variable, providing a useful comparison of Nickel superalloys within this application.

The other performance response within this experiment, the stage efficiency (Figure 88), shows its dependence on the aerodynamic stage design factors. Illustrating how the condition of the flow is paramount in improving stage efficiency.

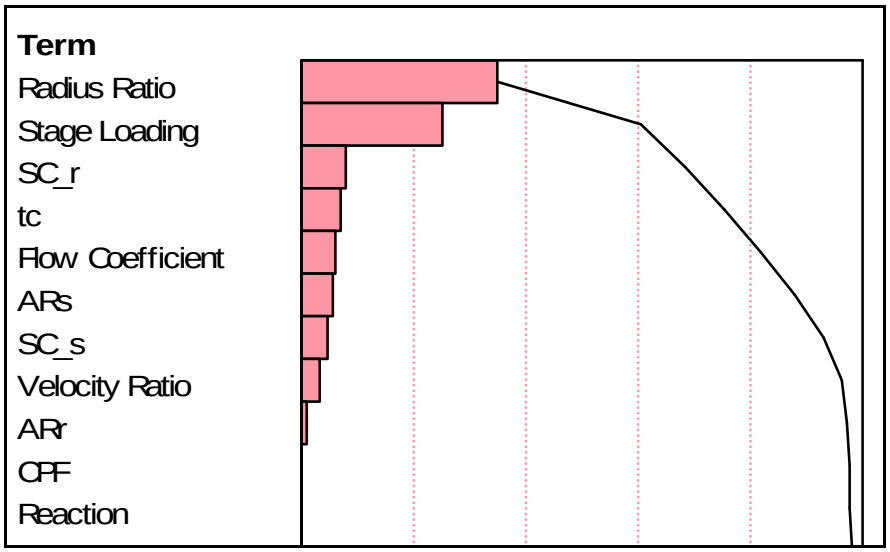

Figure 88: Shortened model one stage efficiency Pareto analysis

The particular reliance of this response on the radius ratio, ν, would suggest that the stage efficiency is particularly influenced due to pressure changes associated with radius change rather than axial flow turning. Investigation of the loss model (section 3.3.5) indicates that work from radius

change can be achieved with little or no loss, whereas the turning of the flow has significant losses associated with it.

The two other responses included within the experiment are more as design guides to provide a better understanding of the design space. Figure 89 shows how the swirl angle response is dominated by the reaction, *r*, and stage loading, λ, coefficients as the theory would suggest.

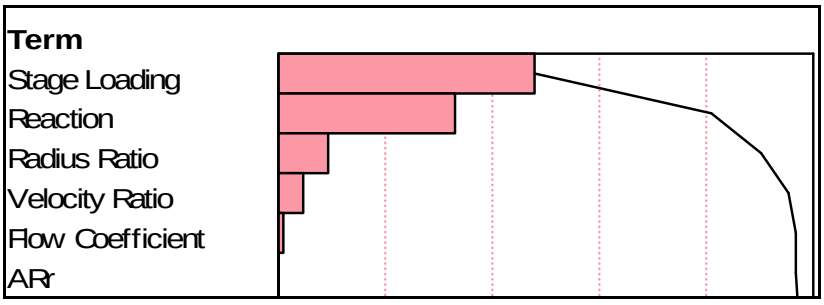

Figure 89: Shortened initial model swirl angle Pareto analysis

The velocity triangle analysis from Schobeiri [80] in Figure 43, illustrates how the magnitude of α_3 depends on the velocity U_3. Therefore, explaining the importance of stage loading, radius ratio and velocity ratio as seen in Figure 89. The dependence on the reaction, *r*, requires the simplification of equation 78 to the form seen in equation 88 below.

$$r = \frac{\Delta h''}{\Delta h' + \Delta h'' S} = \frac{1}{2}\frac{W_{u3} - W_{u2}}{U} \tag{88}$$

This equation illustrates how the stage degree of reaction depends on the component velocities that determine α_3. The fact that these contributing factors pay such an important part in the simplified equation, explains the significance of the variable within the Pareto analysis.

The flare angle as illustrated in Figure 90 is almost entirely dominated by the radius ration, something that both the prediction profiler (Figure 69) and the theory have previously alluded to. If one was to think about it the flare angle is a reflection of the change in angle of the flow through the turbine stage and therefore a change in radius would be the obvious driver for this.

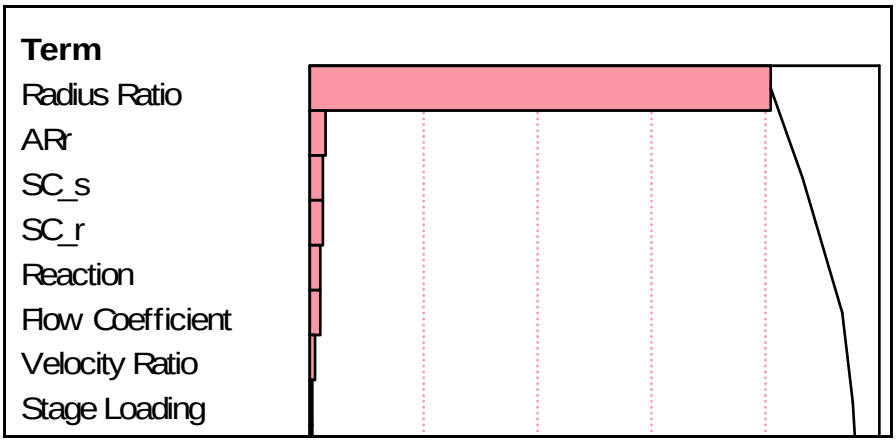

Figure 90: Shortened initial experiment flare angle Pareto analysis

This simple analysis obviously has its shortcomings, in that is only deals with one variable at a time, but addressing that will come later. However the investigation of the Pareto analysis has helped to verify the analysis further

through the understanding of the effects of the input variables and their comparison with the expected theory.

4.3.1.2 System and Material Study Analysis

The Pareto analysis of the second experiment was carried out to find the sensitivity of the responses to the input variables of the neural network model. This analysis confirmed what was to be expected for each of the responses, these being: creep life, cooled efficiency and the factor AN^2. The results of this analysis as discussed in the following section.

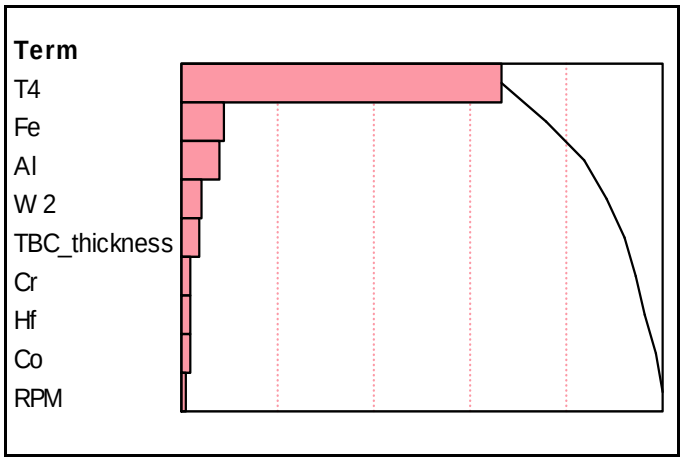

Figure 91: Second experiment creep life Pareto analysis.

The main response of interest in this work is, as with the previous model, the life of the turbine blade. As would be expected the effects screening highlighted the importance of T_4 in the response of the output, expected given its prominence in the thermal analysis, stress analysis and material property determination. The materials contribution came in the noted importance of Iron

and Aluminium on the response, matching up with the fact that the stronger metals all contain some Iron and Aluminium within their compositions. The addition of Iron into the metal matrix actually forms a completely new set of Nickel superalloys known as Ni-Fe superalloys. Thus, it can be shown that the materials model through this analysis environment has picked up on this change in material type very efficiently. A more in depth analysis of the effects of the different metallic compounds with the structure of Ni superalloys can be found in the work of Mr. Chul-Hwa Hong [103]

Additionally the gas flow rate, W_2, through the turbine is shown to have a significant effect on the response of the turbine blade creep life. Figure 86, illustrates how, by increasing W_2 the creep life of the blade reduces. The small effect on the response is due to the fact the effect on the overall stress, is limited just to that of the gas bending stress.

The TBC Thickness is also considered but its overall effect is shown to be small in Figure 86. This makes one consider the need for inclusion of a TBC, however, the extra benefits of its inclusion are not captured within this experiment, these being the improvement of the oxidation and corrosion resistance of the susceptible Nickel superalloys. A true cost analysis would have to be completed before any conclusions could be drawn, since it is often only a small increase in T_4 that is sought from the thermal benefits of this coating.

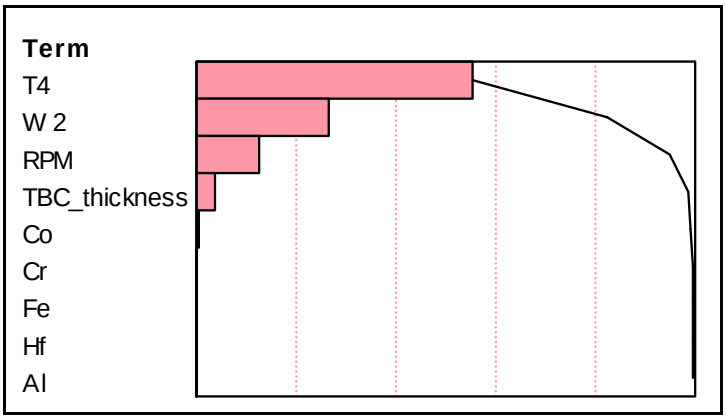

Figure 92: Second experiment cooled efficiency Pareto analysis.

Consideration of the cooled efficiency was driven by an investigation of how much of an effect the turbine inlet temperature would have. It was expected to be one of the major variables from trace profile within the interactive parametric trade-off environment. The Pareto analysis (Figure 92) proved this assumption to be correct, but its relation to the other design variables displayed in Figure 86, raised more questions. From the onset more of a beneficial effect was expected from the use of a TBC layer. However, just as the traces within Figure 86, the results from the Pareto analysis in Figure 92 showed that this was not the case. To understand this one needs to consider the TBC properties used for this work. The figure for the thermal conductivity of the material as suggested in the COOLIT manual [96], is 30 Rankine (30 Fahrenheit) per millimeter. This value is pretty typical of the current coatings used in industry [36, 48, 140], but the actual drop in temperature across say typical two millimeter coating is marginal in comparison to the actual gas temperature, T_4.

It is now being suggested by the likes of Sir John Horlock [46] amongst others that the drive for increased T_4 as designers sought higher performance gains, has reached its peak. This model has helped to capture this possibility at the conceptual stage. The Pareto and parametric analyses, both show just how big of an effect that T_4 has on the performance of the system as a whole (both efficiency and creep life in this case), without any overly beneficial effects to counter it. The increase in the cooling flow requirements (section 3.2.6) that the increase in T_4 requires cannot be offset sufficiently by the increased use of TBC, shown both in Figure 92 and Figure 86. Increasing the speed of the flow, W_2, while reducing the relative temperature at the metal surface, does not offset the overall rise sufficiently either. Additionally, increasing the engine RPM, while it improves the cooled efficiency by speeding up the internal cooling flow through ejection, causes problems with the next response to be considered, AN^2.

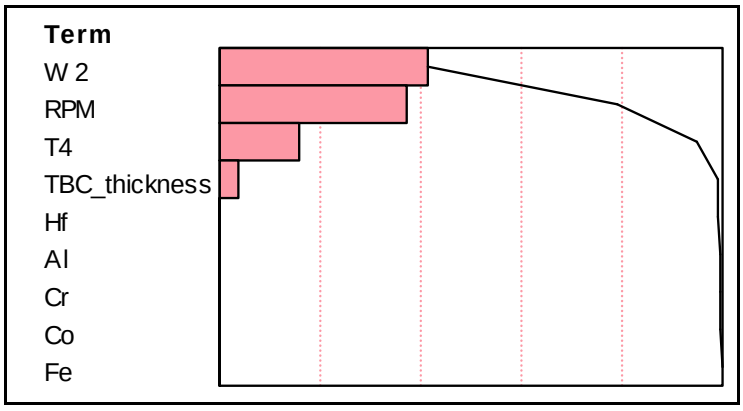

Figure 93: Second experiment AN^2 Pareto analysis

The design limits imposed by AN^2 are meant as an indication of the rotational and centrifugal forces within the engine during operation. Thus it would be expected that the factors directly related to the speed of the engine would have the most significance in the ANOVA analysis in Figure 93. The Pareto analysis did show that the mass flow and rpm of the engine were indeed the most important factors. The mass flow is considered to be the most important in that by increasing the mass flow through a turbine stage often, not only requires the increase in the engine speed but also an increase in the annulus area to accommodate the increased flow.

The inclusion of the ANOVA based Pareto analysis assisted in the understanding of the results of the two design studies. However, the interactive parametric trade-off environment will not suffice when seeking a full design space exploration and understanding for the designer. Thus, as previously mentioned in section 4.3, the consideration of the Multivariate analysis is included within the following section.

4.3.2 Multivariate Analysis

This method has already been approached in chapter five, and the author feels that this is a far more powerful visualization technique than Pareto charts alone when considering a complex system such as the gas turbine. This is a conclusion also drawn by Ender in 2006 [133] through his implementation on a complex system of systems problem. That is not to say that Pareto analysis does

not have its place, but it is just not what one is looking for in a multi response problem. This inverse design multivariate process requires the following the steps outlined below:

- Generate random cases and results through full Monte-Carlo analysis within JMP.
- Each point represents a case, encapsulating associated geometry, operating conditions, material compositions, and creep/stress responses.
- Constraints represented by lines can help identify desired design space
- Select interested points in one block and change their colors (e.g., red), the changes are updated in all dimensions

Select again within these points to meet other design requirements. These requirements such as a flare angle limit can be set within the multivariate environment. The use of these limits and the data filtering that is incurs are more commonly known under the term, "Monte-Carlo with filtering". This approach is used to vastly improve the effectiveness of the multivariate approach. Through the use of JMP the techniques have become fast and simple to use. An example of how this can be put into practice is contained below working from a multivariate scatter plot generated from data gathered utilizing the developed integrated design environment.

The plot, Figure 94, shows where the different data points (design candidates) lie within the design space for each response. This enables the designer to impose constraints (requirements) on the responses, and see what design candidates are meeting all requirements and where they lie in relation to other responses. Figure 94 shows a multivariate scatter plot with two constraints drawn on the plots. The two requirements are blade rupture life beyond a notional 120 hours, and weight less than 400 lbs. The design candidates meeting both requirements are color-coded as red. The data sets of these design candidates behind the plot are also color-coded simultaneously thus allowing the designers to further investigate these data sets.

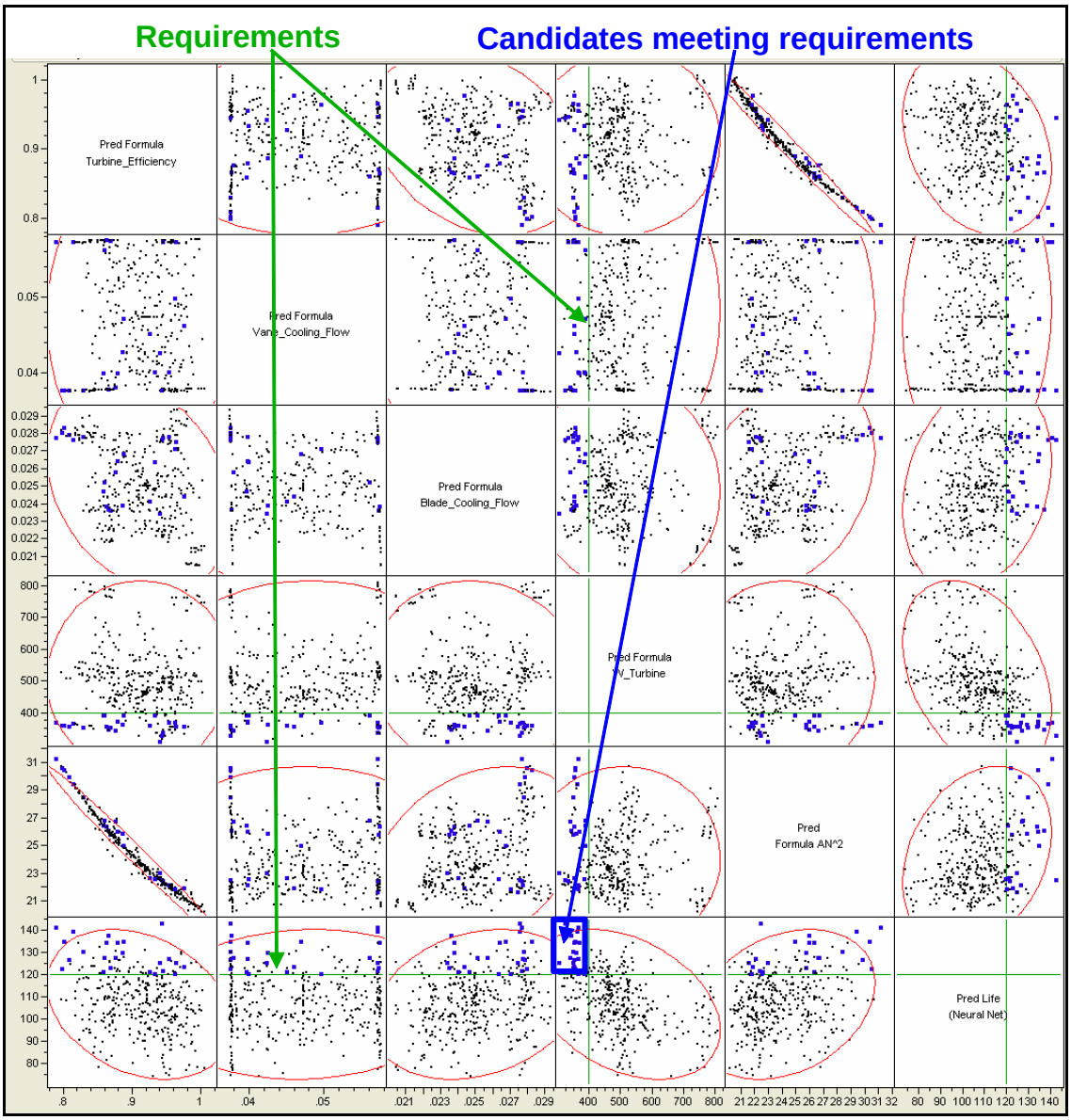

Figure 94: Monte-Carlo filtering example using results from the developed integrated environment. [141]

Applying this technique to the results of both models will demonstrate the great visual power of the proposed techniques, through the marrying of the low fidelity methods within an integrated design environment and the use of advanced modeling and simulation techniques to bring great understanding to the design space. The latest version of JMP has greatly benefited the designer

with the inclusion of the Monte-Carlo simulator within the prediction profiler. Saving much time and effort through removing the need to take the results and modeling equations to other programs for the generation of the results and then transferring them back for visualization. This simulator is easy to use with the choice of the following statistical approximations that can be applied to the design variables:

- Uniform
- Normal
- Normal weighted
- Normal truncated
- Exponential
- Log Normal
- Weibull
- Gamma
- Beta
- Cauchy
- Triangular
- JohnsonSU
- JohnsonSB
- JohnsonSL
- Integer
- Binomial

- Negative binomial
- Geometric
- Poisson
- Sampled.

For simplicity and to maximize the coverage of the design space sampling, the input variables for all the studies were set to uniform distributions. The simulator for the first model is depicted in Figure 95, illustrating how the simulator works off of the prediction profiler from the results of previous surrogate modeling operations.

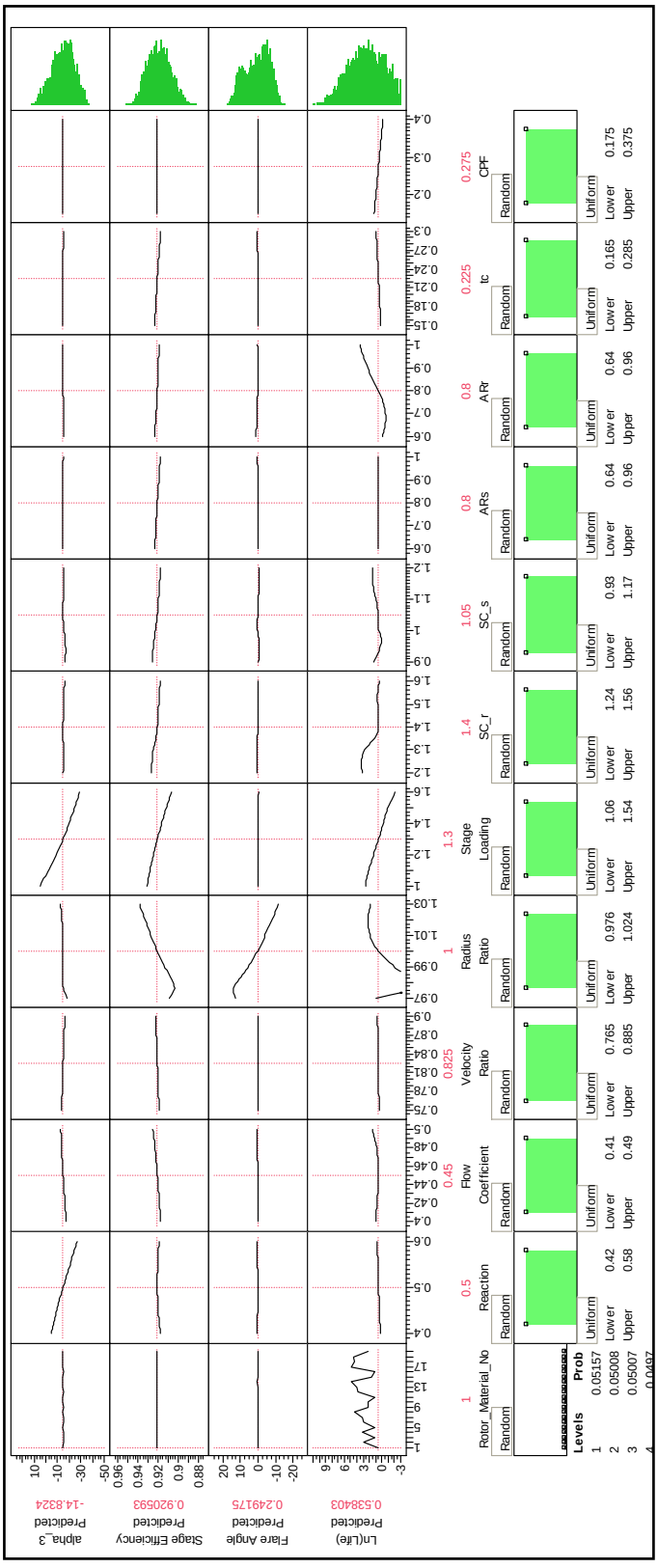

Figure 95: Model one simulator environment.

4.3.2.1 Turbine and Blade Study

Once the results from the simulator were generated they could be used within the following multivariate method as in Figure 96. Applying the techniques discussed earlier would thus provide for the filtered Monte-Carlo.

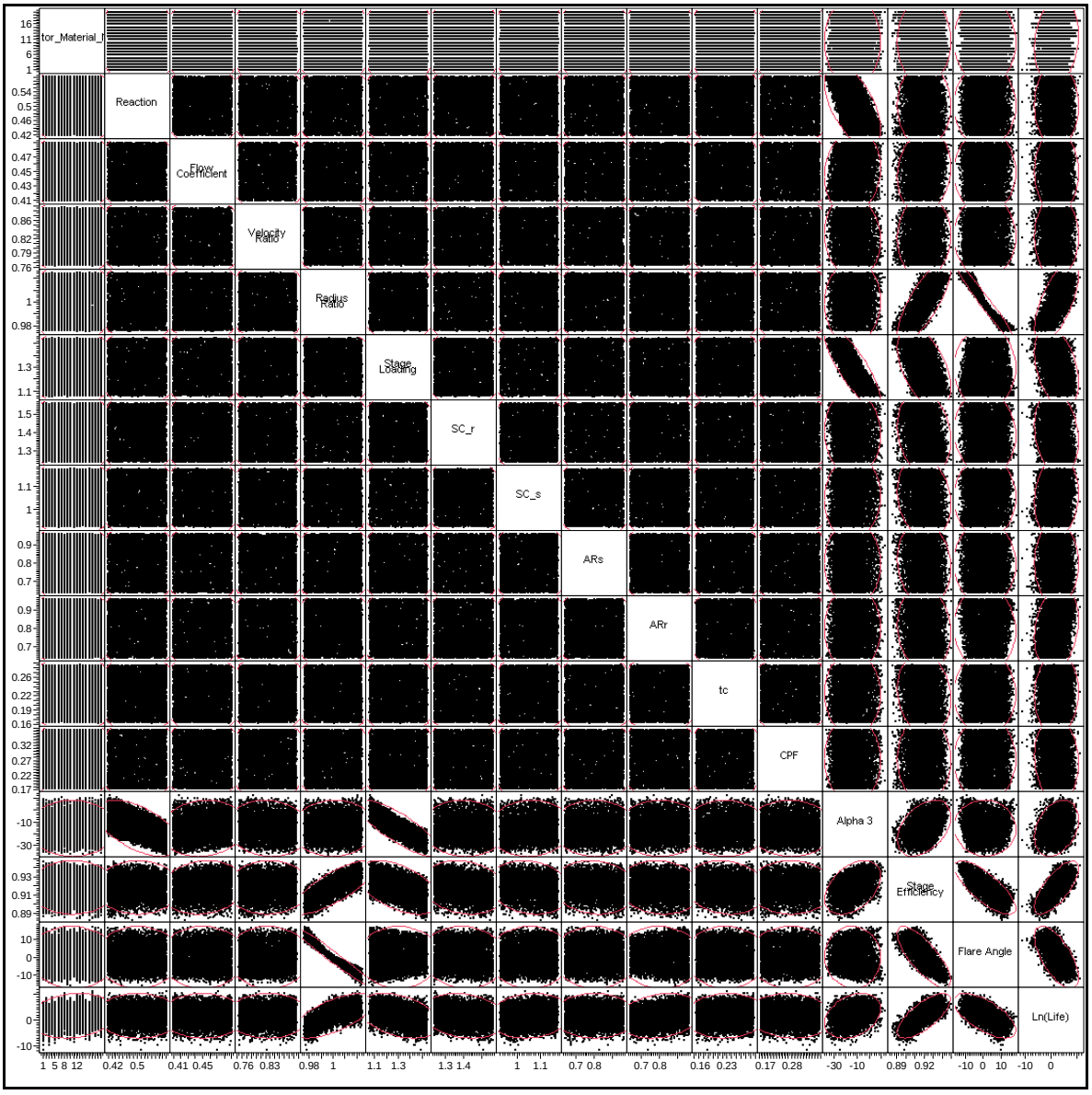

Figure 96: Initial model multivariate analysis environment pre filtering

In addition the identification of feasible design space through the application of design constraints can be utilized with the use of JMP's built in contour profiler. The ability of this to quickly and simply identify the feasible design space is graphically illustrated in Figure 97. The boundaries of the space dynamically change with the alteration of the input variable under study through the use of slide bars in the interface.

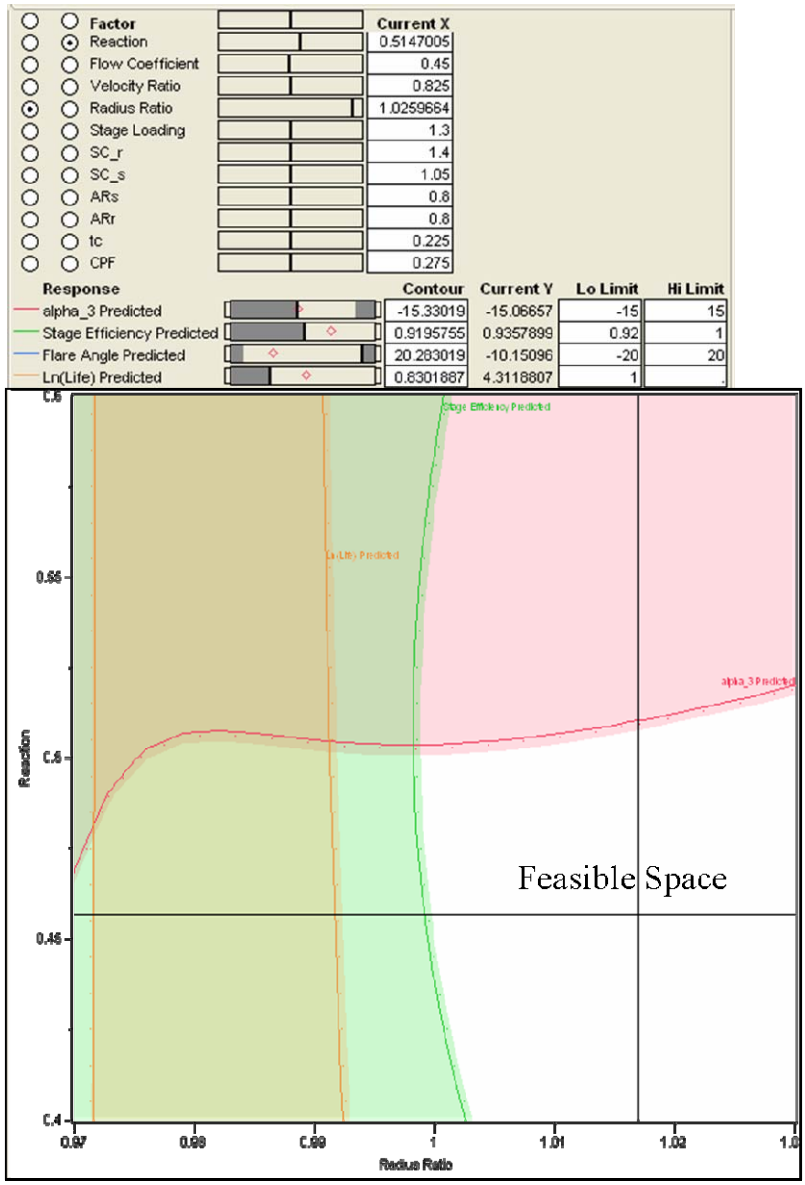

Figure 97: Initial Model contour profiler results

4.3.2.2 System and Material Study

Moving on from the first model but applying the same techniques as described previously the following results were achieved.

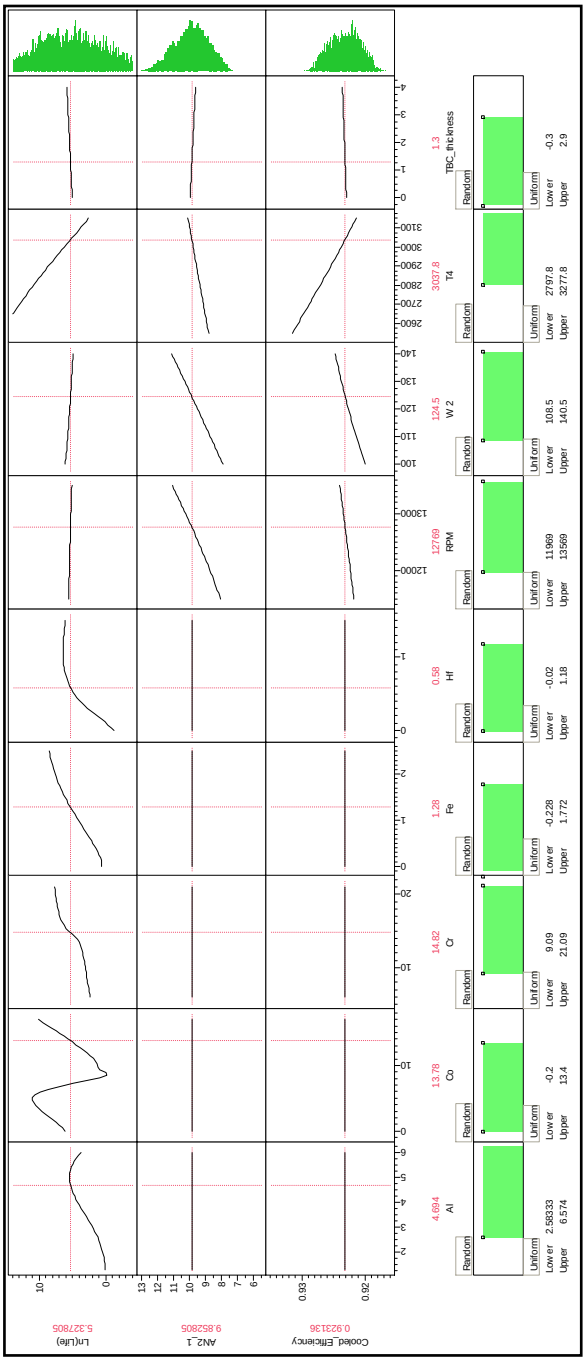

Figure 98: System and material simulator environment

As with the results from the previous model the simulator (Figure 98) was used to generate a, Monte-Carlo based, populated design space from the surrogate modeling equations generated earlier. The resulting multivariate analysis environment is depicted in Figure 99.

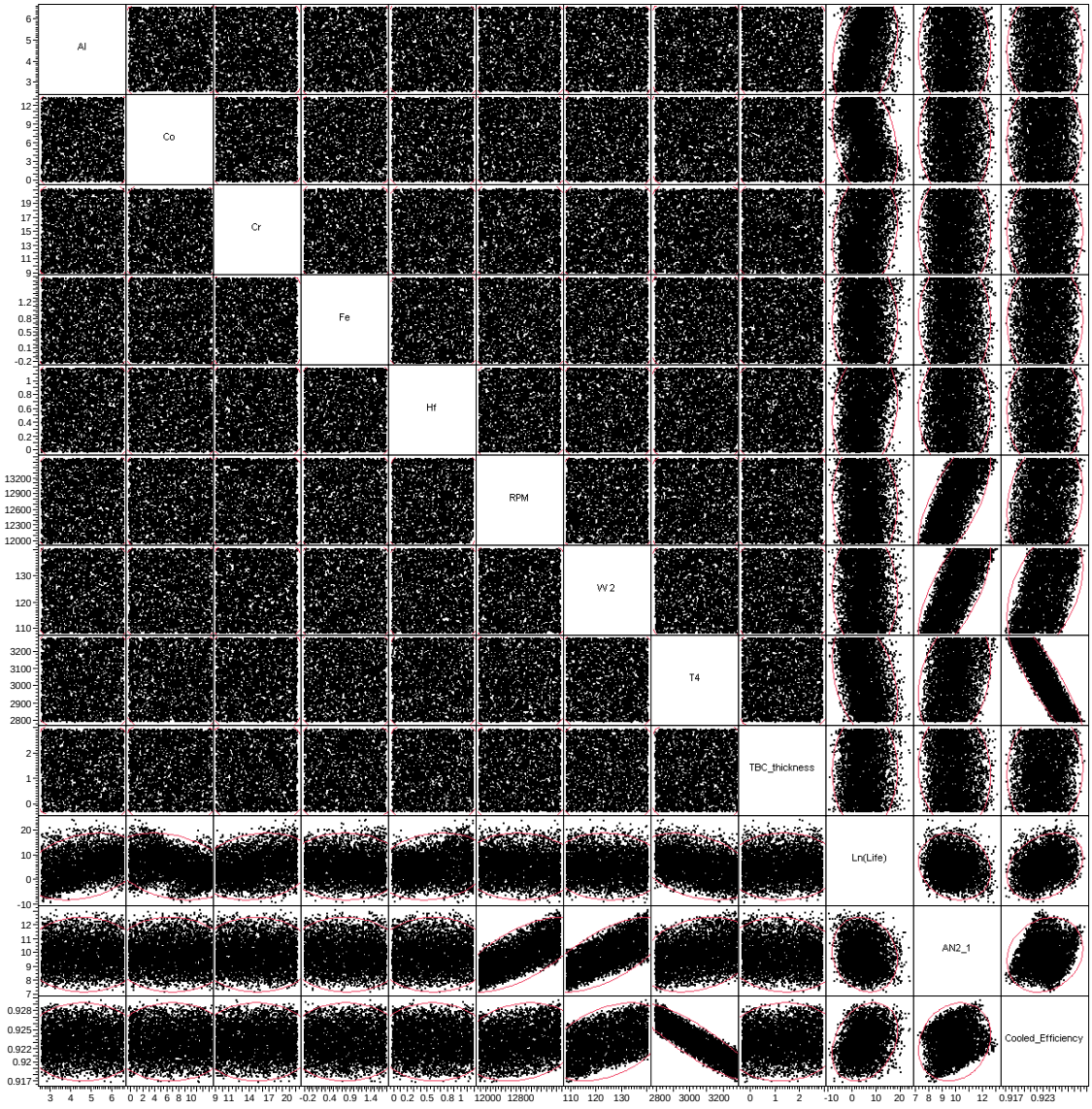

Figure 99: Model two multivariate environment

Figure 99 goes some way to help to demonstrate how powerful the multivariate analysis environment is for the visualization of the design space. The user is immediately drawn to the effects of the inputs on the responses and can easily understand more than one response at the same time. This is especially true with the application of the filtering techniques to the model, as was shown earlier within this section.

Additionally the results from the multivariate process can be used to provide indications as to the success of achieving a desired level response achievement. Here in Figure 100 the creep life of the second model is considered such that an achievement of more than a fifty percent chance of a design being within the stated limits is possible. The resulting data set from this can then be isolated and suited for further improvements to a design.

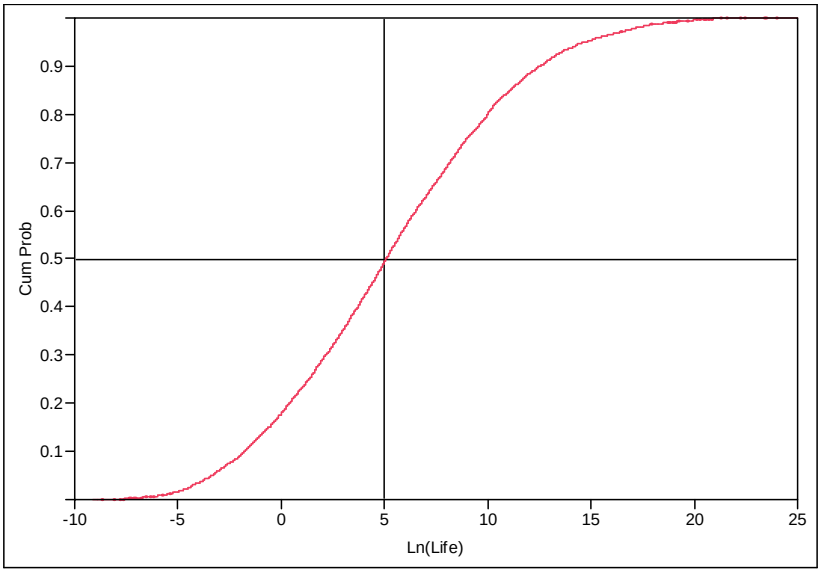

Figure 100: Model two lifing CDF with constraints

As one explores the question of materials composition with respect to the blade life and other possible system level factors, the ability to visualize the space is great detail is beneficial. The particularly non linear nature of the composition space lends itself greatly to such a technique. Using options within JMP this can be achieved. Figure 101, shows how as the percentage of Aluminium changes so does the life of the blade. Add into this the effect of RPM also and a good snippet of the design space has been achieved. Thus, enabling the considering the system and material level effects on one particular response, effectively a smaller version of the prediction profiler or multivariate environment. This technique also helps to depict any interactions that exist within the chosen space, with a simple but powerful technique.

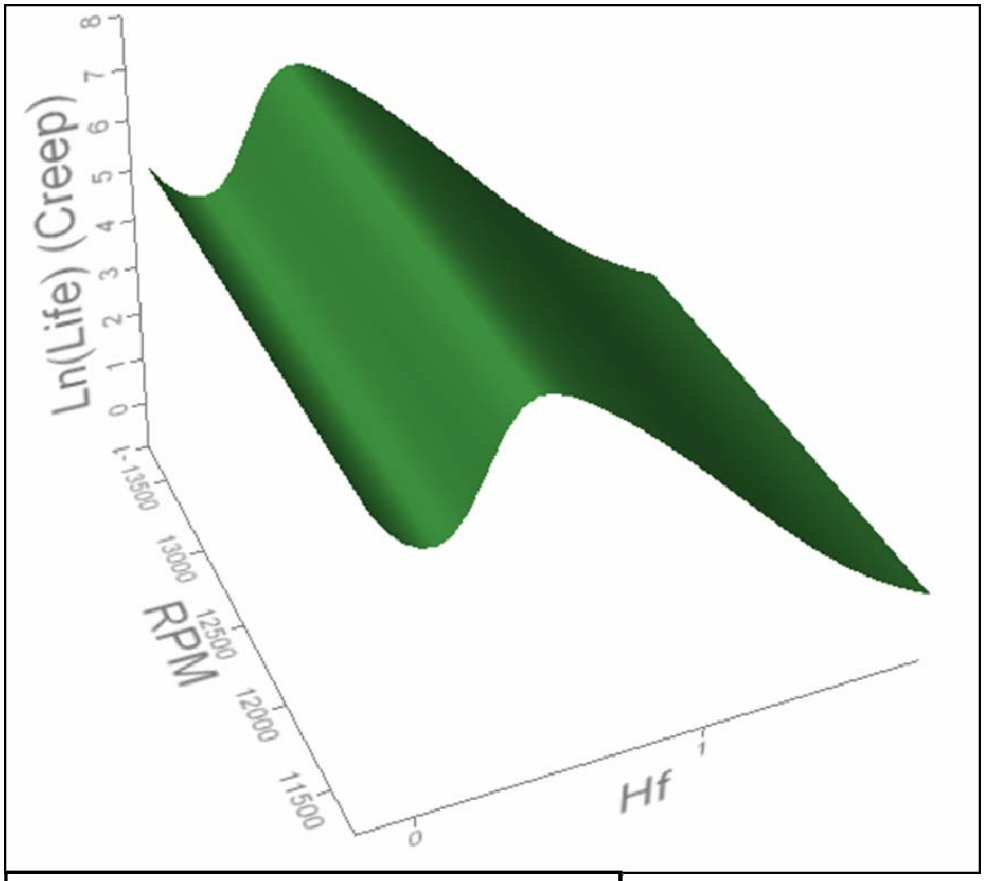

Independent Variables

X	Y				Value	Grid
○	○	Ln(Life) (Creep)			5	
○	○	Al			3.5	
○	○	Co			8.75	
○	○	Cr			14	
○	○	Fe			1.25	
⊙	○	Hf			0.8	☐
○	⊙	RPM			12500	☐
○	○	W2			120	
○	○	T4			2850	
○	○	TBC_thickness			2	

Figure 101: Surface representation of second model design space

CHAPTER 5

CONCLUSION

Blade and material design are necessarily far removed from the aero engine system design. The author puts forward the conclusion that this thesis has shown that at the conceptual design stage the system and blade design can be integrated in terms of blade amongst other factors. This conclusion has been made based on the results of the previous two problems undertaken using the developed environment and approach from this research work. The research questions and hypothesis were developed to help focus the scope of the research, based on the identified need garnered in chapter one. This chapter will lay out how the approach and methods within the previous chapters of this thesis have supported the claims made within chapter two. Additionally, the benefit of this proposed approach will be explored, along with the identification of the contributions and future applications of the work.

5.1 Review of Research Questions and Hypotheses

The research questions and hypotheses had been laid out in such a way as to assist with the exploration of the identified process in Figure 26 as developed within section 1.6. Looking from the system level down and considering the conceptual nature of the intended process the following was posed.

Q.1: How can a conceptual phase creep lifing design approach be achieved without total reliance on historical and empirical methods?

H. 1: *An approach should consider the engine core, right down to the part level creep lifing design, to provide better understanding of the space.*

Chapters 1 and 2 had helped to identify the need for a conceptual design approach that included the full consideration of lifing with in the design decisions. Allowing for the full consideration of the system and part level has enabled the designer to extract much more knowledge from the design at this early stage, considering the system as a whole rather than in its individual parts. In comparison previous consideration of any lifing data in a low fidelity form was limited to either empirical methods or Weibull analysis of existing engine service data.

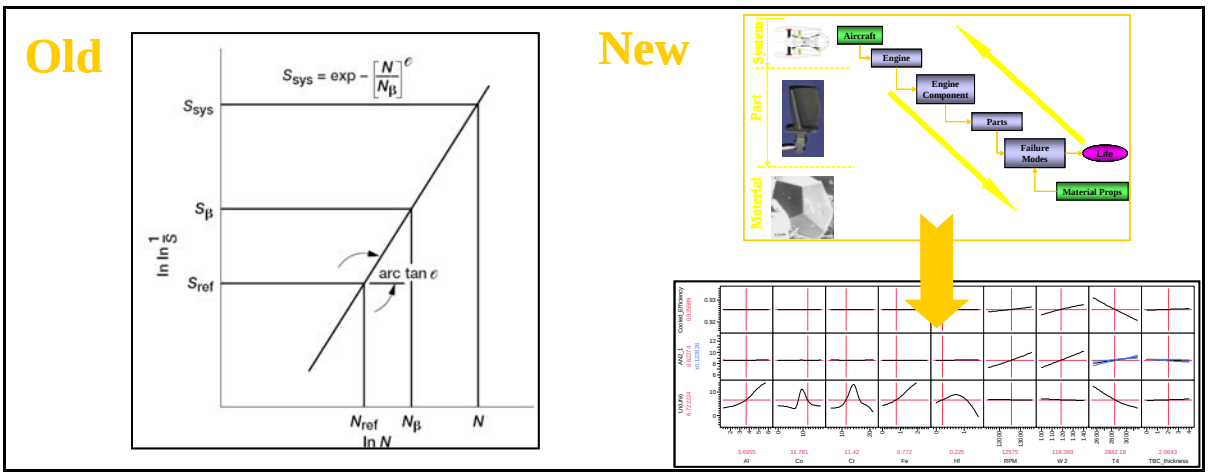

Figure 102: Summary of H. 1contributions

Q. 2: Can the system level and the part level characteristics be considered at the conceptual phase simultaneously? And if so how?

H. 2: *Considering both issues requires the modeling of both considered at a low fidelity level to improve the information flow and thus assist in capturing the interactions.*

The process outlined within this document has shown that this is possible, marrying both systems and part level analysis through the use of various MDO based techniques, not limited to the use of DoE's and DSM based architectures as outlined in chapter four. The models for the system and part levels were of the appropriate fidelity for the particular stage of design and provided for the interactions through the use of the DSM based architecture. This is compared to the previous approach of considering the creep life of a blade much later in the design process, far removed from the cycle considerations.

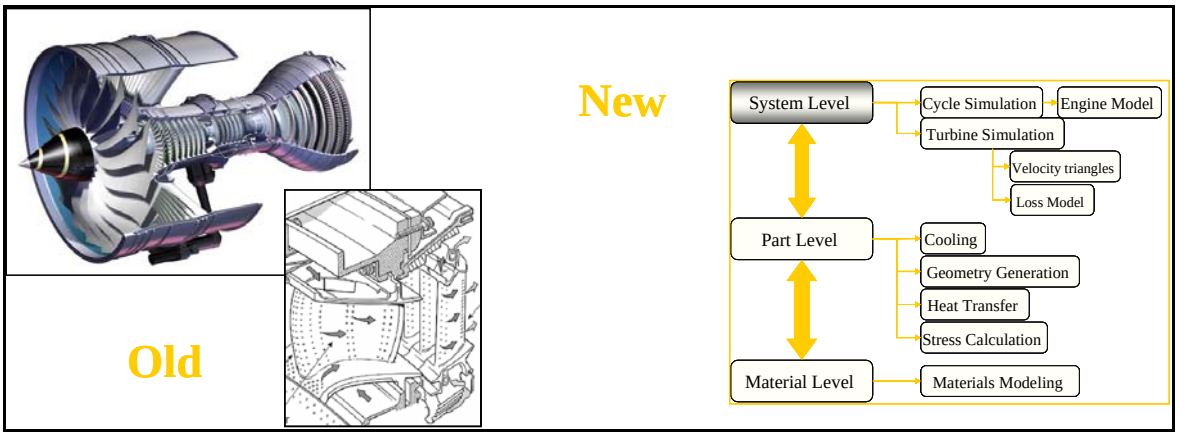

Figure 103: Summary of H. 2 contributions

Q. 3: What is required to bring the blade creep lifing to the conceptual phase of design?

H. 3: *A rapid physics based analysis is needed to consider the blade creep life within an integrated engine design process.*

The methods utilized within the research in this thesis were more physics based than the current empirical methods, utilizing the employment of techniques both classical and modern to achieve this goal. These techniques are

low fidelity physics based methods that given the fidelity level permit the rapid consideration of each design point within a DoE design space exploration.

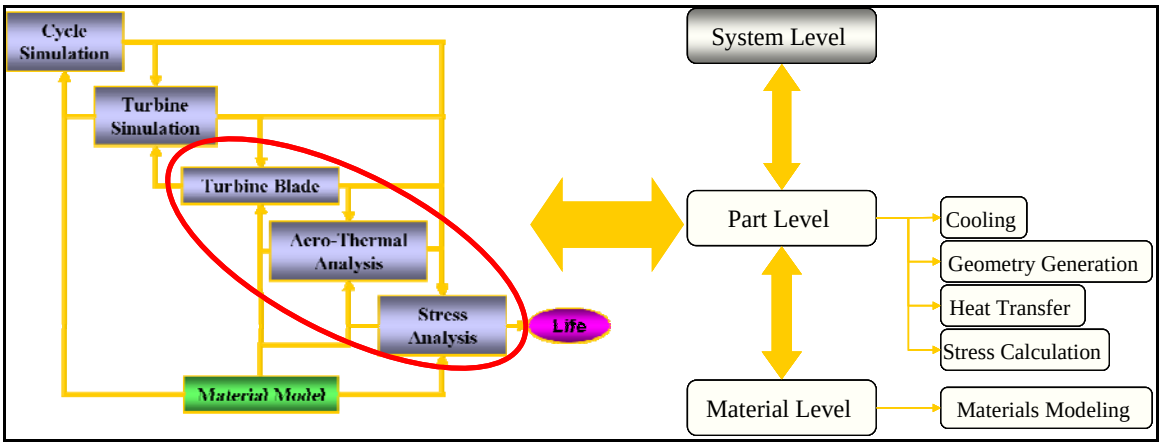

Figure 104: Summary of H. 3 contributions

Q. 4: How can one capture the creep life of the part early in the design process?

H. 4: *One needs to capture the main stress components and aero-thermo-mechanical factors that might combine to affect the service life of a turbine blade.*

Low fidelity turbine blade stress models were used to capture the behavior of the stress at the blade level. These models relied of 0 and 1D approaches to maintain the low fidelity approach and the speed desired for domain spanning. Using a data base of materials property information the creep life information of some select nickel super alloys could be applied to the stresses calculated to retrieve the creep lifing figures for a particular design case. Thus a detailed yet quick approach is possible.

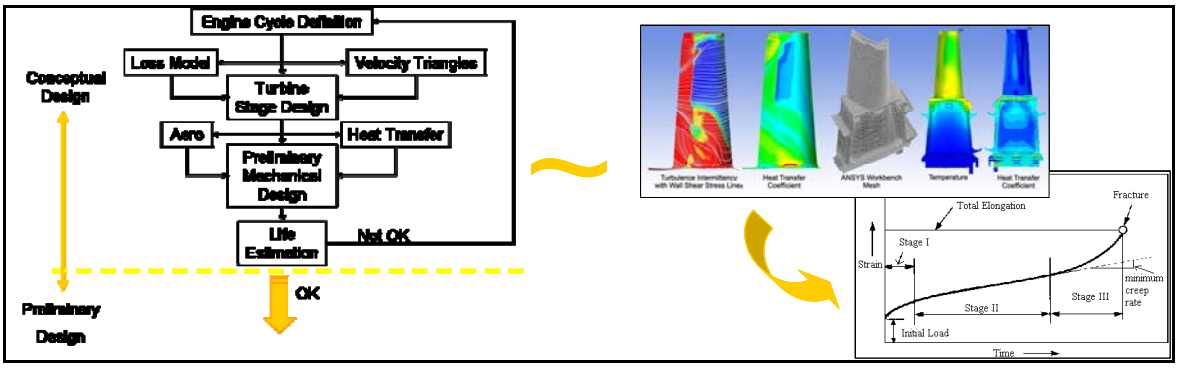

Figure 105: Summary of H. 4 contributions

Q. 5: How can one capture the turbine blade creep lifing interactions within a modern axial gas turbine?

H. 5: *An approach should integrate the physics based analysis of the cycle represented through the engine core, turbine stage and blade into a single design environment.*

The work within this thesis has shown that a lower fidelity method could be developed that linked the whole system under a single analysis approach. The single approach allowed for the spanning of a suitable large design space for creep lifing based design trades. These techniques included the use of an integrated design environment that allowed the connection of the differing levels of the engine. This technique was based around the facilitation offered through the use of Phoenix Integration's Model Center ™. This program permitted the implementation of the DSM designed architecture and thus enabled the linking of the analysis of the whole system.

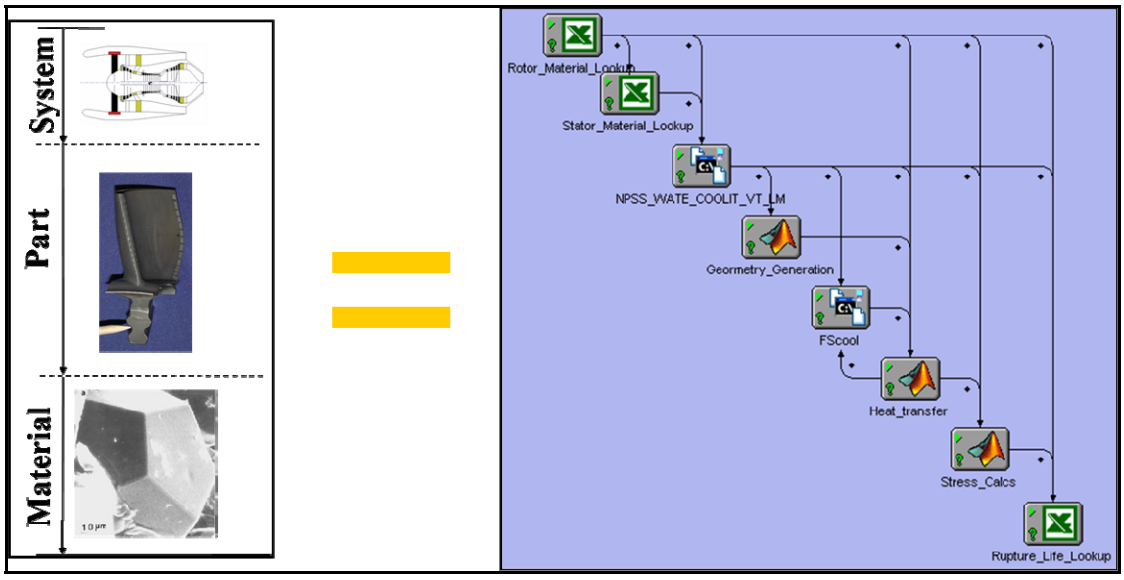

Figure 106: Summary of hypothesis five contributions

Q. 6: How can one help the designer understand the coupling between creep lifing and performance goals?

H. 6: *An approach is needed that samples more of the design space, enables instantaneous trades through surrogate modeling techniques, and provides an informed design direction through interactive visualization.*

Through the use of a CCD/LHC mixed DoE with the analysis environment a good spanning of the design space could be achieved. These results could then be modeled and manipulated using RSM and NN approaches to enable the studying of the design space. Furthermore the additional use of advanced surrogate modeling techniques including Monte Carlo with filtering improved the design space understanding whilst maintaining any possible interactions. These visualization techniques provide the most powerful means to understand the design space, they say a picture paints a thousand words and this

is the epitome of this. Numbers and theory only go some way to understanding the problem at hand. Visualizing the space and the ability to manipulate the variables and responses brings a new kind of understanding of a complex system design.

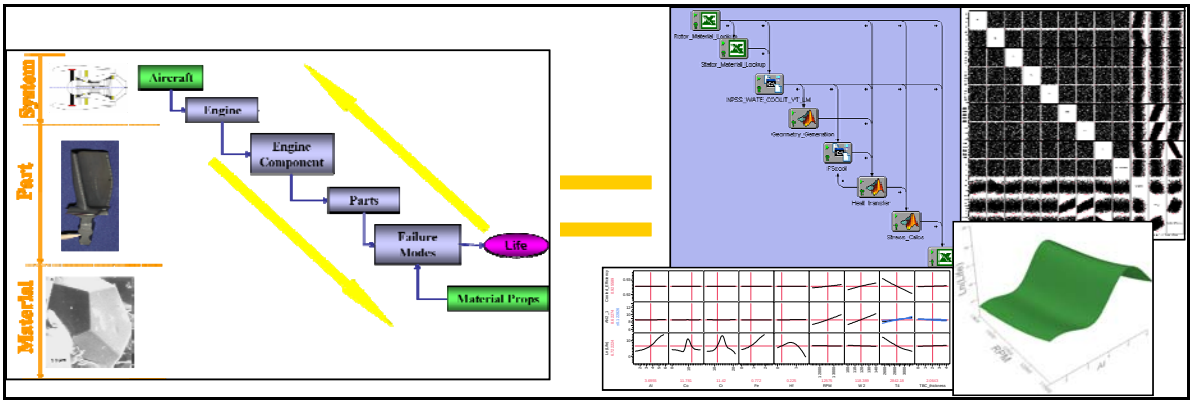

Figure 107: Summary of contributions

Overall it can be concluded that the research goal set in chapter three has been met, that being, that:

"A fast conceptual phase fidelity methodology can be formulated and implemented which may reduce the time required to explore the design space for an optimized turbine blade design solution suited to high temperature applications."

Achieving the above has provided both a great challenge and reward for the author, now looking forward to applying the methods considered within this thesis in industry.

5.2 Overall Benefits of Approach

Understanding the benefits for the inclusion of blade creep life in the conceptual design process, requires that one compares a representative traditional conceptual process with that of the currently proposed approach. A comparison of the values of the desired design variable values when considering the responses for the two forms of approach. A short comparison would involve the results from the initial and final experiments in order to provide the desired insight.

The scenarios behind the two experiments were meant to increase the understanding within the conceptual engine design process through the inclusion of the creep life within the design decisions. Therefore the simplest form of comparison would be to consider the results from these works, with and without the inclusion of the creep life data. The comparison needs to seek out any differences in the suitable values of the design variables that improve upon the desired response.

Beginning with the turbine stage and blade study (the first experiment), this study looked at the creep life and the stage efficiency, while at the same time considering the possible limiting factors of swirl and flare angles. In the previous chapter, it was shown that the results pushed the designer towards considering a design space with the following settings in Table 13, taken from Figure 108:

Table 13: Turbine and blade design model preferred values.

Variable	Preferred Values
Rotor Material	14
Reaction	< 0.52
Flow coefficient	< 0.46
Velocity Ratio	< 0.86
Radius Ratio	0.99 < *v* < 1.02
Stage Loading	~ 1.0
Rotor Solidity	~1.2
Stator Solidity	~ 0.9
Stator Aspect Ratio	~ 0.6
Rotor Aspect Ratio	> 0.9
Blade Thickness to Chord	~ 0.22
Combustor Pattern Factor	0.1

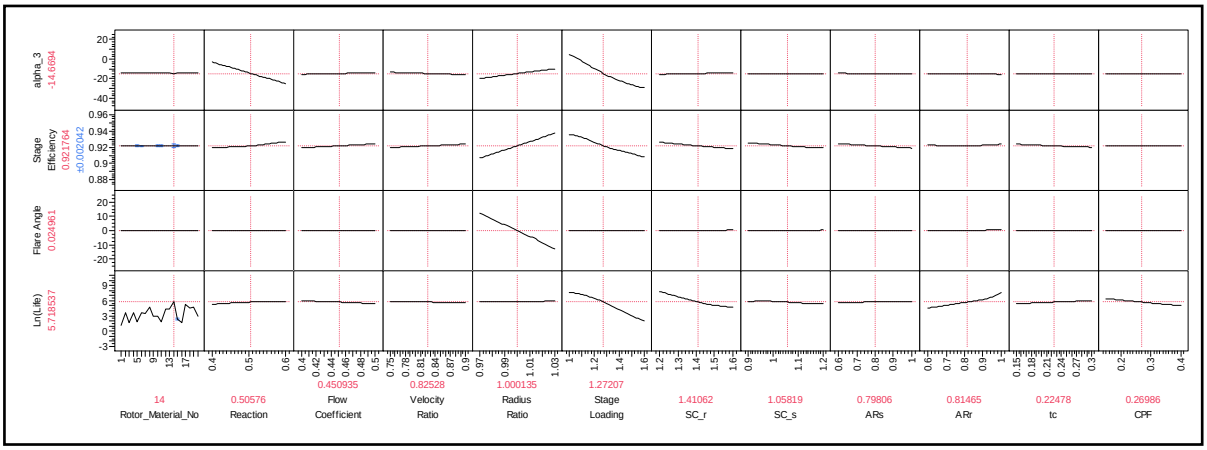

Figure 108: Reminder of initial model results.

Figure 108, has been included as a reminder as to the forms of the responses and the effects the design variables have on them. Thus it can be seen that currently the drive for improvements in creep life and stage efficiency is enabled through the inclusion of the materials comparison (through the use of the materials data table), and the comparison of the response traces whilst

considering magnitudes of the constraint responses. As mentioned previously this lead to the selection of the design variable values in Table 13, the trade offs were most acute for those variables when trends were divergent from one another. These trades were most apparent for the flow coefficient, stator aspect ratio, rotor aspect ratio, and blade thickness to chord. In each of these cases decisions have to be made as to what is the overriding factor that drives the design, to maximize the creep life and stage efficiency. Of particular note is the effect that increasing the thickness to chord has, though a small change, the increase in the creep life that it brings is equally offset by the loss in stage efficiency. Fatter blades are better able to cope with the bending and centrifugal stresses, but this thickness has a detrimental effect on the flow, dropping the efficiency.

The question now arises, what would the difference be without the creep life consideration for this design study. Without the consideration of the blade creep life, the drive to improve eth efficiency of a turbine and blade within the limits of the constraint responses. Table 14, illustrates the difference that the removal of the creep consideration plays on the inputs for the turbine and blade design study. Though this design considers only the stage performance the results are interesting.

Table 14: Comparison of inputs for current and possible previous approach

Variable	Preferred Values	Efficiency Only
Rotor Materials	14	N/A
Reaction	< 0.52	~ 0.52
Flow coefficient	< 0.46	~ 0.5
Velocity ratio	< 0.86	~ 0.9
Radius ratio	$0.99 < \nu < 1.02$	~ 1.02
Stage loading	~ 1	~ 1
Rotor solidity	~1.2	~1.2
Stator solidity	~ 0.9	~ 0.9
Stator aspect ratio	~ 0.6	~ 0.6
Rotor aspect ratio	> 0.9	$0.65 < AR > 0.9$
Blade Thickness to Chord	~ 0.22	~ 0.15
Combustor Pattern Factor	0.1	No Effect

Removing the creep analysis from this conceptual design study has removed the consideration of the materials from this particular work, since the stage efficiency is not affect by material properties, nor are the constraining responses. In addition, a change can be observed in the required settings for the following responses:

- Flow coefficient, φ
- Velocity ratio, μ
- Radius ratio, ν
- Rotor aspect ratio, AR
- Blade thickness to chord, t/c
- Combustor pattern factor, CPF

There is obviously no effect from the combustor pattern factor since it does not feature in the analysis of the stage efficiency in this study, as illustrated

in Figure 108. The other differences highlighted are all purely due to the removal of the creep analysis, and can be observed within Figure 108, by comparing the results for each response.

The first study has shown a particular niche for the inclusion of creep analysis within a turbine and blade design study, when working for improved stage performance. However this has not considered the full scope of the intended approach, the second design study also needs to be considered to really look at the applicability. This second work looked at a design space from the system through to the materials level, in terms of the cooled efficiency, AN^2 and obviously the creep life.

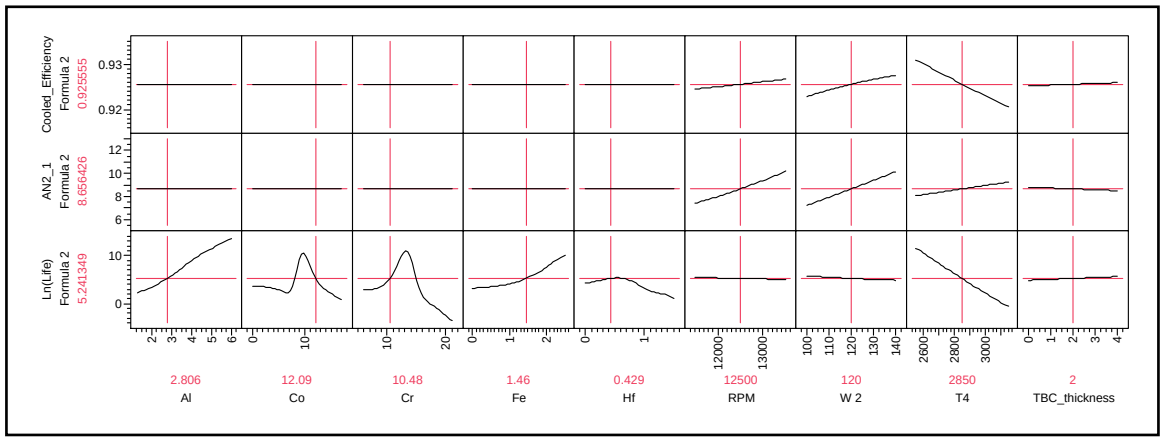

Figure 109: Reminder of second study results

Utilizing Figure 109, once can gather the benefit of the inclusion of the creep analysis within this conceptual design study. As with the previous work, it can be seen that this inclusion highlights trends that would be unavailable to a designer without the consideration of this blade creep life analysis. A simple

determination of the best design direction for the responses was carried out for both cases (the inclusion/exclusion of the creep analysis) and these are summarized in Table 15.

Table 15: Summary of comparison of results for second design study, for both conceptual approaches

Design Variables	Preferred Values	Creep Removed
Al	~ 6 %	N/A
Co	~ 9.5 %	N/A
Cr	~ 13.5 %	N/A
Fe	~ 2.6 %	N/A
Hf	~ 0.6 %	N/A
RPM	~ 12500	~ 13300
Mass flow, W_2	~ 125 lbm/s	~ 137.5 lbm/s
T_4	~ 2300 R	~ 2300 R
TBC Thickness	~ 2 mm	~ 2 mm

Table 15 helps to illustrate the expanded design space that the inclusion of the creep analysis permits. Expanding this design space consideration greatly increases the knowledge for the designer and ability to understand any previously unforeseen problems, even within these simple studies. Within chapter one, it was discussed that the current trend in T_4 is continuing and thus the possibility of need for greater study on the materials utilized is necessary. Providing the key inputs and outputs for such an analysis and integrating them in such a way as to enable the full system to material level analysis, is only available through the inclusion of this conceptual creep analysis approach. This way full consideration can be made at the front end of the design to any manner of design variables and responses.

This work has additionally highlighted the trades necessary outside of the materials selection, as with the first study. This time the size of the study has limited one's insight, but the results are still important. From Table 15, it can be seen that the RPM and mass flow exhibit changes in desired values without the creep analysis. Thus with a drive for performance say in the conceptual stage of a traditional process, without this insight, problems would be encountered as the design progressed, missing out on the potential that this new approach can offer.

The design studies have shown a positive conclusion from the inclusion of the creep analysis based approach at the conceptual stage. The whole point of this thesis work was to expand the knowledge of the designer at the conceptual design stage in a meaningful manner, and even using these simple studies this has been shown. A designer of not just the jet engine as a whole, but even the blade material can investigate the effects of altering their points of interest and their effects on the system, part and material level responses.

5.3 Summary of Contributions

Overall, the work within this thesis has identified an approach that provides the gas turbine conceptual designer with the ability to consider the turbine blade creep lifing amongst systems design consideration. The approach provides a means to quickly and accurately evaluate the impact of changes at the part scale on the system performance and to quickly and accurately set requirements for part scales based on system level requirements.

This has been achieved through a fully integrated analysis technique that considers the systems and part scale analysis through the use of an integrated the system and part level design approach for blade creep lifing. This has brought the blade creep lifing to the conceptual design stage. This consideration is far more detailed than current methods, considering the three main stresses seen operationally by the blade at the design point.

The approach has enabled the consideration of materials modeling within the analysis at the conceptual design stage. Now it is possible for the designer to see the direct correlation between the effects of different material compositions and the performance of the system as a whole.

Taken as a whole, the main contribution of this work has to be the enabling of the consideration of design and technology effects rapidly, in a top down/bottom up, gas turbine conceptual phase design with respect to turbine blade life. Now requirements can be placed and any level of the engine and their effects quickly and efficiently modeled throughout the system. In addition, this work can be used to provide an informed design direction to guide work later in the design process, through the rapid design space exploration. The benefits of the approach have been discussed within the previous section.

5.4 Recommendations for Future Research

It would be nice to assume that the work presented here is the culmination of the research work. However it is really just the beginning of a

new phase. The work within this thesis provides many different avenues for the development of a whole host new research opportunities and possible new uses for this developed approach. Firstly there is the possibility to look into variable fidelity levels to improve analysis accuracy without and associated loss in computational speed. This architecture makes it easy to swap different analysis method in and out and so mixed or higher fidelity approach is entirely possible should the need arise. This would include the improvement to the heat transfer modeling through the use of a more detailed approach with a move to consider outer-surface heating using flow field conditions.

The most obvious future work is the full utilization of the materials codes developed by Mr Hong. This would enable the full utilization of top down bottom up approach that this thesis has gone some way to address. This work would require greater computational effort as the DoE designs would become increasingly difficult, but the level of detail lost be grouping metal by number would be improved upon. As with everything this would be compromise between the needs of the designer and analysis and the time and computation resources available.

Then there is the expansion of the approach to include off design considerations. The approach has been limit thus far in order to simplify the verification of the ideas behind it. However a better understanding of the stresses throughout the flight envelope would be gained through off design considerations. This can be achieved with the addition of extra theory from

Cohen and Rogers and the like and with the possible integration of this approach into an operations research tool. Such integration would make the study of LCF and HCF stress considerations possible, greatly adding to the complete nature of the tool. Now not only would the direct stresses be considered but those time variable one too, greatly adding to the capabilities of such and approach.

This work could also be expanded to the multi-stage analysis. Currently the stages are considered individually and not particularly covered within this thesis topic. However is entirely possible to optimize the turbine stages individually to cope with previous improving the efficiency of the turbine overall. This would however, require more computationally and a different look at the design variables to be considered. In addition the consideration of possibly different ranges too.

Overall I believe that there is great potential in the use of my work not just for the Turbine but the approach could easily be applied to other parts of the engine, with some tweaks of course.

APPENDIX A

EDUCATIONAL REPORT

The following report was added within the appendices to satisfy the reproducibility, objectivity and transparency of the results found within this thesis, as called for within the scientific method. The model folder for use with Model Center that has been provided within the attached C.D. needs to be situated in the wrappers folder as follows:

…\program files\phoenix integration\analysis\wrappers\...

Then with the folder in place the model file (thing) can be selected in the open model window that appears on start up. Once the correct directory has been selected, the model can be manipulated to suit ones analysis needs.

The DoE tool within Model Center ™, allows for simple design space exploration. Input design variables and responses to track can be chosen from the ones that have been laid out within the model. The designer can also choose to use a previously created doe table, or a standardized design contained within the tool, and then run an analysis on this. Whilst this analysis is running Model Center ™ provides useful Pareto graphs visualizing the most significant design variables for the tracked responses. Once finished, the output (in .csv format) can then be passed into statistical analysis software, such as JMP, for use with

Response Surface methods and the like. More information on the use of this tool is available in the help files that come with the software, in addition a short "how to" section is contained within also.

This next section goes through the codes found within the folder for the Blade creep life design environment. The Model Center application also permits the user to alter stress, geometry and heat transfer analysis codes to suit. Additionally, using Phoenix Integration Model Center™ also provides for an easy implementation of DOE tables for the design space exploration that are required within this thesis work.

A1. Parametric Physics Based Design Environment

The added geometry generation and stress calculations are coded in MATLAB. The material properties and blade life calculation are coded in Excel. These additions are integrated with NPSS/VT/LM/COOLIT/WATE through Model Center, as shown in Figure 110.

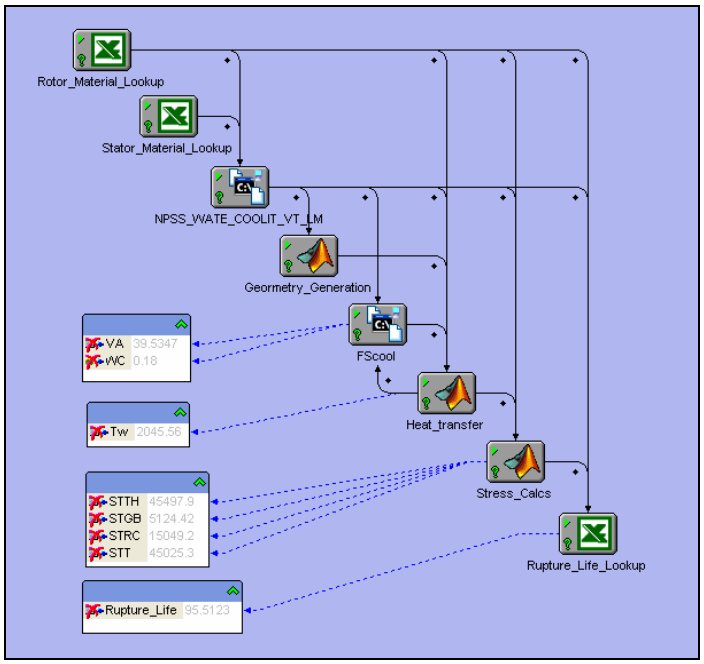

Figure 110: Integrated turbine blade creep life analysis environment

The list below is of the required files placed within the "Marcus Smith Thesis 2008" folder provided. This folder needs to be placed within the wrappers folder in:

…\program files\phoenix integration\analysis\wrappers\...

Within \Marcus Smith Thesis 2008:

- NPSS_v3
  - This is the NPSS wrapper to allow the use of the NASA code within model center. Enables the passing pf variables to the write places etc.
- URETI Lifing Optimisation
  - Model Center™ model file. This file should be opened when opening model center to allow access to model for alterations and DOE execution.
- WATE_NT_Public

    - Public version of WATE is used for this analysis.

- NPSSNT
    - NPSS batch file. The file needs to be altered to match the location of your NPSS NT v1.6.4 folder.
- E3.run
    - NPSS Input file. Currently for core only.
- Rotor and Stator Material lookup.xls
    - Rotor and Stator material information for the model. 20 materials choices. Separate files to ease application within Model Center. Details for each material given within the file.
- Rupture Life material lookup.xls
    - As above, copy of same worksheet just separate to accommodate easy of use within Model Center.
- Materials m-files.
    - Current work from the Materials sub section, the m-files have been included to give an insight to their application within the future model.
- Fscool
    - Gathers cooling flow property data from NPSS.
- CoolProp.run
    - Runs NPSS for Fscool.
- heattrans.m

- Calculates internal wall temperature from metal temperature and cooling flow properties

- Stress_code.m
  - Stress Calculations for the finding of the rupture life of the turbine blade, includes the following calculations:
    - Thermal Stress
    - Gas Bending Stress
    - Centrifugal Stress
    - Von Mises Stress
- ChungBlade_Jun2007.m & find_epsilon_out.m
  - M-file containing the geometry generation analysis.

There are 3 sub folders within the URETI folders. The following is a brief description of each with a list of the contents:

- …/SRC
  - Source code for NPSS add-ons and model files, includes the following
- E3.mdl
  - E^3 model file, core only.
- Coolit2.int
  - Updated COOLIT algorithm
- VelocityTriangle.int
  - Velocity triangle model file

- LossModel.int
  - Loss Model file
- …/View/Npss.case.view
  - Standard NPSS view file
- …/Geometry
  - All files contained are for the visualization and recording of blade profiles from the analysis.

A1.2 Analysis Environment User Information

1.2.1 Having placed the folder in the correct place, Analysis Server™ and Model Center ™, need to be started in that order.

1.2.2 Open the model by choosing the *.pwc file from the folder.

1.2.3 With the model open one can observe the inputs and output on the right and side of the screen and the Design Structure Matrix (DSM) on the left as shown in Figure 111.

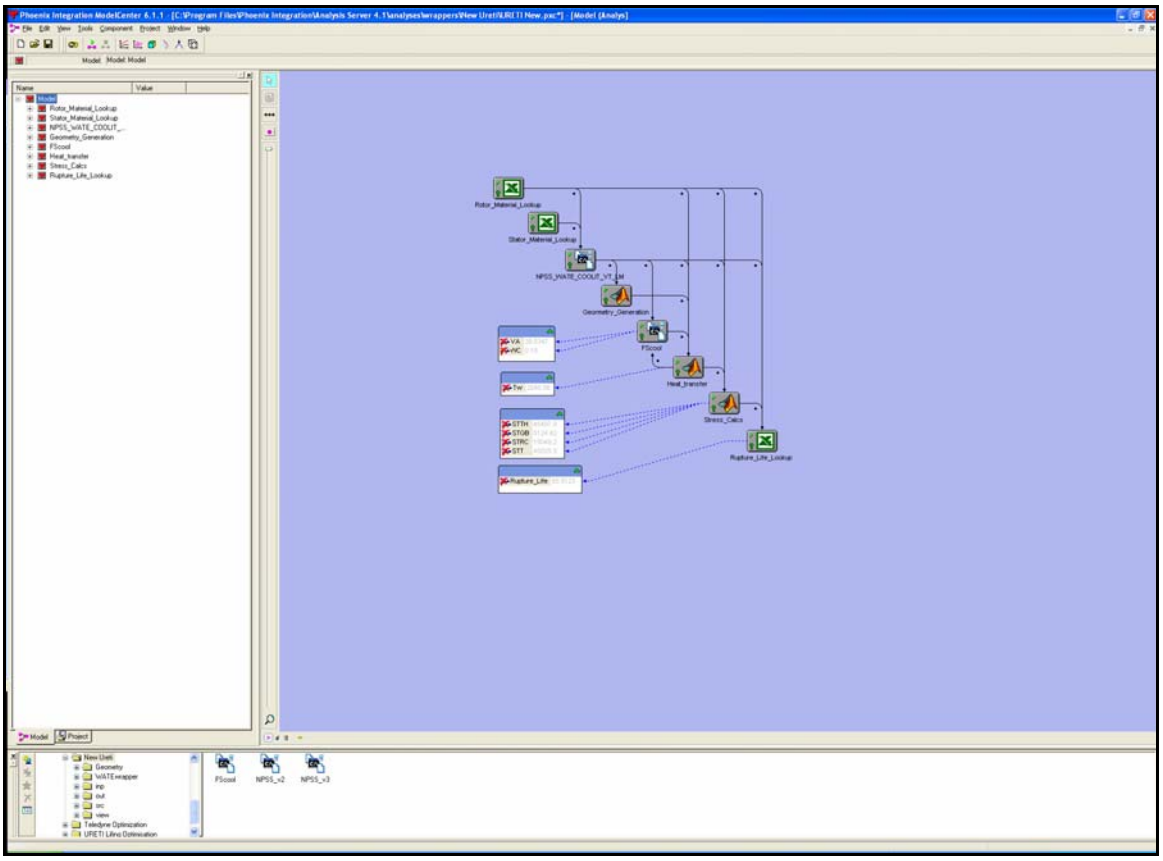

Figure 111: Model Center ™ based design environment

1.2.4 The inputs and outputs can be seen very easily by just expanding and contracting the model on the right hand side of the screen. This is highlighted in Figure 112.

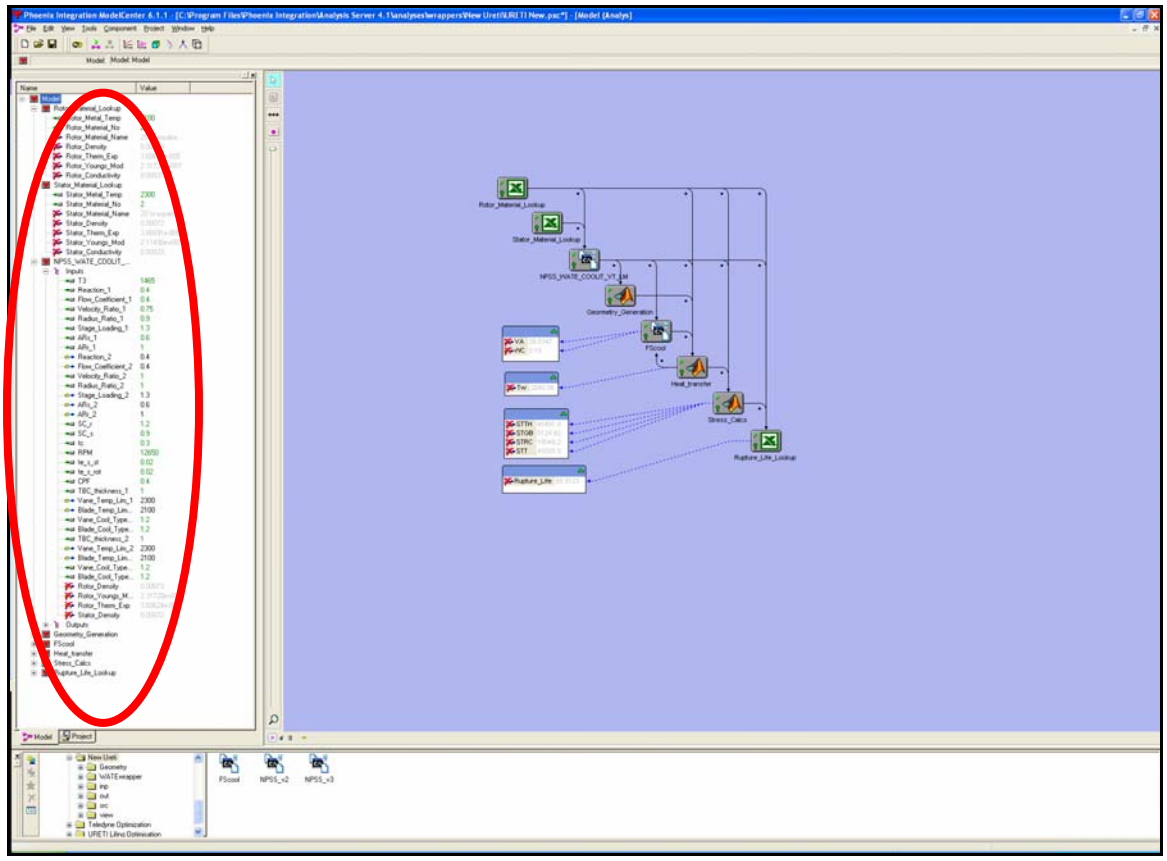

Figure 112: Location of model inputs and outputs

1.2.5 Using the DoE tool involves opening the too window from the icon bar in Model Center. With the window open the desired input and output variables for the study, can be dragged into the associated areas. See Figure 113.

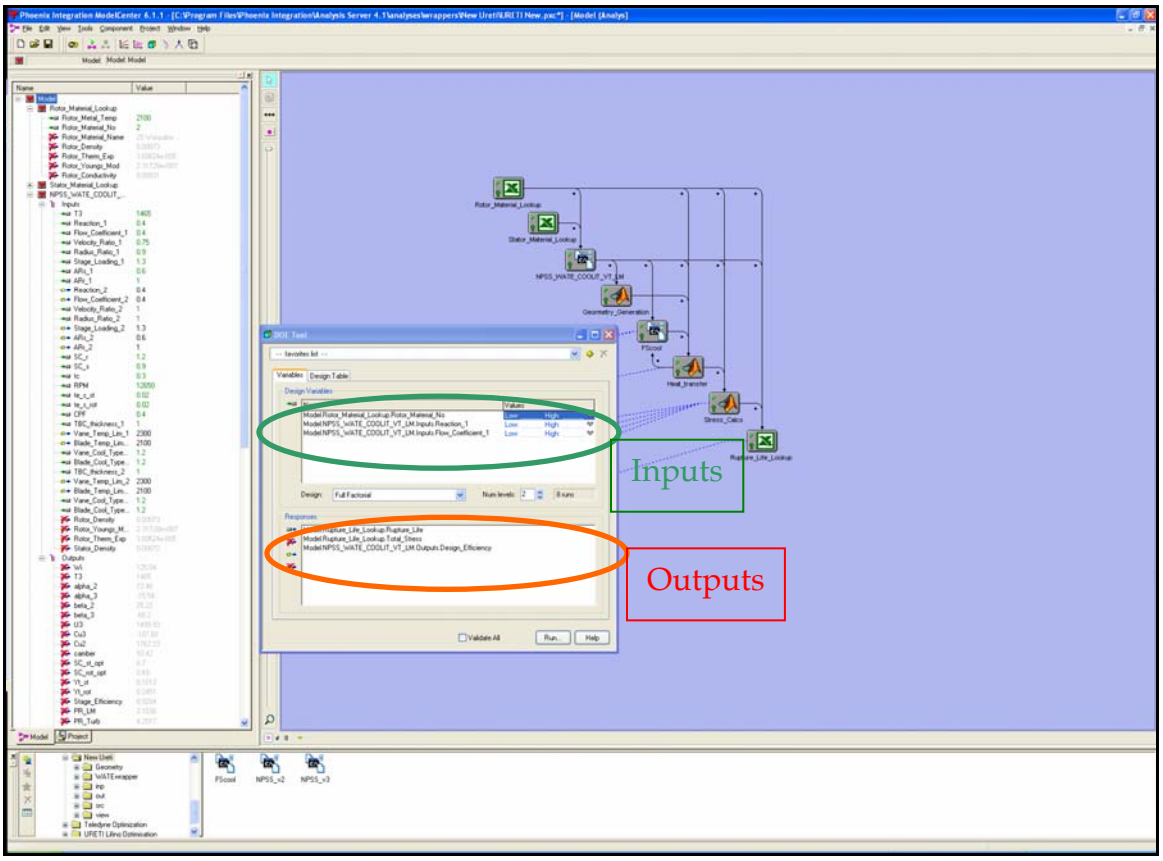

Figure 113: Using the integrated DoE tools within Model Center™

1.2.6 The DoE tool allows for the use of either user defined or its own DoE tables, these can be entered using the other tab in the DoE window, as shown in Figure 114. The user defined tables need to be in *.csv format, with the columns in the same order as that of the input variables in the study.

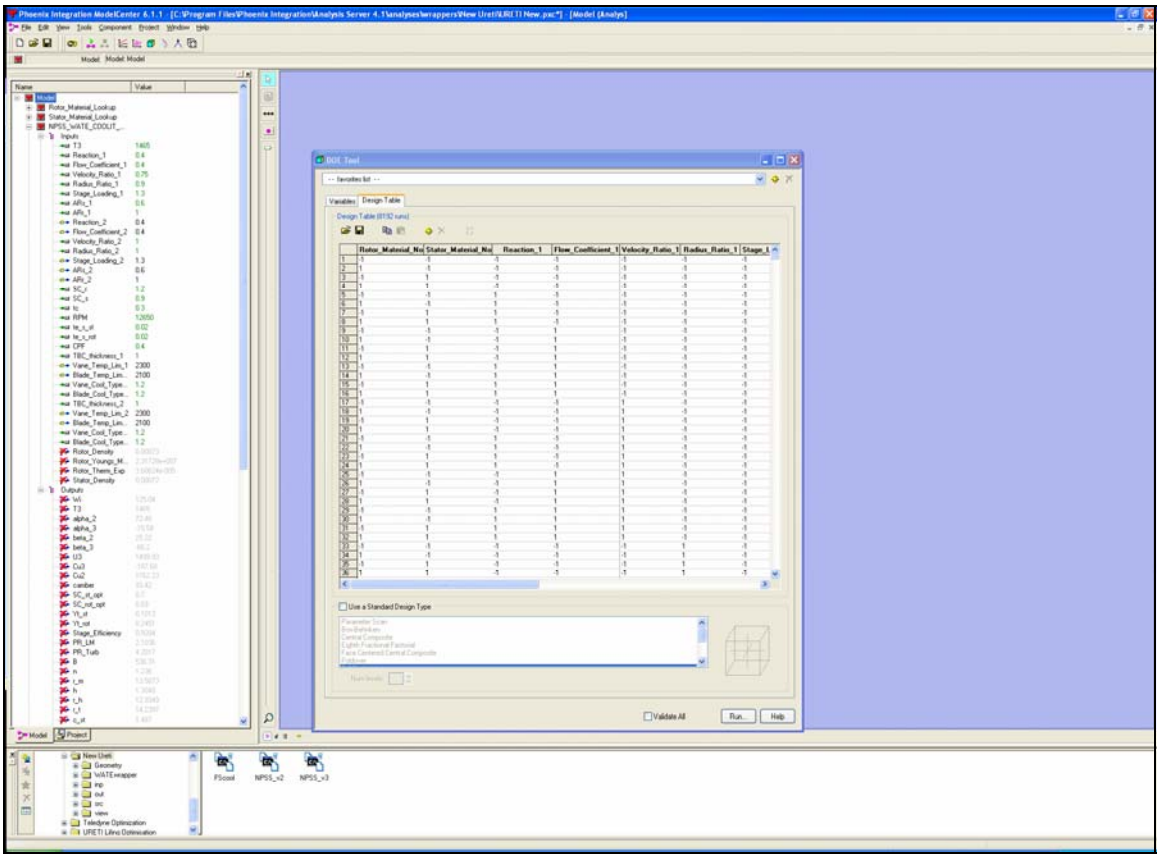

Figure 114: Model Center ™ DoE tool, design table input

1.2.7 During the analysis the results are tracked and displayed in both tabular and Pareto format. An example plot is show in Figure 115. These plots allow for good indicators as to the major effects for the different outputs.

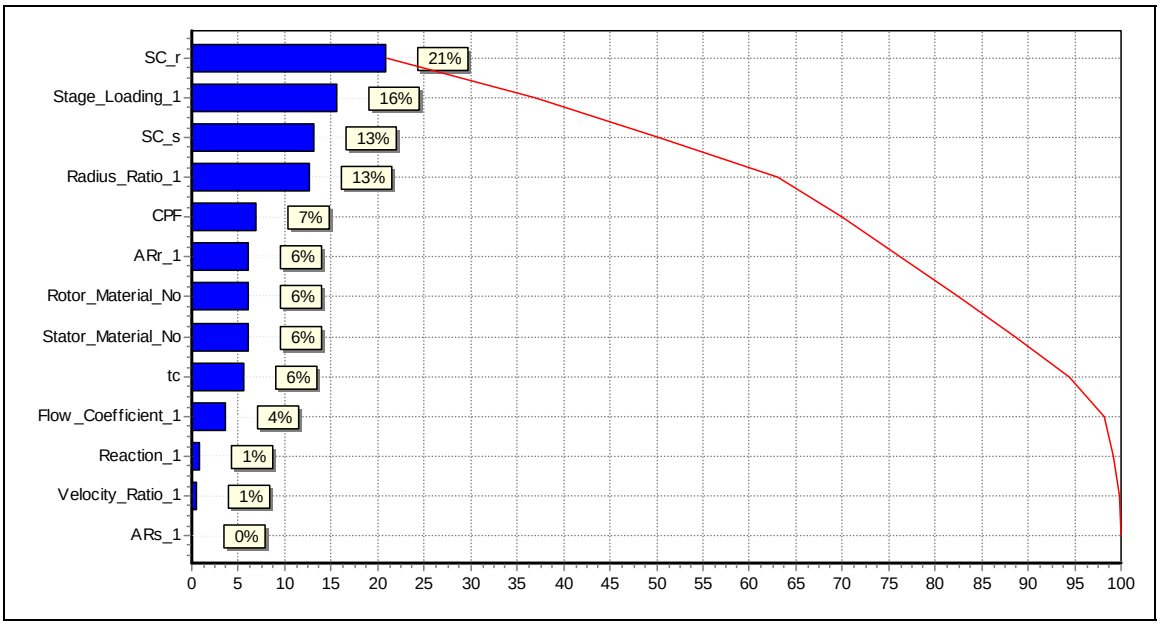

Figure 115: Pareto plot for blade creep life from sample analysis

1.2.8 Once the analysis has been completed the data table can then be saved as a *.csv file for use within a further statistical analysis software, such as JMP. This extra step will permit the surrogate modeling and design space visualization necessary for this approach.

A2. Computer Usage

All analysis was carried out using a Dell Optiplex GX620 with Pentium D 3.0 GHz and 1.0 GB of RAM located within ASDL.

The following is the required software to complete the studies listed herein: Windows XP, Microsoft Excel®, Mathworks MATLAB, SAS JMP, Phoenix Integration Analysis Server and Model Center ™ and finally NASA NPSS NT v1.6.4.

APPENDIX B

ANALYSES OF PARTICULAR NOTE

The following sections include analyses of particular note that have been utilized within the previously described parametric physics based gas turbine blade creep life design environment.

B1. Loss Model NPSS Code

```
#define __LOSSMODEL__
class LossModel extends Element {
//-------------------------------------------------------------
//     ******* DOCUMENTATION *******
//-------------------------------------------------------------
#ifndef __LOSSMODEL__
          title = "LOSSMODEL ELEMENT ";
 description = isA() + " is a general purpose element used to
 calculate the losses for a turbine stage based on the method
 presented in Japikse.";
  usageNotes =
"
";
//-------------------------------------------------------------
```

```
//     ******* SETUP VARIABLES ********

//-------------------------------------------------------

setThermoPackage("GasTbl");


//INPUT VARIABLES

real Tt1 {

        value = 2000.0;

        description = "Total temperature at stage inlet";

        IOstatus = "input";

}

real Pt1 {

        value = 60.0;

        description = "Total pressure at stage inlet";

        IOstatus = "input";

}

real alpha1 {

        value = 0.0;

        description = "Flow angle at stage inlet";

        IOstatus = "input";

}

real ARs {

        value = 2;
```

```
        description = "Stator blade aspect ratio";
        IOstatus = "input";
}
real ARr {
        value = 2;
        description = "Rotor blade aspect ratio";
        IOstatus = "input";
}
real tc {
        value = 0.2;
        description = "Stator thickness to chord ratio";
        IOstatus = "input";
}
real SC_st {
        value = 0.8;
        description = "Stator pitch/chord ratio";
        IOstatus = "input";
}
real SC_rot {
        value = 0.8;
        description = "Rotor pitch/chord ratio";
        IOstatus = "input";
```

```
}
real te_s_st {
        value = 0.02;
        description = "Stator blade trailing edge to pitch ratio";
        IOstatus = "input";
}
real te_s_rot {
        value = 0.02;
        description = "Rotor blade trailing edge to pitch ratio";
        IOstatus = "input";
}
//CONSTANTS
real J = 778.1692626;
real g = 32.174049;
//VARIABLES RECIEVED FROM VELOCITY TRIANGLES
real alpha2, beta2, beta3, lambda, C1, C2, W2, C3, W3, U3, U2, Cx2, Cx3, Cx1,
nu12;
//LOSS CALCULATION VARIABLES
real SC_st_opt, SC_rot_opt;
real Yp0st, Yp23st, Yp_st, lambdaS_st, alpha_m, Clsc_st, B_st, kh_st, YsYk_st,
Yt_st;
```

```
real Yp0rot, Yp23rot, Yp_rot, lambdaS_rot, beta_m, Clsc_rot, B_rot, kh_rot,
YsYk_rot, Yt_rot;
//STATIONS 1 AND 2 VARIABLES
real ht1, S1, gamma2, R, Cp, exp2, gam2, Tt2, Ts1, Ts2, a2, M1, M2, M2rel, Ps1,
Ps2, Pt2rel, Pt2, PR_1, PR_cr;
real M1rel; //for data viewer
//STATION 3 VARIABLES
real ht3, gamma3, Tt3, gam3, exp3, Ts3, a3, M3rel, M3, Pt3, Ps3;


//ISENTROPIC STATION 3 VARIABLES
real ht3isen;
//STAGE EFFICIENCY VARIABLES
real eta_s;
real PR;
//STRESS ANALYSIS VARIABLES
real camber, B, n, h, rho2, mu2, rho3, mu3, W, r_m, omega, r_h, r_t, c_st, c_rot,
Nvanes, Nblades, R_te_st, R_te_rot;
real r_m1, r_m2, r_m3, h1, h2, h3, r_h1, r_h2, r_h3, r_t1, r_t2, r_t3;
real alpha_s_inp, alpha_s_calc, Re2, Re3,Re;
real x1, x2, x3, gap, theta_h_12, theta_h_23, theta_t_12, theta_t_23;
x1=0;
real Aex;                    //Turbine exhaust area
```

```
real AN2;                //AN^2 based on Aex (billions (RPM-in)^2

//-------------------------------------------------------

// ****** SETUP PORTS, FLOW STATIONS, SOCKETS, TABLES ********

//-------------------------------------------------------

// FLUID PORTS

// FUEL PORTS

// BLEED PORTS

// THERMAL PORTS

// MECHANICAL PORTS

// FLOW STATIONS

FlowStation One;

FlowStation Two;

FlowStation Three;

FlowStation ThreeA;

FlowStation ThreeB;

// SOCKETS

// TABLES

#include "src/CRtables.map";

#include "src/trig.fnc";

//-------------------------------------------------------

// ******* INTERNAL SOLVER SETUP *******

//-------------------------------------------------------
```

```
//-------------------------------------------------------
//  ******  ADD SOLVER INDEPENDENTS & DEPENDENT  ******
//-------------------------------------------------------
//-------------------------------------------------------
//   ******* OPTION VARIABLE SETUP *******
//-------------------------------------------------------
//-------------------------------------------------------
// Set total conditions in the fluid input port
//-------------------------------------------------------
//-------------------------------------------------------
// ******* VERIFY ELEMENT *******
//-------------------------------------------------------
//-------------------------------------------------------
//   ******* PERFORM ENGINEERING CALCULATIONS *******
//-------------------------------------------------------
int i;
int calc_stagger = 0;
void calculate() {
        //check if stagger angle should be calculated
        if (alpha_s_inp < 1) {calc_stagger = 1;
}
        //Link omega to Shaft speed
```

```
omega = Sh_O.Nmech;

//OPTIMAL PITCH/CHORD RATIO

SC_st_opt = Fig714(alpha1, alpha2);

SC_rot_opt = Fig714(beta2, beta3);

//VALUES AT STATION 1

if (One.Tt < 520) {//if One hasn't been linked to anything

        One.copyFlow("Fl_I"); }

//cout <<"!!!!!!!!!! Pt1:   "<<One.Pt<<endl;

Tt1 = One.Tt;

Pt1 = One.Pt;

ht1 = One.ht;

S1 = One.S;

R = One.Rt;              //constant across all stages

Cp = One.Cpt;

//One.V = C1;

One.MNdes = 0.5;

One.MNdes = C1/sqrt(One.gams*R*J*g*One.Ts);

One.MNdes = C1/sqrt(One.gams*R*J*g*One.Ts);

One.MNdes = C1/sqrt(One.gams*R*J*g*One.Ts);

One.MNdes = C1/sqrt(One.gams*R*J*g*One.Ts);

//cout <<"!!!!!!!!!! Pt1:   "<<One.Pt<<endl;

//cout<<"C1:  "<<C1<<"  V1:  "<<One.V<<endl;
```

```
        Ps1 = One.Ps;
        Ts1 = One.Ts;
        M1 = One.MN;
        //STATOR PERFORMANCE AND VALUES AT STATION 2
        Yp0st = Fig724noz(SC_st, alpha2);
        //Yp23st = 0.0;
        Yp23st = Fig724imp(SC_st, alpha2);
        Yp_st=(Yp0st+(alpha1/alpha2)**2*(Yp23st-Yp0st))*(tc/0.2)**
(alpha1/alpha2);
//lambdaS_st = 0.0334/ARs*cos(rad(alpha2))/cos(rad(alpha1));
        //Small Turbines
        lambdaS_st = Fig726((1.066*cos(rad(alpha2))/cos(rad(alpha1)))**2/(1.88));
        //Large Turbines (E3 numbers used)
        alpha_m = deg(atan((tan(rad(alpha2))-tan(rad(alpha1)))/2));
        Clsc_st = 2*(tan(rad(alpha1))+tan(rad(alpha2)))*cos(rad(alpha_m));
        B_st = 0.0;
        kh_st = 0.02;
        YsYk_st                                                    =
(lambdaS_st+B_st/ARs*(kh_st*ARs)**.78)*Clsc_st**2*(cos(rad(alpha2)))**2/(cos(r
ad(alpha_m)))**3;
        gamma2 = One.gamt;          //b/c gamma2 is same as gamma1
        exp2 = gamma2/(gamma2-1);    //for use in isentropic flow calculations
```

```
gam2 = (gamma2-1)/2;        //for use in isentropic flow calculations
Tt2 = Tt1;
Ts2 = Tt2-gam2*C2**2/(gamma2*R*J*g);
a2 = sqrt(gamma2*R*J*g*Ts2);
M2 = C2/a2;
M2rel = W2/a2;
if(M2 >= 1) {
        Yp_st = Yp_st*(1+60*(M2-1)**2);
}
Yt_st = Yp_st+ YsYk_st;
Yt_st = Yt_st*Fig727(te_s_st);
Ps2 = Pt1/(Yt_st*((1+gam2*M2**2)**exp2-1)+(1+gam2*M2**2)**exp2);
Pt2rel = Ps2*(1+gam2*W2**2/a2**2)**exp2;
PR_1 = Pt1/Ps2;
PR_cr = ((gamma2+1)/2)**(gamma2/(gamma2-1));
Pt2 = Ps2*(1+gam2*C2**2/a2**2)**exp2;
//Two.copyFlow("One");
Two.setTotalTP(Tt2, Pt2);
Two.V = C2;
//ROTOR PERFORMANCE AND VALUES AT STATION 3
Yp0rot = Fig724noz(SC_rot, beta3);
Yp23rot = Fig724imp(SC_rot, beta3);
```

```
        Yp_rot=(Yp0rot+(beta2/beta3)**2*(Yp23rot-Yp0rot))*
(tc/0.2)**(beta2/beta3);
        if (Yp_rot>10) {
        Yp_rot = 10.0;
        }
//      lambdaS_rot = 0.0334/ARr*cos(rad(beta3))/cos(rad(beta2));
                //Small Turbines
        lambdaS_rot = Fig726((1.066*cos(rad(beta3))/cos(rad(beta2)))**2/(1.88));
        //Large Turbines (E3 numbers used)
        beta_m = deg(atan((tan(rad(beta3))-tan(rad(beta2)))/2));
        Clsc_rot = 2*(tan(rad(beta3))+tan(rad(beta2)))*cos(rad(beta_m));
        B_rot = 0.47;
        kh_rot = 0.01;
        YsYk_rot                                                    =
(lambdaS_rot+B_rot/ARr*(kh_rot*ARr)**.78)*Clsc_rot**2*(cos(rad(beta3)))**2/(c
os(rad(beta_m)))**3;
        ht3 = ht1-lambda*U3**2/J/g;
        //ThreeA.copyFlow("Two");
        ThreeA.setTotal_hP(ht3,300.0);
        gamma3 = ThreeA.gamt;
        Tt3 = ThreeA.Tt;
        gam3 = (gamma3-1)/2;
```

```
exp3 = gamma3/(gamma3-1);
Ts3 = Tt3-gam3*C3**2/(gamma3*R*J*g);
a3 = sqrt(gamma3*R*J*g*Ts3);
M3rel = W3/a3;
M3 = C3/a3;
if(M3rel >= 1) {
        Yp_rot = Yp_rot*(1+60*(M3rel-1)**2);
}
Yt_rot = Yp_rot+ YsYk_rot;
Yt_rot = Yt_rot*Fig727(te_s_rot);

Ps3 = Pt2rel/(Yt_rot*((1+gam3*M3rel**2)**exp3-
1)+(1+gam3*M3rel**2)**exp3);
Pt3 = Ps3*(1+gam3*M3**2)**exp3;
//cout<<"Pt1: "<<Pt1<<" Pt2: "<<Pt2<<"Pt3: "<<Pt3<<endl;
//VALUES AT ISENTROPIC STATION 3
Three.copyFlow("ThreeA");
Three.setTotalSP(S1,Pt3);
ht3isen = Three.ht;
//CALCULATIONS TO SUPPORT STRESS ANALYSIS (MEAN RADIUS)
AND OTHER CALCULATIONS
B = Fig716B(camber);
```

```
n = Fig716n(camber);
ThreeB.copyFlow("ThreeA");
ThreeB.setTotalTP(Tt3, Pt3);
ThreeB.V = C3;
//Flowpath
W = One.W;
r_m = U3*60./(omega*2.*PI)*12.;                    //inches
h = W/(ThreeB.rhos*Cx3*2.*PI*r_m/12.)*12.;         //inches
r_h = r_m-h/2.;                                    //inches
r_t = r_m+h/2.;                                    //inches
 r_m2 = U2*60./(omega*2.*PI)*12.;                          //inches
 r_m1 = nu12*r_m2;
 r_m3 = U3*60./(omega*2.*PI)*12.;                          //inches
h1 = One.W/(One.rhos*Cx1*2.*PI*r_m1/12.)*12.;
h2 = Two.W/(Two.rhos*Cx2*2.*PI*r_m2/12.)*12.;              //inches
h3 = Three.W/(ThreeB.rhos*Cx3*2*PI*r_m3/12.)*12.;          //inches
r_h1 = r_m1-h1/2.;
r_h2 = r_m2-h2/2.;                                 //inches
r_h3 = r_m3-h3/2.;                                 //inches
r_t1 = r_m1+h1/2.;
r_t2 = r_m2+h2/2.;                                 //inches
r_t3 = r_m3+h3/2.;                                 //inches
```

```
c_st = h2/ARs;                                          //inches

c_rot = h3/ARr;                                         //inches

Nvanes = round(2.*PI*r_m2/(SC_st*c_st));

Nblades = round(2.*PI*r_m3/(SC_rot*c_rot));

R_te_st = te_s_st*SC_st*c_st/2.;                        //inches

R_te_rot = te_s_rot*SC_rot*c_rot/2.;                    //inches

alpha_s_calc = Fig638(alpha1, alpha2);  //Stagger Angle

Re2 = One.rhot*C2*c_st/12./One.mut;

Re3 = ThreeB.rhot*W3*c_rot/12./ThreeB.mut;

Re = (Re2+Re3)/2.;

//STAGE EFFICIENCY WITH CORRECTION FOR REYNOLDS NUMBER

eta_s = (ht1-ht3)/(ht1-ht3isen);

eta_s = 1.-(Re/(2.*10.**5.))**-0.2*(1.-eta_s);

PR = Pt1/Pt3;

//AXIAL LOCATION OF FLOW STATIONS AND FLARE ANGLES

//assumes rotor/stator spacing is 1/4 stator chord

//x1 = 0;

if (calc_stagger) {

        alpha_s_inp = alpha_s_calc;

        }

gap = c_st*cos(rad(alpha_s_inp))/4.;
```

```
        x2 = x1+gap*(4.+1./2.);
        x3 = x2+gap/2.+cos(rad(alpha_s_inp))*c_rot;
        theta_h_12 = deg(atan2((r_h2-r_h1),(x2-x1)));
        theta_h_23 = deg(atan2((r_h3-r_h2),(x3-x2)));
        theta_t_12 = deg(atan2((r_t2-r_t1),(x2-x1)));
        theta_t_23 = deg(atan2((r_t3-r_t2),(x3-x2)));
        Aex = PI*r_m3*h3;
   AN2 = Aex*omega**2.0/10.**9.;

        //flowpath based on isentropic expansion
        //One.V = C1;
        // Two.setTotalSP(One.S,One.Pt);
        // Two.V = C2;
        //
ThreeB.setTotal_hP(ht3,(One.Pt*(ThreeB.Tt/One.Tt)**(ThreeB.gams/(ThreeB.ga
ms-1))));
        // ThreeB.V = C3;
        // h1 = One.W/(One.rhos*Cx1*2.*PI*r_m1/12.)*12.;
        // h2 = Two.W/(Two.rhos*Cx2*2.*PI*r_m2/12.)*12.;          //inches
        // h3 = Three.W/(ThreeB.rhos*Cx3*2*PI*r_m3/12.)*12.;
        //inches
        // r_h1 = r_m1-h1/2.;
```

```
        // r_h2 = r_m2-h2/2.;                                    //inches
        // r_h3 = r_m3-h3/2.;                                    //inches
        // r_t1 = r_m1+h1/2.;
        // r_t2 = r_m2+h2/2.;                                    //inches
        // r_t3 = r_m3+h3/2.;                                    //inches
}
} //end LossModel
#endif
```

B2. Stress Code (NPSS version)

```
#ifndef __STRESSCALC__
#define __STRESSCALC__
class StressCalc extends Element {
//-------------------------------------------------------
//    ******* DOCUMENTATION *******
//-------------------------------------------------------
         title =
"
                  STRESSCALC ELEMENT
 ";
 description = isA() + " Programme for determining the Centrifugal Stress of a
Gas Turbine Blade
```

```
        Marcus Smith
        ";
 usageNotes =
"
";
 //-------------------------------------------------------
//     ******* SETUP VARIABLES ********
//-------------------------------------------------------
//INPUTS
real RHOB {
        value = 1.;
        description = "RHOB - lbf*s**2/in**4 (from materials spreadsheet?)";
        IOstatus = "input";
}
real RPM {
        value = 1.;
        description = "shaft speed";
        IOstatus = "input";
}
real RT {
        value = 1.;
        description = "Tip Radius (inches)";
```

```
        IOstatus = "input";
}
real RH {
        value = 1;
        description = "Hub Radius (Inches)";
        IOstatus = "input";
}
real THRA {
        value = 0.5;
        description = "Blade Thickness Ratio";
        IOstatus = "input";
}
real BLADEL {
        value = 0.5;
        description = " is in TURWT from (BH/AR)";
        IOstatus = "input";
}
real WI {
        value = 0.5;
        description = "airflow into turbine (input from NPSS)";
        IOstatus = "input";
}
```

```
real n {
        value = 1.27;
        description = "from Mean line code";
        IOstatus = "input";
}
real B {
        value = 570;
        description = "from Mean line code";
        IOstatus = "input";
}
real h {
        value = 0.5;
        description = "blade height";
        IOstatus = "input";
}
real Cw2 {
        value = 1.0;
        description = "";
        IOstatus = "input";
}
real Cw3 {
        value = 1.0;
```

```
        description = "";
        IOstatus = "input";
}
real NB {
        value = 1.0;
        description = "Number of blades calculated in WATE (TMECH)";
        IOstatus = "input";
}
real TG {
        value = 1.0;
        description = "Gas temp from Coolit (R)";
        IOstatus = "input";
}
real TM {
        value = 1.0;
        description = "Metal temp from Coolit (R)";
        IOstatus = "input";
}
real TC {
        value = 1.0;
        description = "Wall temp from Thermal Code (R)";
        IOstatus = "input";
```

```
}
 real YM {
        value = 1.0;
        description = "Young's Modulus from materials spreadsheet. //
lbf/in**2";
        IOstatus = "input";
}
real alpha {
        value = 1.0;
        description = "thermal expansion coeff, from spreadsheet // 1/R";
        IOstatus = "input";
}
real NU {
        value = 1.0;
        description = "";
        IOstatus = "input";
}
real STT {
        description = "";
        IOstatus = "output";
}
real STRC {
```

```
        description = "";
        IOstatus = "output";
}
real STGB {
        description = "";
        IOstatus = "output";
}
real STTH {
        description = "";
        IOstatus = "output";
}
real RT_RH {
        description = "";
        IOstatus = "output";
}
real Flare_angle {
        description = "";
        IOstatus = "output";
}
real pi = 3.14159265;
//-------------------------------------------------------
// ****** SETUP PORTS, FLOW STATIONS, SOCKETS, TABLES ********
```

```
//-------------------------------------------------------

        // FLUID PORTS

        // FUEL PORTS

        // BLEED PORTS

        // THERMAL PORTS

        // MECHANICAL PORTS

        // FLOW STATIONS

        // SOCKETS

//-------------------------------------------------------

// ******* INTERNAL SOLVER SETUP *******

//-------------------------------------------------------

//-------------------------------------------------------

//  ******  ADD SOLVER INDEPENDENTS & DEPENDENT  ******

//-------------------------------------------------------

//-------------------------------------------------------

//   ******* OPTION VARIABLE SETUP *******

//-------------------------------------------------------

//-------------------------------------------------------

// Set total conditions in the fluid input port

//-------------------------------------------------------

//-------------------------------------------------------

// ******* VERIFY ELEMENT *******
```

```
//-------------------------------------------------------

//-------------------------------------------------

//   ******* PERFORM ENGINEERING CALCULATIONS *******

//-------------------------------------------------------

void calculate() {

// Need:

// RPM - revolutions per minute

// RT - Tip radius (inches)

// RH - Hub Radius (inches)

// TR - Taper Ratio

// A - Annulus area (square inches)

// RHOB - lbf*s**2/in**4 (from materials spreadsheet?)

// W = RPM * ((2*PI())/60);

//Declarations for Internal variables

real A,tc,zs,hb,DT,STL,R;

A = pi * (RT**2. - RH**2.);

// Centrifugal Stress  (lbf/in**2)

STRC = (4./3.) * pi * (RPM/60.)**2. * RHOB * A; //Eqn 7.30 from C&R

//Gas Bending (lbf/in**2)

//BLADEL is in TURWT from (BH/AR)

//THRA = Blade thicknes ratio

//n = 1.27; //from Mean line code
```

```
//B = 570; //From meanline code

//WI = airflow into turbine (input from NPSS)

//NB = Number of blades calculated in WATE (TMECH)

tc = THRA;

zs = (10.*tc)**n / B; // non dimensional

hb = h;//0.5 * (h2+h3); // inches

STGB = ((WI * (Cw2 - Cw3)/32.2)/NB) * (hb/2.) * (1. / (zs * BLADEL**3.));

      // [lbm/s]*[ft/s]*[inches]*[1/inches**3] = lbf/in**2

//Thermal Stress (lbf/in**2)

//TG = Gas temp from Coolit // R

//TM = Metal temp from Coolit //R

//TC = Wall temp from coolit // R

//YM = Young's Modulus from materials spreadsheet. // lbf/in**2

//Alpha = thermal expansion coeff, from spreadsheet // 1/R

//DT = (1.0*TG) - (TC*1.0);

DT = (1.0*TM) - (TC*1.0);

STTH = YM * alpha * DT;

//Von Mises (lbf/in**2)

STL = STGB + STTH;

// Total Stress (lbf/in**2)

STT = (0.5 * ((STL-STRC)**2. + (STL)**2. + (STRC)**2.))**0.5;

// Calculate tip to hub ratio
```

```
RT_RH=RT/RH;
// Calculate Mean-line radius
R=(RT+RH)/2.;
// Calculate Flare angle
Flare_angle=atan((R-NU*R)/(BLADEL+h/12.))*180./pi;
        }
} //end StressCalc
#endif
```

B3. Velocity Triangle Model (from Schobeiri)

```
#ifndef __VELOCITYTRIANGLE__
#define __VELOCITYTRIANGLE__
class VelocityTriangle extends Element {
//-------------------------------------------------------
//    ******* DOCUMENTATION *******
//-------------------------------------------------------
        title =
"
                VELOCITYTRIANGLE ELEMENT
 ";
 description = isA() + " is a general purpose element used to
 calculate the velocity triangle for a turbomachinery blade row.";
```

```
 usageNotes =
"
";
 //-------------------------------------------------------
//     ******* SETUP VARIABLES ********
//-------------------------------------------------------
//INPUTS
real mu {
        value = 1.;
        description = "Axial velocity ratio, Vm2/Vm3";
        IOstatus = "input";
}
real phi {
        value = 1.;
        description = "Flow coefficient, Vm3/U3";
        IOstatus = "input";
}
real nu {
        value = 1.;
        description = "Radial displacement, r2/r3 = U2/U3";
        IOstatus = "input";
}
```

```
real lambda {
        value = 1;
        description = "Work coeffienct, Im/U3^2";
        IOstatus = "input";
}
real r_s_t {
        value = 0.5;
        description = "Reaction, static/total";
        IOstatus = "input";
}
real r_s_s {
        value = 0.5;
        description = "Reaction, static/static";
        IOstatus = "input";
}
real alpha2 {
        value = 0.5;
        description = "Blade inlet gas angle, stationary reference frame";
        IOstatus = "input";
}
real alpha3 {
        value = 0.5;
```

```
        description = "Blade outlet gas angle, stationary reference frame";
        IOstatus = "input";
}
real beta2 {
        value = 0.5;
        description = "Blade inlet gas angle, rotating reference frame";
        IOstatus = "input";
}
real beta3 {
        value = 0.5;
        description = "Blade outlet gas angle, rotating reference frame";
        IOstatus = "input";
}
real deltah {
        value = 1.0;
        description = "Work output of Turbine";
        IOstatus = "input";
}
real alpha1 {
        value = PI/2.;
        description = "stator inlet angle";
        IOstatus = "input";
```

```
}
real mu12 {
        value = 1.0;
        description = "stator axial velocity ratio Vm1/Vm2";
        IOstatus = "input";
}
real nu12 {
        value = 1.;
        description = "Radial displacement, r1/r2";
        IOstatus = "input";
}
real eqn1;
real eqn2;
real eqn3;
real eqn4;
real eqn5,eqn5_r_s_s,eqn5_r_s_t;
real U3, Cx3, C3, Cu3, W3, U2, Cx2, C2, Cu2, W2, camber, C1, Cx1, r_w;
real alpha1deg;
real alpha2deg;
real alpha3deg;
real beta2deg;
real beta3deg;
```

```
//for data viewer
real beta1deg,U1,W1;
//CONSTANTS
real J = 778.1692626;
real g = 32.174049;
//-------------------------------------------------------
// ****** SETUP PORTS, FLOW STATIONS, SOCKETS, TABLES ********
//-------------------------------------------------------
        // FLUID PORTS
        // FUEL PORTS
        // BLEED PORTS
        // THERMAL PORTS
        // MECHANICAL PORTS
        // FLOW STATIONS
        // SOCKETS
#include <src/trig.fnc>
//-------------------------------------------------------
// ******* INTERNAL SOLVER SETUP *******
//-------------------------------------------------------
//-------------------------------------------------------
//  ******  ADD SOLVER INDEPENDENTS & DEPENDENT  ******
//-------------------------------------------------------
```

```
Dependent dep_eqn1 {
        eq_lhs = "eqn1";
        eq_rhs = "0";
        description = "Equation (1)";
        autoSetup = TRUE;
}
Dependent dep_eqn2 {
        eq_lhs = "eqn2";
        eq_rhs = "0";
        description = "Equation (2)";
        autoSetup = TRUE;
}
Dependent dep_eqn3 {
        eq_lhs = "eqn3";
        eq_rhs = "0";
        description = "Equation (3)";
        autoSetup = TRUE;
}
Dependent dep_eqn4 {
        eq_lhs = "eqn4";
        eq_rhs = "0";
        description = "Equation (4)";
```

```
        autoSetup = TRUE;
}
Independent ind_alpha2 {
        varName = "alpha2";
        autoSetup = TRUE;
}
Independent ind_alpha3 {
        varName = "alpha3";
        autoSetup = TRUE;
}
Independent ind_beta2 {
        varName = "beta2";
        autoSetup = TRUE;
}
Independent ind_beta3 {
        varName = "beta3";
        autoSetup = TRUE;
}
Independent ind_r_s_t {
        varName = "r_s_t";
        autoSetup = FALSE;
}
```

```
Dependent dep_eqn5_r_s_s {
        eq_lhs = "eqn5_r_s_s";
        eq_rhs = "r_s_s";
        description = "Equation (5)";  //Added to force equilibrium at stator inlet
        autoSetup = FALSE;
}
//used to link to previous stage if there is one
Dependent dep_C1 {
        eq_lhs = "C1"; //the actual dep/ind structure is set in the parent element
        eq_rhs = "C3";
        description = "Equation (1)";
        autoSetup = FALSE;
}
Independent ind_C1 {
        varName = "mu12";
        autoSetup = FALSE;
}
/*Independent ind_C1 {
        varName = "phi";
        autoSetup = TRUE;
}*/
//-------------------------------------------------------
```

```
//   ******* OPTION VARIABLE SETUP *******
//---------------------------------------------------------
r_s_s.trigger = TRUE;
r_s_t.trigger = TRUE;
int reactionset = 0;
void variableChanged(string name, any oldVal)
 {
 if ( name == "r_s_s"  || name == "r_s_t" ){
 reactionset = 1;                              //FIX   could include some type of
warning if the reaction isn't set
        if (name == "r_s_s") {
                ind_r_s_t.autoSetup = TRUE;
                dep_eqn5_r_s_s.autoSetup = TRUE;
        }
 r_s_s.trigger = FALSE;
 r_s_t.trigger = FALSE;
 }
 }
//---------------------------------------------------------
// Set total conditions in the fluid input port
//---------------------------------------------------------
//---------------------------------------------------------
```

```
// ******* VERIFY ELEMENT *******
//-----------------------------------------------------------
//-------------------------------------------------
//   ******* PERFORM ENGINEERING CALCULATIONS *******
//-----------------------------------------------------------
void calculate() {
        eqn1=((mu**2)*(phi**2)*(1-
nu**2)*(cot(alpha2)**2))+(2*mu*nu*phi*lambda*cot(alpha2))-(lambda**2)-(2*(1-
r_s_t)*lambda)+((mu**2-1)*(phi**2));
        eqn2=((phi**2)*(1-
nu**2)*(cot(alpha3)**2))+(2*phi*lambda*cot(alpha3))+(lambda**2)-(2*(1-
r_s_t)*lambda*(nu**2))+((mu**2-1)*(phi**2)*(nu**2));
        eqn3=((1-
nu**2)*((mu*phi*cot(beta2)+nu)**2)+(2*nu*lambda*(phi*mu*cot(beta2)+nu))-
(lambda**2)-(2*(1-r_s_t)*lambda)+((mu**2-1)*(phi**2)));
        eqn4=((1-
nu**2)*((phi*cot(beta3)+1)**2)+(2*lambda*(phi*cot(beta3)+1))+(lambda**2)-(2*(1-
r_s_t)*lambda*nu**2)+((mu**2-1)*(phi**2)*(nu**2)));
        //CONVERT ANGLES TO BE MEASURED RELATIVE TO THE AXIAL
DIRECTION
        alpha2deg = 90. - deg(alpha2);
        alpha3deg = 90. - deg(alpha3);
```

```
beta2deg = 90. - deg(beta2);

beta3deg = 90. - deg(beta3);

alpha1deg = 90. - deg(alpha1);

//CALCULATION OF VELOCITY TRIANGLE DIMENSIONAL VALUES

U3 = sqrt(deltah*J*g/lambda);

Cx3 = phi*U3;

C3 = Cx3/cos(rad(alpha3deg));

Cu3 = Cx3*tan(rad(alpha3deg));

W3 = Cx3/cos(rad(beta3deg));

U2 = nu*U3;

Cx2 = mu*Cx3;

C2 = Cx2/cos(rad(alpha2deg));

Cu2 = Cx2*tan(rad(alpha2deg));

W2 = Cx2/cos(rad(beta2deg));

camber = beta2deg-beta3deg;

Cx1 = Cx2*mu12;

C1 = Cx1/cos(rad(alpha1deg));

//for data viewer

beta1deg = alpha1deg;

W1 = C1;
```

```
        eqn5_r_s_s = (deltah+(C3**2-C2**2)/(2*J*g))/(deltah+(C3**2-
C1**2)/(2*J*g));
        }
} //end VelocityTriagnle
#endif
```

APPENDIX C

MATERIAL DATABASE METALLIC COMPOSITIONS

The numbers of different chemical compounds that go into a nickel superalloy are large and diverse in nature. The literature search for the best available materials database with the most complete data lead the author to using the Special Metals ™ data base, since it was open access and contained the most diverse nickel superalloy collection. The large numbers of compounds within the compositions has required that the table of the compositions be split in two (Table 16 & Table 17) below.

Table 16: Nickel superalloy properties utilized within thesis, part 1.

	Materials	Percent Composition									
		Ni	Al	Co	Cr	Fe	Hf	Mn	Mo	Nb	Re
1	Waspaloy	61.4	1.3	13.5	19.5	0	0	0	4.3	0	0
2	Waspaloy derivative	61.8	2.5	14.7	18	0	0	0	3	0	0
3	Waspaloy derivative	61.5	5.5	13.2	14.3	2.5	0	0	3	0	0
4	Nimonic115	61.9	4.9	13.2	14.3	2.5	0	0	3.2	0	0
5	Rene41	56.25	1.51	10.82	19.31	2.34	0	0	9.77	0	0
6	Udimet700	59	4	17	15	0	0	0	5	0	0
7	IN713LC	75.6	5.9	0	12	0	0	0	4.5	2	0
8	MarM002	74	5.5	10	9	0	1.5	0	0	0	0
9	MarM002 derivative	75	5.5	11	6	1	1.4	0.1	0	0	0
10	Astroloy derivative	61.7	3	15	16	0	0	0	4.3	0	0
11	Rene41 derivative	55	2	11	20	2	0	0	10	0	0
12	Udimet 700 derivative	61	5	16	14	0	0	0	4	0	0
13	Nimonic derivative	66.1	6	11	12.5	1.5	0.1	0	2.8	0	0
14	Waspaloy derivative	57	3.5	14.7	21	0	0	0	3.8	0	0
15	Arbitrary Material	66.1	1.9	10	21	0	0	0	0	1	0
16	Rene41 derivative	62	2	11	15	2	0	0	8	0	0
17	Udimet 700 derivative	66	3	12	15	0	0	0	4	0	0
18	Nimonic derivative	73.4	4	8	11	1.5	0.1	0	2	0	0
19	MarM002 derivative	75.4	4.9	9.5	8.8	0	1.4	0	0	0	0
20	Waspaloy derivative	59.6	2	14	20.1	0.1	0	0	4.2	0	0

Table 17: Nickel superalloy compositions utilized within this thesis, part 2.

	Material	Percent Composition								
		Ru	Si	Ta	Ti	W	Zr	B	C	N
1	Waspaloy	0	0	0	3	0	0	0.006	0.08	0
2	Waspaloy derivative	0	0	0	5	1.25	0	0.033	0.035	0
3	Waspaloy derivative	0	1	0	4	1	0.04	0.16	0.15	0.2
4	Nimonic115	0	0	0	3.7	0	0.04	0.16	0.15	0
5	Rene41	0	0	0	3.23	0	0	0.006	0.08	0
6	Udimet700	0	0	0	3.5	0	0	0.03	0.06	0
7	IN713LC	0	0	0	0.6	0	0.1	0.01	0.05	0
8	MarM002	0	0	2.5	1.5	10	0.05	0.015	0.15	0
9	MarM002 derivative	0	0.1	0	0	11	0.05	0.01	0.15	0
10	Astroloy derivative	0	0	0	3.7	0	0	0.03	0.06	0
11	Rene41 derivative	0	0	0	3	0	0	0.007	0.09	0
12	Udimet 700 derivative	0	0	0	3.7	0	0	0.04	0.05	0
13	Nimonic derivative	0	0	0	4.6	0	0.08	0.2	0.05	0
14	Waspaloy derivative	0	0	0	2.87	0	0	0.007	0.09	0
15	Arbitrary Material	0	0	1.4	3.7	2	0	0.009	0.15	0
16	Rene41 derivative	0	2	0	4	0	0	0.003	0.08	0
17	Udimet 700 derivative	0	0	0	7	0	0	0.03	0.06	0
18	Nimonic derivative	0	0	0	9	0	0.07	0.3	0.06	0
19	MarM002 derivative	0	0	2.25	2.8	9.5	0.08	0.01	0.1	0
20	Waspaloy derivative	0	0	0	4.5	0	0	0.008	0.04	0

The compounds included above are the following:

Table 18: Glossary of chemical compounds within metal compositions.

Symbol	Name	Symbol	Name
Ni	Nickel	Ru	Ruthenium
Al	Aluminium	Si	Silicon
Co	Cobalt	Ta	Tantalum
Cr	Chromium	Ti	Titanium
Fe	Iron	W	Tungsten
Hf	Hafnium	Zr	Zirconium
Mn	Manganese	B	Boron
Mo	Molybdenum	C	Carbon
Nb	Niobium	N	Nitrogen
Re	Rhenium		

REFERENCES

1. Koff, B., *Gas Turbine Technology Evolution: A Designer's Perspective.* Journal of Propulsion and Power, 2004. **20**(4): p. 577-595.

2. Whittle, F., *Improvements in Aircraft Propulsion* in *UK Intellectual Property Office*, U.I.P. Office, Editor. 1930: United Kingdom.

3. Spittle, P., *Gas turbine technology.* Physics Education, 2003. **38**(6): p. 504-511.

4. *UK Aerospace Industry Research Report*. 2006, Market & Business Development: Manchester UK.

5. *2006 Annual Report*. 2007, GE Aircraft Engines: Cincinnati OH.

6. Barros, C., *Measuring performance in defense-sector companies in a small NATO member country.* Journal of Economic Studies, 2004. **31**(2): p. 112-128.

7. Ingram, P. (2001) *The Subsidy trap: British Government Financial Support for Arms Exports and the Defence Industry*. Building Bridges for Global Security http://www.oxfordresearchgroup.org.uk/publications/books/online/subsidytrap01exec.php

8. Singh, R., *Civil Aerospace Propulsion: The Challenge of the Environment*. 2006, Cranfield University, UK.

9. (2001) *Rolls-Royce Signs $360 Million Total Care Agreement with Continental Airlines*. London Stock Exchange Regulatory News Service http://ir.rolls-royce.com/rr/investors/latestnews/rns/story?id=995626467nRNST2533H

10. *Rolls-Royce Engine Support, Heavy Metal Hardball*, in *Aviation Maintenance*. 2006, Access Intelligence, LLC: Rockville MD.

11. Kemp, K., *Cost of engine failure*, in *The Sunday Herald*. 2001: Glasgow, UK.

12. (2001) *Rolls-Royce profits dip*. British Broadcasting Corporation, http://news.bbc.co.uk/2/hi/business/1505455.stm

13. *2006 Business & Market Report*, in *Citigroup Aerospace and Defence Conference*. 2007, Rolls-Royce Group plc: New York.

14. Tai, J. and e. al, *University Research Engineering Technology Institute (URETI) on Aeropropulsion and Power Technology* 2006, Georgia Institute of Technology.

15. Winstone, M., *The Contribution of Advanced Nickel Alloys to Future Aero-Engines.* Journal of Defence Science 2000. **5**(4): p. F65-F71.

16. Gauntner, J., *Algorithm for Calculating Turbine Cooling Flow and the Resulting Decrease in Turbine Efficiency*, N.L.R. Center, Editor. 1980, NASA: Cleveland, OH.

17. Esgar, J., R. Colladay, and A. Kaufman, *An Analysis of the Capabilities and Limitations of Turbine Air Cooling Methods*, N.L.R. Center, Editor. 1970, NASA: Cleveland, OH.

18. Torbidini, L. and A. Massardo, *Analytical Blade Row Cooling Model for Innovative Gas Turbine Cycle Evaluations Supported by Semi-Empirical Air-Cooled Blade Data.* Journal of Engineering for Gas Turbines and Power, 2004. **126**: p. 498-506.

19. Vittal, S., P. Hajela, and A. Joshi, *Review of Approaches to gas turbine life management*, in *10th AIAA/ISSMO Multidisciplinary Analysis and Optimization*. 2004, AIAA: Albany, NY.

20. Spang, H. and H. Brown, *Control of jet engines.* Control Engineering Practice, 1999. **7**(9): p. 1043-1059.

21. Faith, N., *Black Box*. 1996, London: Boxtree Ltd.

22. Raynor, G. and D. Millward, *Experts probe Heathrow plane's crash landing*, in *Daily Telegraph*. 2008, Telegraph Media Group Ltd: London.

23. Asimow, M., *Introduction to Design*. 1962, Englewood Cliffs, NJ: Prentice-Hall.

24. Dieter, G., *Engineering Design: A Materials and Processing Approach*. 3rd ed, ed. K. Kane. 2000: McGraw-Hill Higher Education.

25. *Improving Engineering Design*, N.R. Council, Editor. 1991, National Academy Press: Washington DC.

26. Glegg, G., *The Design of Design*. 1969, New York: Cambridge University Press.

27. Cohen, H., G. Rogers, and H. Saravanamuttoo, *Gas Turbine Theory*. Second ed. 1974, London, UK: Longman Group Limited.

28. Denton, J. and W. Dawes, *Computational fluid dynamics for turbomachinery design.* Proceedings of Institute of Mechanical Engineering, 1999. **213**(C): p. 107-124.

29. Denton, J. and L. Xu, *The exploitation of three-dimensional flow in turbomachinery design*. Proceedings of Institute of Mechanical Engineering, 1999. **213**(C): p. 125-137.

30. Duboue, J., N. Liamis, and L. Pate, *Recent Advances in Aerothermal Turbine Design and Analysis*, in *36th AIAA/ASMA/SAE/ASEE Joint Propulsion Conference and Exhibit*. 2000, AIAA: Huntsville, AL.

31. McQuilling, M., M. Wolff, S. Fonov, and e. al, *An Experimental Investigation of Low-Pressure Turbine Blade Suction Surface Stresses Using S3F*. 2006: Reno, Nv.

32. Sindir, M. and E. Lynch, *Overview of the State-of-the-Art Practice of Computational Fluid Dynamics in Advanced Propulsion System Design*. 1997, AIAA.

33. Cervenka, M., *Trent 800 breakdown with pressure and temperature considerations*, Rolls-Royce Group PLc: Derby UK.

34. Aungier, R., *Axial-Flow Compressors - A Strategy for Aerodynamic Design and Analysis*. 2003, New York: ASME Press.

35. Denney, R., Z. Liu, M. Smith, and J. Tai, *2.1.1 Final Report*, in *NASA/DoD URETI UAPT*. 2008, Georgia Institute of Technology: Atlanta.

36. Gleeson, B., *Thermal Barrier Coatings for Aeroengine Applications.* Journal of Propulsion and Power, 2006. **22**(2).

37. Han, J.-C., *Turbine Blade Cooling Studies at Texas A&M University: 1980-2004.* Journal of Thermophyics and Heat Transfer, 2004. **20**(2): p. 161-186.

38. Mattingly, J., *Elements of Gas Turbine Propulsion*. 1996, New York: McGraw-Hill.

39. Zaretsky, E., R. Hendricks, and S. Soditus, *Weibull-Based Design Methodology for Rotating Aircraft Engine Structures*, N.G.R. Center, Editor. 2002, NASA: Cleveland, OH.

40. Melis, M., E. Zaretsky, and R. August, *Probabilistic Analysis of Aircraft Gas Turbine Disk Life and Reliability.* Journal of Propulsion and Power, 1999. **15**(5): p. 658-666.

41. Tong, M., I. Halliwell, and L. Ghosn, *A Computer Code for Gas Turbine Engine Weight and Disk Life Estimation*, in *ASME Turbo Expo 2002*. 2002, ASME: Amsterdam, The Netherlands.

42. Casey, M., *Accounting for Losses and Definitions of Efficiency in Turbomachinary Stages.* Proceedings of Institute of Mechanical Engineering, 2007. **221**(A).

43. Bunker, R., *Axial Turbine Blade Tips: Function, Design and Durability.* Journal of Propulsion and Power, 2006. **22**(2): p. 271-285.

44. Coplin, J., *Aircraft Jet Engines*. Now Books. 1967, London: Macdonald & Co (Publishers) Ltd.

45. Schulz, U., C. Leyens, L. Fritscher, M. Peters, B. Saruan-Brings, O. Lavigne, J. Dorvaux, M. Poulain, R. Mevrel, and M. Caliez, *Some recent trends in research and technology of advanced thermal barrier coatings.* Aerospace Science and Technology, 2003. **7**: p. 73-80.

46. Horlock, J.H., D.T. Watson, and T.V. Jones, *Limitations on Gas Turbine Performance Imposed by Large Turbine Cooling Flows.* JOurnal of Engineering for Gas Turbines and Power, 2001. **123**: p. 487.

47. *Creep and Stress Rupture*, in *Metallurgical Consultants*. 2007, www.materialsengineer.com: Altamonte Springs, FL.

48. Sourmail, T. (2003) *Coatings for Turbine Blades*. http://www.msm.cam.ac.uk/phase-trans/2003/Superalloys/coatings/index.html

49. Gektin, V., A. Bar-Cohen, and S. Witzman, *Coffin-Manson based fatigue analysis of underfilled DCAs.* IEEE Transactions on Components, Packaging, and Manufacturing Technology, Part A, 1998. **21**(4): p. 577-584.

50. Hamed, A. and W. Tabakoff, *Erosion and Deposition in Turbomachinery.* Journal of Propulsion and Power, 2006. **22**(2): p. 350-360.

51. Eskner, M., *Mechanical Behavior of Gas Turbine Coatings*, in *Department of Materials Science and Engineering*. 2004, Royal Institute of Technology: Stockholm.

52. Talya, S., J. Rajadas, and A.Chattopadhyay, *Multidisciplinary Optimization of Gas Turbine Blade Design*. 1998, AIAA.

53. Tai, J., R. Denney, M. Smith, and Z. Liu, *Year 3 Review*, in *NASA/DoD URETI UAPT*, J. Tai, Editor. 2005, Georgia Institute of Technology: Columbus, OH.

54. Wallace, J. and D. Mavris, *Creep Life Uncertainty Assessment of a Gas Turbine Airfoil*, in *44th AIAA/ASME/ASCE/AHS Structures, Structural Dynamics and Materials Conference*. 2003, AIAA: Norfolk, VA.

55. Haubert, R., H. Maclin, M. Noe, E. Hsia, and R. Brooks, *High Pressure Turbine Blade Life Sensitivity*. 1980, AIAA 1980-1112.

56. Yue, Z., Z. Lu, and C. Zheng, *Evaluation of Creep Damage Behavior of Nickel-Base Directionally Solidified Superalloys with Different Crystallographic Orientations.* Theoretical and Applied Fracture Mechanics, 1996. **25**: p. 127-138.

57. Antunes, F., J. Ferreira, C. Branco, and J. Byrne, *High temperature fatigue crack growth in Inconel 718.* Materials At High Temperatures, 2000. **17**(4): p. 439-448.

58. Liu, Z. and D. Mavris, *A Methodology for Probabilistic Creep-Fatigue Life Assessment of Hot Gas Path Components*, in *45th AIAA/ASCE/AHS/ASC Structures, Structural Dynamics & Materials*. 2004: Palm Springs CA.

59. Shepherd, D., *Principles of Turbomachinery*. 1956, New York: The MacMillan Company.

60. Haldeman, C. and M. Dunn, *Heat Transfer Measurements and Predictions for the Vane and Blade of a Rotating High-Pressure Turbine Stage*, in *ASME/IGTI Turbo Expo 2003*. 2003, ASME: Atlanta, GA.

61. *Model Center 7.0 Design Your Success*. 2006, Phoenix Integration: Blacksburg, VA. p. 2.

62. Phoenix Integration. (2008) *Model Center Desktop Trade Studies*. http://www.phoenix-int.com/products/modelcenter.php,

63. Mavris, D., L. Phan, and E. Garcia, *Formulation and Implementation of an Aircraft - System - Subsystem Interrelationship Model for Technology Evaluation*, in *ICAS 2006*. 2006: Hamburg, Germany.

64. Kurzke, J., *GasTurb Details 4 - A Utility for Gas Turbine Performance Calculations*. 2003: Dachau, Germany.

65. Naiman, G.F.a.C., *Numerical Propulsion System Simulation -- A Common Tool for Aerospace Propulsion Being Developed*, N.G.R. Center, Editor: Cleveland, OH.

66. Follen, G., *An Object Oriented Extensible Architecture for Affordable Aerospace Propulsion Systems*, in *Reduction of Military Vehicle Acquisition Time and Cost through Advanced Modelling and Virtual Simulation*. 2002, NATO Research and Technology Organisation: Paris, France.

67. Evens, A., G. Follen, C. Niaman, and I. Lopez, *Numerical Propulsion System Simulation's National Cycle Program*. 1998, NASA Lewis Research Center: Cleveland OH.

68. Stauber, L. and C. Naiman (2001) *Numerical Propulsion System Simulation (NPSS): An Award Winning Propulsion System Simulation Tool*. http://www.grc.nasa.gov/WWW/RT2001/9000/9400naiman.html

69. Cline, S., P. Halter, J. Kutney, and T. Sullivan, *Fan and quarter-stage component performance report*, in *Energy efficient engine*. 1983, NASA Lewis Research Center: Cleveland OH.

70. Holloway, P., C. Koch, G. Knight, and S. Shaffer, *High pressure compressor detail design report*, in *Energy efficient engine*. 1982, NASA Lewis Research Center: Cleveland OH.

71. Timko, L., *High pressure turbine component test performance report*, in *Energy Efficient Engine*. 1984, NASA Lewis Research Center: Cleveland OH.

72. Halila, E., D. Lenahan, and T. Thomas, *High pressure turbine test hardware detailed design report*, in *Energy Efficient Engine*. 1982, NASA Lewis Research Center: Cleveland OH.

73. Bridgeman, M., D. Cherry, and J. Pedersen, *Low Pressure Turbine Scaled Test Vehicle Performance*, in *Energy Efficient Engine*. 1983, NASA Lewis Research Center: Cleveland OH.

74. Cherry, D., C. Gay, and D. Lenahan, *Low Pressure Turbine Test Hardware Detailed Design Report*, in *Energy Efficient Engine*. 1982, NASA Lewis Research Center: Cleveland OH.

75. Stearns and E. Marshall, *Integrated coreflow spool design and performance report*, in *Energy Efficient Engine*. 1985, NASA Lewis Research Center: Cleveland OH.

76. Stearns and E. Marshall, *Core Design and Performance Report*, in *Energy Efficient Engine*. 1982, NASA Lewis Research Center: Cleveland OH.

77. Onat, E. and G. Klees, *A Method to Estimate Weight and Dimensions of Large and Small Gas Turbine Engines*, N.L.R. Center, Editor. 1979: Cleveland, OH.

78. Boley, B.A. and J.H. Weiner, *Theory of Thermal Stresses*. 1960, New York: Wiley.

79. Fielding, L., *Turbine Design - The Effect on Axial Flow Turbine Performance of Parameter Variation*. 2000, New York: ASME Press.

80. Schobeiri, M., *Turbomachinery Flow Physics and Dynamic Performance*. 2005, New York: Springer Berlin Heidelberg.

81. Dunham, J. and P. Came, *Improvements to the Ainley-Mathieson Method of Turbine Performance Prediction.* Journal of Engineering for Power, 1970.

82. Japikse, D. and N. Baines, *Introduction to Turbomachinery*. 1994, Oxford, UK: Oxford University Press.

83. Rao, S. and R. Gupta, *Optimum Design of Axial Flow Gas Turbine Stage Part 1: Formulation and Analysis of Optimisation Problem.* Journal of Engineering for Power, 1980. **102**: p. 782-789.

84. Rao, S. and R. Gupta, *Optimum Design of Axial Flow Gas Turbine Stage Part 2: Solution of the Optimisation Problem and Numerical Results.* Journal of Engineering for Power, 1980. **102**: p. 790-797.

85. Young, J. and R. Wilcock, *Modeling the Air-Cooled Gas Turbine: Part 1 - General Thermodynamics*, in *46th International Gas Turbine and Aeroengine Congress and Exhibition*. 2001, ASME: New Orleans, LA. p. 207-213.

86. Young, J. and R. Wilcock, *Modeling the Air-Cooled Gas Turbine: Part 2- Coolant Flows and Losses*, in *46th International Gas Turbine and Aerospace Congress and Exhibition*. 2001, ASME: New Orleans, LA. p. 214-222.

87. Ainley, D. and G. Mathieson, *A Method of Performance Estimation for Axial Flow Turbines*, A.R. Council, Editor. 1951, HMSO: London, England.

88. Sieverding, C., *Recent progress in the understanding of basic aspects of secondary flow in turbine blade passages.* Journal for Gas Turbines and Power, 1985. **107**: p. 248 - 257.

89. Dunham, J., *A review of cascade data on secondary losses in turbines*. Journal of Mechanical Engineering Science, 1970. **12**: p. 48-59.

90. Horlock, J., *Losses and Efficiencies in Axial-Flow Turbines.* International Journal of Mechanical Science, 1960. **2**: p. 48-75.

91. Horlock, J., *Further comments on "Losses and efficiencies in axial-flow turbines"*. International Journal of Mechanical Science, 1961. **12**: p. 312-313.

92. Horlock, J., *Axial flow turbines: fluid mechanics and thermodynamics*. 1966, London: Butterworth.

93. Dunn, M., *Convective Heat Transfer and Aerodynamics in Axial Flow Turbines*, in *ASME Turbo Expo 2001*. 2001, ASME: New Orleans, LA.

94. Beeton, A., *A method of estimating the performance of a gas turbine stage*, R.A. Establishment, Editor. 1944, HMSO: Beford.

95. Reeman, J., P. Gray, and C. Morris, *Some Calculated Turbine Characteristics* P.J. Report, Editor. 1945, HMSO: London.

96. *Updated COOLIT Algorithm for Turbines*. 2001, NASA: Cleveland, OH.

97. Nordland, R. and A. Kassab, *A conjugate BEM optimization algorithm for the design of turbine blade cooling channels*. Boundary Element Technology: WIT Press.

98. Oates, G., *The Aerodynamics of Aircraft Gas Turbine Engines*, A.A.P. Laboratory, Editor. 1978.

99. Ashby, M. and K. Johnson, *Materials and Design*. 2002: Butterworth Heinemann.

100. Maine, E. and M. Ashby, *An investment methodology for materials.* Materials and Design, 2003. **23**: p. 297-306.

101. Ashby, M., *Materials Selection in Mechanical Design*. 2nd ed. 1999, Oxford: Butterworth-Heinemann.

102. *High Performance Alloys*. 2007, Special Metals Corp.

103. Hong, C.-H. and Z. Liu, *Milestone 11 Develop and Document Material Properties Meta-Model*, in *URETI/UAPT Task 2.1.1*, J. Tai, Editor. 2006, Georgia Institute of Technology: Atlanta.

104. Hong, C.-H., *Thesis Proposal*, in *Aerospace Engineering*. 2008, Georgia Institute of Technology: Atlanta, GA.

105. Colladay, R., *Turbine Cooling*, in *Turbine Design and Application*, A. Glassman, Editor. 1975, NASA. p. 59-98.

106. Meitner, P., *Computer Code for Predicting Coolant Flow and Heat Transfer in Turbomachinery*, N.L.R. Center, Editor. 1989, NASA: Cleveland, OH.

107. Incropera, F.P. and D.P. DeWitt, *Fundamentals of heat and mass transfer*. 4th ed. 2001, New York: Wiley.

108. Megson, T.H.G., *Structural and Stress Analysis*. 1996: Edward Arnold.

109. Simitses, G., *An Introduction to the Elastic Stability of Structures*. 1986, Malabar: Kreiger Publishing Company.

110. Tresca, H., *On the flow of solid bodies subjected to high pressures.* CR Acad Sci Paris, 1864. **59**: p. 754.

111. McGuire, J. (1995) *Notes Concerning Yield Criteria*. FEMCI The Book http://femci.gsfc.nasa.gov/yield/,

112. Von Mises, R., *Gottingen Nachrichten.* Math Phys Klasse, 1913. **582**.

113. Pritchard, L., *An Eleven Parameter Axial Turbine Airfoil Geometry Model*, in *Gas Turbine Conference and Exhibit*. 1985, IMECHE: Houston, TX.

114. Smith, M., R. Denney, and Z. Lui, *Milestone 14: Materials and Lifing Final Report*, in *NASA/DoD URETI UAPT Milestone Reports* D.J. Tai, Editor. 2006, Georgia Institute of Technology: Atlanta.

115. Taguchi, G., M.E. Sayed, and C. Hsaing, *Quality Engineering and Production Systems*. 1989, New York: McGraw-Hill.

116. Weisstein, E., *Least Square Fitting*, Wolfram Research Inc. www.mathworld.wolfram.com/LeastSquaresFitting.html

117. Kirby, M., *An Overview of Response Surface Methodology*. 2007, Georgia Institute of Technology: Atlanta GA.

118. Weisstein, E., *Residuals*. 1999, Wolfram Research Inc. http://mathworld.wolfram.com/Residual.html

119. Myers, R. and D. Montgomery, *Response Surface Methodology*. 1995, New York: Wiley Inter-Science.

120. Kamdar, N., M. Smith, R. Thomas, J. Wikler, and D. Mavris, *Response Surface Utilization in the Exploration of a Supersonic Business Jet Concept with Application of Emerging Technologies*, in *World Aviation Conference* 2003, SAE: Montreal, Canada.

121. *Neural Networks*. Electronic Textbook - StatSoft 2003 http://www.statsoft.com/textbook/stneunet.html#pnn.

122. Johnson, C. and J. Schutte, *Basic Regression Analysis for Integrated Neural Networks (BRAINN) Documentation* 2007, Georgia Institute of Technology: Atlanta GA.

123. Hida, T. and M. Hitsuda, *Gaussian Processes*. Translations of Mathematical Monographs. Vol. 120. 1976, Providence: American Mathematical Society.

124. Olea, R., *Geostatistics for Engineers and Earth Scientists*. 1999, Boston: Kluwer Academic Publishers.

125. Cressie, N., *Statistics for Spatial Data*. 1993, New York: Wiley.

126. Chiles, J.-P. and P. Delfiner, *Geostatistics, Modeling Spatial uncertainty*. Series in Probability and Statistics. 1999, New York: Wiley.

127. Hill, W. and W. Hunter, *A Review of Response Surface Methodology: A Literature Survey.* Technometrics, 1966. **8**(4): p. 571-590.

128. Myers, R., A. Khuri, and W. Carter, *Response Surface Methodology: 1966-1988.* Technometrics, 1989. **31**(2): p. 137-157.

129. Saunders, N., M. Fahrmann, and C. Small, *The Application of CALPHAD Calculations to Ni-Based Superalloys*, in *Superalloys 2000*, K. Green, T. Pollock, and R. Kissinger, Editors. 2000, The Minerals, Metals, & Materials Society: Warrendale, PA.

130. Saunders, N., A. Miodownik, and J. Schille, *Modelling of the Thermo-Physical and Physical Properties for Solidification of Ni-Based Superalloys*, in *Liquid Metals Procession 2003*. 2003: Nancy, France.

131. Johnson, C., *Advanced Surrogate Modeling Techniques - Neural Networks*, in *Advanced Design Methods III: Strategic Decision Making*, D. Mavris, Editor. 2007, Georgia Institute of Technology: Atlanta, GA.

132. Villeneuve, F., *A Method for Concept and Technology Exploration of Aerospace Architectures*, in *School of Aerospace Engineering*. 2007, PhD Thesis, Georgia Institute of Technology: Atlanta.

133. Ender, T., *A Top-Down, Hierarchical, System-of-Systems Approach to the Design of an Air Defense Weapon*, in *School of Aerospace Engineering*. 2006, PhD Thesis, Georgia Institute of Technology: Atlanta.

134. Baker, A., *The Role of Mission Requirements, Vehicle Attributes, Technologies and Uncertainty in Rotorcraft Systems Design*, in *School of Aerospace Engineering*. 2002, PhD Thesis, Georgia Institute of Technology: Atlanta.

135. Baker, A. and D. Mavris, *Assessing the Simultaneous Impact of Requirements, Vehicle Characteristics, and Technologies during Aircraft Design*, in *39th Aerospace Sciences Meeting & Exhibit*. 2001, AIAA-2001-0533: Reno, NV.

136. Biltgen, P., T. Ender, and D. Mavris, *Development of a Collaborative Capability-Based Tradeoff Environment for Complex System Architecture*, in *44th AIAA Aerospace Sciences Meeting and Exhibit* 2006, AIAA-2006-0728: Reno, NV.

137. *JMP Help Manual*. 2007, SAS Institute Cary, NC.

138. Walsh, P. and P. Fletcher, *Gas Turbine Performance*. Second ed. 2004, New York: ASME Press. 646.

139. Pareto, V., *Manuel d'Economie Politique*. 1909, Paris: Giard et Briere. 695.

140. Vasinonta, A. and J. Beuth, *Measurement of iInterfacial toughness in thermal barrier coating systems by indentation.* Engineering Fracture Mechanics, 2001. **68**(7): p. 843-860.

141. Smith, M., C.-H. Hong, Z. Liu, and R. Denney, *Milestone 15: Low Fidelity Life Prediction Theory*, in *URETI UAPT Task 2.1.1*. 2007, Georgia Institute of Technology: Atlanta, GA.

VITA

MARCUS E. B. SMITH

Marcus Smith was born in Peterborough Cambridgeshire in the United Kingdom. He attended Stamford School in the United Kingdom, read Aeromechanical Systems Engineering at Cranfield University (Defence College of Management and Technology), achieving a BEng(hons) with first class honors in 2001. Following a year off working on a farm, then for an outdoor clock manufacturing company, he ventured to the USA, to Georgia Tech to read Aerospace Engineering at the graduate level in the Aerospace Systems Design Laboratory. His time at Georgia Tech culminates with the award of a Ph.D in Aerospace Engineering in April of 2008, following the award of a Master's Degree in 2003. When not working on his research, Mr. Smith enjoys walks with his wonderful fiancée Laura, playing field hockey and going fishing in the mountains.